Antibacterial agent formulation and delivery with external triggered release

A Thesis Submitted to the University of London for the Degree of

Doctor of Philosophy

By

Dong Luo

Supervisor: Professor Gleb B. Sukhorukov

School of Engineering and Materials Science

Queen Mary University of London

July 2017

Declaration

I certify that the present work is prepared solely by me during the course of my studies at Queen Mary University of London. It has not been submitted for a degree at this or any other university. Any words and/or figures from the work of other people are fully acknowledged according to standard referencing.

This thesis fully combines with the regulations set by the University of London and the Queen Mary, University of London.

Dong Luo

December 2016

Abstract

Antibacterial agent delivery is of great importance in medicine and dentistry since the bacterial infections are still one of the major reasons for hospitalization and mortality. Despite of the development of technique and pharmacy, more antimicrobial agents are optimized and utilized to treat infections, and their action of principal is better understood which lay a foundation for developing strategies for infection treatment. Over the last decades, many delivery systems have been established to deliver bacterial agents and maintain a sustained activity against them. However, the bacteria are always developing and finding a way to defend themselves. A more responsive antibacterial agent delivery system, which can release the active substances on demand to match the stages of diseases, is highly desirable.

Therefore, it motivates us to carry out the work to develop a multifunctional delivery system for antibacterial particle formulation and encapsulation based on the layer-by-layer self-assembly technique and electrospinning, to manipulate the release with external triggers, such as near-infrared (NIR) light and alternating magnetic field (AMF). Strategically, two different kinds of antibacterial agents, chlorhexidine and doxycycline, were studied. Chlorhexidine was fabricated into spherical particles and functionalized with both gold and magnetite nanoparticles, and doxycycline was encapsulated within microcapsules which were also functionalized with magnetite nanoparticles. Their release kinetics and possibilities to trigger the release with either a NIR light or AMF was explored.

The first two chapters of the thesis give a general introduction and literature review on the current use of antibacterial agents and the problems concerned, strategies already developed for antibacterial agent delivery, and the potential triggers to induce a smart release. In chapter 3, a brief description of materials and methods, and instruments is presented. Chapter 4 is about chlorhexidine particle formulation. Firstly, particulation of chlorhexidine and mechanism of

spherical interconnected structure formation was explored, and then the chlorhexidine particles are encapsulated either by LbL assembly or spray-drying. The chlorhexidine spheres were also functionalized with gold nanorods and Fe_3O_4 nanoparticles to achieve NIR light and magnetic field manipulated release, and the effect of nanoparticles on the formation of chlorhexidine spheres was also studied. When the chlorhexidine particles were incorporated into electrospun fibers, a sustained antibacterial activity was demonstrated. Chapter 5 is about the delivery of doxycycline to cells with microcapsules and the sustained intracellular doxycycline activity was demonstrated via EGFP expression when the cells were engineered with a tetracycline regulated gene expression system. Intracellular triggered release and upregulation of EGFP expression was achieved by an AMF. The results successfully demonstrated the possibility of chlorhexidine and doxycycline delivery and NIR light/AMF triggered release, which is promising for a future application in medicine and dentistry.

Table of Contents

Acknowledgements

First of all, I would like to thank my PhD supervisor, Professor Gleb B. Sukhorukov, who offered me the opportunity to study at QMUL, and was always there during the past three years providing with constant guidance and encouragements.

I would also like to express my thanks to Dr. David Gould (William Harvey Institute, QMUL), Dr. Mike Cattell (School of Dentistry, QMUL), Dr. Saroash Shahid (School of Dentistry, QMUL), without whom I would never have had my work done so smoothly.

I am grateful for all the colleagues at QMUL, who helped me a lot with the experimental things, particularly, Dr. Dongsheng Wu, Dr. Alice Williams, Dr. Rory Wilson, Dr. Russell Bailey, Dr. Nadezda Tarakina, Dr. Krystelle Mafina. Specially, I have to thank Mr Chris Mole and Mr Shafir Iqbal for their constant help with the general lab equipment use and lab management.

I feel so lucky to be a member of Gleb's group that it was always easy to share experimental skills and ideas. Especially, I really appreciate the senior members of our group, Dr. Anton Pavlov, Dr. Qingrong Wei, Dr. Qiangying Yi, Dr. Maria Lomova, who led me into the lab at QMUL and offered a lot of help at the beginning. I also thank the other group members, visitors to our lab, and all my friends.

List of Figures

List of Tables

List of Symbols and Abbreviations

AMF, alternating magnetic field

BSA, bovine serum albumin

BSEM, back scattering electron microscopy

CTAB, cetyl-trimethylammonium bromide

CHX, chlorhexidine

CLSM, confocal laser scanning microscopy

DLS, dynamic light scanttering

DPPC, 1,2-Dipalmitoyl-sn-glycero-3-phosphocholine

DS, dextran sulfate sodium salt

E. coli, escherichia coli

EDTA, ethylenediaminetetraacetic acid

EDX, Energy-dispersive X-ray spectroscopy

EGFP, enhanced green fluorescent protein

FITC, fluorescein isothiocyanate

FIB, focused ion beam

FTIR, fourier Transform Infrared Spectroscopy

GNR, gold nanorod

HEMA, hydroxyethyl methacrylate

HFMF, high frequency magnetic field

LbL, Layer-by-Layer

MF, melamine formaldehyde

MIC, minimum inhibitory concentration

MSNs, mesoporous silica nanoparticles

MTT, 3-(4,5-dimethylthiazol-2-yl)-2,5-diphenyltetrazolium bromide

NIR, near-infrared light

O/W, oil-in-water

PAH, poly(allylamine hydrochloride)

Parg, poly-L-arginine

PDADMAC, poly(diallyldimethylammonium chloride)

PEC, polyelectrolyte complex

PEI, poly(ethylene imine)

PLA, poly-lactic acid

PLGA, poly(lactides-co-glycolide)

PNIPAM, poly(N-isopropylacrylamine)

PS, polystyrene

PSS, poly(sodium 4-styrenesulfonate)

QCM, quartz crystal microbalance

RhB, rhodamine B

SEM, scanning electron microscopy

TEM, transmission electron microscopy

TGA, thermo-gravimetric analysis

TRITC, tetramethylrhodamine-5-(and 6)-isothiocyanate

TRITC-Dextan, tetramethylrhodamine isothiocyanate-dextran

UDMA, urethane dimethacrylate

UV-Vis, ultraviolet-visible (Spectroscopy)

W/O, water-in-oil

1. Introduction

We are sharing the world with numerous forms of life, animals, plants, and microorganisms, a harmonious living together of which ensures us a happy and high quality life. Microorganisms, or more specific bacteria, are more directly contacted with us every day. Some of them are good and essential for our health, while the others may cause us troubles. When harmful bacteria invade and reproduce in our body, we may suffer from infections or even death. So actually, the immune system of human body is fighting with these harmful bacteria every seconds. However, sometimes our body still fails to defend the invasion of harmful bacteria and has infection diseases, ranging from cutaneous infections to deep-seated life threatening infections such as pneumonia, endocarditis, septicemia, osteomyelitis, and other metastatic complications.[1] Therefore, some treatments are needed to help to get rid of these bacteria.

Various antibacterial agents are developed and used for infection treatment, ensuring a happier and healthier life. Nevertheless, the battle is never ended. We still face huge challenges to fight with the bacterial infections, such as bacterial resistance, intracellular infections, and formation of biofilms.[2] The direct application of antibacterial agents cannot ensure a depletion of bacteria, so in this case, some delivery systems which can facilitate a local sustained activity of antibacterial agents are needed to enhance their performance.[1, 3]

Local and sustained delivery of antibacterial agents is a novel concept for the treatment of recurrent and chronic infections, as an increased drug concentration at the site of infection could reduce the need for systemic drug administration, and avoid side effects.[4-5] A high local drug concentration is essential to eliminate bacteria initially and with a sustained drug release in the long term to prevent secondary infection.[6] Many delivery systems, such as microparticles, nanogels, foams, films and nanofibers have been developed to deliver antibacterial agents.[7-10]

Polyelectrolyte microcapsules generated on a dissolvable matrix core using the layer-by-layer (LbL) assembly method are good candidates for antibacterial agents delivery.[11] Their construction utilizes electrostatic interactions between oppositely charged polyelectrolytes to add layers to the core. Assembly is performed under native conditions which permit the inclusion of various molecules within the structure, the positioning of these, influences activity in intact capsules as well as stability and release kinetics.[12-13] Microcapsules have been extensively studied in isolation and have been successfully employed for the delivery of drugs to cells, which is potentially beneficial for intracellular infections. Their fate within cells depends upon their chemical composition that those composed of biodegradable polymers will be broken down and release their contents whilst those assembled with synthetic polymers can potentially remain intact. On the other hand, nano-/micro- fibers are advantageous for drug delivery because of their small diameter, high specific surface area and easy of surface functionalities.[14-15] The fibers are commonly produced by electrospinning and there are various approaches to load the fibers with antibacterial agents. They are especially attractive to be used as wound dressings.[16]

On the other aspect, how to target delivery of the antimicrobial agents and tailor the release in a desired manner is of great interest for a more effective and responsive treatment of infections. It can be achieved by carriers functionzalization. For example, the inclusion of metal nanoparticles (gold or magnetite) into carriers may facilitate a near-infrared light or magnetic field responsive properties, the exposure to which can thus induce a triggered release of cargos. The inclusion of gold nanoparticles and magnetite nanoparticles as a charged species in microcapsule layers is already extensively studied.[17-19] With magnetic nanoparticles encapsulated, movement of carriers can be navigated with an external magnetic field[20] and the specific targeted delivery of drug can greatly improve the efficiency and reduce dosage used,

which is important for infection treatment. The in situ release of cargo is also reported with either NIR light or an alternating magnetic field.[21-23]

According to all mentioned above, this thesis describes experiments on delivery of antibacterial agents (chlorhexidine and doxycycline). For chlorhexidine part, a novel formulation of chlorhexidine spherical particles was produced and functionalized with gold nanorods and iron oxide nanoparticles. The possibility to achieve a more sustained activity by incorporating them into polymer films and electrospinning fibers, and a triggered release by NIR light or magnetid field was studied. Doxycycline, on the other hand, was encapsulated into LbL microcapsules and sustained effect in cells was evaluated via the tet-on system. When the microcapsules were functionalized with magnetic particles, targeted doxycycline delivery to cells and alternating magnetic field induced release were also explored.

2. Literature Review

2.1 Antimicrobial agents

Bacteria are the most common life forms which we contact with every day, and even many of the normal functions of human body are relied on some of the bacteria. However, despite the improvement of medicine, infection by the harmful bacteria is one other leading causes of diseases nowadays.[1] There is a wide variety of agents which have an antibacterial activity, including metal ions (e. g. zinc, silver), nanoparticles, antibiotics, chlorhexidine, and other agents such as chitosan and quaternary ammonium compounds, also demonstrate a good antimicrobial capability.[24-26] The review here mainly focuses on the application of chlorhexidine and doxycycline.

2.1.1 Chlorhexidine

2.1.1.1 Chlorhexidine and its compounds

Chlorhexidine is a broad spectrum antimicrobial agent, which is effective against both the gram-positive and gram-negative microbes.[27] The molecular structure of chlorhexidine is given in Figure 2.1. The antimicrobial properties of chlorhexidine are assumed to be that the guanidium groups from its structure have strong coordinating ability, which enables binding to bacteria cell membranes to cause cell function disruption.[28] At a low concentration, the action of chlorhexidine is bacteriostatic while at a higher concentration, its action is bactericidal.[29] Chlorhexidine has a very solubility, so it is normally used in the form of salts, such as chlorhexidine diacetate, chlorhexidine digluconate, and chlorhexidine dihydrochloride. The solubility properties of the chlorhexidine as a function of salts type and concentration are well studied in by Zeng et al..[30]

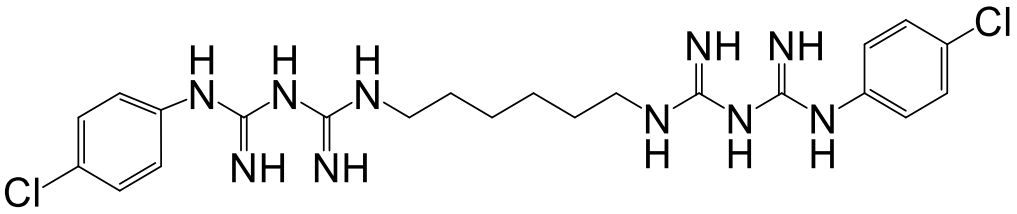

Figure 2.1 The chemical structure of chlorhexidine.

The biguanide groups of chlorhexidine have remarkable coordination ability, which are utilized to produce other formulation of chlorhexidine compounds.[31] For example, new copper (II) complex compounds have been reported, which utilized the biguanidine of chlorhexidine to coordinate with Cu^{2+}, and the structure of proposed interaction between copper ions and chlorhexidine is showed in Figure 2.2.[28-29] Moreover, the incorporated Cu^{2+} ions, or other ions such as Zn^{2+}, Sn^{2+}, and Ag^{+} can enhance the antimicrobial activities.[29] Another study also used chlorhexidine digluconate to precipitate with sodium hexametaphosphate, and produced a new formulation of chlorhexidine nanoparticles.[32]

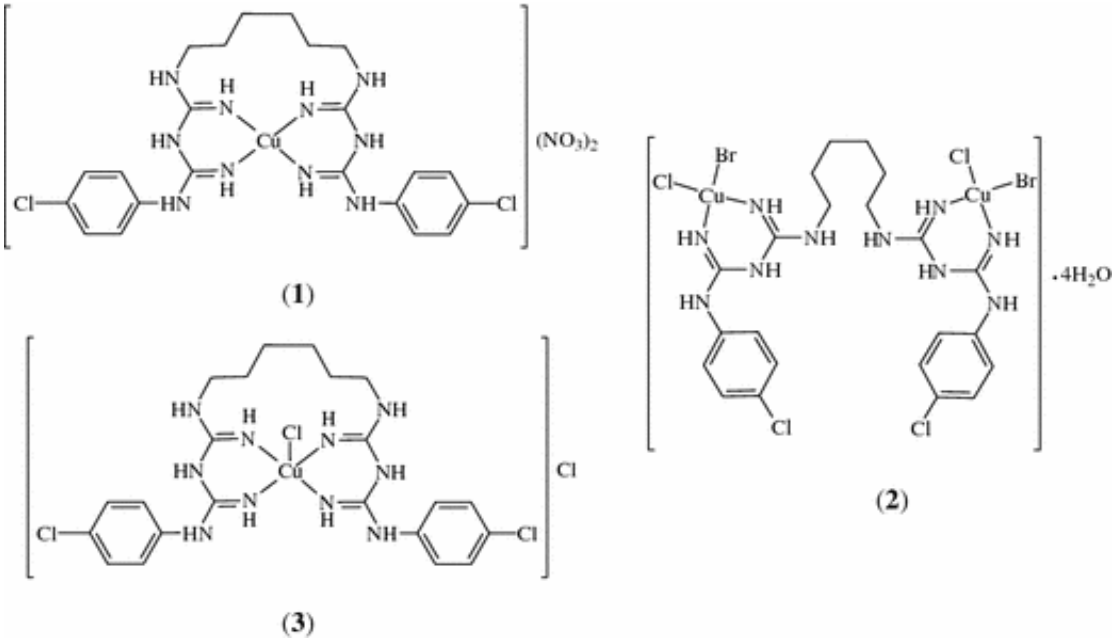

Figure 2.2 Proposed coordination mode for the chlorhexidine and copper complexes. [28]

2.1.1.2 Application of chlorhexidine in dentistry

Chlorhexidine is widely used in our everyday life to disinfect of our skin and hand. It also has broad applications in dentistry, which is used in the toothpaste, mouthwashes and other products to control dental plaque and to treat gingivitis and endodontic disease.[6, 33-34] The problem concerned with its oral performance nevertheless is always sustained function against microbes, and a lack of long term effect, which can lead to repetitive infection or failure for implants. For example, chlorhexidine contained in mouth rinse is effective for general oral bacteria but for those bacteria in periodontal pockets, a longer and sustained activity is required.[35] A delivery system which allows a sustained release of chlorhexidine (2% aqueous solution) may be useful in the treatment of endodontic infections,[6] and to reduce the prevalence of dental infections. A commercially available product now for the treatment of periodontal (gum) disease is known as PerioChip, which combines chlorhexidine digluconate with cross-linked gelatine. The problems with these kinds of carriers however, are low drug loading capacity and release of the preloaded drug is dependent on polymer degradation rate. Many delivery systems have been developed for sustained chlorhexidine delivery and most of those are based on biodegradable polymeric carriers, nano/micro particles or gels.[7, 36-38] Interestingly, β-cyclodextrin was also reported to form reversible complexes with chlorhexidine to promote drug loading and sustained release.[35]

For restoration, chlorhexine is also incorporated into resins and other resin based dental composites.[39-41]The functionalization of the restoration materials with chlorhexidine is beneficial to reduce secondary caries and inhibit cariogenic biofilms. To achieve a sustained antimicrobial activity, inorganic particles such as mesoporous silica nanoparticles (MSNs) are used for chlorhexidine loading, since MSNs have porous surface structure. Moreover, this approach can also display rechargeable properties.[42]

2.1.2 Antibiotics

2.1.2.1 Doxycycline

Antibiotics are another category of antibacterial agents, which can either stop microbes growing or kill them outright.[43] The mechanism of their action against bacteria is more complicated than chlorhexidine and varies from different type of antibiotics. They can either interfere with the cell wall synthesis (e.g. β-lactams and glycopeptides) or nuclei acid synthesis (e.g. fluoroquinolones and rifampin), or inhibit protein synthesis (e.g. macrolides, aminoglycosides, tetracycline and oxazolidinones), or inhibit a metabolic pathway (e.g. sulfonamides and folic acid analogs), or just interrupt the bacteria membrane (e.g. polymysins and dapomcin).[1, 43]

Tetracycline is a kind of broad spectrum antibiotics which is effective against both gram-positive and gram-negative bacteria. They are named according to the chemical structure, four (tetra) hydrocarbon rings (cycl). Doxycycline is one derivative from the tetracycline family, and its chemical structure is given in Figure 2.3.

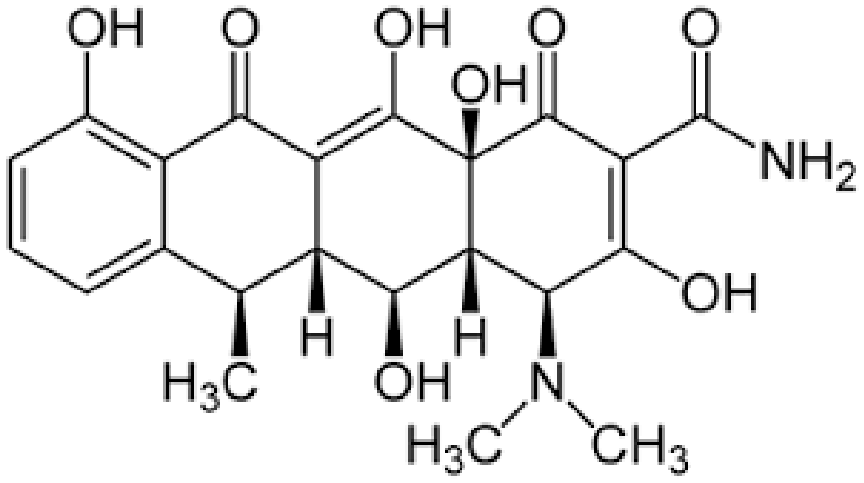

Figure 2.3 Chemical structure of doxycycline.

2.1.2.2 Application of doxycycline

Doxycycline is a widely used antibiotic in the treatment of infections in humans. At low concentrations below those required for antimicrobial effects doxycycline also exerts anti-inflammatory effects due to inhibition of matrix metalloproteinases[44] so has potential use in treatment of inflammatory conditions.[45] Doxycycline is typically administered orally as tablets or suspensions and also topically in creams. Doxycycline has been incorporated into both nano and microstructures however sustained biological activity of the antibiotic has not been explored in these studies.[46-47] Take the commercially available product containing doxycycline, Atridox™ as an example (Figure 2.4). Atridox™ is a subgingival controlled release product composed of bioabsorbable, flowable polymeric formulation, poly(DL-lactide) (PLA) dissolved in N-methyl-2-pyrrolidone (NMP), and doxycycline hyclate. The constituted product is a pale yellow to yellow viscous liquid with a concentration of 10% of doxycycline hyclate. Upon contact with the crevicular fluid, the liquid product solidifies and then allows for controlled release of drug for a period of 7 days.

Figure 2.4 The commercial available product Atridox™, which contains doxycycline.

Besides, doxycycline can also be used for gene regulation based on the *tet-on* system. The *tet-on* system is the most efficient and broadly used one among all of the gene regulatory systems, and it is optimized in various ways to promote sensitivity and robust induction by tetracycline or its derivatives[48-50]. *Tet-on* system is based on the specific and affinity binding between reverse Tet repressor protein (rtTA) and operator DNA sequence (*tet*O), which at the present of tetracycline, the binding would be enhanced and transgene switch is kept on[51]. Doxycycline, is more routinely used for its penetration of cell and nuclear membranes[52]. Based on doxycycline, light and pH regulated gene expression system could be established by chemically modifying the molecule with photoactivatable cage [53-54] or conjugating it to dendritic polymers via pH-sensitive binding[55].

2.2 Various polymers-based drug delivery system

2.2.1 Resin composites

Since being introduced to dentistry in the 1950s, dental composites have undergone considerable changes; the modification of fillers to enhance the mechanical properties and the optimisation of the polymeric matrix to improve their biocompatibility [56]. Resin composites are used extensively in dentistry as restorative materials, cavity liners, cores and buildups, crowns, inlays, sealants and cements for tooth prostheses.[57] According to different applications, the resin composites can be distinguished, but they are normally made of polymeric matrix, reinforcing fillers, silane coupling agents to bind the filler to the matrix, and chemicals that promote or modulate the polymerization reaction. The most commonly used base monomers in the resin composites are bis-GMA, which is usually mixed with other dimethacrylates, such as TEGDMA, UDMA or other monomers.[58] Currently available dental composites have

exceptional aesthetics and comparable mechanical properties (flexural strength, fracture toughness and tensile strength) when compared with porcelain and amalgam, and superior to that of glass ionomers[57]. This allows their wide use for anterior and posterior tooth restorations, as well as pit and fissure sealants [59]. Most composites are light-activated, and the most common photoinitiator system is camphoroquinone, accelerated by a tertiary amine. When dental composites are cured by light and chemically initiated by free radical polymerization, there will be 2-5.63 vol. % shrinkage of the material [60]. This can lead to the formation of gaps between the restoration and the tooth [61]. Bacterial microleakage through these gaps can cause marginal discolouration, sensitivity, inflammation, recurrent caries and apical periodontitis [62]. Furthermore, accumulation of bacterial biofilms on the surface of dental composites can lead to degradation of the polymer matrix, resulting in the weakening of the restoration. Dental composites with antimicrobial properties are therefore highly desirable to overcome these problems.

Chlorhexidine has been incorporated in a variety of resin composites [40, 63-64]. Chlorhexdidne also stabilizes the resin-dentine bond by inhibiting matrix metalloproteinases (MMP) which are responsible for the breakdown of the bond at the dentine-restoration interface [65]. Inclusion of chlorhexidine into dental composites has been achieved by mixing the chlorhexidine diacetate with monomers [42, 66-67]. This composite however suffers from an uncontrollable release of chlorhexidine, due to its rapid diffusion from the methacrylate based resin. To overcome these drawbacks efforts have been made to develop new chlorhexidine formulations [28, 32, 68-69] and investigate novel drug carriers [70-71]. Interestingly, a recent study used the mesoporous silica nanoparticles as carriers for chlorhexidine loading, which were further incorporated into resin composites. The chlorhexidine release of which was more controllable compared with the resin mixed with chlorhexidine directly (Figure 2.5). [42]

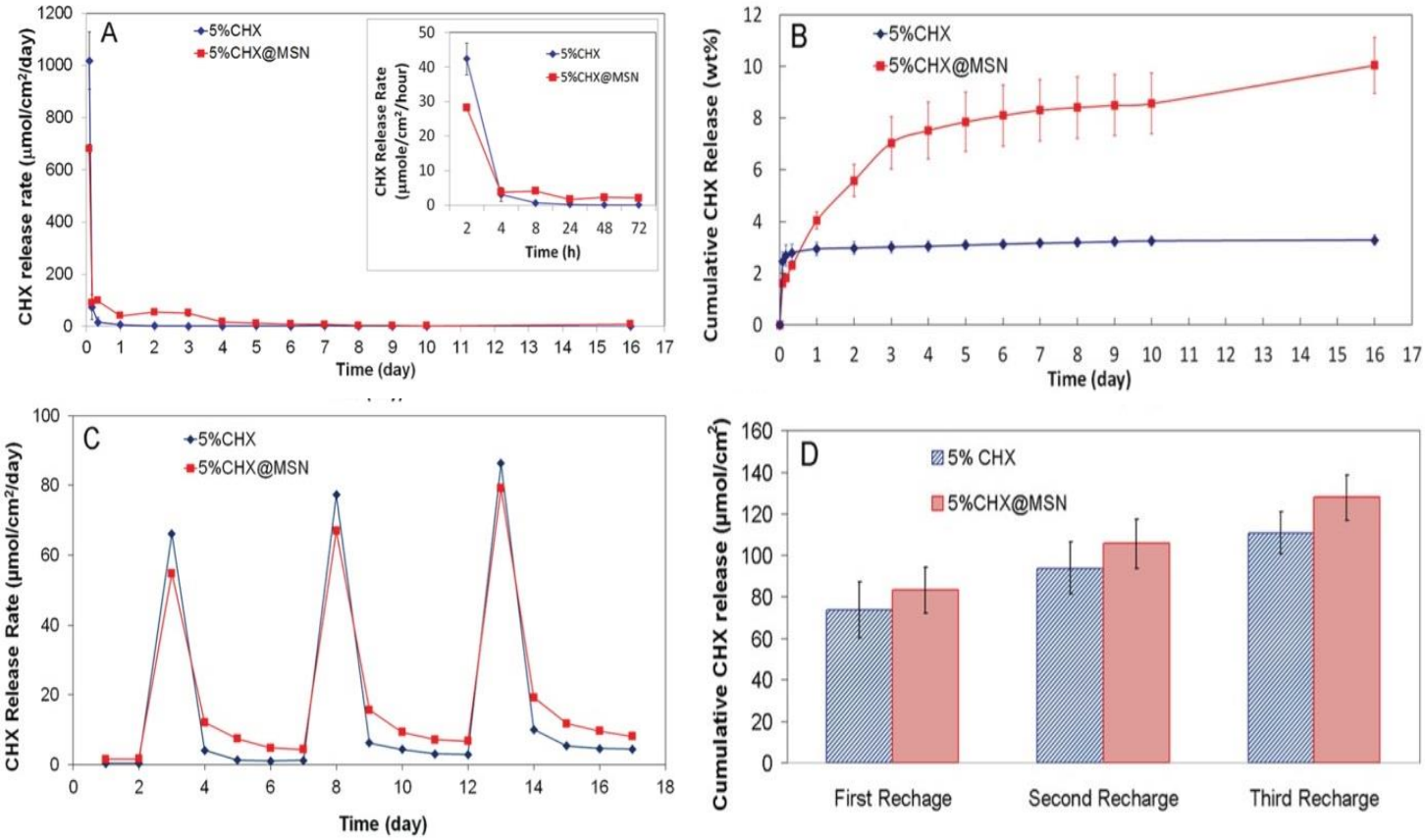

Figure 2.5 CHX release and recharge. (a) CHX release profiles from composites containing directly mixed CHX or CHX@MSN. (The insert is the release rate (μmol/cm^2/hr) during the first 72 hr.) (b) Cumulative CHX release as the weight percentage of the total loaded CHX. (c) CHX recharge profile in 3 repeated recharges. (d) Cumulative CHX release over 3 days after recharge. [42]

2.2.2 Spray dry particles

A more straightforward and simpler approach to produce drug crystals or drug loaded polymeric spheres is spray-drying.[72-74] Particles fabrication by spray-drying is mainly based on the atomization of fluid in a hot drying gas stream, which will transform the liquid droplets

into solid dry powders. The spry-drying process is schematically demonstrated in Figure 2.6. Briefly, it consists of four main steps, firstly, liquid feed is pumped into the drying chamber through an atomizer or nozzle to form atomization; then solvent will evaporate in the hot gas stream and the small droplets will transfer into dry particles; finally, the resulting dry particles will be separated from the dry gas and collected via a cyclone.[72]

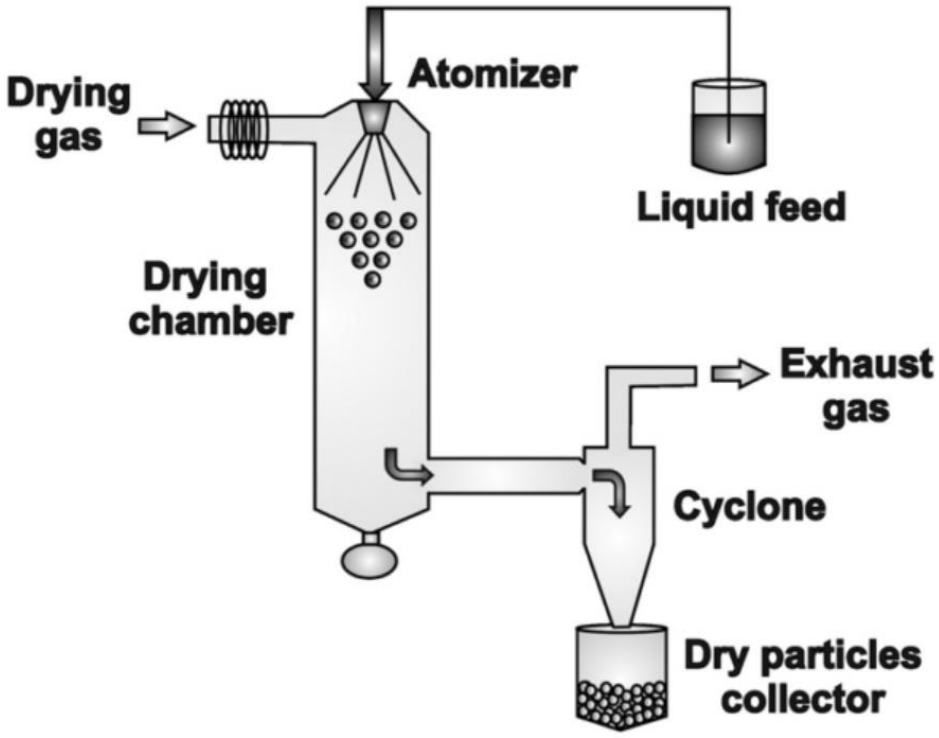

Figure 2.6 Diagram of the equipment and process of conventional spray-drying. [72]

The flow of drying gas can be in the same direction (co-current flow) or in the opposite direction (counter-current flow) as that of liquid atomization. For the co-current flow method, solvent is evaporated quickly at the beginning and the final dried particles are contacted with the coolest air, which is preferred for the heat sensitive materials. While for the counter-current flow method, though is not good for heat sensitive materials, the thermal efficiency is higher.

The fluid feeds which are used for spay-drying vary from solutions, suspension, emulsions, melts, or pastes, and the gas used for drying can also be air or other inert gas.[72, 75]

All the parameters involved in the four steps of spray-drying process will affect the final particles. First of all, the concentration of liquid feeds, viscosity, and the boiling point of solvent will have a profound influence on the particle size and morphology. A high concentration and viscosity of liquid feeds will result in large particles and a fast solvent evaporating rate will lead to porous morphology of particles. Besides, flow rate of liquid feeds and the diameter of nozzle will affect the atomization process, which also have fundamental effect on the dry particles. Other factors, such as temperature of flow gas, type of gas and its flowing direction also matter for particles fabrication.[72, 75]

Spray-drying has many advantages over other methods to produce particles and for drug encapsulation.[76-77] The process of spray-drying is simple, rapid, continuous, and reproducible, therefore, it is easy to scale up, which is attractive for industrial production. In fact, the spray-drying technique is already widely used in pharmaceutical, chemical, materials, cosmetic and food industries.[72]

As for drug encapsulation, spray-drying also has remarkable advantages.[78] A variety of substances can be dried via this method, and since the evaporation of atomized droplets is so fast, the detrimental effects to heat sensitive compounds can be reduced to the minimum. Similar to the ultrasonication approach to produce pure drug particles, spray-drying can also be used, which is simpler and faster, and the yield is higher. Drugs can also be mixed together with polymers, and spray-dried to encapsulate them into polymeric particles. Compared to the emulsion/solvent evaporation method, spray-drying has less limitations on the solubility of drugs and polymers. The fabricated particles are stable and can be re-dispersed into aqueous

solutions without size changing of particles. Besides, the drug encapsulation rate is also higher than the other methods.

The biggest advantage to used spray-drying for encapsulation is that the activity of biological agents can be protected.[76-77] For instance, proteins and genes are sensitive to harsh conditions, which may reduce or lose their activity during the other encapsulation process, such as ultrasonication in the emulsion/solvent evaporation approach. When siRNA was encapsulated into spry-dried PLGA nanoparticles, their activity was not affected by comparing to the free siRNA control in the cell transfection assay.[77] In addition, for antigen delivery, particulation of which can protect the immunity against intracellular pathogens, and thus enhance intracellular immune response. Encapsulation of antigens into polyelectrolytes and mannitol by spray-drying produced porous particles, which promoted enzymatic processing of antigens in cells and thus enhanced cross-presentation *in vitro* (Figure 2.7).[79]

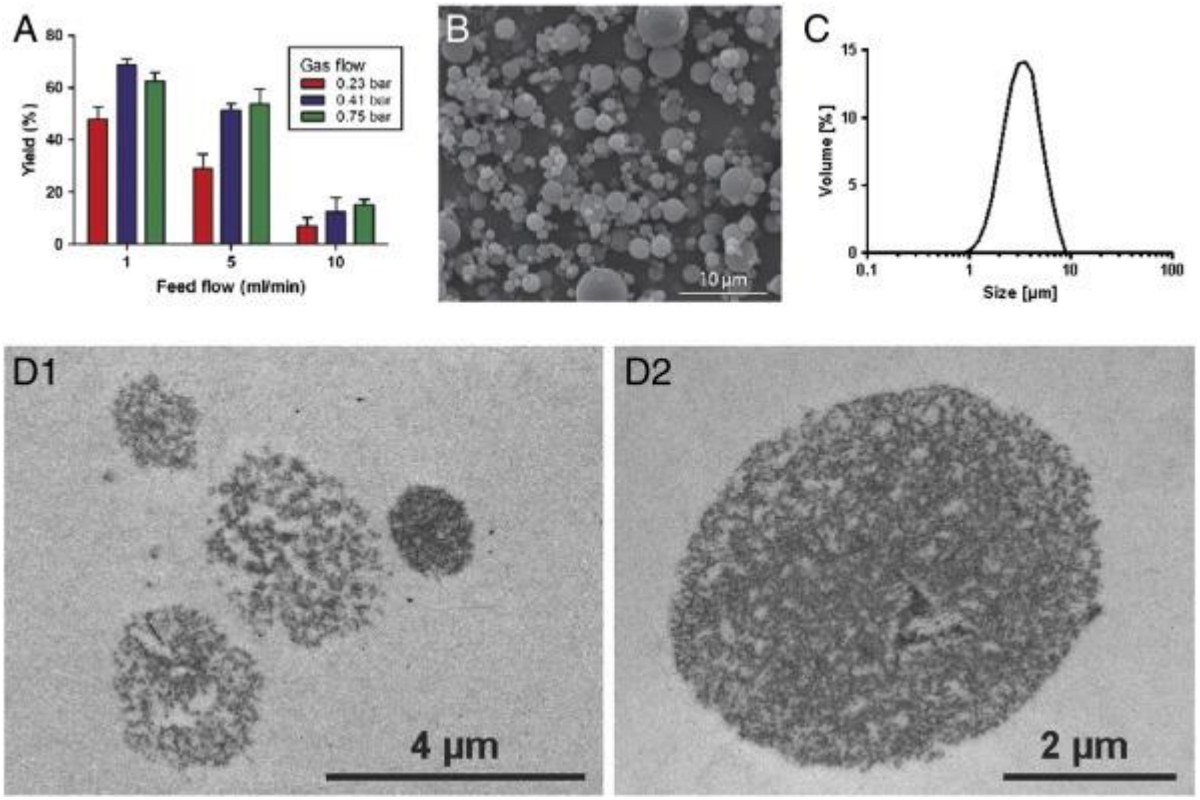

Figure 2.7 Encapsulation of antigens into polyelectrolytes and mannitol by spray-drying. (A) Microparticle recovery expressed as the weight percentage of the microparticles collected in the recipient after the cyclone to the original dry weight of the formulation prior to spray drying. (B) Scanning electron microscopy image of the spray dried microparticles before resuspension in aqueous medium. (C) Size distribution measured by laser diffraction of the microparticles redispersed in water. (B) and (C) were recorded from microparticles produced at optimal formulation and processing conditions. (D) Transmission electron microscopy images of epoxy-embedded and ultramicrotomed porous microparticles obtained after resuspension in aqueous medium. [79]

2.2.3 Electrospun fibers

Micro- and nano-fibers are another category of carriers for drug delivery.[14-15] Different from the microcapsules, polymeric spheres, the fibers are in two dimensions, with continues structure and flexible shapes. They are advantageous for drug delivery because of their small diameter, high specific surface area and surface functionalities.[10, 14] Many polymers, such as PCL, PLGA, and PLA, are fabricated into fibers. PLA is particularly attractive to produce fibers due to its good mechanical strength, excellent biocompatibility and biodegradability and is currently used in biomedical applications.[80]

The fibers are commonly produced by a method named electrospinning, which polymers in solution or melt polymers are fabricated into fibrous structure. Basically, to produce electrospun fibers, three major components are needed, high voltage source, syringe pump and collector (Figure 2.8).[15] Briefly, the polymer solution or melt is loaded into the syringe and pumped with a very low rate (normally a few ml per hour). The liquid drop comes out from the tip of needle will be electrified in the applied high voltage (1- 30kv). The induced charges will distribute over the pendant drop surface evenly and deformed it into a conical shape which is called Taylor cone. When the threshold is reached, electric force will overcome the surface tension of droplets, and charged jets of solution will eject from the tip and reach the collector, during which the solvent will evaporate and fibers are formed.

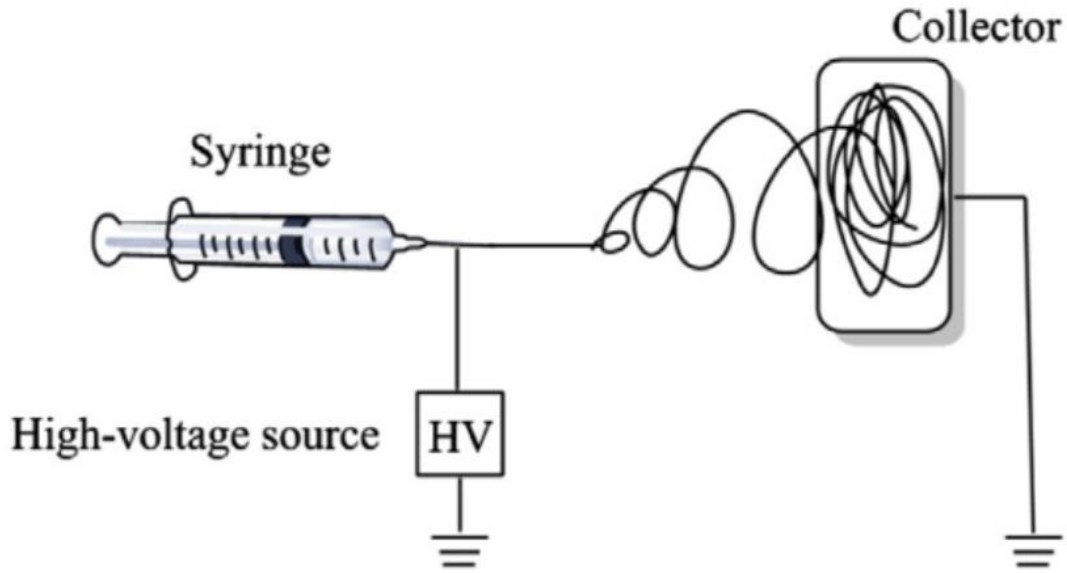

Figure 2.8 Schematic illustration of the basic setup for electrospinning. [15]

The properties of electrospinning polymer solutions play a dominant role in fibers formation, such as concentration, viscosity, conductivity, surface tension and homogeneity.[81] Polymer solutions with a too high concentration will result in a high viscosity, which is not beneficial for fiber formation. It is reported that viscosities range from 1 to 20 P is suitable for fiber fabrication, which viscosity above 20 P will result an instable flow and viscosity below 1 P will lead to formation of droplets.[15] A homogeneous polymer suspension is also key to produce continuous fibers. Other process factors, such as applied voltage, pump speed of solution, humidity and temperature, distance between needle and collector, will also determine the formation of fibers. For example, humidity less than 35% is good for electrospinning and higher than that will result a non-continuous jet. Therefore, it is better to record every parameter during electrospinning to ensure reproducible of fibers.

Electrospinning fibers are especially advantageous to be used as wound dressing materials and for postoperative local therapy.[82-84] There are various approaches to load the fibers with antibacterial agents. The most straightforward method is directly mixing the drug in the

electrospinning solution. The antimicrobial effect of fibers made using this approach is not durable, as the release cannot be controlled.[85-86] Chemically binding of antibacterial agents to fibers can however improve the controllability of release. For instance, cyclodextrins were utilized in fibers to complex with chlorhexidine digluconate,[35] and chitosan fibers were functionalized with thiol groups to covalently bind with gentamicin-loaded liposomes.[10] Other drug carriers, such as mesoporous silica nanoparticles,[87] Ca-alginate microspheres,[88] chitosan nanoparticles[89] and clay nanotubes,[90] can also be combined with electrospinning fibers, which facilitate a more controllable drug release.[91] For instance, the halloysite clay nanotube doped microfibers can extend the drug release to over 20 days, compared to just 4 days for fibers with drugs mixed directly.[90] The drug loading ratio is however always a concern with these methods, as is vital to achieve a high local drug concentration to avoid reapplication of the treatment.

The development of electrospinning also brings new strategies for drug loading and controlled release. Coaxial electrospinning, for example, produce fibers with a core-shell structure, which is beneficial for a programmed drug delivery. Different for the normal electrospinning setup, for coaxial electrospinning, a concentric spinneret with different diameters is used, which are connected to different syringes and pumps. The pumping of different polymer solutions at the same time through the core-shell nozzle will result core-shell fibers. Moreover, this method greatly broad the materials which can be used for electrospinning, as the core materials cannot necessary be able to form fibers by themselves. This coaxial structure of fibers provides different release profiles, as the drug loaded in the core is better isolated from outside thus a sustained release is ensured, but the drug in the sheath layer will has a burst release. This characteristic of fibers is better demonstrated for controlled release with a triaxial fibers (Figure 2.9).[92]

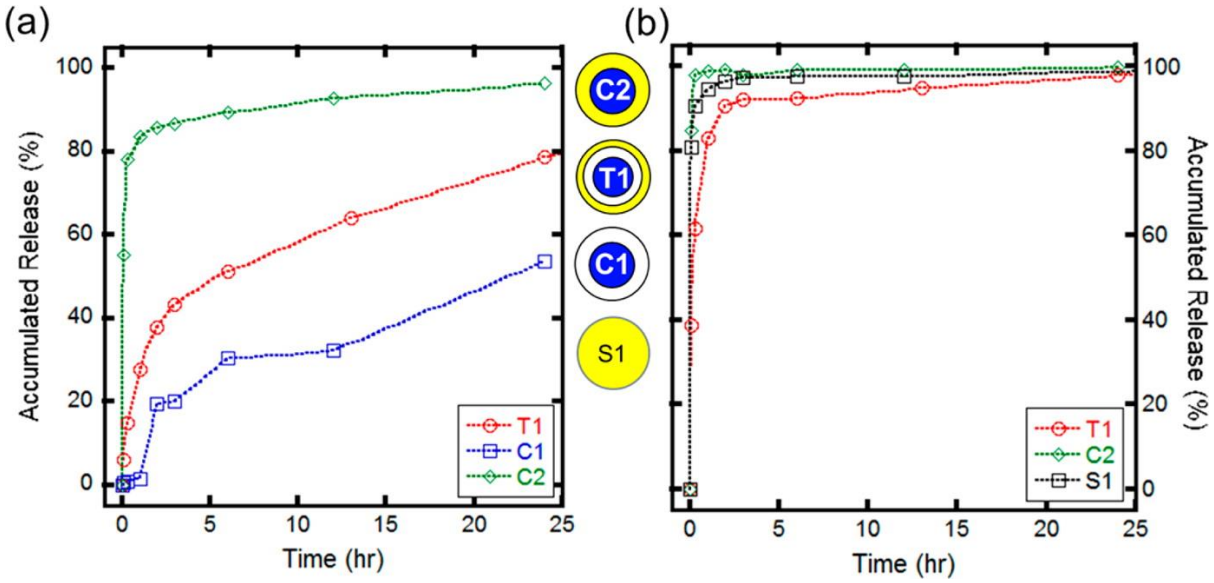

Figure 2.9 Comparison of drug release behaviors from different type of fiber mats. (a) KAB release from PVP core of coaxial/triaxial fiber mats; (b) KAU release from PCL sheath of coaxial/triaxial fiber mats or single fiber mat (S1). Inserts: Cross-sections of fibers are illustrated with indication of dye loading. [92]

2.2.4 Polyelectrolyte microcapsules

2.2.4.1 Polyelectrolytes

Polyelectrolytes refer to a category of polymers which consist of charged or ionizable monomers and the counterpart ions. When the polyelectrolytes are dissolved in aqueous solution, the solution will also have a charge. According to the charge of solutions, either positive or negative, the polyelectrolytes can be classified into polycations and polyanions. Some of the them, which can dissociate completely in solution, are known as strong polyelectrolytes, while others can only partly dissociate are called weak polyelectrolytes. Many of the natural polymers are polyelectrolytes, such as polypeptides and DNA. Therefore, to further understand their dissociating behavior and interaction is important.

When dissolved in water, the polyelectrolyte ion pair will reversibly dissociate as indicated by the following equation:

$$HA \leftrightarrow H^+ + A^- \qquad (2.1)$$

The dissociation behavior can be described by dissociation constant $K\alpha$, which is given as the following equation (brackets represent the concentration of each species):

$$K\alpha = \frac{\left[H^+\right]\left[A^-\right]}{\left[HA\right]} \qquad (2.2)$$

The Henderson-Hasselbalch equation will be showed as below when logarithm is taken for the dissociation equation:

$$pK_\alpha = pH - n\log\frac{\left[\alpha\right]}{\left[1-\alpha\right]} \qquad (2.3)$$

Where pK_α represents the acid dissociation constant, n is the charge density along the polymer chains, α is the protonation degree.

From the equation (2.3), we can see that pH has a dominating influence on the charge density along the polyelectrolyte chains, and thus affects the interaction between polyelectrolytes.

Polyelectrolyte complexes (PEC) will form when oppositely charged polyions are mixed together. The polycations and polyanions will attract and bind to each other via the force of Coulombic and hydrophobic interactions. It is supposed that the entropy will increase when the counter-ions are released into the solutions. Therefore, the change of charges of polyelectrolytes will affect their interaction and PEC formation. For example, the presence of salts in the polyelectrolyte solutions will have a profound influence on the PEC formation, since the structures of polyelectrolytes will change as a function of salt concentration. Basically,

with a small amount of salt, the polyelectrolytes will rearrange, and the reaction will shift to the thermodynamic equilibrium, resulting in a uniform distribution of short chain components. Further increasing the salt in solution will lead to polyelectrolyte molecule chains shrinkage, as the changes of the polymers will be shielded, and at a critical salt concentration, disproportionation will happen, leading to a completely complexed and precipitation. With a higher salt concentration, the PEC will completely dissociate, with free polyelectrolyte chains in solution. Theory about the PEC structure and the conformation is well studied and demonstrated schematically in Figure 2.10.[203]

For strong polyelectrolytes, they are highly aggregated and the addition of small amount of salt will help to reduce the aggregation, however, a higher salt concentration will lead to macroscopic flocculation and precipitation.

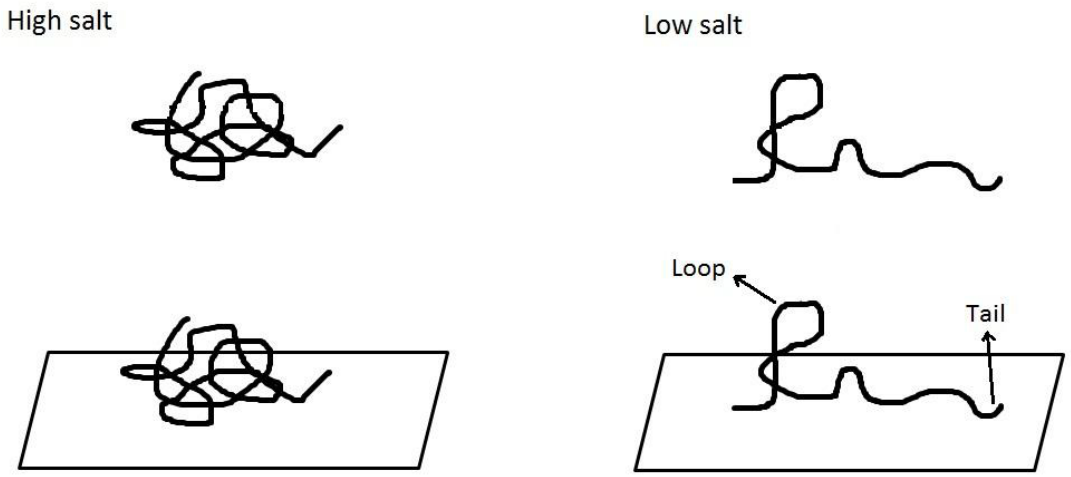

Figure 2.10 Effect of salt concentration on polyelectrolytes in solution

2.2.4.2 Layer-by-layer assembly and microcapsules

Layer-by-layer (LbL) assembly refers to a technique which builds multilayers by alternately absorbing oppositely charged macromolecules on the surface of substrates. Briefly, this process

can be demonstrated schematically in Figure 2.11.[93] Firstly, when a charged surface is placed into an oppositely charged polyelectrolyte solution, and kept immersed for a specific duration, the polyelectrolytes in solution will travel towards the substrate and adhere on the surface, and thus change the surface to an opposite electrical charge. By rinsing the surface with polyelectrolyte-free solvent, excess polyelectrolytes are removed. Then introducing the surface to another oppositely charged polyelectrolyte solution, a second layer will be deposited. By repeating these procedures, multilayers can be built to as many layers as desired.

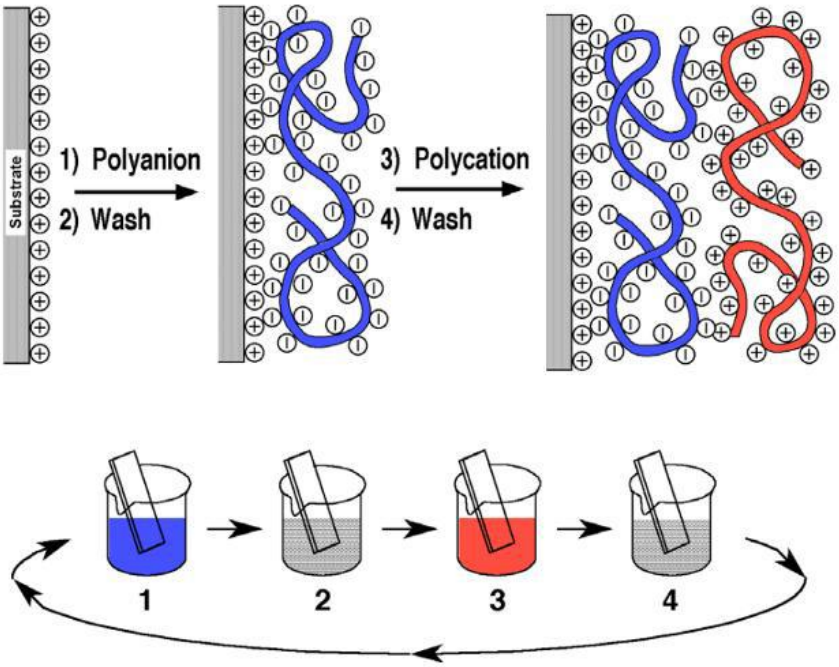

Figure 2.11 Polyelectrolyte multilayer assembly process. [93]

The main driving force for the multilayer assembly is the electrostatic interaction, which the absorption of polyelectrolytes will decrease the free energy of whole system. Besides, non-electrostatic interactions such as hydrogen bonding, van der Waal force and hydrophobic interactions also help to form LbL multilayers. There are various factors which will have an influence on the finally multilayers formed (e.g. thickness, permeability). First of all, since the assembly is dominated by electrostatic interactions, the charge density of polyelectrolytes and

configuration of polymers will have profound effect on the layers. When the charge of surface is high, and the ratio to the charge of polyelectrolytes is 1:1, a flat conformation will be formed. But when the surface charge is not at 1:1 stoichiometric ratio to that of polyelectrolyte, a loose conformation will be deposited. In addition, presence of salts in the polyelectrolyte solutions will also affect the interaction between polymers and charged interfaces. When the salt concentration is low, the polyelectrolytes are better stretched and the layer formed will be thin. However, when the concentration of salts in solutions is high, the polyelectrolytes will shrink and coil, so the absorption in this form will lead to a thicker layer with polymer tails and loops. The type of ions in the solutions will also affect the multilayer assembly. It is reported that small ions have more fundamental influence than the large ions due to the small polarizability.

Basically, quartz crystal microbalance (QCM) and zeta-potential measurement are two common ways to study the kinetics of the multilayer assembly. Theoretically, the QCM measurement is based on the oscillator resonant frequency change during the deposition of each layer. The resonance frequency is related with the oscillating mass, that when the deposited layer numbers increase, the mass will increase, leading to the change of resonance frequency. According to the Sauerbrey equation below:

$$\Delta M = -K\Delta F \qquad (2.4)$$

In which, ΔM refers to the mass change, K is the coefficient, and ΔF is the resonance frequency change. Therefore, there is a linear relationship between change of mass and resonance frequency.

Zeta-potential measurement is another technique to evaluate the surface charge changes during LbL assembly. But because the measurement is based on the movement of particles in the electrical field, it is normally used for investigate deposition on small templates.

LbL process can be carried out on particulate templates and when the templates are removed, hollow polymeric shells are remained, which are well known as microcapsules. The process of producing microcapsules is similar to that of making LbL multilayers, which is shown schematically in Figure 2.12.[94] Briefly, various particles, regardless the size and shape, are employed as colloidal templates, and then first layer of oppositely charged polyelectrolytes is deposited and incubated for a period. Wash steps are also needed to remove the excess non-absorbed polymers by either centrifugation or micro-filtration. Then the second layer of polymers is assembled with the same procedure. Subsequently assembly of polycations and polyanions leads to colloids with multilayers coated. At the end, the colloidal templates are removed and hollow microcapsules are formed.

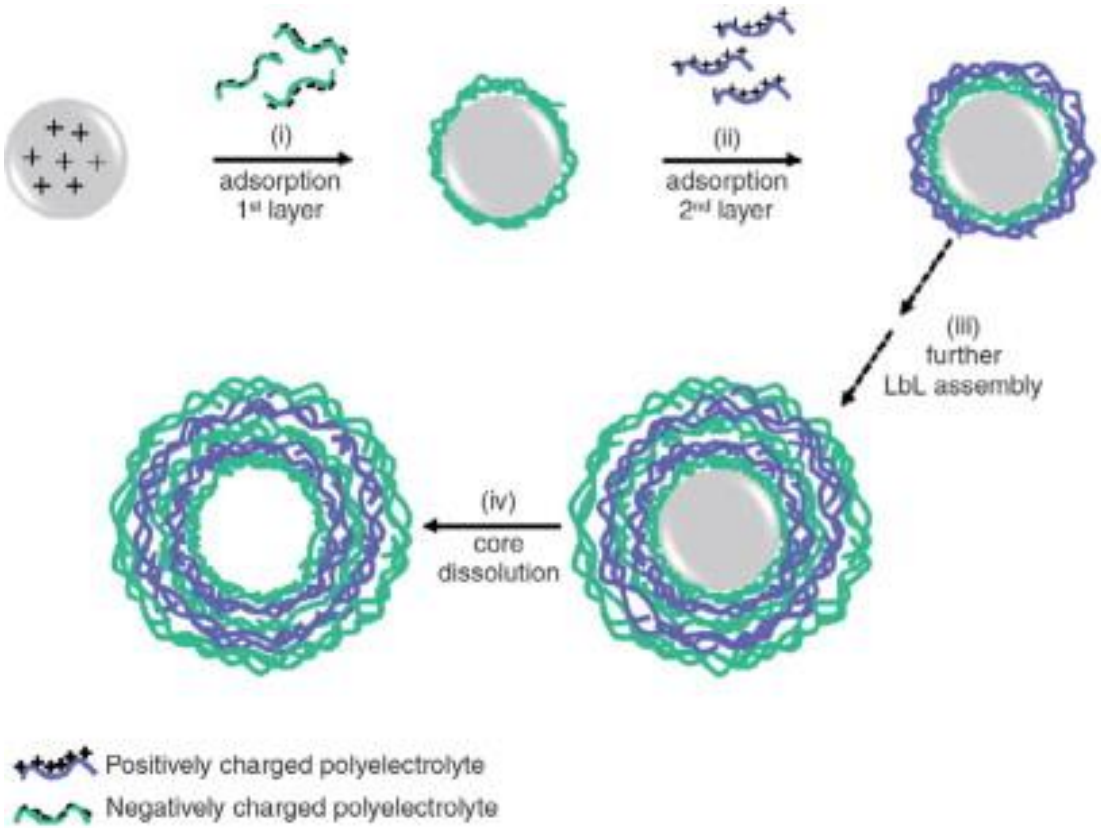

Figure 2.12 LbL assembly to produce microcapsules. [94]

Many particles can be used as templates, including organic, inorganic particles, metal nanoparticles, oil emulsions, microbubbles and even living cells. The most commonly used organic templates are crosslinked melamine formaldehyde (MF) particles. The MF particles are stable at neutral pH and once encapsulated with multilayers, they can be dissolved with 0.1 M HCl or solvents such as N, N-dimethylformamide (DMF) and tetrahydrofurane (THF). The problem with MF templates is that the remained oligomers from dissolution are hard to diffuse out from the multilayer shells, which will tend to damage or rupture the capsules. Also the positively charged MF oligomers can stick to the negatively charged layers, bringing challenges to completely get rid of the cores. Polystyrene particles (PS) are also used as templates for LbL assembly, but the same problems remain as the same as MF templates.

Inorganic particles, on the other hand, are advantageous for using as templates, because they can easily be dissolved and removed from the shells and no large oligomers will be remained in capsules. $CaCO_3$ particles are the most frequently used inorganic templates, as they are easy to produce and dissolve with EDTA or HCl solutions. The calcium ions or CO_2 are easy to get rid of. Moreover, the porous structure of $CaCO_3$ particles can act as excellent reservoirs for cargos, such as large molecular drugs, proteins and DNA. After removing the core, these cargo molecules will be trapped within the cavity of capsules, which provides a good strategy for encapsulation. Silica (SiO_2) particles are another kind of good inorganic templates. They are monodispersed and not porous, and with addition of hydrofluoric acid (HF), they can be quickly dissolved. But attention must be paid to during the silica dissolution as the HF is dangerous to handle. Other inorganic particles, such as cadmium carbonate ($CdCO_3$) and manganese carbonate ($MnCO_3$) are also reported.

Any charged polymers can be used to construct microcapsules, either synthetic polymers or natural biodegradable polymers, peptides, proteins, even DNA. The most commonly used synthetic polyelectrolytes are poly(allylamine hydrochloride) (PAH) and poly(sodium 4-

styrenesulfonate) (PSS). Other biodegradable polymers such as chitosan, poly-L-arginine, dextran sulfate sodium salts, are also widely used for LbL assembly. The main advantage of using biodegradable polymers for LbL is that they can be decomposed inside living cells, and encapsulated cargos can thus be released intracellularly. This is clearly demonstrated by encapsulating a fluorogenic protein, DQ-OVA, into both synthetic and biodegradable capsules, which is self-quenched (red fluorescence) and only when enzymatic cleavage into single dye-labelled peptides, a bright green fluorescence will appear (as shown in Figure 2.13). [95]

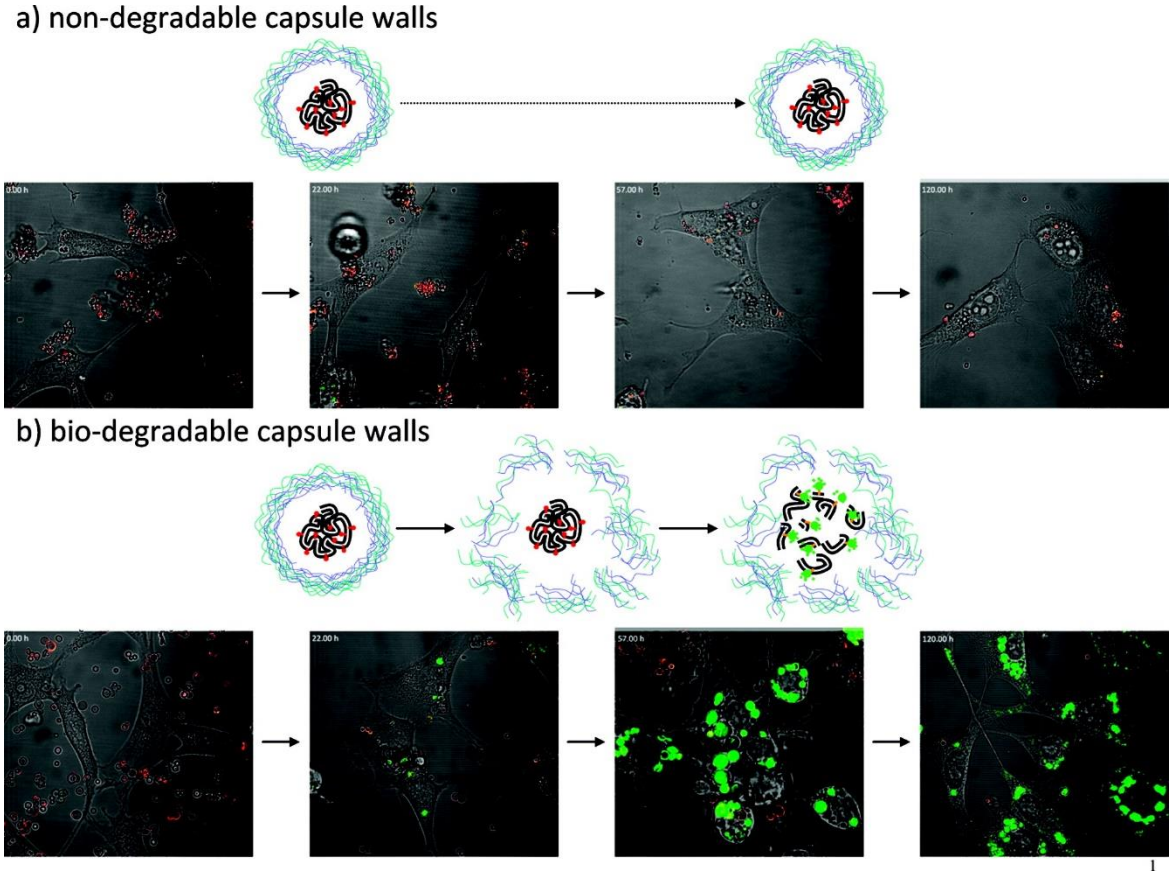

Figure 2.13 Enzymatic cleavage of protein cargo. Embryonic NIH/3T3 fibroblasts were incubated with (a) nondegradable PSS/PAH or (b) degradable DEXS/pARG capsules filled with the fluorogenic protein cargo, DQ-OVA. Images were taken immediately after addition of the capsules (t = 0h) over time up to 120 h with a confocal microscope in different channels, green, red, and transmission. [95]

Metal nanoparticles, such as gold, silver and magnetite nanoparticles, can also be incorporated into the polyelectrolyte shell of microcapsules by electrostatic interaction. The imbedding of nanoparticles into microcapsules facilitates mult-functionalities. For instance, the gold encapsulated capsules have a near infrared absorption, thus a site specific rupture of capsules and cargo release can be achieved by laser irradiation. Microcapsules with magnetite nanoparticles can be used for targeted delivery and alternating magnetic field triggered release, since the nanoparticles are magnetic responsive. Detailed application of triggered release will be discussed in Section 2.3.

2.2.4.3 Drug encapsulation

Large molecular weight drugs, and bioactive molecules can be directly encapsulated into microcapsule, as the polyelectrolyte shells are not permeable to molecules larger than 5 kDa.[96] These large molecular cargos can be co-precipitated with the templates, calcium carbonate for example. The resulting hybrid particles are used commonly for LbL assembly. After that, templates are removed, and the desired substances will be trapped inside the cavity of capsules. This is the simplest method for encapsulation, and the encapsulation rate is always high. This encapsulating method is affected by their solubility, molecular weight, as well as the affinity to the template ($CaCO_3$). Proteins, DNA, and other bioactive molecules are usually encapsulated in this way, as the precipitation inside calcium carbonate can very well preserve their activity during LbL process, and the dissolution with EDTA is also mild. Besides, they can also be encapsulated as a layer of capsules shells via an electrostatic interaction. In previous study by our group, luciferases are encapsulated into to microcapsules at different locations, in the cavity by co-precipitation with $CaCO_3$, in the middle of polyelectrolyte layers, and at the

out most layer of microcapsules. Activities of luciferase at the different locations are proved to be different, that luciferase in the cavity and at the surface of capsules are more active that these within the shells (Figure 2.14). [13, 97]

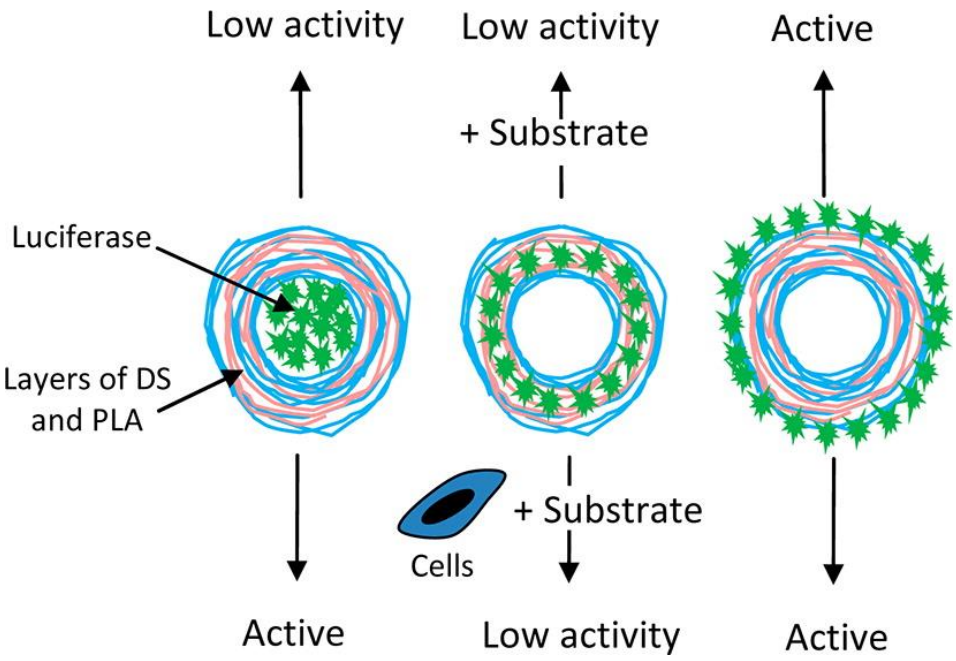

Figure 2.14 Schematically showing the locations of luciferases encapsulated in microcapsules. [13]

Another method to load the microcapsules with desired substances is by diffusing. Briefly, the fabricated hollow microcapsules are incubated with the solutions of molecules of interest, and they will then diffuse into the microcapsules, driven by either electrical interaction or concentration gradient between the bulk solution and the interior of capsules. For example, bovine serum albumin (BSA) was co-precipitated with $CaCO_3$ to produce hybrid particles, and after core dissolving, a charged network remained in the capsules, which can attract the oppositely charged doxorubicin molecules. Moreover, since the charge of BSA can be tuned by adjusting the pH, a pH controlled drug release cab be achieved.[98-99] However, the disadvantage of this method is that the encapsulation efficiency is low (encapsulated amount compared to the high concentration bulk solution added).

Since it is always easy for the small molecular drugs to diffuse out from the microcapsules, many methods are developed to seal the microcapsules after drug loading. Basically, the problem is how to reduce the permeability of polyelectrolyte shells.

Heat treating the microcapsules is the simplest way. It is proved that with an increase in the temperature, the capsules will shrink, which is due to the change of building block polymers from two-dimensional arrangement to a more coiled arrangement. With an elevated temperature, the microcapsules will shrink, resulting a decrease in size and increase in shell thickness, and the permeability is thus reduced (Figure 2.15). [100-101]

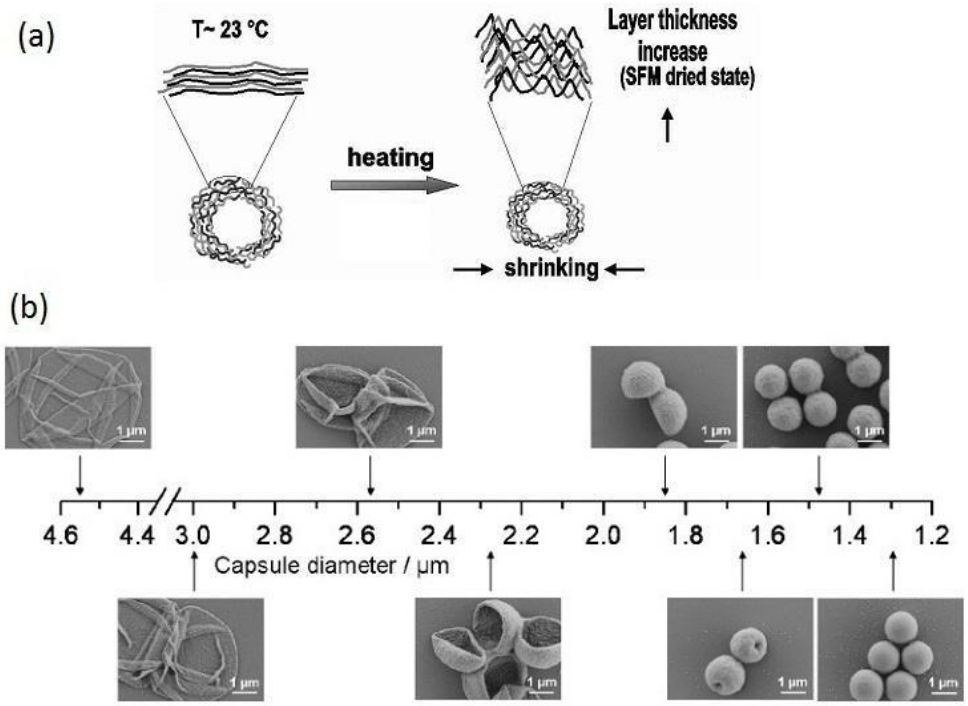

Figure 2.15 Schematic illustration (a) and SEM (b) images of heat shrinkage. (a) Configurational arrangements of the (PSS/PAH)5 capsules before and after heating. The reduction of the capsule diameter is accompanied by an increase of the thickness of the layer. (b) SEM images of (PDADMAC/PSS)4 capsules shrunk to different sizes as a function of diameter after temperature treatment. The first image shows an initial capsule with a diameter of 4.55 μm. [100-101]

Coating the microcapsules with a hydrophobic layer is another method to reduce the permeability and enhance the encapsulation efficiency. Phospholipid, for example, is a good candidate for capsule sealing. The lipids are hydrophobic, and the their absorption on the surface of capsules can effectively reduce the permeability to small hydrophilic molecules. Besides, polypyrrole (PPy) also exhibited outstanding low permeability, due to the π electron delocalization along the polymer chains and their high rigidity. Depositing a PPy layer on microcapsule surface was proved to be efficient to entrap low molecular weight compounds.[102]

Crosslinking the microcapsule building block polymers is also utilized to encapsulate low molecules weight cargos. Chemical crosslinker can be used to bind the related functional groups of polyelectrolytes, or it can also be externally triggered, such as by UV light. Polymers containing a photoactive diazonium groups are normally utilized. In previous study by our group, a novel microcapsule system consisting of diazoresion and Nafion was produced, which upon UV illumination, the diazonium groups and the sulfonate groups reacted and sealed the microcapsules (Figure 2.16). [103]

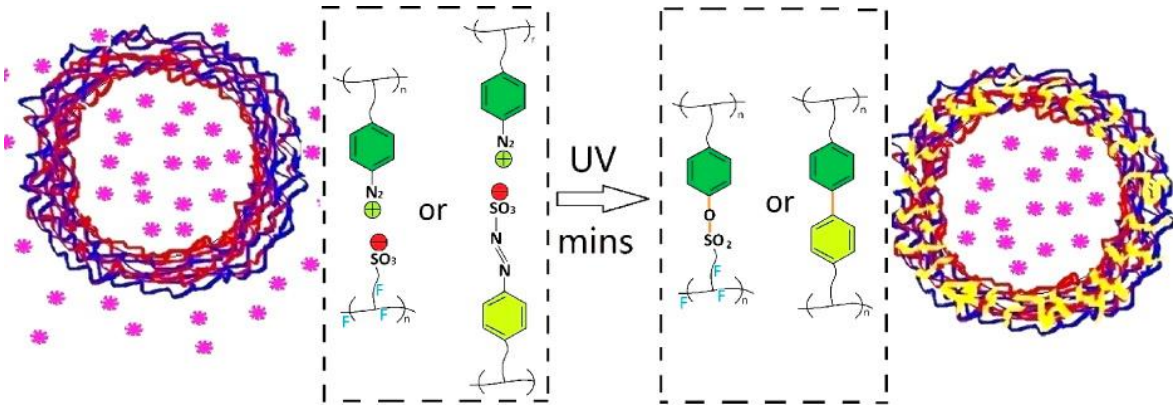

Figure 2.16 UV induced crosslinking of DAR/Nafion capsules and rhodamine B encapsulation.[103]

The low soluble drug crystals, on the other hand, can be directly used as cores for LbL assembly and producing capsules with a high drug loading capability. This approach was first reported to encapsulate fluorescein particles. At normal aqueous solutions, fluorescein crystals are very easy to dissolve, so the LbL encapsulation was carried out at pH 2 hydrochloric acid solution to prevent the preliminary core decomposition. The number of polyelectrolyte layers sufficient to sustain fluorescein release was found to be 8-10, and with increasing layers, the release time was also prolonged.[104] Other water soluble drugs, such as ibuprofen, furosemide, nifedipine, and insulin, are also successfully encapsulated by tuning the LbL assembly conditions carefully.[105] Poorly soluble drug crystals, including paclitaxel, tamoxifen, curcumin, resveratol, are also encapsulated by LbL assembly.[106] However, for those poorly soluble drug crystals, ultrasound is usually applied to ensure a better dispersion of crystal size, and the ultrasonication formation of drug cores is accompanied by simultaneous polyelectrolytes coating. According to the difference of sonication process, it can be classified as top-down and bottom-up approaches. In the top-down approach, the drug powder is added into water and sonicated to break the big crystals into smaller one, and re-aggregation is prevented by absorption of polyelectrolytes. While for the bottom-up approach, drug crystals are completely dissolved in water/organic solvent mixture and ultrasonication with polyelectrolytes at presence will evaporate the organic solvent and precipitate fine drug crystals (Figure 2.17).[107] Therefore, the bottom-up method is more efficient to produce smaller capsules compared to the top-down method. The traditional LbL technique to produce encapsulated drug crystals always need intermediate washings to remove excess polyelectrolytes, which is time and polymer consuming, and dissolution of drug crystals is not avoided. More recently, an optimized method by carrying out the assembly in equilibrium or reduced concentrated polyelectrolyte solutions can solve this problem.[108]

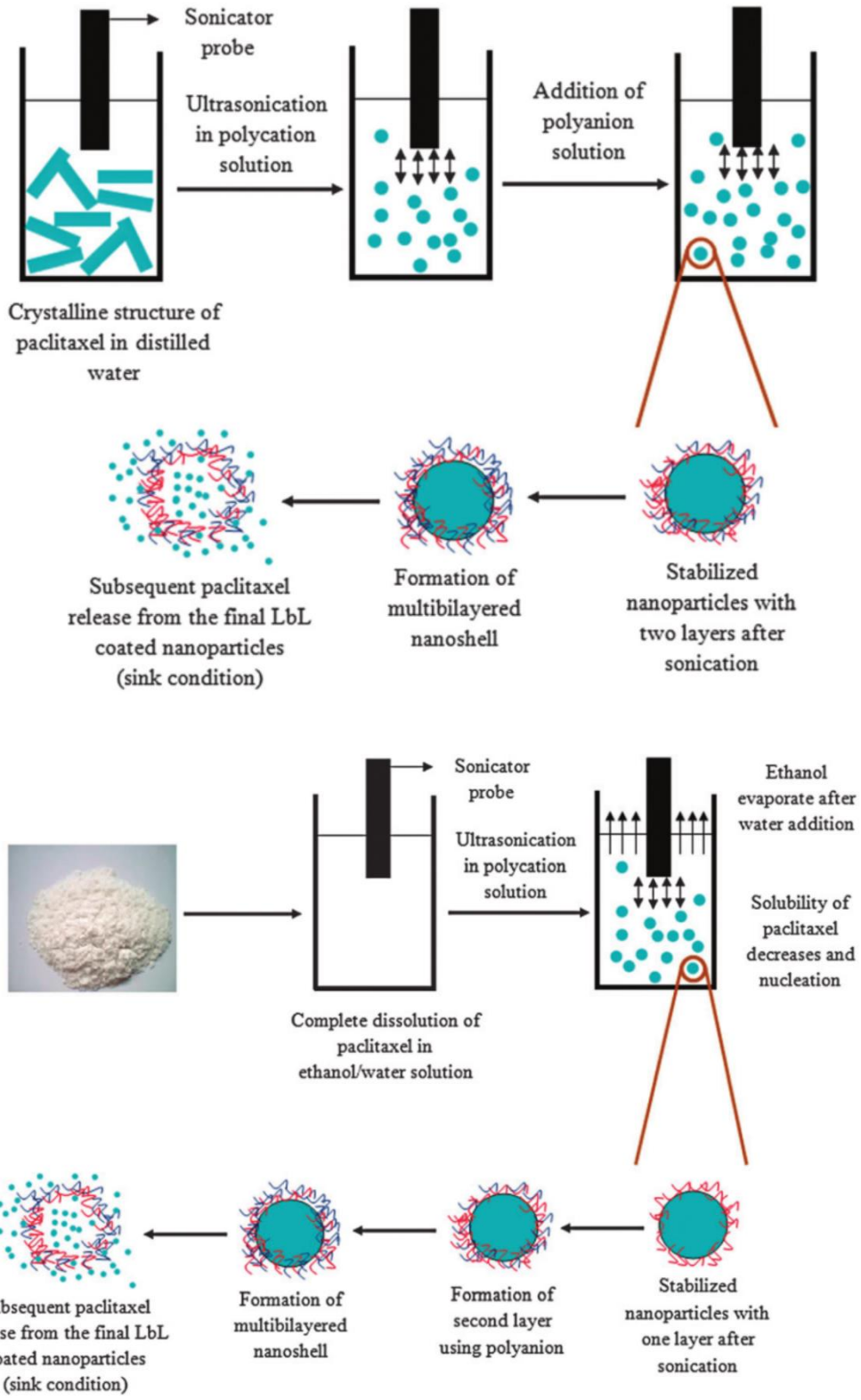

Figure 2.17 Schematic representation of ultrasonication assisted layer-by-layer assembly using the top-down and bottom-up approach. [107]

2.3 Triggered release

Methods to trigger the release are one of the main tasks, since a desired release kinetic is beneficial for not only a safe performance but also an enhanced activity of encapsulated substances.[19, 109] For the delivery of antibacterial agents, it is even more important to have a precise control of the release kinetics. A smart and on demand release will be essential to treat chronic infections and eliminate the bacteria.

There are various methods which can control the release from carriers. Basically, these triggers can be divided into physical, chemical and biological approaches.[110] Here the physical way to induce encapsulated cargo release is presented, including ultrasound, NIR light and alternative magnetic field (AMF).

2.3.1 Ultrasound

Ultrasound is a kind of sound wave with a high frequency (20 kHz and above) which is beyond human's hearing limit. It is usually generated by piezoelectric transducers which can transfer the voltage into mechanical displacement surface, and mediums such as water and gel, then transmit the ultrasonic waves.[111] Ultrasound is widely used in our everyday life, such as detecting object and distance. As a non-invasive and no surgery method, it also has useful applications in medicine, for example, ultrasound imaging, and its ability to be focused at specific site in human body make it attractive for diseases treatment.[112] In dentistry, ultrasound is mainly used for mechanical removal of hard tissues, debris, apical root structure, plaques and biofilms, and more interestingly ultrasound was proved to be beneficial for tooth growth.[113] Ultrasound, with the benefits of improving cell membrane permeability and being focused at targeted tissue, has widely been used for controlled drug delivery.[111, 114] Ultrasound has the potential to control the delivery of antibacterial agents as it was demonstrated in the bone

cements that the synergistic effect of ultrasound and antibiotics had enhanced antimicrobial efficiency.[67, 115] And moreover, a more recent studies have tried to use the high frequency ultrasound to delivery antimicrobial chitosan nanoparticles into dentinal tubule, which may open up new approaches for root canal infection treatment (Figure 2.18).[113, 116]

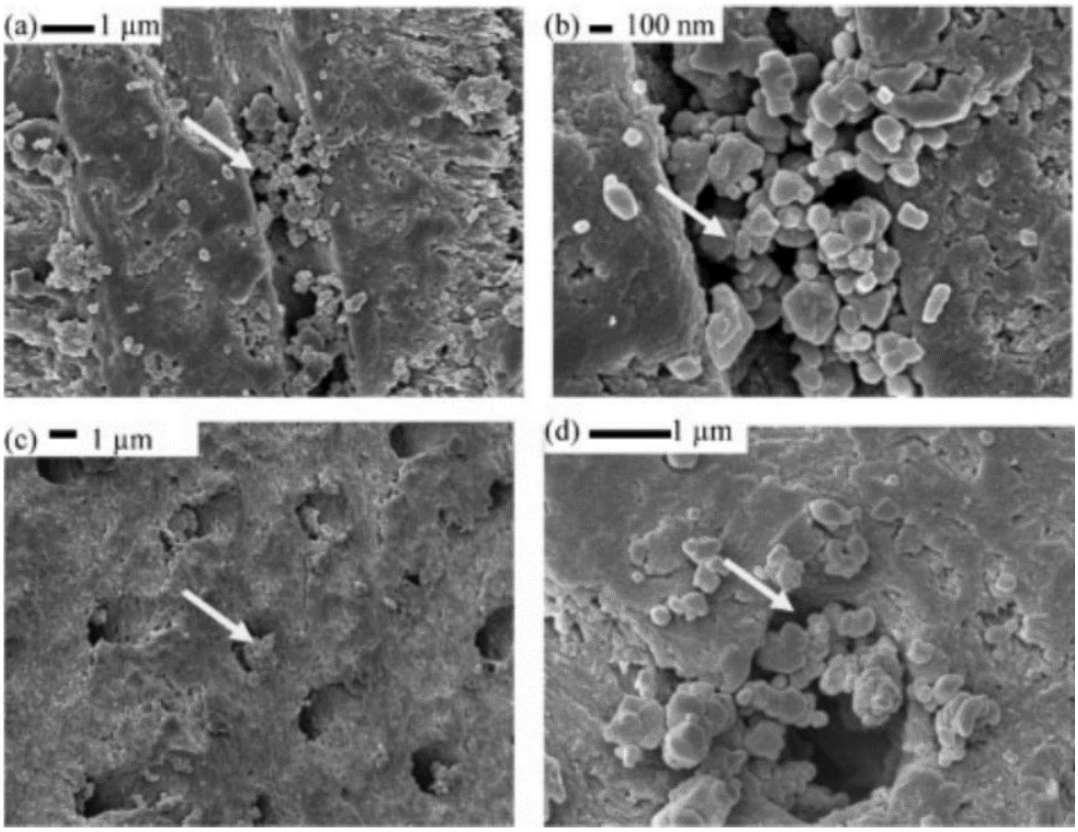

Figure 2.18 Field emission scanning electron micrographs of a sample from the treatment group showing the nanoparticles penetration into the dentinal tubules. Penetration up to 1000mm deep from the opening of the tubules is seen; however, the distribution of the particles is not uniform. (a) The nanoparticles lining inside the tubule (white arrow) and on the side of another tubule. (b) Magnified view of the nanoparticles cluster inside the dentinal tubule. (c) Nanoparticles penetration at the openings of the dentinal tubules. (d) Nanoparticles aggregates penetrating into the tubules. [113]

When drugs are loaded in various carriers, ultrasound can efficiently trigger the release. Basically, ultrasound induced thermal effect can change the phase of polymers which used as carrier composition, the phase transition of which will disrupt their original close and ordered packing, thus increasing permeability for drug release.[117] Another explanation for ultrasound enhanced drug release is the intense acoustic streaming field which accelerate the fluids exchange. For instance, liposome vesicles with sonication will demonstrate transient pores in the membrane, and intra and extra-vesicular substance exchange is promoted.[118] The cavitation generated by sonication, especially at the presence of microbubbles is proved to be very efficient to enhance the drug and gene delivery.[119]

In addition, sometimes the mechanic oscillation resulted from sonication is dominant to release the encapsulated substances. It is reported that the pressure generated to the vesicles is uniform and the pressure gradient is negligible when the vesicles are small compared to the ultrasound wavelength. But when their size is comparable to ultrasound wavelength, the pressure is not uniform and shear force will be generated.[118] On the other hand, by increasing rigidity of carriers, the mechanical effect will be more remarkable. Normally, the LbL assembly microcapsules are quite stable upon ultrasound irradiation, however, by incorporating nanoparticles in the polyelectrolyte shells, ultrasound can easily rupture the microcapsules.[111] More interestingly, recent work by our group revealled that with a layer of SiO_2 deposited on the surface, the microcapsules are highly sensitive to ultrasound, which 6s of exposure to ultrasound will completely destroy the microcapsules (Figure 2.19).[120]

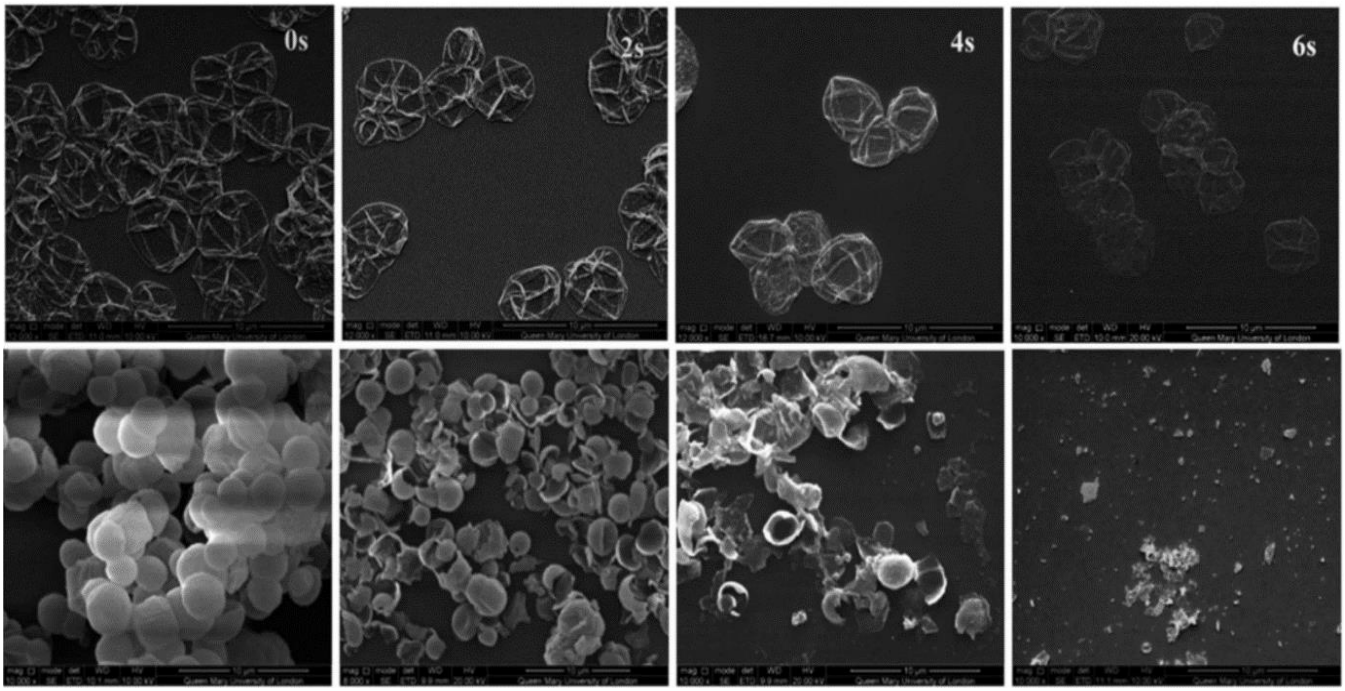

Figure 2.19 Normal and SiO_2 coated PAH/PSS capsules upon ultrasound irradiation. [120]

2.3.2 NIR light based stimuli

Near infrared (NIR) light with the advantage of high tissue penetration ability, is widely used for medicine, such as cancer therapy and controlled drug delivery.[121-122] The NIR light can be focused at specific site and functionalize locally, and due to it photothermal effect, NIR light is used for cancer therapy, which the cancer cells can be burned to death by the absorbed energy from NIR light. For drug delivery, many metal or metal oxide nanoparticles can absorb the energy from the light and generate local heating to trigger the release of delivered cargos. It is due to the surface plasmon resonance effect of these particles. This no-invasive method for therapy and drug delivery is advantageous and extensively studied during the past decades.

2.3.2.1 Gold nanoparticles and nanorods

Gold nanoparticles and nanorods are the most commonly used laser responsive particles. Gold nanoparticles with controlled shape and size are normally synthesized via a seed-mediated method ($HAuCl_4$), in which the nucleation and growth of nanoparticles are separated.[123] By adjusting the synthesis parameters, such as kinds of reduction agents, initial gold salt concentration, temperature, solvent, the size of gold nanoparticles can be ranged from a few nanometers to hundreds of nanometers. To further control the morphology of gold nanoparticles, for example to get gold nanorods, the cetyl-trimethylammonium bromide (CTAB) can be used to navigate the growth of gold particles.[124-125] The gold nanorods are also synthesized via a seed-mediated growth method, which the gold seeds are synthesized first and further grow in an anisotropic CTAB solution. Interestingly, the axial ratios of gold nanorods can be tuned by changing the concentration of reagents, which even rods with 200 nm in length and 100 nm in width can be produced. More recently, by using a mixing competitors of CTAB and cuprous ions to guide the growth of nanorods, single-crystalline gold nanorods with various facets are obtained (Figure 2.20).[126-127]

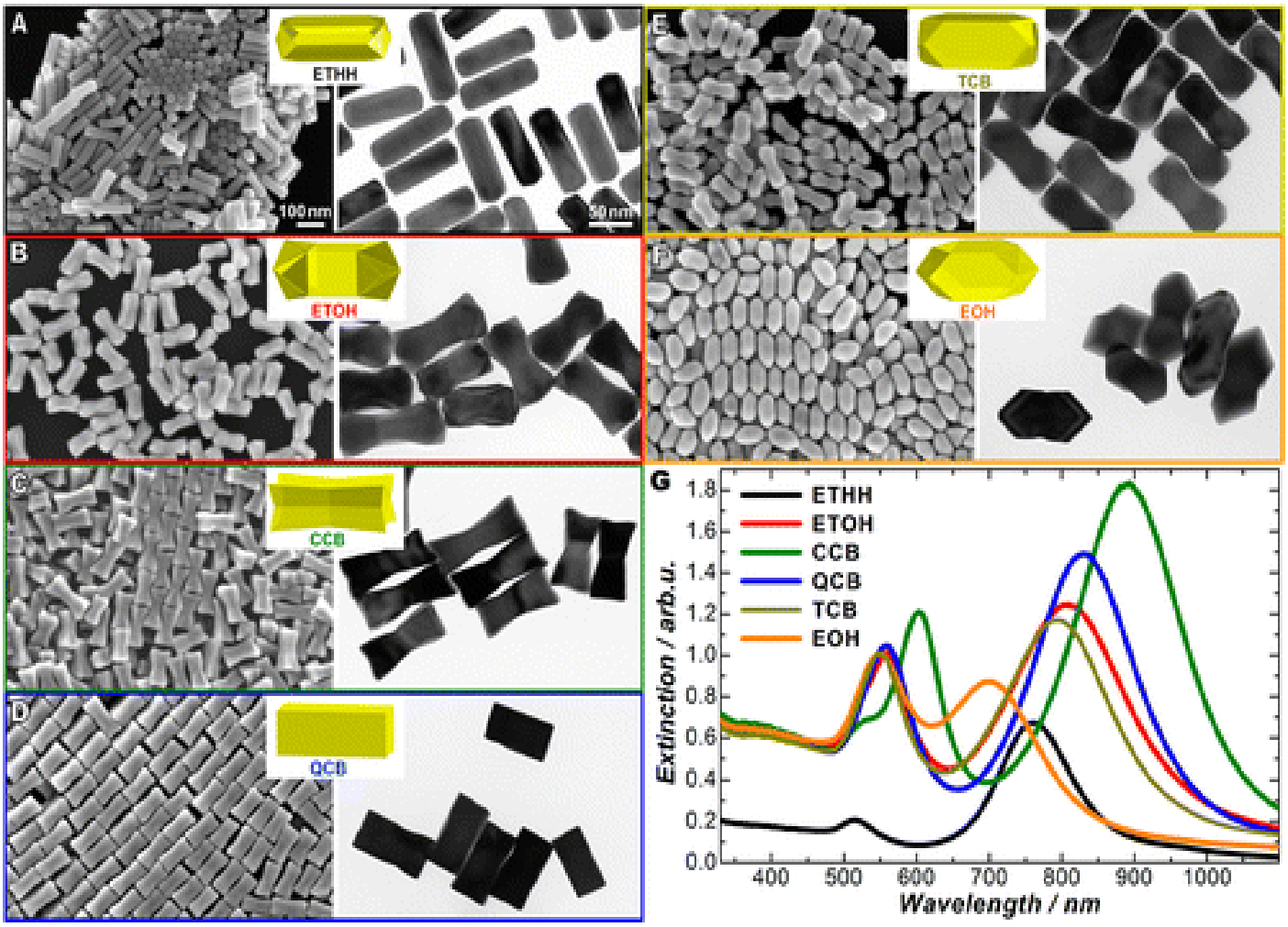

Figure 2.20 SEM and TEM images of Au (A) ETHH, (B) ETOH, (C) CCB, (D) QCB, (E) TCB, and (F) EOH NPs. The SEM images and TEM images are shown in the left and right columns, respectively. The insets show the geometric models of individual NPs. All the SEM and TEM images share the same scale bars in panel A. (G) Extinction spectra of colloidal Au ETHH, ETOH, CCB, QCB, TCB, and EOH NPs. The particle concentration was ~1.0 × 1011 particles mL^{-1} for all the samples. [126]

Basically, due to the surface resonance effect, the gold nanoparticles have absorbance peak ranging from 400 nm to 800 nm, the position of maximum absorption is predominately

determined by the size and shape of nanoparticles. By increasing the diameter of gold nanoparticles, the absorption peak will shift to longer wavelength, which is known as red shift. Gold nanoparticles with an average size of 10 nm show a peak at 520 nm, however, for 109 nm gold nanoparticles, the main resonance band will peak at 574.5 nm and the shape of which will also broaden.[123] The aggregating state of gold nanoparticles will also affect the absorbance band. Take advantage of the surface charge of gold nanoparticles, they can be aggregated by introducing oppositely charged molecules or NaCl solution in the suspension. By forming large clusters, their absorption band can be shifted to the NIR light region due to the plasmon coupling effect between particles, which enables promising biological uses. Moreover, the light absorption efficiency of gold clusters is also proved to be dramatically improved. Coating the gold nanoparticle surface with other components is another way to shift the absorption position of gold nanoparticles.

For gold nanorods, due to their geometry, there are usually two absorption bands at the spectrum, one transverse band around 520 nm which is similar to that of gold nanoparticles, and the other longitudinal band which is determined by the aspect ratio of nanorods. The absorption band of gold nanorods can be tuned from 550 nm to infrared spectral region by simply adapting their length or axial ratio. As the axial ratio increases, their absorption red shift and the oscillation strength is also turned out to be enhanced. Their shapes and facets will also have an influence on the absorption band as indicated in Figure 2.20.

Local heating of gold particles induced by NIR light irradiation is an important property which is used for triggered release. Many studies have been carried out to investigate the mechanisms of heat generation and how it transfers to the surroundings. Basically, the temperature distribution from the gold particles can be given by the following equation[128]:

$$\Delta T(\mathrm{r}) = \frac{V_{NP} Q}{4\pi k_0} \frac{1}{r} (r > R_{NP}) \qquad (2.5)$$

In which, k_0 is the thermal conductivity of surrounding substances, r is the distance to center of the gold particle, and the Q is heat dissipation rate which is depend on the induced electric field inside gold particles.

Gold is highly thermally conductive, so that upon NIR light irradiation, instantaneous and homogeneous heat will generate around the particles within nanoseconds. The temperature around the gold particles drops as a function of increased distance from their surface as indicated by the equation. It is reported that with a 2 mW laser illumination, 80 nm gold nanoparticle can be instantly heated up to 340 °C, and temperature decreases dramatically to 78.9 °C with a distance of 80 nm away from the particle surface (Figure 2.21).[129] So an intimate contact with the gold particles is essential to make the most of heat generated. A good example is encapsulating gold nanoparticles into LbL assembled microcapsule shells, which can rupture the polyelectrolyte shells with laser irradiation.

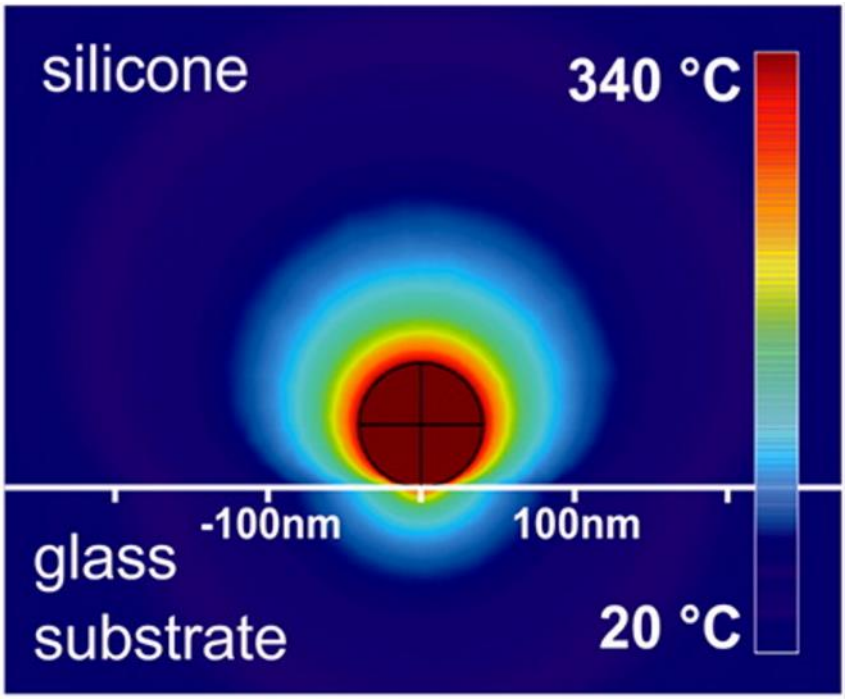

Figure 2.21 Simulation of the heat distribution of an 82 nm gold nanoparticle irradiated with a laser beam at a laser power density of 378 kW/cm^2 (~2 mW). [129]

The thermal effect of gold particles can be enhanced by assemblying them into clusters, as the heat fluxes from each individual particle cumulate. Simply, individual gold particles can be aggregated by mixing with oppositely charged components. The gold clusters showed five times increase in absorption coefficient than the single ones.[130] Also, nanowires assembled by gold nanoparticles in cylindrical complexes were reported, in which gold nanoparticles acted as photonic amplifier.[131]

2.3.2.2 NIR light triggered release

Gold nanoparticles and nanorod based carriers are extensively used for drug delivery and photothermal therapy due to their facile surface modification and intrinsic plasmonic properties.[132-134] Upon near infrared (NIR) light irradiation, the gold particles can efficiently convert the energy into heat, inducing release of loaded cargos. The general approach is to attach drug molecules or therapeutic agents, such as DNA and RNA, to their surface and then selective release can be achieved via photothermal treatment.[135-136] They are also incorporated into carriers such as micelles,[137] liposomes,[138] polyelectrolyte microcapsules,[139] and nanogels[140] to facilitate stimuli responsive drug release. Previously a NIR mediated tumor cell apoptosis was achieved with gold nanorod based carriers *in vivo*.[136] Hollow vesicles consisting of gold nanoparticles and gold nanocages were also reported, which were supposed to be more sensitive to NIR light because of the high gold content.[141-142] Moreover, their hollow structure was also advantageous over the other carriers due to the drug loading capability. The advantage of NIR light induced release is high specific and that drug release pattern can be precisely controlled.[143] A specific and sequential intracellular release of cargo triggered by light irradiation was demonstrated by Carregal-Romero et al., with a 3.8 $mW/\mu m^2$ laser spot and less than 2s exposure.[144] The gold nanoparticles embedded ruptured the microcapsule shells upon laser irradiation, releasing the encapsulated cascade blue labelled dextran intracellularly and one hour after, by irradiating another TRITC-dextran encapsulated capsule in the same cell, sequential cargo release was achieved (Figure 2.22).[144] This observation shows potential for NIR light controlled intracellular biochemical reactions.

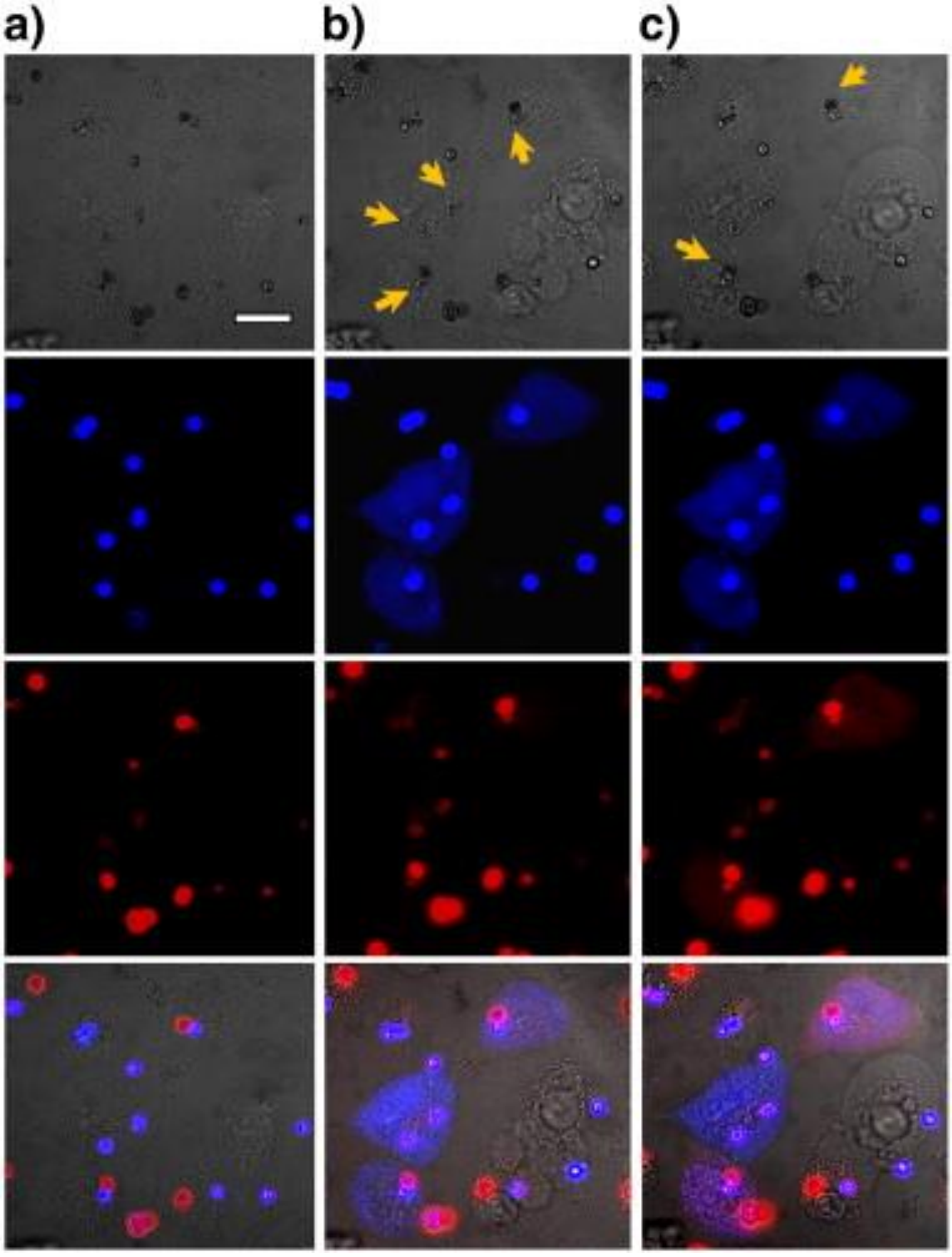

Figure 2.22 Sequential release in A549 cells. (a) before, (b) after the opening of $(PSS/PAH)_2$ Au_{agg} $(PSS/PAH)_2$ capsules loaded with 10 kDa Cascade Blue-dextran, and (c) after the opening of capsules loaded with dextran-Tetramethylrhodamine.[144]

Another approach is to make the most of the photothermal properties of gold nanoparticles and nanorods for drug delivery, by directly constructing a drug on top of the particles. For instance mesoporous silica shells were deposited on the surface of gold particles to produce core-shell nanocomposites.[145-146] Since this was first reported by Liz-Marzan et al., (1996),[147] these gold/silica composites have attracted great attention for usage in controlled drug delivery. This is due to the porous silica shells acting as a good drug container and the gold core serving as an efficient photothermal convertor. The release kinetics of the payload from such composites can be easily tuned by NIR light illumination and with targeted delivery realised via modification of the silica surface.[132, 136] The mechanism of formation of these core/shell structures consists of two stages: hydrolysis to form silica oligomers and mesoporous silica growth on the surface of the gold seeds via Ostwald ripening.[148] Because gold has little affinity for silica, silane coupling agents are usually used as surface primers.[145, 147] Since most of the payload molecules are physically entrapped in silica cavities, gating moieties on the composite particle surface are usually needed to regulate the release behavior.[149]

2.3.3 Magnetic field based stimuli

Efficient delivery of therapeutic agents to the specific target site is of great interest in disease treatment since the capability of concentrating a drug locally can reduce the overall dose and adverse effect of off-targeted molecules to normal cells or tissue.[150-151] The requirement of targeted delivery has motivated people to design various carriers in recent decades. Basically, the idea is how to navigate the drug loaded carriers in a programmed route. Magnetic nanoparticles which can respond to magnetic field, provide a good approach to achieve it. Carriers, such as micelles, liposomes, emulsions and microcapsules, can be functionalized with magnetic nanoparticles and directed to the targeted tissue with a magnetic field.[17-18, 152]

Moreover, the release of loaded cargos can be triggered by an external alternating magnetic field, which is a promising method for remote controllable release.

2.3.3.1 Magnetic particles

Magnetite (Fe_3O_4) nanoparticles and the other forms of iron oxide nanoparticles have been highlighted for targeting drug delivery and other biomedical applications. There are many chemical approaches developed during the past decades to synthesize magnetite nanoparticles with various size and morphology.[153-155] The basic method is well known Massart's co-precipitation method, where the particles were stabilized with citric acid into the aqueous solution.[156] The ratio of Fe^{3+} and Fe^{2+} has to be tuned to 2 to 1 and the reaction has to be carried out in the atmosphere of nitrogen to avoid oxidation. Other methods such as reverse micelle method, sol-gel techniques, hydrothermal or solvothermal reactions are also used to synthesized magnetic nanoparticles. The properties of synthesized magnetic nanoparticles depend not only on their composition, but also their structure, shape, size and size distribution.[157] Normally, without any templates or external forces, the synthesized magnetic nanoparticles have a spherical shape, and the size of which are largely depended on the reaction conditions (e.g. temperature, time). Magnetic nanoparticle with other shapes are also synthesized to enhance their performances. For example, iron oxide nanocubes have been demonstrated with better specific absorption rate (SAR) and magnetic properties. They are synthesized by using dibenzyl ether as the solvent, the decomposition product of which can control the nucleation and size of the nano cubes. By adding different amount of squalene to the reaction mixture, the size of nanocubes can be tuned (Figure 2.23).[158] By using other template, such as polyethylene glycol, magnetite nanoparticles with spherical, cubic, rod-like and dendritic morphologies can be produced, which the concentration of Fe^{3+}, Fe^{2+}, and the molecular weight of polyethylene glycol are key factors.[153] In addition, with the assistance of external magnetic field, magnetite nanoparticles with a rod-like structure can also be

synthesized via a conventional co-precipitation method.[159] More interestingly, magnetic nanoparticles with a hollow structure can also be synthesized via a solvethermal reaction at the presence of urea or other ammonium salts.[160] It is supposed that the urea and ammonium salts would decompose at a high temperature and generate bubbles, which is the key to form the hollow structure.[161]

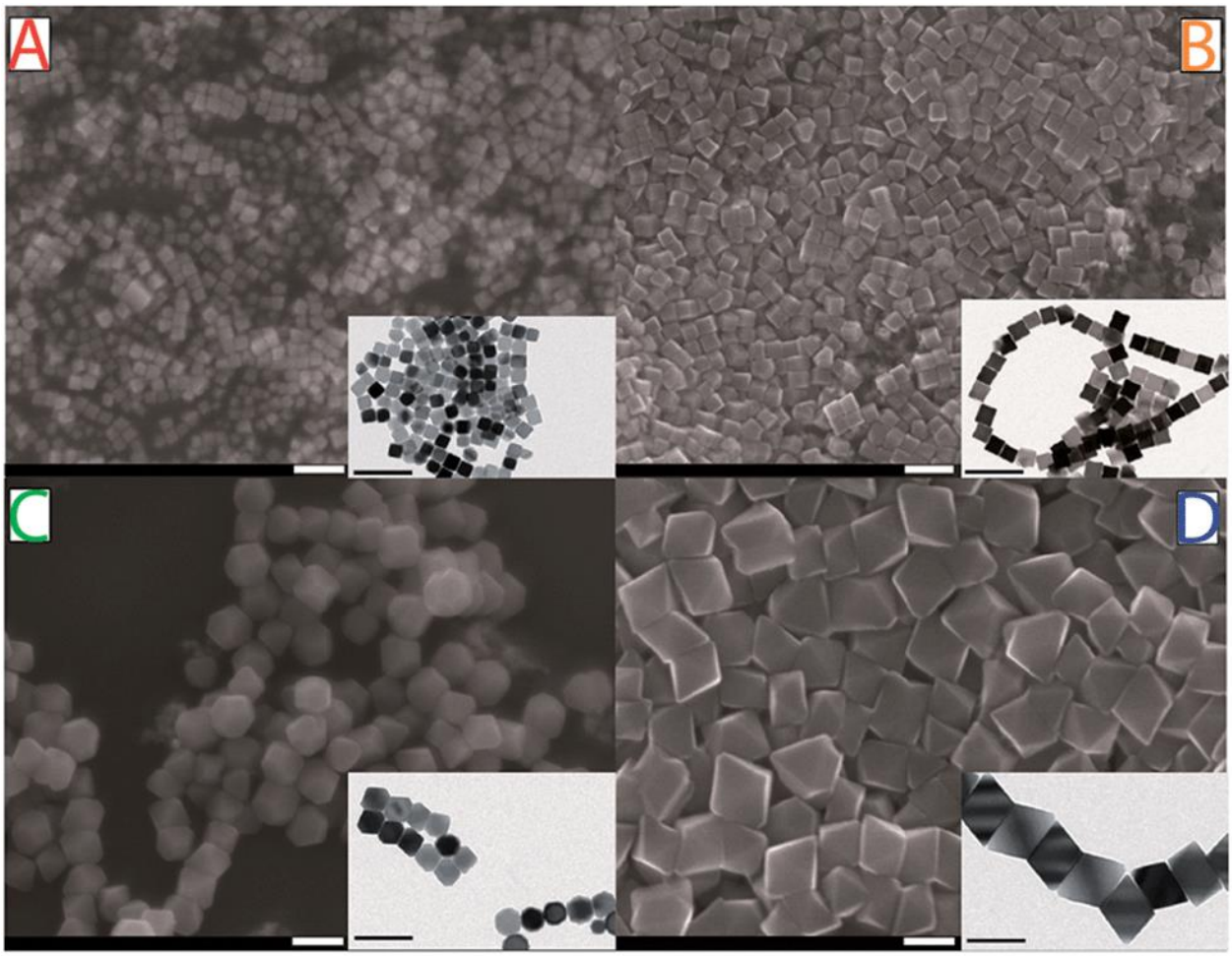

Figure 2.23 Representative scanning and transmission (inset) electron microscopy images of iron oxide nanocubes synthesized by tuning the relative amount of squalane. The total volume of solution was equal to 25mLin all syntheses and the volume ratio between DBE and squalene was: 23: 2 (A), 7: 18 (B), 4: 21 (C) and 3: 22 (D). These conditions lead to nanocrystal sizes equal to 14 ± 2 nm(A), 26± 2 nm(B), 38± 4nm (C) and 100± 7 nm (D). [158]

2.3.3.2 Alternating magnetic field triggered release

Magnetic nanoparticles are a good candidate for targeted delivery of a variety of substances, including small molecular drugs, biomolecules and DNA. Moreover, the magnetic particles, including magnetite, strontium ferrite, manganese ferrite and others, are sensitive to alternating magnetic fields, which can be utilized for triggered release.[23, 162-163] Basically, under an alternating magnetic field, the magnetic nanoparticles will vibrate and generate heat, which will lead to change in permeability or carrier breakdown, and enhance the release.[23] Magnetically mediated hyperthermia was employed to induce cancer cells apoptosis, that upon antitumor chemotherapy agent delivery, the hyperthermia effect can greatly enhanced the performance.[164] For instance, magnetite nanoparticles and thermosensitive poly(N-isopropylacrylamine) (PNIPAM) nanogels were incorporated into the ethyl cellulose membrane, and an external oscillating magnetic field was applied to activate the embedded magnetic nanoparticles, and the heat generated by which leaded to the shrinkage of PNIPAM nanogels and increase of permeability of membrane. The flux of sodium fluorescein through the membrane was successfully tuned by an on-off states of magnetic field (Figure 2.24).[165-166] Magnetic nanoparticles are also incorporated into spherical polymer particles together with drugs via emulsification to enable a AMF induced release.[140, 167] A more straightforward method to utilize the heat generated by magnetic nanoparticles is growing mesoporous silica on surface of the nanoparticles, which can be used as drug reservoirs, and the release of cargo can be further tuned by modifying the surface with some gate moieties.[168-169] Other carriers, such as liposomes[170-171] and micelles,[172-173] are also reported for AMF triggered release.

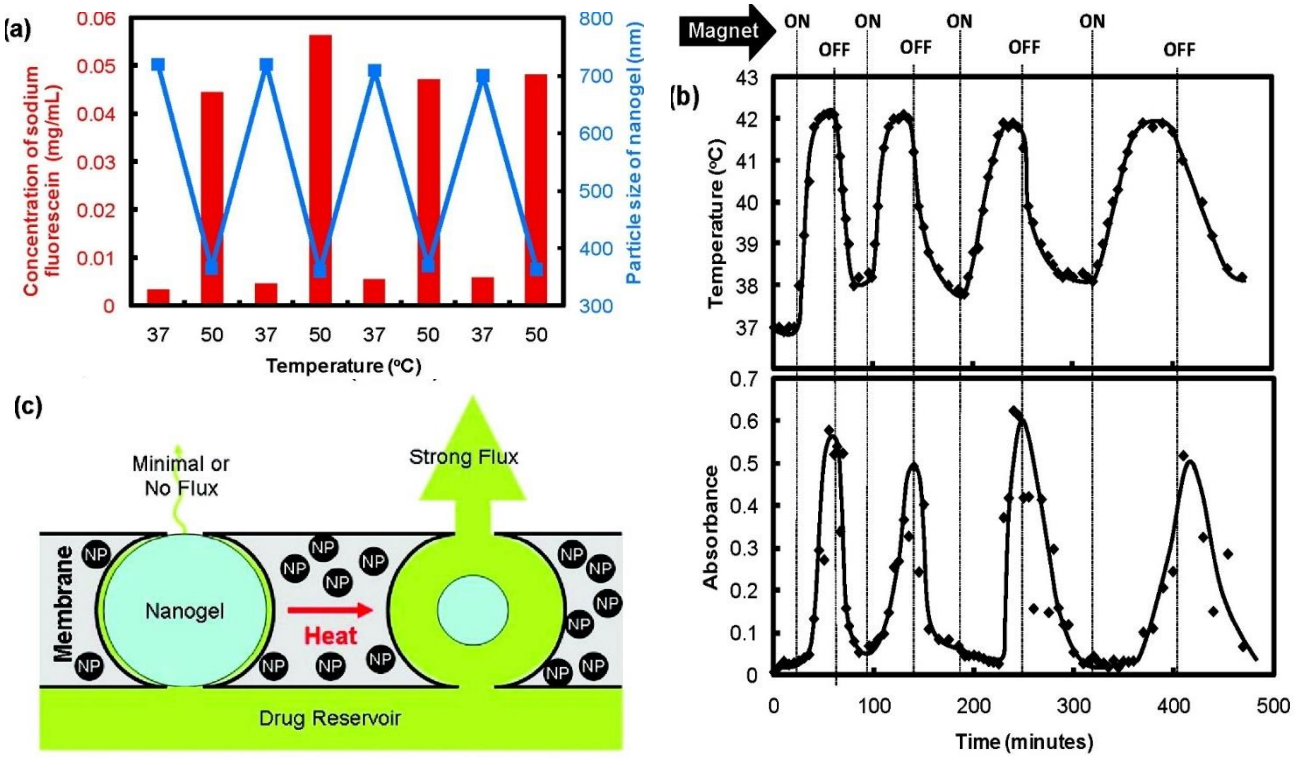

Figure 2.24 Stimulus-responsive membrane triggering in vitro. (a) temperature-triggering, comparison of nanogel particle size in suspension (blue data, right y-axis) and differential flux of sodium fluorescein through the nanogel-loaded membranes (red data, left y-axis) as a function of temperature; (b) magnetic triggering, temperature profile in the sample chamber and differential flux of sodium fluorescein out of membrane-capped devices as a function of time over four successive on/off cycles of the external magnetic field; (c) schema of the proposed mechanism of membrane function.[165]

The magnetic nanoparticles can also be assembled into the LbL microcapsules. In the alternating magnetic field, the magnetic particles will vibrate corresponding to the frequency of AMF and lead to relaxing of polyelectrolytes and loose of capsule walls, which increases the permeability for encapsulated cargos. Sometimes when the frequency and strength of alternating magnetic field is high, the microcapsules can be ruptured. The morphology change of microcapsules was recorded by a previous study (Figure 2.25).[174] Though, it is reported that

the local heating at surface of magnetic particles decays with increasing distance,[175] the non-heating effect produced by low frequency AMF is preferred for delivery bioactive substances (e.g. enzymes, DNA) to normal tissues.[176-177] In fact, it is known that the low frequency AMF (up to 150 Hz) can more efficiently increase the permeability of a polymer matrix.[178]

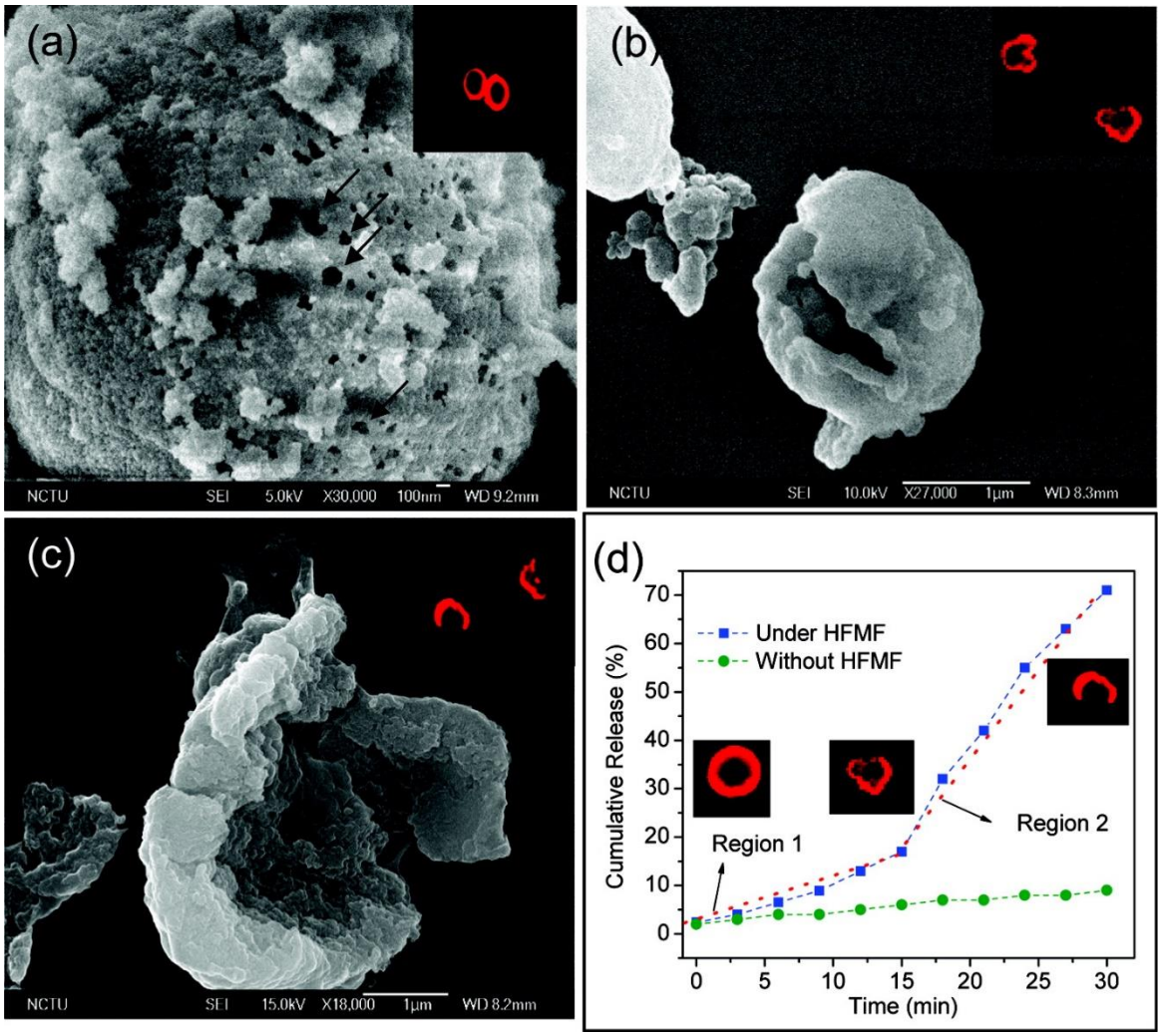

Figure 2.25 SEM and CLSM images of $(Fe_3O_4/PAH)_4$ capsules after HFMF treatment for (a) 10 min, (b) 15 min, and (c) 30 min. After 10-min stimulus, a certain amount of nanocavities 50−100 nm in size appeared on the surface of the microcapsules. Upon further increasing the HFMF stimulus to 30 min, the microcapsules were ruptured to a large extent. (d) The drug release behavior and morphologies of $(Fe_3O_4/PAH)_4$ capsules under continue HFMF.[174]

2.4 Motivation and Aims

The use of antibacterial agents greatly improves the efficiency to treat infections, but there are still many problems concerned with their performance. First of all, they are easy to be excreted from the body or metabolized.[179] Increasing the administration amount of drug can rapidly improve the effective drug concentration in the whole body, but the overuse of which will lead to the resistance of bacteria, which are able to survive exposure to one or several antibacterial agents.[180-181] Resistance of bacteria will bring great challenges to the treatment. For the bacteria in the biofilms, it will be harder to kill them since the structure of biofilm retards antibiotics from penetration and bacteria there are also more resistance.[2, 182] Finally, for the intracellular infections, antibiotics also vary greatly on their penetration into cells, and even if they are internalized inside cells, they could be impaired intracellularly and be inefficacious against the bacteria.[183] Therefore, a delivery system which can maintain a high sufficient concentration of drug as well as their activity, is highly admired.

To overcome these problems, approaches can be taken by either developing new formulation of antibacterial agents or using other carriers to enhance their delivery. For the first method, modification to the current form of drug would improve its performance, as the examples listed previously for chlorhexidine. For the carriers assisted delivery, it is more straightforward because antibacterial agents encapsulated in the carriers or polymer matrixes are well protected and the drug concentration can be maintained at a high level. Since some of the antibacterial agents have trouble to penetrate biological barriers, the polymeric carriers will also facilitate their transport across the critical and specific barriers. A sustained activity of which can ensure an efficient activity against bacteria locally.

For these reasons, the motivation of the thesis is to develop new formulation of antibacterial agents, which can not only have a sustain activity against bacteria but also demonstrate external

stimuli responsive properties. Rare studies were reported for controlled antibacterial agent delivery and external triggered release. In fact, the lack of controllable release of antibacterial drug is always the main reason leads to secondary infections. For the less water soluble chlorhexidine, it is easy to precipitate it with various of salts, but to get homogeneous chlorhexidine particles is a challenge. So parameters such as type of salts, concentration, temperature, needed to be investigated. The benefit to produce drug crystals with uniform size and morphology is that they can be easily encapsulated or incorporated into other polymeric systems. Besides, the size of drug crystals also has a fundamental effect on its release kinetics. Functionalization the drug delivery system with other triggers responsive components is a way to facilitate smart release. If these components could be directly incorporated into drug crystals, it may be easier to manipulate the release kinetics. So precipitation was explored to produce chlorhexidine particles, and incorporation of which into various polymer systems to investigate the sustained activity. The possibility of external triggered release (ultrasound, NIR light, magnetic field) was investigated.

For doxycycline, with a very good solubility, the encapsulation could be achieved with LbL microcapsules and coating with hydrophobic lipid layer could help to reduce the release. From the point of view of targeted delivery, magnetic nanoparticles could be assembled in microcapsule shells and even have a AMF triggered release. But most of the reported AMF triggered release system were based on high frequency magnetic field, which was not preferred to be applied to normal cells or tissues as the hyperthermia effect. Therefore, it was decided to deliver doxycycline with microcapsules, and use a low frequency AMF to trigger its release intracellularly. By engineering the cells with a tetracycline based gene regulation system, the intracellular doxycycline activity could be effectively monitored.

The ultimate goal of the thesis was to explore the possibility to deliver antibacterial agents (chlorhexidine and doxycycline) with various polymer based systems to achieve a sustained

activity, and to further facilitate an external triggers responsive release by functionalizing the systems with gold or magnetic nanoparticles. Hopefully, the developed antibacterial formulations could help to solve the current problems concerned with antibacterial agent delivery and enhance the its performance against bacterial infections.

3. Materials, Methods and Instruments

3.1 Materials

Chlorhexidine diacetate (C6143, Lot: 19H0417), Doxycycline Hydrochloride, Rhodamine B (RhB, 283924, lot: 063K3407), Fluorescein isothiocyanate isomer I (FITC, Lot: 020M5305), Rhodamine B Isothiocyanate dye (RBITC, 283924), camphorquinone, Calcium Chloride (C8106, Lot: SLBF7416V), Boric Acid (B6768, Lot: 119K0067), NH4OH (Sigma, 320145), citric acid (Sigma, 27490, Lot: 23405C03), Ethylenediaminetetraacetic Acid disodium salt (EDTA), Sodium Carbonate and all other salts were purchased from Sigma-Aldrich.

$FeCl_3$ (Fluka, 44944, Lot:30607125) and 0.86g $FeCl_2$ (Fluka, 44939, Lot:24606139), Agar (Fisher BioReagents) and LB Broth, Miller (Fisher BioReagents) were used for antimicrobial studies.

Poly(allylamine hydrochloride) (PAH, 56 kDa, 283223, Lot: MKBJ4274V), Poly(sodium 4-styrenesulfonate) (PSS, 70 kDa, 243051, Lot: BCBF6120V), Dextran sulphate sodium salt (DS, 100 kDa), FITC-Dextran (70 kDa), Poly-L-arginine hydrochloride (Parg, 15-70 kDa), 1,2-Dipalmitoyl-sn-glycero-3-phosphocholine (DPPC),L-α-Phosphatidylcholine (lecithin, from egg yolk), hydroxyethyl methacrylate (HEMA), dimethylamino ethyl methacrylate were purchased from sigma-aldrich.

Poly (lactic acid) (PLA, 2002D) was from Nature works.

2-dipalmitoyl-sn-glycero-3-phosphoethanolamine-N-(lissaminerhodamine B sulfonyl) (ammonium salt) was purchased from Avanti Polar-lipids.

urethane dimethacrylate (UDMA) (Esschem, UK, Lot: 591-22), 0.08% of N, N-dimethyl-P-toluidine (Acros Organics)

Agar (BP1423, Lot 127054), Tryptone (BPE9726, Lot 21012), Yeast Extract (BCE800, Lot4381720) and Sodium chloride (S3160, Lot 1333838) were bought from Fisher BioReagents.

Phosphate buffered Saline (PBS, Lot RNBD7772), DMEM (41966, Lot 1513243) Thiazolyl Blue Tetrazolium Bromide (MTT, M5655, Lot 052K5328), Cell Lysis Reagent (CelLytic™ M), Protease Inhibitor Cocktail, were all purchased from Sigma-Aldrich.

Foetal calf serum, penicillin and trypsin were purchased from Lonza Biologics Inc (Newington, NH, United States).

All the reagents were used directly as received without further purification. All the solutions were prepared with H_2O from hree stage Millipore Milli-Q 185 water purification system (Millipore, USA) with a resistivity higher than 18.2 Ω·cm.

3.2 Methods

3.2.1 Nanoparticles/Nanorods synthesis

3.2.1.1 Fe_3O_4 nanoparticles synthesis

Fe_3O_4 nanoparticles were synthesized by mixing 2.35g $FeCl_3$ and 0.86g $FeCl_2$ in 40 ml H_2O in a three-neck flask, which was placed in an oil bath and heated up to 80 ℃ in an argon atmosphere. The mixture was next stirred, whilst 5 ml NH_4OH was added slowly with a syringe. The reaction was maintained at 80 ℃ for 30 mins and then 2ml of 0.5 g/ml citric acid was added. The temperature was next raised to 95 ℃ and held for 90 mins. The magnetic nanoparticles were dialysed against H_2O in a 14 kDa cut-off membrane for one week. The Fe_3O_4 nanoparticles were then characterized with TEM and zeta measurement.

3.2.1.2 Gold nanorods synthesis

Gold nanorods were synthesized according to a reported seed mediated growth protocol. Briefly, the seed solution was prepared by mixing 10 mL of 0.1 M CATB and 0.25 mL of 10 mM of $HAuCl_4$. While stirring, 0.6 mL of ice-cold 0.01 M $NaBH_4$ was added. The mixture was kept at 25 ºC. Then 40 mL of 0.1 M CTAB, 0.32 mL of 10 mM $AgNO_3$, 10 mL of 10 mM $HAuCl_4$ and 95 mL of deionized water were mixed to produce the growth solution. 0.5 mL of 0.1 M ascorbic acid was added to the growth solution. 50 µl of the seed solution was finally added to the growth solution at 27 ºC and the reaction was kept constant at this temperature for 6 hours.

3.2.2 Chlorhexidine particles preparation

Chlorhexidine particles were fabricated by precipitation of chlorhexidine diacetate with $CaCl_2$. The chlorhexidine diacetate concentration was fixed at 15mg/ml. $CaCl_2$ solutions with various concentrations from 2M, 1M, 0.5M, 0.33M, 0.25M to 0.125M, were mixed with the chlorhexidine diacetate solution at 1:1 by volume at room temperature. The mixtures were shaken for 1 min, and then centrifuged at 2000 rpm for 1 min (Eppendorf centrifuge 5417C, Germany). The precipitates were washed three times with corresponding concentrated $CaCl_2$ solutions to reduce the dissolution of chlorhexidine compounds. The resulting chlorhexidine compounds were characterized using scanning electron microscopy (SEM, FEI inspect-F, USA) and the freeze-dried powder was analyzed using Fourier Transform Infrared Spectroscopy (FTIR-Bruker, USA).

To evaluate the influence of temperature on spherical chlorhexidine particle formation, 15 mg/ml chlorhexidine diacetate and 0.33 M $CaCl_2$ solutions were kept in an ice bath and the temperature of the solutions was monitored. At 1, 5, 10, 15, 20 and 25 ℃, specifically, the

solutions were mixed and centrifuged as previous and the precipitations were washed with corresponding $CaCl_2$ solutions (three times) and then characterized using SEM. The particle size of spherical chlorhexidine compounds prepared at different temperatures was analyzed using a particle size analyzer (Nano Measurer, version 1.2).

Labelled spherical chlorhexidine particle was prepared using the same procedure, but before mixing the chlorhexidine diacetate solution with $CaCl_2$ solution, Rhodamine B was added to the chlorhexidine diacetate solution. The produced particles were centrifuged, washed and freeze dried as described previously. Particles were characterized using confocal microscopy (Leica TS confocal scanning system, Germany).

To functionalize the chlorhexidine spheres with gold, the gold nanorod suspension was pre-mixed with 0.8 mL of 0.33 M $CaCl_2$, and then the mixture was introduced to 0.8 mL of 15 mg/mL chlorhexidine diacetate solution. Specifically, a series of gold suspensions, 5, 10, 50, 100, 200, and 400 µl (0.45 mg/mL), were premixed with $CaCl_2$ solution to determine the influence of nano particles on chlorhexidine growth. All the procedures were the same as previous described and the gold nanorod functionalized chlorhexidine spheres were also freeze dried. The number of particles produced from all the mixtures was counted using a hemocytometer. Both Field emission and back scattered SEM were used to characterize the synthesized particles, and the size of the gold-chlorhexidine composites were measured using a Nano Measure (version 1.2). The gold nanorod functionalized chlorhexidine spheres were also characterized using Thermo-gravimetric analysis (TGA, Q50, USA) at 10°C/min under a nitrogen atmosphere and over a temperature range of 100-1000 °C.

Similar here, to functionalize the chlorhexidine spheres with Fe_3O_4 nanoparticles, 200ul of Fe_3O_4 nanoparticles suspension was premixed with 1 ml of 0.33M CaCl2 (C8106, Lot: SLBF7416V). Then the mixture was introduced to 1 ml of 15 mg/ml chlorhexidine diacetate

solution (C6143, Lot: 19H0417). The mixtures were shaken for 1 min, and then centrifuged at 2000 rpm for 1 min (Eppendorf centrifuge 5417C, Germany). To reduce the dissolution of the particles, the precipitates were washed three times with 0.33M $CaCl_2$ solutions. All the supernatants were collected for UV-vis measurement. The resulting chlorhexidine spheres were characterized using a scanning electron microscope (SEM, FEI inspect-F, USA) with voltage of 10 kV, working distance of 10 mm and spot of 3.5. The presence of Fe in the spheres was confirmed by EDX analysis. The chlorhexidine spheres were freeze dried (ScanVac Cool Safe Freeze Drying, Denmark) at -107 ^{o}C, 0.009 mBar for 1 day and proportion of chlorhexidine in the powders was calculated. In addition, the freezing dried chlorhexidine spheres were analyzed by Thermo-gravimetric analysis (TGA Q50) at 10°C/min under nitrogen atmosphere, over a temperature range of 50-800°C.

Growth of chlorhexidine spheres was also tuned and separated into two stages. The first stage involved the slow growth of small chlorhexidine crystals at low temperature and second the fast growth of chlorhexidine shells on top of the initial primary crystals. To visualize the two stages, chlorhexidine diacetate solutions were mixed with FITC and RhB accordingly. To produce small chlorhexidine primary crystals, both the chlorhexidine diacetate (15mg/ml) and $CaCl_2$ solutions (0.33 M) were kept in an ice bath for one hour. The mixing of these solutions as described in section 2.3 resulted in immediate precipitation of small chlorhexidine crystals. These pre-produced chlorhexidine crystals at 5, 50, 100, 200 and 400 µl (1.63×10^7 crystallites/mL) were separately added to 0.33 M room temperature $CaCl_2$, and 15 mg/ml chlorhexidine diacetate solutions. After 1 minute, the mixtures were washed with $CaCl_2$ and characterized using confocal microscopy. The size effect induced by the chlorhexidine primary crystals was determined by analyzing the size distribution of produced chlorhexidine spheres using Nano Measure (version 1.2).

3.2.3 LbL assembly to produce microcapsules

3.2.3.1 Polymers labelling

To visualize the microcapsules with confocal microscopy or fluorescence microscopy, the polymers (PAH, Parg) used for LbL encapsulation were labelled with dyes (RBITC or FITC).

Briefly, 100 mg polymers (PAH or Parg) were dissolved in 50 ml 0.1 M borate buffer. The pH of the borate buffer was adjusted to 8.5 with NaOH. After that, the dye solutions (RBITC or FITC) with a concentration of 1 mg/ml in ethanol were added dropwise into the polymer solutions under vigorous magnetic stirring, and kept stirring for one day. Then, to remove the unbound dyes, the mixtures were transferred into 25 kDa cut-off dialysis membrane and dialysed against deionized H_2O for 1 week. The water was changed frequently every day. The resulting labelled polymers were then kept in dark at 4 ℃ for further study.

3.2.3.2 Hollow microcapsules and doxycycline encapsulation

The LbL self-assembly technique was used to produce microcapsules, and the commonly used $CaCO_3$ sacrificial templates were employed. The multilayers assembly on $CaCO_3$ cores were described in detail in previous studies. But here, subsequent loading of doxycycline into capsules, DS was co-precipitated within $CaCO_3$ according to the method for encapsulation of large molecules[13]. DS (20 mg/ml) was added to 0.33 M $CaCl_2$ solution and was then immediately mixed with 0.33 M Na_2CO_3 by vigorous stirring for 20 seconds and then incubated for a further 10 seconds. The hybrid $CaCO_3$ particles were washed three times with deionized H_2O, and were immediately used for microcapsule assembly. PAH and PSS were used for synthetic shells, and Parg and DS as biodegradable ones. Due to the DS trapped in the templates, the cores were initially negatively charged so PAH or Parg was assembled as the first layer.

All the polymer solutions were prepared at 2 mg/ml with NaCl (0.2 M), and after absorbing each layer, microcapsules were triple washed with deionized H_2O. For fluorescent visualization, the second positive layer was replaced with TRITC-PAH or TRITC-Parg. Six layers were deposited for all the capsules before dissolving the templates with 0.2 M EDTA solution.

DS trapped in the hollow cavity of microcapsules was used as attraction for doxycycline molecules. This method has been used for encapsulating soluble low molecular weight drugs,[98] which are loaded via electrostatic interaction or as a shell component. Herein, doxycycline molecules penetrate the shells and react with DS and form a complex within the microcapsule. Microcapsules were counted with a haemocytometer and the concentration adjusted to 6×10^7 capsules per ml before mixing with 1 ml of doxycycline solution (10 mg/ml) and shaking for 8 hours. At the end of this incubation maximum encapsulation was achieved by placing the mixture at 60℃ for 10 min to shrink the capsules according to a previously reported procedure.[184] Then the capsules were washed three times with deionized water and supernatants were collected to determine amount of loaded doxycycline. Besides, to determine encapsulated doxycycline amount per gram of microcapsules, equal quantity of microcapsules (both empty capsules and doxycycline loaded ones) were freezing dried (ScanVac Cool Safe Freeze Drying, Denmark) at -107 ℃, 0.009 mBar for 2 days. Then each sample was weighed (CP2-P microbalance, Sartorius AG Gottingen, Germany) and encapsulated doxycycline weight was calculated.

Phospholipids, DPPC or lecithin, were coated as outmost layers on microcapsules to further reduce the permeability and thereby reduce the doxycycline leakage. DPPC (for synthetic capsules) and lecithin (for biodegradable capsules) were dissolved in chloroform at 0.5 mg/ml and were then evaporated using a rota vap at 42℃, after which a thin layer of phospholipids was formed.[146, 185] Liposomes were then constructed by adding water (final lipid concentration of 1mg/ml) to the lipid film and sonicating for 1 hour at 60℃. The formed lipid vesicles were

added to the doxycycline loaded capsules and shaken for 20 min. Then the mixture was washed 3 times with deionized water to remove excessive lipid, and supernatants were also collected for doxycycline concentration measurement. To visualize the lipid coating, Rhodamine B labelled lipid (0.2 mg/ml) was mixed with the DPPC or lecithin. Permeability of microcapsules was tested with FITC under the confocal microscope.

To evaluate the influence of AMF on permeability of microcapsules, FITC labelled dextran (70 kDa), which cannot penetrate the polyelectrolyte shells, were used model molecules. Firstly, 200 µl microcapsule suspensions (1×10^8 capsules) were added into cuvettes and then placed on top of electron magnet. The microcapsule suspensions were kept still in the AMF for duration of 30, 60, 90, and 120 min. Then the microcapsules were mixed with FITC labelled dextran solution and characterized with confocal microscopy. Since the microcapsules were labelled with TRITC, block of FITC-dextran outside capsules shells would lead to dark shadow inside the microcapsule, while penetration of which would display green fluorescence. Therefore, the ratio of microcapsules which were permeable to FITC-dextran was statistically analyzed as a function of exposure duration to AMF.

200 µl microcapsule suspensions (1×10^8 capsules each) were added into cuvettes. As control, microcapsule suspensions were keep still in the cuvette, while for the AMF treated group, cuvettes were placed directly on top of the electromagnet. At each time point (from 10 min to 270 min), the microcapsules in cuvette were precipitated by a magnet and half of the supernatants were collected for evaluation of the doxycycline released and equal volume of fresh H_2O was replaced. Also, one group of microcapsules were exposed to AMF from the 120 min. All the supernatants for each group at each time point were measured by UV-Vis spectrometer at 274 nm according to an established calibration. The cumulative release profile of doxycycline from microcapsules was plotted.

3.2.3.3 Solid chlorhexidine microcapsules

Spherical chlorhexidine particles (15 mg/ml chlorhexidine diacetate and 0.33 M $CaCl_2$) were used for LbL self-assembly. PAH (2 mg/ml, with 0.33 M $CaCl_2$) was added to the spherical chlorhexidine particles as the first layer and the mixture was shaken (Vortex-Genie 2, Germany) for 10 min. Then the mixture was centrifuged (Eppendorf centrifuge 5417C, Germany) at 2000 rpm and washed with 0.33 M $CaCl_2$ solution (3 times) to remove the excess PAH. The second PSS layer (2 mg/ml, with 0.33 M $CaCl_2$) was deposited using the same procedure. After assembling 7 layers, the encapsulated chlorhexidine particles with the structure Chlorhexidine/$(PAH/PSS)_3$/PAH was produced. To prevent dissolution, all the assembly and wash steps were carried out in a solution of 0.33 M $CaCl_2$. The supernatant during each layer assembly and after washing was collected for UV measurement to determine chlorhexidine loss during the LbL process. To monitor the assembly process, SEM images were taken for the spherical chlorhexidine compounds after the assembly of each subsequent layer. FIB SEM (Quanta 3D, FEI, E.U./U.S.A.) was also used to characterize the cross-section of the chlorhexidine capsule and the shell thickness was measured. The fifth layer of PAH was labelled with FITC for fluorescence imaging of the encapsulated chlorhexidine particles.

3.2.4 Spray drying

Spray-drying solutions were prepared by mixing freezing dried chlorhexidine particles with PLA solutions (1 wt.% and 3 wt.% PLA in mixing solvent of chloroform and acetone). The mixtures were then sprayed (Sprühflaschen), and the atomized product was collected with foil. The dried powder was characterized with SEM and confocal.

3.2.5 Electrospinning of PLA fibers

PLA fibers were fabricated by electrospinning at room temperature, with a working distance of 15 cm, pumping rate of 1 ml/h, and a voltage of 18 kV. PLA was dissolved in a mixed solvent of chloroform and acetone (3:1 by volume) at 7 %. All the chlorhexidine particles were added at 0.5, 1 and 5 % (wt/wt) to the PLA and mixed using a Rotomix (ESPE RotoMix, USA). PLA fibers were collected on foil and characterized using SEM and their mean (SD) diameter was analysed using Nano Measure software (version 1.2). Confocal microscopy and FTIR (Bruker, Billerica, MA) were also used to confirm the presence of chlorhexidine.

3.2.6 Preparation of chlorhexidine UDMA- HEMA resin discs

UDMA-HEMA resin was prepared by mixing 64% urethane dimethacrylate (UDMA) (Esschem, UK, Lot: 591-22), 36% hydroxyethyl methacrylate (HEMA) (Aldrich, UK), 0.08% of N, N-dimethyl-P-toluidine (Acros Organics) and 0.05% dimethylamino ethyl methacrylate (Aldrich, UK). The mixture was stirred at 800 rpm for 15 min (VWR Stirrer, USA). Finally, camphorquinone (Aldrich, UK) was added at the proportion of 0.1%. The mixture was stirred for another 15 min, and then the viscous liquid resin was prepared.

Freezing dried spherical chlorhexidine particles were weighed and incorporated within the resin at 5% by weight. To evenly mix the resin with the chlorhexidine spheres, the mixture was placed in an Eppendorf tube and then mixed for 15 s in a Rotomix mixer (120V/60Hz, 2850 rotations/min) (ESPE RotoMix, USA). A separate set of sample containing chlorhexidine diacetate powder was also incorporated in the prepared resin in the same way, with loading rates of 5%. The resin mixture was then placed into a Teflon mold (10 mm in diameter ×2 mm thick) and cured through a Mylar film with a curing light (Bluedent LED pen, Bulgaria) (430-

490nm, 600 mW/sq.cm) for 30 s on both sides. Then the discs were next weighed on a microbalance (Salter Ander-180A weighing scale, UK), and chlorhexidine amount in each disc was calculated.

For the visualization of chlorhexidine spheres distribution in the resin composites, the spheres were labelled by rhodamine B. Spherical chlorhexidine particle were fabricated as described above, however before mixing chlorhexidine diacetate solution with $CaCl_2$ solution, minimum amount of rhodamine B was added to the chlorhexidine diacetate solution. The produced particles were centrifuged and washed in the same way, and freezing dried. The labelled spherical chlorhexidine particles were mixed within UDMA-HEMA resin at 5 wt. % and filled into Mylar film mold (L 10 mm, W 10 mm, H 1mm), and cured to produce a very thin film. The spherical chlorhexidine incorporated resin film was characterized by confocal microscope (Leica TS confocal scanning system, Germany).

UDMA-HEMA resin was prepared by mixing 50% urethane dimethacrylate (UDMA) (Esschem, UK, Lot: 591-22), 50% hydroxyethyl methacrylate (HEMA) (Aldrich, UK), 0.08% of N, N-dimethyl-P-toluidine (Acros Organics) and 0.05% dimethylamino ethyl methacrylate (Aldrich, UK). The mixture was stirred at 800 rpm for 15 min (VWR Stirrer, USA). Finally, camphorquinone (Aldrich, UK) was added at the proportion of 0.1%. The mixture was stirred for another 15 min, and then the viscous liquid resin was prepared. Freezing dried spherical Fe3O4-chlorhexidine spheres were weighed and incorporated within the resin at 5 wt.%. Incorporation of the chlorhexidine particles within the resin was carried out by rotating the mixture for 15 s in a Rotomix (120V/60Hz, 2850 rotations/min) (ESPE RotoMix, USA). For the control group, the resin mixture was then placed into a Teflon mold (10 mm in diameter ×1 mm thick) and cured through a Mylar film with a curing light (Bluedent LED pen, Bulgaria) (430-490nm, 600 mW/sq.cm) for 60 s. For the magnetic field treated groups, the mixed resin was placed into Teflon mold which was placed on a MACS magnet. The resin mixtures were

kept still on the magnet for 5 min or 10 min, and then cured for 60 s. The discs were next weighed on a microbalance (Salter Ander-180A weighing scale, UK), and chlorhexidine amount in each disc was calculated.

The resin discs containing Fe3O4-chlorhexidine spheres were emerged in liquid nitrogen and broke to analyse the distribution of spheres. Briefly, cross-section SEM images were taken continuously from one side of resin disc to the other side, and then all the images were put together to make a panoramic image. The panoramic image was divided into 21 frames with length along the x-axis, and each frame presented one single point on the graph. Number of chlorhexidine spheres in each of the frames was counted and summed to get the total number, and a point was draw accordingly on the graph. Fe3O4-chlorhexidine spheres distribution in the resin discs was plotted in percentage as a function of distance to the magnet. Distribution for control resin disc, with 5 min and 10 min magnetic field treatment discs was displayed.

3.2.7 Drug release measurement assays

The content of chlorhexidine in the compound (0.33M $CaCl_2$ and 15 mg/ml chlorhexidine diacetate), was determined by using a UV-Vis spectrometer (Lambda 35, Perkin Elmer, USA). Initially, a series of chlorhexidine diacetate solutions with standard concentrations of 0.25, 0.5, 1, 2, 3, 4, 5, 10, 20, 40 ppm were prepared, and the absorption was measured. The absorption peak at 254 nm and the reference concentration had a linear relationship, and the calibration curve was established. All concentrations were determined by measuring the absorption of the supernatant and calculated accordingly. The number of chlorhexidine spheres in solution was counted using a hemocytometer (Neubauer Chamber, UK) and chlorhexidine content in each particle was also calculated.

Spherical chlorhexidine particles or encapsulated chlorhexidine particles (n=3) were stored in 2 ml H_2O or PBS and agitated (Vortex Genie 2). At specified time points from 5 to 420 mins, the samples were centrifuged and supernatants were collected for UV-Vis absorption measurement (Lambda 35, Perkin Elmer, USA). After each time interval, the removed supernatant was replaced with fresh deionized water or PBS. In addition, the release test for chlorhexidine capsules was also carried out in 15.6, 31.3, 62.5, 125, 250 mM NaCl and Na_2HPO_4 solutions to determine the influence of Cl^- or PO_4^{3-}on release kinetics. The accumulative release was calculated according to the calibration curve. Following the release experiment the chlorhexidine capsules were characterized using confocal microscopy and SEM.

Release of doxycycline from microcapsules was determined by a fluorescence spectrum assay. The doxycycline concentration in solution was calculated according to the emission fluorescence intensity at 536 nm. Typically, a series of standard doxycycline solutions (40, 30, 20, 15, 10, 5, 4, 3, 2, 1, 0.5, 0.25, 0.1, 0.05 ug/ml) were prepared and emission intensity at 536 nm was measured (excited at 350nm). The calibration curve was used to determine amount of doxycycline in supernatants collected during the assembly process and therefore enable calculation of the amount of doxycycline retained in each capsule.

In the release experiments, $12\times10^7$of synthetic or biodegradable capsules were prepared in a 1 ml suspension in either deionized water, PBS or NaCl (0.15M). The suspensions were shaken on a vortex for specified intervals, after which it was centrifuged and the supernatant was collected for evaluation of the doxycycline released. The removed supernatant was replaced with 1 ml of fresh solution and the incubation continued. To demonstrate 100% release, doxycycline loaded microcapsules were mixed with 2 M NaOH.[186] At this pH, microcapsules were disassembled and doxycycline concentration in the solution was measured.

3.2.8 Cell studies

3.2.8.1 Myoblasts and fibroblasts

The lentiviral vectors used to engineer mouse C2C12 myoblast cells (ATCC® CRL-1772™) were pLOX-TwGFP which encodes EGFP from the P_{tet} and pUCL-MIK which encodes the rtTA-2SM2 transactivator[187] and the *tet*RKRAB repressor[188] from a bicistrontic cassette[189] under the control of the constitutive SFFV promoter.[190] Lentivirus was prepared as previously described[191] then C2C12 cells were multiply infected with pUCL-MIK before multiple infection with pLOX-TwGFP. The resulting cell population was then stimulated with doxycycline hydrochloride (1 µg/ml) and after 24 hours the cells with the highest expression of EGFP were sorted using a BD FACS Aria II. These cells were plated on a 96 well plate at 1 cell per well and clones expanded. The selected clone was not fluorescent in the unstimulated state but ubiquitously expressed high levels of EGFP upon doxycycline stimulation.

3.2.8.2 Cell viability assays

The myoblast cells were cultured in the Dulbecco's minimum essential media, containing 10% fetal bovine serum (FBS) and 1% penicillin–streptomyosin, at 37 °C and 5% CO_2. The standard MTT assay was used to assess the cell viability after treatment with doxycycline solution, empty capsules and doxycycline-loaded capsules for 48 hours. Cells were seeded in 96-well plates with 1×10^4 cells per well and capsules were added at 10:1 ratio. After 48 hours, medium was removed, 20 µl of MTT solution (in PBS) was added to each well and cells were cultured for 3.5 hours. Then 150 µl MTT solvent (4 mM HCl, 0.1% Nondet P-40 in isopropanol) was added to each well. The plate was read in a BMG Fluostar Galaxy plate reader (filter 570 nm).

Toxicity of microcapsules to myoblast cells with and without AMF treatment was evaluated by MTT assay. Cells were seeded in 96-well plates at density of 1×10^4 cells per well, and cultured in Dulbecco's minimum essential media, containing 10% fetal bovine serum (FBS) and 1% penicillin-streptomyosin. After 24 hours, normal and magnetic microcapsules were added to each well, and free doxycycline solution was added as a control (n=5). Doxycycline concentration in each well was 4 μg/ml. AMF was placed at the bottom of each well for 30 min/well after incubating with magnetic or PEI coated magnetic capsules for 1 day, and then cultured for another day. Then, the culture mediums were replaced with 0.2 mg/ml MTT solution (in DMEM medium) and cultured for 4 hours. After which, 150 μl MTT solvent (4 mM HCl, 0.1% Nondet P-40 in isopropanol) was added to each well. The plates were read in a Multiskan Ascent Plate Reader (Thermo Fisher Scientific, UK) with the filter at 570 nm.

The cytotoxicity of chlorhexidine containing fibers to fibroblasts was determined using the MTT assay. Both fibers with 0.5, 1 and 5 % (wt/wt) chlorhexidine particles, and PLA fibers without chlorhexidine, were rinsed with 70% ethanol and sterilized by exposing to UV for 2 h. The fibers were then immersed in culture medium at 1 mg/ml and were kept in the incubator for 24 h or 48 h. The fibers were next removed and the medium used for cell culture. The 3T3 cells were seeded in 96-well plates at 1×10^4 per well, and cultured with fresh medium for 24 h. The medium was then removed and replaced with the chlorhexidine fiber release medium, and cells were cultured for another 24 h or 48 h. After which, the medium was removed and 20 μl of MTT solution was added to each well and cells were cultured for 4 h. Then 150 μl MTT solvent (4 mM HCl, 0.1% Nondet P-40 in isopropanol) was added to each well. The plate was read in a Multiskan Ascent Plate Reader (Thermo Fisher Scientific, UK) with the filter at 570 nm.

Both fibers with 0.5, 1 and 5 % (wt/wt) chlorhexidine particles were cut into 0.8 cm × 1 cm mesh, and sterilized using the method described in 2.6. PLA fibers without chlorhexidine

particles were used as a control. Prior to cell seeding, the fiber meshes were fixed at the bottom of a removable cell culture chamber (Lab-Tek® II, Chamber Slide™). An Engineered 3T3 cell (expressing EGFP) [50] suspension was added to each well at 2×10^4 cells per well, and then cultured for 24 h. The fiber meshes were collected and rinsed with PBS to remove any of the dead or detached cells. Confocal microscopy images were acquired with a confocal microscope using a 63x/ Oil DIC (WD=0.19mm) objective. All the fiber meshes were spread on glass slides and scanned in x–y–z mode. The interval between sections was set as 0.3 µm. All the images along the z position were stacked and three-dimensionally displayed using Imaris software (Bitplane, version7.7).

3.2.8.3 Targeted delivery and Triggered release

Mouse C2C12 myoblast cells (ATCC® CRL-1772™) were engineered with lentiviral vectors to express EGFP at the present of doxycycline according to the method described in our previous study. So the cells could be used as reporters for doxycycline delivery which fluorescence could be observed when doxycycline was delivered intracellularly. Here, C2C12 cells were cultured in 8-well glass chamber slides (well size 10.7 mm×9.4 mm, ibidi USA Inc) at 1×10^4 cells per well and incubated for one day. Then the doxycycline loaded magnetic microcapsules were added to the cells at a 1:1 ratio. To attract the magnetic capsules to the site of interest and induce EGFP expression locally, one magnet was placed at the bottom of well. The cells together with the magnet were kept in incubator for 24 hours. Cells incubated with magnetic capsules but without magnetic field treatment was used as control.

Intracellular doxycycline delivery and locally induced EGFP expression was imaged with a Leica confocal microcopy with 40× oil emersion objective. To visualize the distribution of microcapsules and cells with fluorescence, images were taken continuously from one side of

the well to the other side in the red, green and transmission channels. Each of the individual images were put together to make a panoramic image.

EGFP expression was quantitatively analyzed using a Fluostar Galaxy plate reader. The cells were seeded in 96-well plate at 1×10^4 cells per well and cultured for one day. Then free doxycycline, doxycycline loaded normal and magnetic capsules, PEI coated magnetic capsules were added to each well with doxycycline concentration fixed at 4 µg/ml, 2 µg/ml and 0.4 µg/ml per well (n=5), and cultured for 24 hours. Then the electromagnet was place at the bottom of wells with magnetic microcapsules or PEI coated magnetic microcapsules for 10 min or 20 min per well. Cells with no AMF exposure were used as comparison. After all the AMF treatment, the cells were cultured for another day. To evaluate the EGFP expression, the cells were then washed with PBS and lysed for 30 min by 20 µl lysis reagent (0.05% Protease Inhibitor Cocktail in CelLytic™) each well. Then, 80 µl PBS was added to each well. EGFP fluorescent intensity was measured with excitation wavelength fixed at 480 nm and emission fixed at 520 nm. Cells with no free doxycycline or doxycycline loaded microcapsules were lysed as the control and 100 µl lysis reagent in PBS was used as the blank. The EGFP fluorescent intensity was calculated as follow, EGFP fluorescence intensity = (test well - control)/control.

3.2.8.4 EGFP fluorescence intensity assay

Quantitative analysis of EGFP expression kinetics was performed with a Fluostar Galaxy plate reader. Engineered C2C12 cells (1×10^4 cells per well) in a 96-well plate were treated with free doxycycline, doxycycline-loaded synthetic or biodegradable capsules (7 wells for each group). After specific intervals (2, 4, 6, 8, 10, 12 days), culture medium was removed, and cells were washed with PBS and lysed for 30 min by addition of 20 µl lysis reagent (CelLytic™ M, with

0.05% Protease Inhibitor Cocktail added) to each well. Then 80 µl PBS was added, and EGFP fluorescence intensity was measured in the reader with excitation and emission wavelengths fixed at 480 nm and 520 nm accordingly. Control lysates were prepared using untreated cells and the assay blank consisted of lysis reagent and PBS up to 100 µl volume. EGFP intensity was calculated according to the following equation, EGFP fluorescence intensity = (intensity of test well – intensity of control well) / intensity of control well ×100%.

3.2.9 Antibacterial assay

The antibacterial activity of doxycycline loaded microcapsules was tested by growth inhibition of *Escherichia coli* (*E. coli*, DH5a). Bacterial suspensions in LB Broth were cultured at 37°C/200rpm shaking until they were in the linear phase of growth indicated by an optical density between 0.4-0.6 measured using a spectrophotometer (Cecil CE2021) at 400nm. Bacterial suspension (0.4 ml) was spread on the surface of dried LB agar plates. The sensitivity of the *E. coli* to inhibition with doxycycline was firstly demonstrated using filters (diameter 7 mm) treated with doxycycline concentrations from 5 mg/ml to 8 µg/ml and placed on an agar plate pre-spread with *E. coli*. Filters remained on the plate which was incubated at 37°C overnight and then diameter of zones of inhibition were measured in mm. Sustained release of doxycycline from microcapsules was examined in a transfer experiment in which filters were initially loaded with 40 µl of doxycycline solution (0.1 or 1 mg/ml) or 40 µl of microcapsule suspension equivalent 1 mg/ml of doxycycline. After incubation for 90 minutes on an agar plate pre-spread with *E. Coli*, filters were transferred to a second pre-spread plate with addition of 10 µl sterile water to the filter, the process was repeated every 90 minutes. After 12 hours, all the filters were disposed and all the plates were incubated overnight at 37°C. Images were taken and the inhibitory zones against *E. coli* growth were measured using Nano Measurer(1.2).

The antibacterial properties of chlorhexidine particles loaded electrospun PLA fibers were tested by growth inhibition of Escherichia coli (*E. coli*, DH5a), using both an agar diffusion assay and broth transfer assay. The LB broth base solution was prepared (with 0.5 g NaCl, 10 g tryptone, 5 g yeast extract per liter). To make the LB agar plates, agar was added to the LB broth base solution at 15 g/L. Bacterial suspension in LB broth base solution was cultured at 37°C/200 rpm shaking, and the density of the suspensions was adjusted to that of a McFarland 0.5 turbidity, which corresponded to 1.5×10^8 cells/ml using a spectrophotometer (Cecil CE2021, USA) at 625 nm. 0.4 ml of the bacterial suspension was spread on the surface of LB agar plates. The sensitivity of the *E. coli* to inhibition with chlorhexidine was firstly demonstrated using filters (diameter 7 mm) treated with chlorhexidine particles or encapsulated chlorhexidine particles with chlorhexidine concentrations from 5 mg/ml to 50 µg/ml and placed on agar plates pre-spread with *E. coli*. The fibers were cut into discs (diameter 7 mm, thickness 0.1 mm) and rinsed with 70% ethanol and H_2O, and then placed on LB agar plates which was incubated at 37°C for 24 h and then the diameter (SD) (n=3) of zones of inhibition were measured in mm.

The sustained antibacterial effect of the chlorhexidine containing fibers was also examined in a transfer experiment. Bacterial suspensions in LB broth base, with McFarland 0.5 turbidity were diluted 200 times. Each of the fiber discs (fibers with chlorhexidine particles or encapsulated chlorhexidine particles containing 0.5, 1 and 5 % (wt/wt) chlorhexidine, n=3) were immersed into the bacterial suspensions (1 ml) and cultured at 37°C/200rpm shaking. After each hour, the fiber discs were transferred into fresh bacterial suspensions. After 9 hours, all the fiber discs were discarded and all the bacterial suspensions were incubated for another 24 hours. The optical absorptions were measured at 625 nm (Cecil CE2021, USA).

3.3 Instruments

3.3.1 Zeta potential and size

The Malvern Nano ZS zetasizer instrument was used for the size and zeta potential measurement (Figure 3.1). The technique allows for clear (or light colored) solutions to be characterized in terms of sample particle size, zeta potential and molecular weight, three fundamental parameters of nano-sized particles or molecules in a liquid medium.

For particle size measurement, basically, it is based on the Brownian motion of particles in a simple using Dynamic Light Scattering (DLS). When the monochromatic light beam travels through the particles suspension, the particles will cause the light to be scattered at different intensities, the intensity fluctuation of which is determined by the size of particles. The light fluctuation can be detected and analyzed, giving the particle size distribution based on the following relationship:

$$r = \frac{k_B T}{6\pi\eta D}\Delta m \qquad (3.1)$$

Where r is the radius of particles, k_B is Boltzmann's constant, T is temperature, η is viscosity and D is the diffusion constant.

Zeta potential refers to the charge at the interface of particle surface and the liquid medium, and usually is measured in mV. In the electric field, the charged particles will move towards the electrode of the opposite polarity. The zeta potential is calculated according to the following formula:

$$\zeta = \frac{4\pi\eta}{\varepsilon} \times U \times 9 \cdot 10^7 \qquad (3.2)$$

$$U = \frac{\nu L}{V}$$

Where ζ is zeta potential, η is solution viscosity, ε is dielectric constant, U is electrophoretic mobility, ν is speed of particles, V is voltage and L is the distance between electrodes.

Figure 3.1 Image of Malvern Nano ZS zetasizer instrument.

3.3.2 UV-Vis spectroscopy

The Lambda 35 UV-Vis spectroscopy (Perkin Elmer) covering a wavelength range from 175 to 1500 nm was used for the measurement concentration of chlorhexidine (at 254 nm) and doxycycline (at 274nm) in solutions (Figure 3.1). It has to be noted that in the ultraviolet range (200 to 400 nm), all the measurements were carried out in the quartz cuvette, which has little absorption in this range.

Basically, when the monochromatic light with specific wavelength pass through the organic molecules, they will absorb the energy of light and transit to a higher orbital. The transition of molecules normally includes the multiple-bond (π), single bond (σ) and n-caused by lone pairs (*n*). For most of the organic samples, the transition of *n* or π electrons to π^* excited state will result absorption region from 200 nm to 700 nm. In addition, the UV-Vis spectroscopy is also used to for measuring transition metal ion solutions, for example the gold or iron oxide nanoparticles, and DNA or protein samples.

For the concentration determination, since the absorption intensity of samples (chlorhexidine and doxycycline) has a correlation with its concentration, the amount of molecules in solutions can be calculated based on the calibrated relationship.

In addition, for the measurement of bacterial concentration, the optical light spectroscopy (Cecil CE2021) was used, and cell concentrations in suspension was determined according to the McFarland standard. McFarland standard with different numbers which refer to the turbidity of bacterial suspensions, have a correlation with the cell numbers. At McFarland 0.5 turbidity, the cell density is around 1×10^8 CFU/ml. and the absorbance is between 0.08 and 0.1 at 625 nm wavelength.

Figure 3.2 Image of Lambda 35 UV-Vis spectroscopy.

3.3.3 Fluorescence spectroscopy

The fluorescence spectrometer (Perkin Elmer LS55) was used to measure the fluorescence intensity and determine concentration of dyes and fluorescence drugs (doxycycline) (Figure 3.3). Similar to the UV-Vis spectroscopy, the measurement is also based on a linear relationship between fluorescence and substance concentration. So a standard calibration is needed to measure the release. But to ensure an accurate measurement, the samples should always be kept away from the light and concentration for each sample should not too high. With a too concentrated solution, it will self-quenching, thus leading to a lower measurement concentration. As for quantification of doxycycline concentration, the excitation and emission wavelength was set at 350 nm and 536 nm respectively.

Briefly, a light beam generated by a high energy pulsed Xenon source is used to excite the sample molecules, leading to emission of fluorescent light. The excitation light should be monochromatic with a specific wavelength, and the emission light is recorded. Also, the fluorescence spectrometer can also be measured in an excitation model, which with emission light set at specific wavelength and the excitation light is recorded.

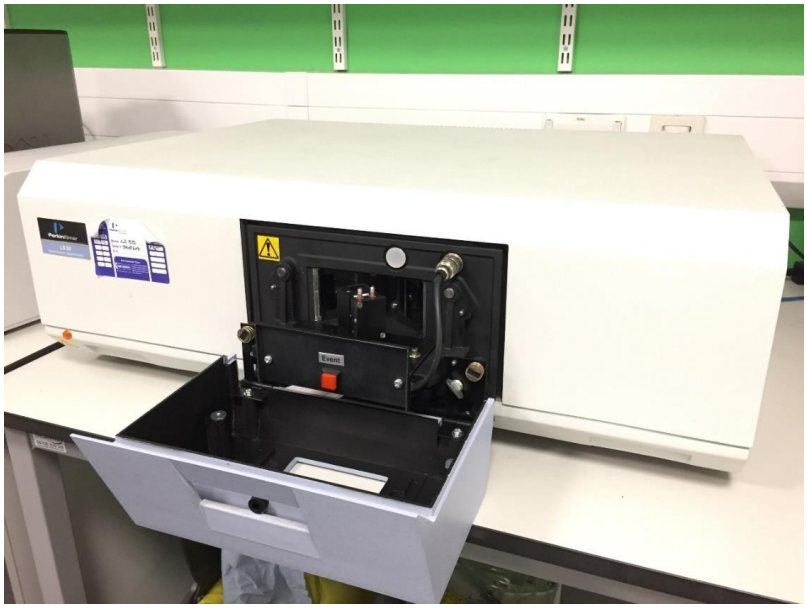

Figure 3.3 Image of fluorescence spectrometer.

3.3.4 Fourier transform infrared spectroscopy

The FTIR spectrometer (Pekin Elmer) was used for chemical structure analysis (Figure 3.4). Both the chlorhexidine and doxycycline samples were analyzed with the spectral resolution set at 4 cm^{-1} from the range of 4000 cm^{-1} to 600 cm^{-1}. FTIR is a basic technique for chemical structure analysis, functional groups of molecules identification, and detect of certain compounds. Either solid or liquid samples could be directly examined.

Basically, the FTIR consists of an infrared source which emits full spectrum of wavelengths of infrared radiation. The infrared radiation then goes into a Michelson interferometer, which contains a fixed mirror and a moving mirror, and then is modulated to monochromatic lights. It then passes through the samples and be absorbed at different wavelength by different bonds and molecular groups. After that, the infrared beam intensity is detected, Fourier transferred, and generate a spectrum.

Different molecules have different bonds and functional groups, so the vibrating of bonds will be at different frequencies. Even if the same group in different molecular structures will have various vibrating frequency. But we can interpret their chemical bonds and positions by refer to the standard spectrums. By comparing the shift of vibrating band and intensity, the chemical structure or interaction between functional groups can be interpreted.

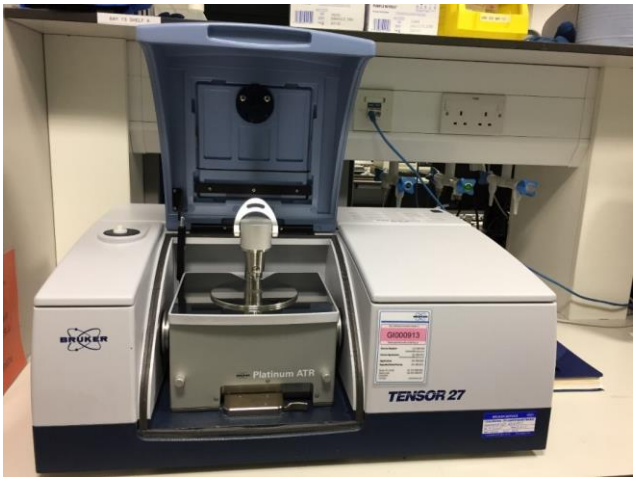

Figure 3.4 Image of FTIR spectrometer.

3.3.5 Thermogravimetric analysis

Thermo-gravimetric analysis (TGA Q50, USA) was used to determine the composition of chlorhexidine spheres (Figure3.5). The TGA analysis for all the samples was carried out at 10°C/min under nitrogen atmosphere, over a temperature range of 50-800°C. And the samples were dried and loaded as powder in the pan of TGA machine for analysis.

TGA is a method to measure the mass change of solid samples over a range of temperature. Basically, when the sample is heated, its weight will lose when it starts to decompose or evaporate. But sometimes the weight also increases when oxidation happens. The dynamic of weight changes is recorded via the microbalance and the temperature is monitored by a thermocouple. By referring to the TGA result, we can learn the stability of samples and their decomposition temperature. For the metal nanoparticle functionalized chlorhexidine spheres, we can even calculate the percentage of the organic and inorganic components.

Figure 3.5 Image of thermo-gravimetric analysis instrument.

3.3.6 Fluorescence microscopy

Fluorescence microscopy (Leica DMI 4000B Epifluorescence microscope) were used for characterize samples (microcapsules and cells) with fluorescence. For the microcapsule samples, polyelectrolyte shells are normally labelled with dyes (FITC or TRITC). Doxycycline is also fluorescent, which can be visualized in the ultraviolet range. For cells imaging, the myoblast cells (C2C12) were engineered to express EGFP, therefore, they were imaged directly with the fluorescence microscopy to monitor the EGFP expression.

When the specimen is illuminated with monochromatic light, they will emission light from the excited singlet state to the ground state. The microscopy is consisted of light source, dichroic mirror, excitation filter and emission filters, both of which are chose corresponding to the excitation and emission wavelength of fluorophores. For the Epifluorescence microscopy, each time only one fluorophore is imaged, and multicolor samples have to be imaged separately and images at different channels then are merged (Figure 3.6).

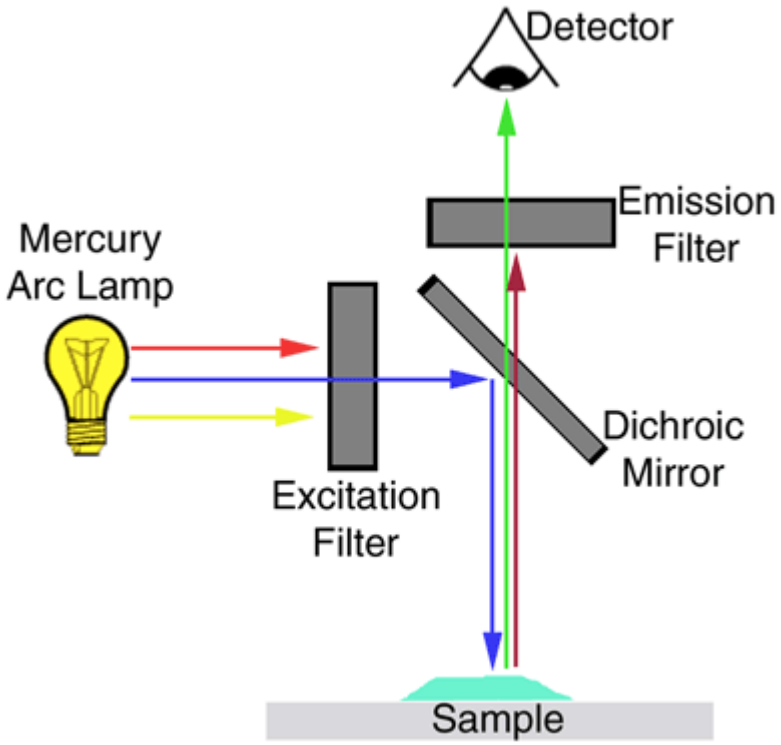

Figure 3.6 Fluorescent microscopy schematics.

3.3.7 Confocal laser scanning microscopy

Confocal laser scanning microscopy (CLSM, Leica TS confocal scanning system) was used for microcapsules characterization, permeability test, and all the cells imaging. The microscope is equipped with 10×, 20×, 40×, 40× oil, 63× oil immersion objectives. For microcapsule samples, the suspensions were deposited on thin glass slide and covered with cover glass. Cells adhered on electrospum fibers were also transferred on thin glass slides. For cell samples, cells were cultured in Ibidi 8-well glass chamber and imaged directly.

The advantage of confocal microscope over the fluorescence microscope is that high resolution images can be taken and a 3-D reconstruction can be achieved. For the traditional fluorescence microscope, the light cannot not be focused on a specific area, but whole the sample is excited. However, for confocal microscope, focus of light to sight of interest is realized by placing a pinhole in front of the detector to eliminate the out-of-focus signal, and only signals very close to the focal plane can be detected. The confocal microscope can acquire optical sections as thin as 0.5 μm. Therefore, specimen at specific section depth can be easily imaged. To reconstruct a 3-D image, we just have to set the start and end depths by adjusting the z-position, number of sections, and then take the images continuously. Then the acquired images stack to make the 3-D image. Therefore, the 3-D structure of samples, positions between cells compartment and capsules can be viewed and analyzed (Figure 3.7).

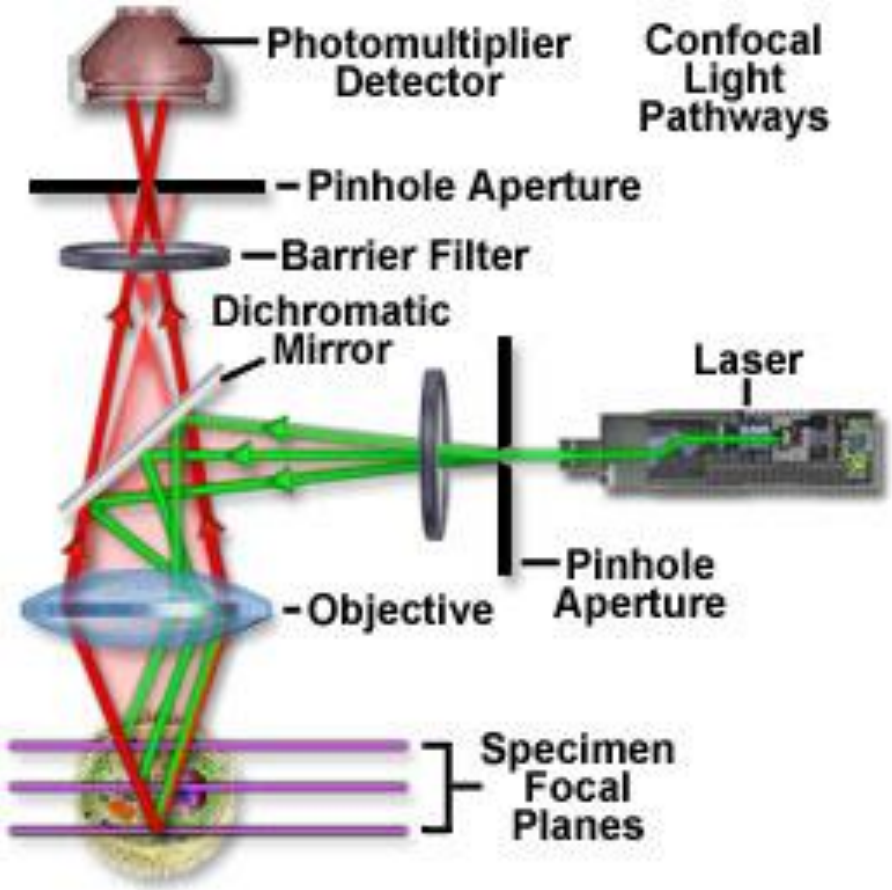

Figure 3.7 Laser scanning confocal microscopy schematics.

3.3.8 Scanning electron microscopy

Scanning electron microscopy (SEM, FEI inspect-F) was used for characterizing chlorhexidine samples and microcapsules (Figure 3.8). The samples, either in powder or in suspension, were prepared on a glass wafer, and coated with gold or carbon to make the samples conductive. For gold or Fe_3O_4 functionalized chlorhexidine spheres, back-scattered detector was used to visualize the distribution of metal elements, so carbon coating was preferred. The voltage used for imaging was 10 kV, and spot size was set at 3.5, and working distance was around 10 mm. Statistical analysis of particle size based on the SEM images and fiber diameters were carried out using Nano Measure (version 1.2).

The principle of SEM is basically that when a focused electron beam scans on the surface of specimen and interact with the surface, signals were detected by detectors, which produce

images of sample morphology and composition. The most common detectors used are secondary electrons (SE), back-scattered electron (BSE) and photons of characteristic X-rays detectors. Secondary electron detector monitors the secondary electrons emitted by the surface of samples and can produce images with resolution as high as 1 nanometer. BSE detector collects elastic scattering electrons from much deeper surface of samples, and the resolution is poorer than the SE images. But elements distribution for the samples can be provided in the BSE model. For the characteristic X-rays detector, an inner shell electron from the sample was removed and filled by a higher-energy electron, and information is collected. So the composition of samples can be identified in this model. To get better images, normally the samples should be electrically conductive, therefore, a thin layer of Au, Pt or carbon is sputtered on the sample surface. For biology samples, carbon is preferred. And the voltage of electron beam ranging from 5 kV to 20 kV is chose depending on the properties of samples, as electon beam with a too high voltage may penetrate and damage the sample.

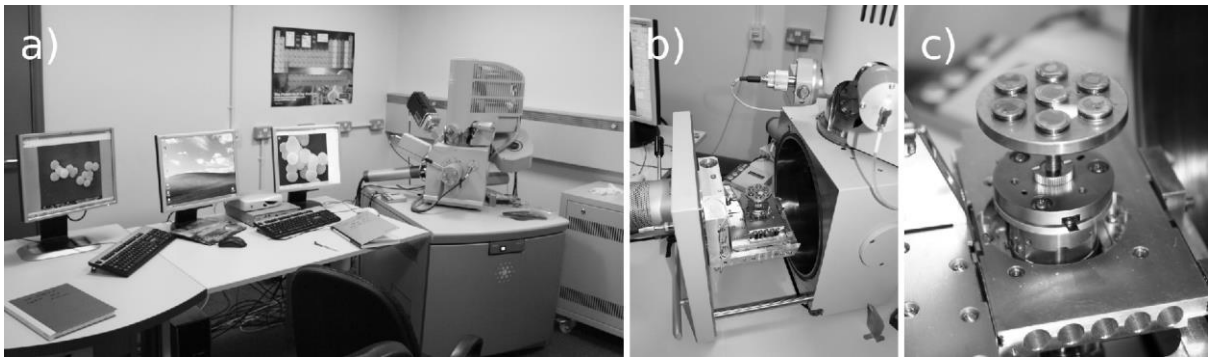

Figure 3.8 FEI Inspect F scanning electron microscope photographs: a) microscope general view, b) vacuum chamber with specimens fitted, c) sample holder with specimens close-up.

3.3.9 Transmission electron microscopy

Transmission electron microscopy (JEOL 2010) was used for Fe3O4 nanoparticles, Au nanoparticles/Nanorods, and microcapsule characterization (Figure 3.9). Samples were prepared by put one drop of diluted suspension on the copper grid with carbon film, and dried in air. The copper grid was fixed into a holder and placed into vacuum chamber before analyzed at acceleration voltage of 200 kV.

Different from the SEM, the electron beam used in TEM transmit directly through the sample and interacting with the it, giving the information of the structure of the sample. So the samples should be ultra-thin for electron penetration, and the electron beam is accelerated. The images generated based on the information are then magnified and focused, or detected by a sensor underneath the sample. The resolution of TEM images is extra high, which makes it possible to examine the details of samples such as a single column of atoms.

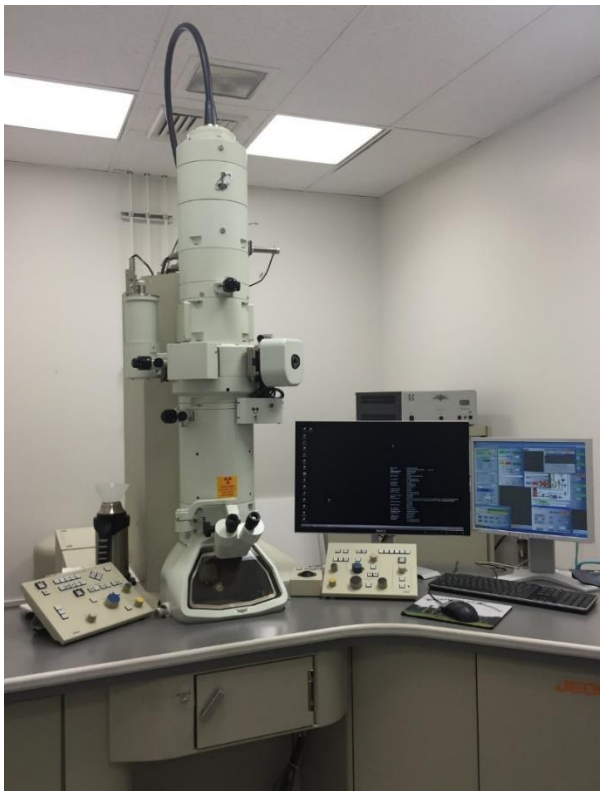

Figure 3.9 Image of TEM instrument.

3.3.10 Ultrasonic unit

Ultrasound (Piezon Master 400) was used in the study to trigger the release of chlorhexidine from HEMA-UDMA resin (Figure 3.10). This ultrasonic unit is frequently used in dentistry for the purpose of subgingival calculus removal, periodontal treatment, cavity preparation, root canal preparation, cleaning and irrigation and so on. In our experiment, the ultrasound probe (27-30 kHz) was contacted with the resin disc surface and sonicated for different durations to trigger chlorhexidine release.

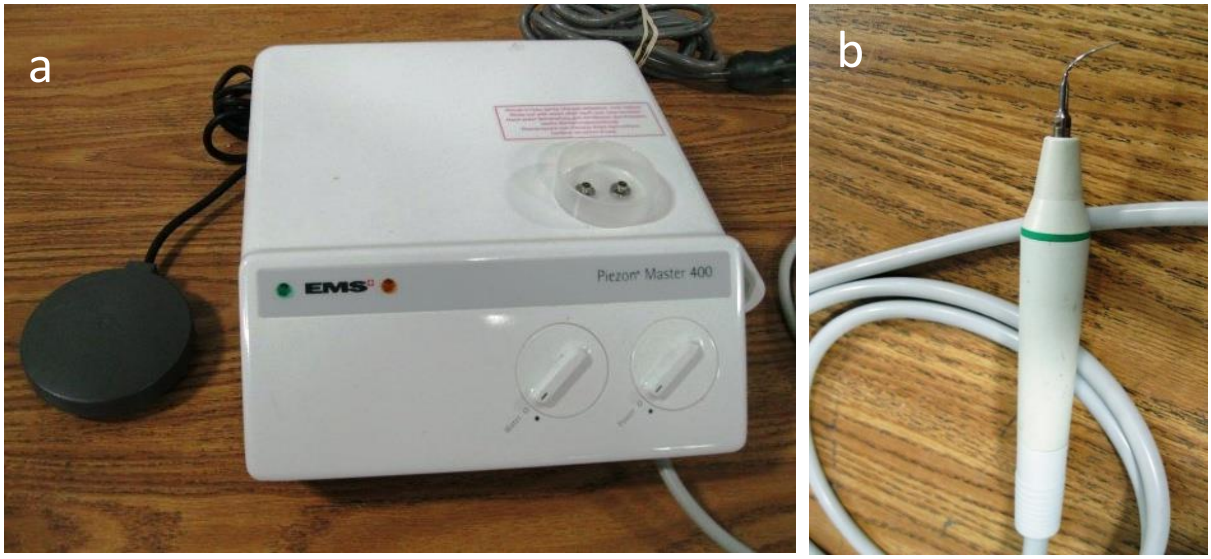

Figure 3.10 Image of ultrasound unit (a) and the probe (b).

3.3.11 Laser irradiation setup

To irradiate the chlorhexidine capsules a customised laser setup was used (Figure 3.11).[192] The chlorhexidine capsule suspension was placed on a thin glass slide and the glass slide was marked to locate the particles. A 100 mW laser diode (840 nm) was coupled with a simple optical microscope (100 × objective, Edmund Scientific, USA), and the focused laser spot was tuned by adjusting the operating laser voltage. In addition, the white light source and XYZ stages allowed samples to be easily located and focused. The laser beam passed through the objective in the Z direction and was focused at the sample to irradiate the specific site. A CCD camera was connected to a computer to capture this event. Thus, once aligned and focused, an image of sample and a laser spot could be observed on the screen. In the current work, remote triggering of the gold functionalized chlorhexidine capsules was carried out using this laser setup.

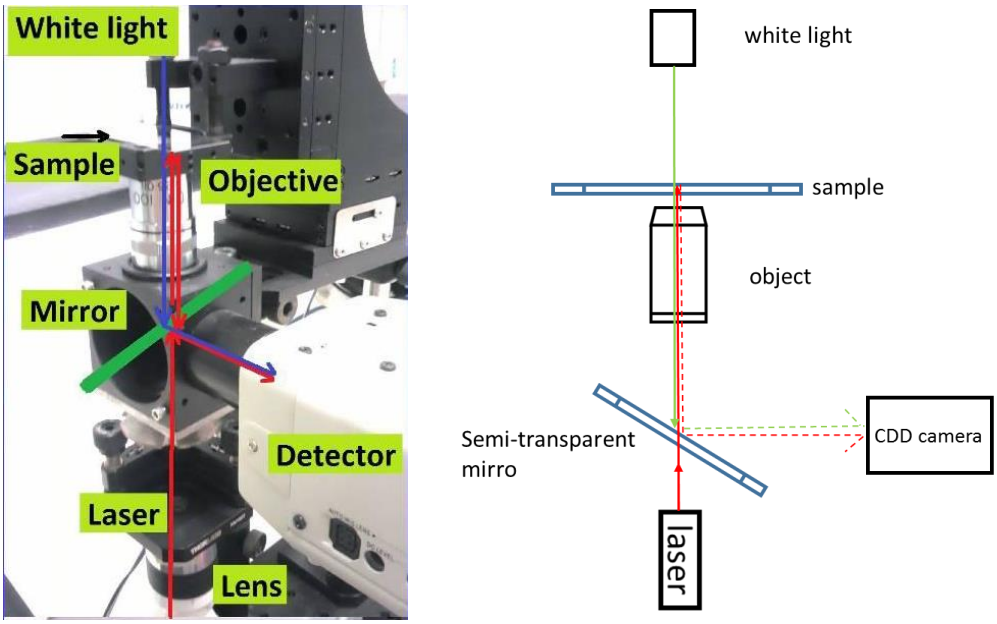

Figure 3.11 Laser irradiation setup (left) and schematics (right).

3.3.12 AMF setup

As an AC electromagnet, a 7 cm long, 2.2 cm diameter linear coil wound on a cylindrical solid soft iron core of 1.5cm diameter was obtained from a low voltage electromechanical relay switch (manufacturer unknown). It had a DC resistance of 2kΩ, and an impedence of 5kΩ at 50Hz, indicating an inductance of 14.6 Henrys.

A power supply was constructed with a 230v to 110v 50Hz mains transformer. A variable voltage was supplied to the electromagnet through a stepped potential divider circuit connected across the transformer output consisting of seven 1kΩ 1W resistors in series connected to a rotary switch. To avoid damage to the coil from high voltage transients, a resistance of 1kΩ was connected in series with the electromagnet, and a 200V surge limiter was placed across its terminals. The maximum voltage supplied to the coil was 98V.

The magnetic field was measured by a Gaussmeter at full voltage. the electromagnet gave an AC field of 16.4 milli Tesla (164 Gauss) at the centre of the end of the core. For the experiments, the magnet was mounted vertically and the test wells were placed immediately above the end of the core. At the spacing of the bottom of the interior of the plastic wells from the core, the field was 16.0 milliTesla (160 Gauss). The field at 1 cm directly above the centre of the core end fell to one third of level with the probe touching it. At lower voltages, the magnetic field had a linear relationship with the applied voltage, indicating that the core was not saturated.

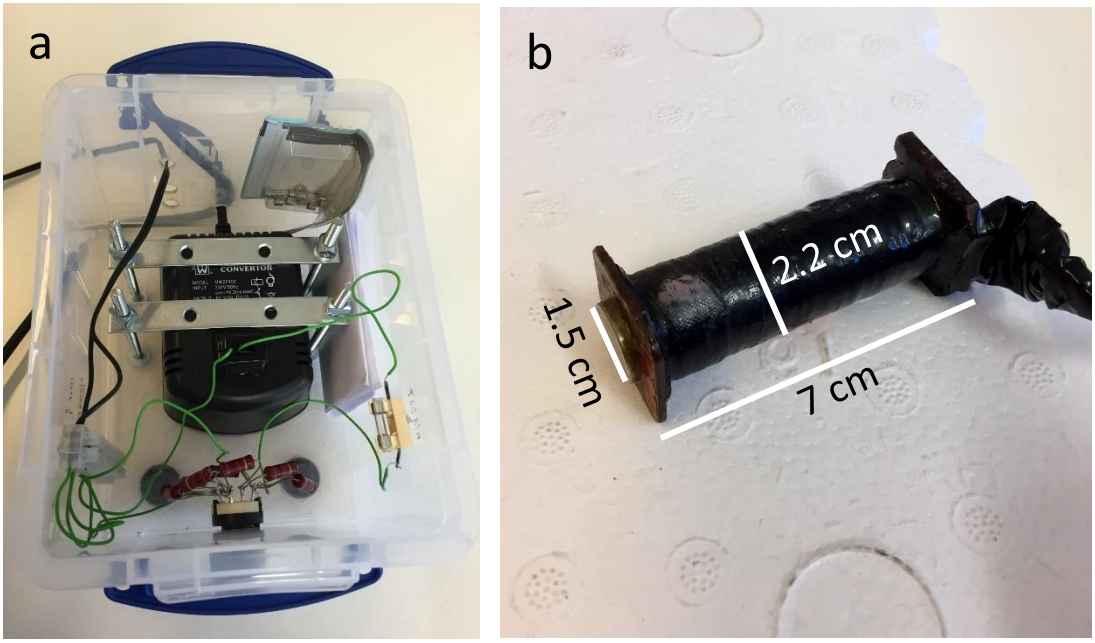

Figure 3.12 Image of AMF setup (a) overview of the AMF setup and (b) the coil.

4. Chlorhexidine spheres

4.1 Chlorhexidine spheres and their encapsulation

4.1.1 Fabrication of chlorhexidine spheres

4.1.1.1 Chlorhexidine precipitation with salts

Chlorhexidine cannot readily crystallize,[193] so it is commonly used in the form of chlorhexidine digluconate, chlorhexidine diacetate and chlorhexidine dihydrochloride. Chlorhexidine diacetate has a relatively low solubility (2% in H_2O),[30] therefore many salts or ions could lead to precipitation, enabling the possibility to further modify the formulation and morphology of chlorhexidine precipitation.

Here we used different salts to precipitate chlorhexidine. Briefly, 15 mg/ml chlorhexidine diacetate was mixed with solutions of Na_2CO_3 (Figure 4.1a), Na_2HPO_4 (Figure 4.1b), $NaHCO_3$ (Figure 4.1c), Na_2SO_4 (Figure 4.1d), and not homogeneous precipitations were produced. But when chlorhexidine diacetate was mixed with NaBr and KI, some fibrous structure was observed as illustrated in Figure 4.4e, f. Especially for the precipitation of 15 mg/ml chlorhexidine diacetate solution and 0.66 M NaBr, individual clusters were precipitated. According to the enlarged image, a dendritic-like structure was observed, however intact spherical particles could not be identified. So we assume that the halogen elements may have the potential to help produce homogeneous chlorhexidine particles. Because comparing to the precipitation from I^-, those precipitated with Br^- have a more ordered appearance, so next we tried Cl^- salts.

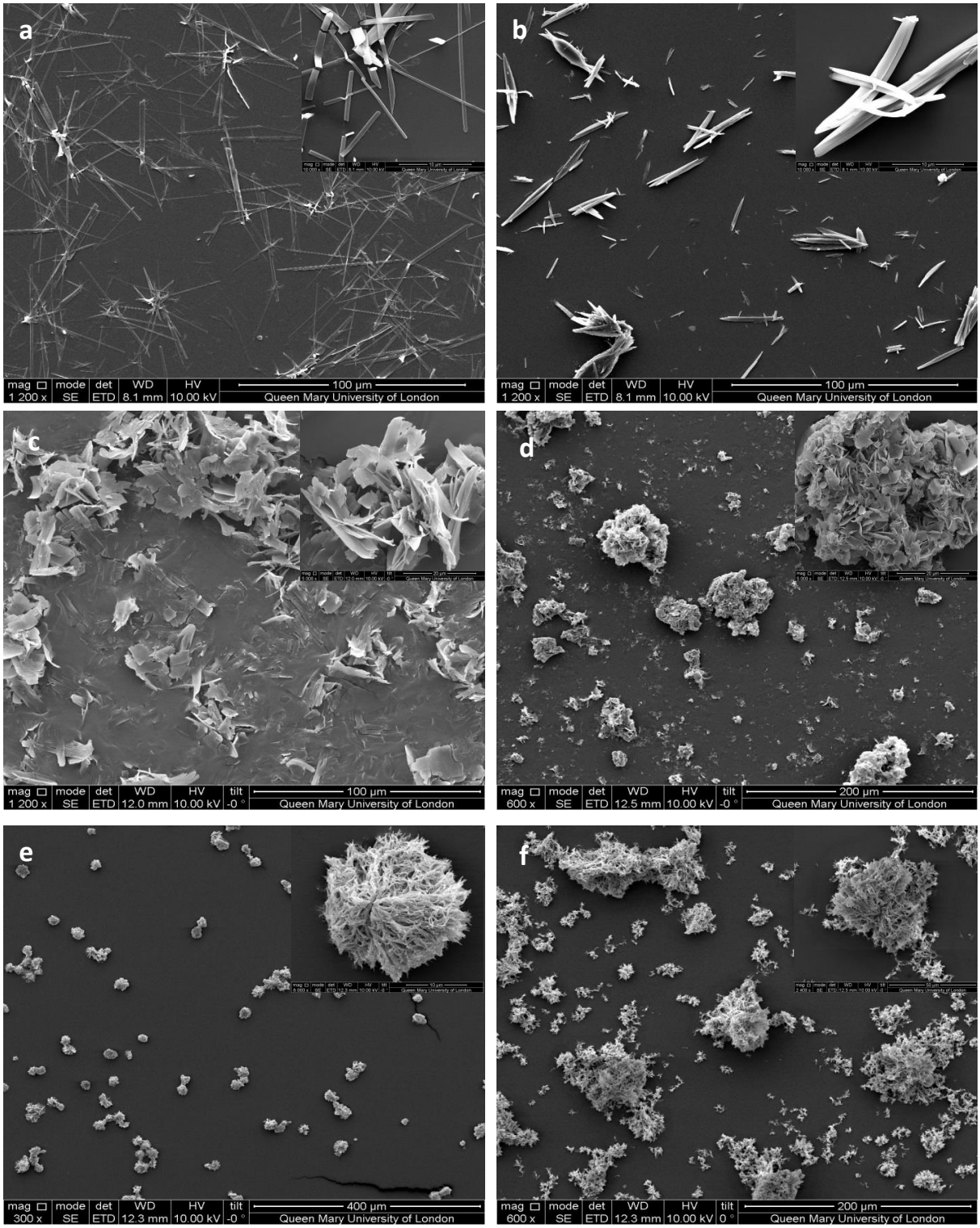

Figure 4.1 SEM images of chlorhexidine diacetate precipitated with 0.33 M (a) Na_2CO_3, (b) Na_2HPO_4, (c) $NaHCO_3$, (d) Na_2SO_4, and 0.66 M (e) NaBr and (f) KI. The inset images are individual clusters at high magnification (×8000).

Similarly, 15 mg/ml chlorhexidine diacetate solution was used with different $CaCl_2$ concentrations to synthesize spherical chlorhexidine particles. As demonstrated in Figure 4.2, spherical chlorhexidine particles could be fabricated with low $CaCl_2$ concentration and the formation of spheres were dependent on the amount of ions in solutions. When the chlorhexidine diacetate concentration was fixed at 15 mg/ml, 2 M $CaCl_2$ this led to irregular precipitation (Figure 4.2a). When the concentration was reduced to 1 M a similar clustered structure was presented (Figure 4.2b). The 0.5 M $CaCl_2$ solution produced precipitation of individual particles, most of which were spherical or semi-spherical with a high porosity (Figure 4.2c). The distinct texture revealed the nucleation and growth direction which originated from the core. When the $CaCl_2$ concentration was 0.33 M, more regular spheres were produced (Figure 4.2d). The interconnected structure was highly porous and homogeneous and the mean particle diameter (SD) was 19.9 (3.1) µm. This formulation was used for all the following experiments. Further reducing the $CaCl_2$ concentration to 0.25 M and 0.125 M resulted in the synthesis of particle morphology with a more spherical, compact and interconnected structure (Figure 4.2e-f). The $CaCl_2$ concentrations however did not have much influence on the chlorhexidine precipitation efficiency, since all solutions used could precipitate over 95% chlorhexidine (Table 4.1). The chlorhexidine content in the spheres was 90 wt. % as determined by measuring the remaining chlorhexidine in the supernatant and the weight of the dried spheres. The chlorhexidine content was higher than the other carriers which are used for chlorhexidine delivery.[71] Chlorhexidine content in each particle was 2.57 ng. The minimum inhibitory concentration (MIC) of chlorhexidine reported for *E. coli* was 2-8 µg/ml and for *S. epidermidis* was 0.5-2 µg/ml.[86] Therefore, the concentration of the chlorhexidine spheres may be beneficial for sustained antibacterial activity.

To further confirm the effect of Cl^-, chlorhexidine diacetate solution was mixed with other equivalent chloride salt solutions (such as NaCl, KCl, $ZnCl_2$, and $MgCl_2$), that similar

interconnected porous spherical structures were produced, in a range of differing sizes (Figure 4.3).

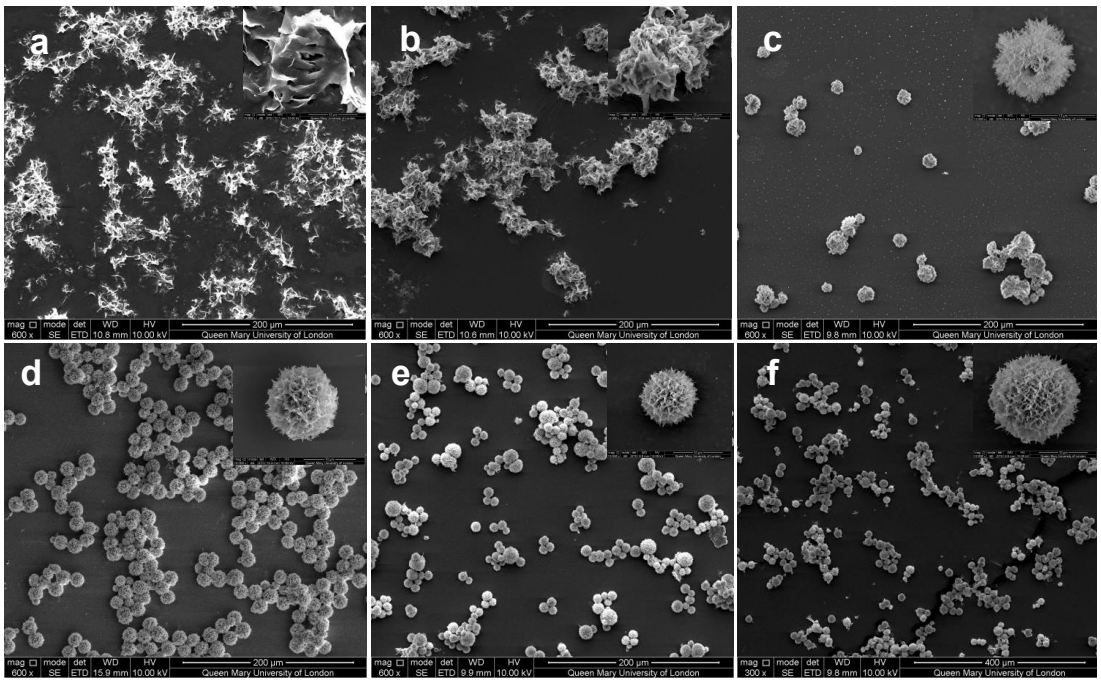

Figure 4.2 SEM images of chlorhexidine compounds precipitated with: (a) 2 M, (b) 1 M, (c) 0.5 M, (d) 0.33 M, (e) 0.25 M, and (f) 0.125 M $CaCl_2$. The inset images are individual particles at high magnification (×8000).

Table 4.1 Chlorhexidine precipitating efficiency with $CaCl_2$ solutions of different concentration.

$CaCl_2$ concentration	CHX precipitate efficiency (%)	Standard deviation (SD)
2	99.1	0.02
1	98.9	0.11
0.5	98.7	0.05
0.33	98.4	0.12
0.25	97.4	0.01
0.125	95.5	0.15

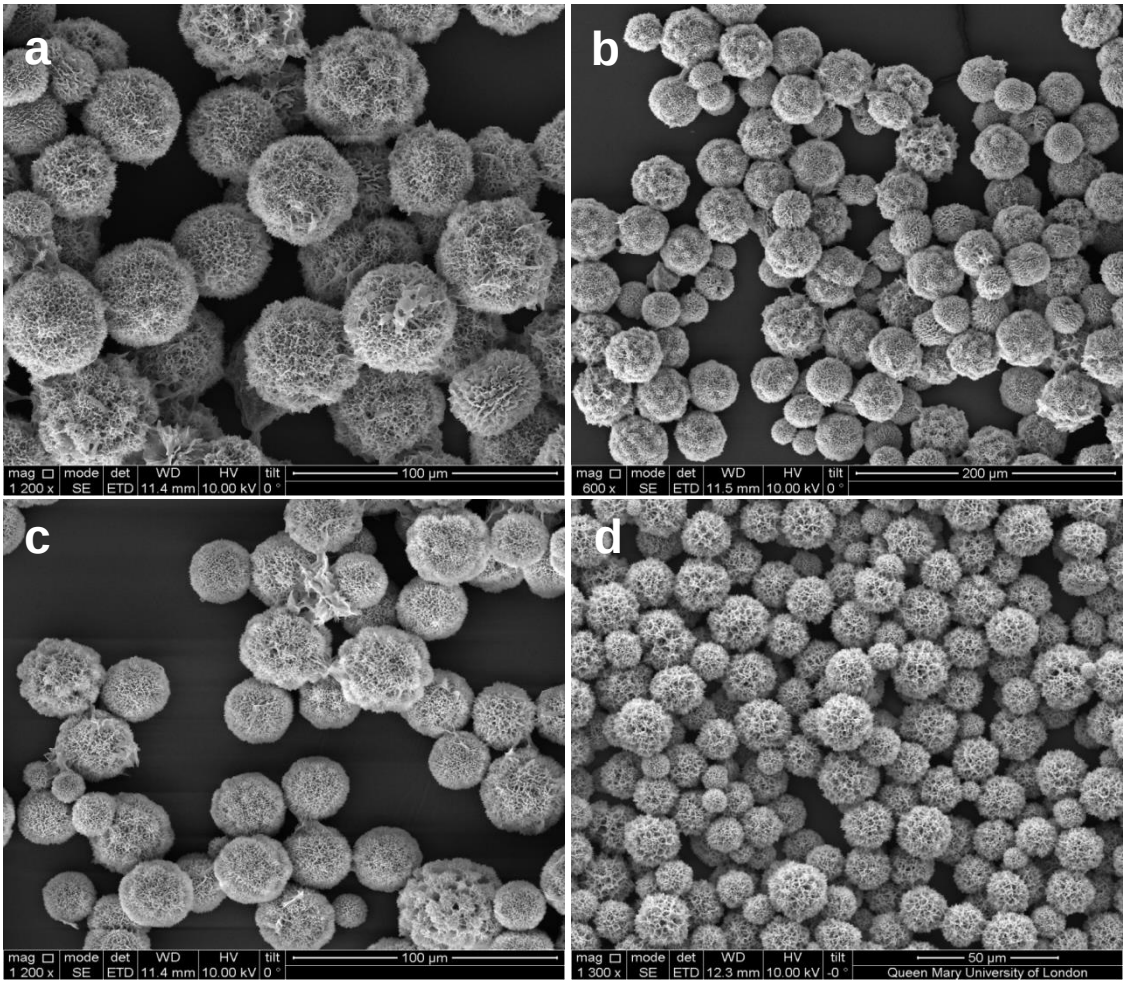

Figure 4.3 SEM images of chlorhexidine compounds formed with (a) NaCl, (b) KCl, (c) $MgCl_2$ and (d) $ZnCl_2$.

The spherical chlorhexidine particles made form chlorhexidine diacetate and $CaCl_2$ were characterized by Fourier Transform Infrared Spectroscopy (FTIR). Compared to the spectrum of chlorhexidine diacetate which was used for particle synthesis, the typical band of C=N for chlorhexidine was shifted from 1610 cm^{-1} to 1621cm^{-1} (Figure 4.4). The reported position for the amine group stretching vibration for chlorhexidine dihydrochloride was 1651cm^{-1}. [194] There was a distinct intensity increase at 3118, 3303 and 3190 cm^{-1}, which was assigned to the stretching vibration N-H of the groups Alkyl-NH-Aryl and $(Alkyl)_2NH$ and the group =NH.[28] The band shift and intensity change was due to the electron density change for the =NH group, which showed that the biguanides of chlorhexidine may have coordinated with Ca^{2+}. The

mechanism for the formation of the radiating interconnected structure is however still unclear, but similarly Cu^{2+} coordinated chlorhexidine complexes were reported and the chelation mechanism was well studied.[28-29]

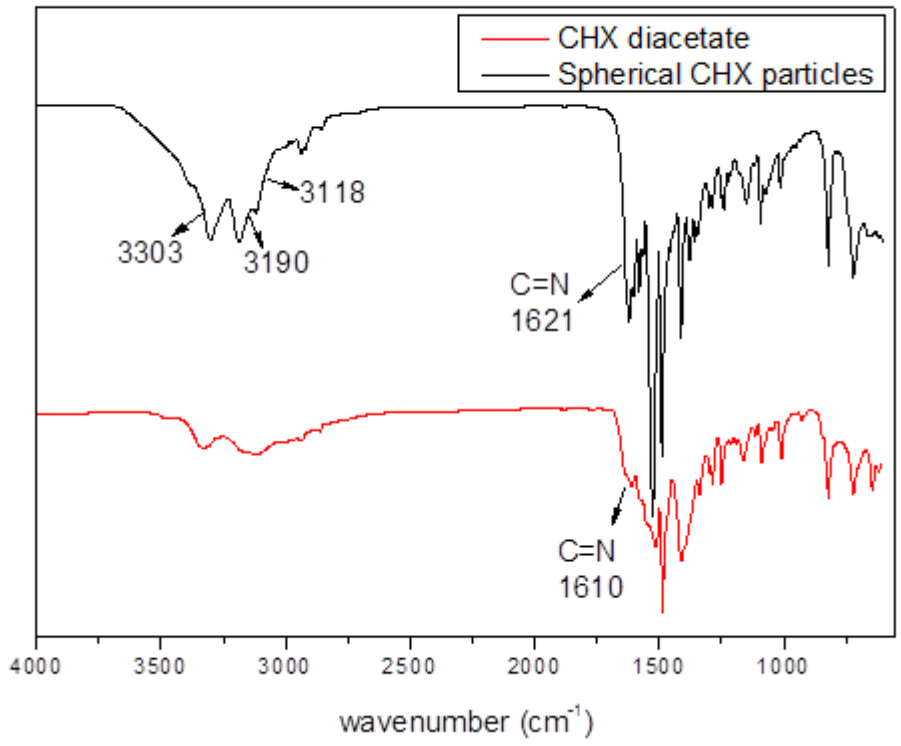

Figure 4.4 FTIR spectra of chlorhexidine diacetate and spherical chlorhexidine compounds.

The elemental analysis of chlorhexidine spheres also confirmed the presence of Ca^{2+} in the structure (data not shown). Since the spheres were washed more than 3 times with NaCl solution to get rid of the residual Ca^{2+}, we assumed that the Ca^{2+} was bound in the spherical structure instead of physically absorbed on the surface. Moreover, by mixing chlorhexidine diacetate solution with 0.33 M $Ca(NO_3)_2$, a similar interconnected spherical structure was observed (Figure 4.5). This structure was however coarser and the dendrites were thicker. Therefore, combining the EDX results with the FTIR spectra, we assume that coordination of biguanides to Ca^{2+} happened during the formation of spherical chlorhexidine particles.

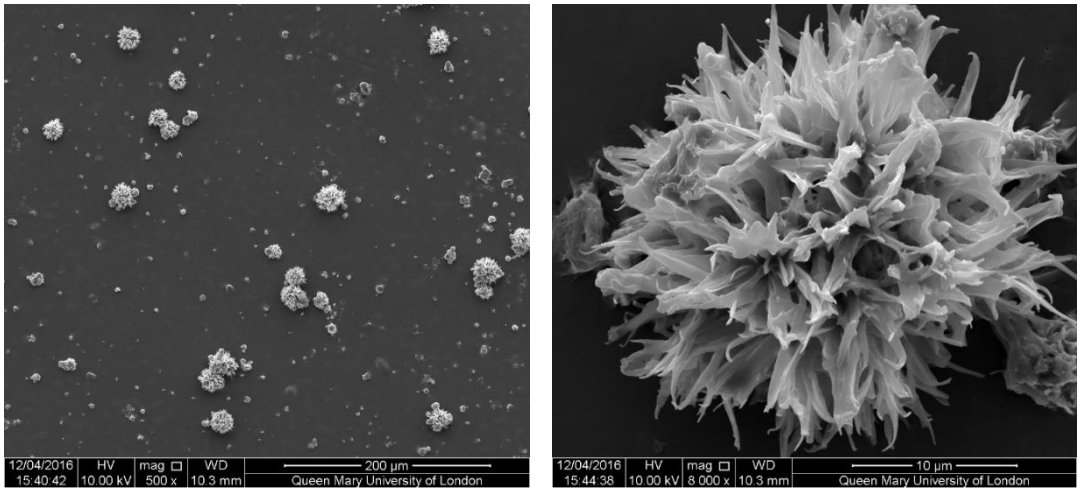

Figure 4.5 SEM images of chlorhexidine compounds formed with $Ca(NO_3)_2$.

The chloride ions may play a vital role in the formation of the chlorhexidine spheres. Chlorhexidine diacetate has a relative low solubility in H_2O, and the presence of Cl^- in solution accelerated the precipitation. When a highly concentrated $CaCl_2$ solution (2 M) was added, turbidity was immediately observed, while more time was required to precipitate with the 0.125 M $CaCl_2$ solution. Chlorhexidine solubility was highly dependent on salt type and concentration of the solution, as demonstrated by previous studies.[30] Since the addition of sodium gluconate into solution would improve chlorhexidine diacetate solubility, while the presence of chloride would reduce it.[6]

Therefore, we conclude that the formation of spherical chlorhexidine particles with homogeneous size distribution is a combined function of chloride anions and the counterpart cations (Ca^{2+} in our case). The chloride anions may help to reduce solubility of chlorhexidine and the rate of formation of the interconnected structures, while the cations are responsible for the assembly of more compact spherical structures.

The structure of the spherical chlorhexidine particles was further analyzed with powder XRD. There was a clear change in the 2 theta positions (missing peaks, peak shifts, peak broadening) and the peak intensities, when the chlorhexidine compounds were compared to the chlorhexidine diacetate powder (Figure 4.6), indicating a different polymorph and crystallite size. The inset SEM image of the chlorhexidine diacetate crystal also confirmed a morphology and size which was completely different from the finer, porous interconnected spherical chlorhexidine particles. The crystal structural differences in the new compounds were therefore in evidence, with crystals growing dendritically from a nucleation site central to the structure.

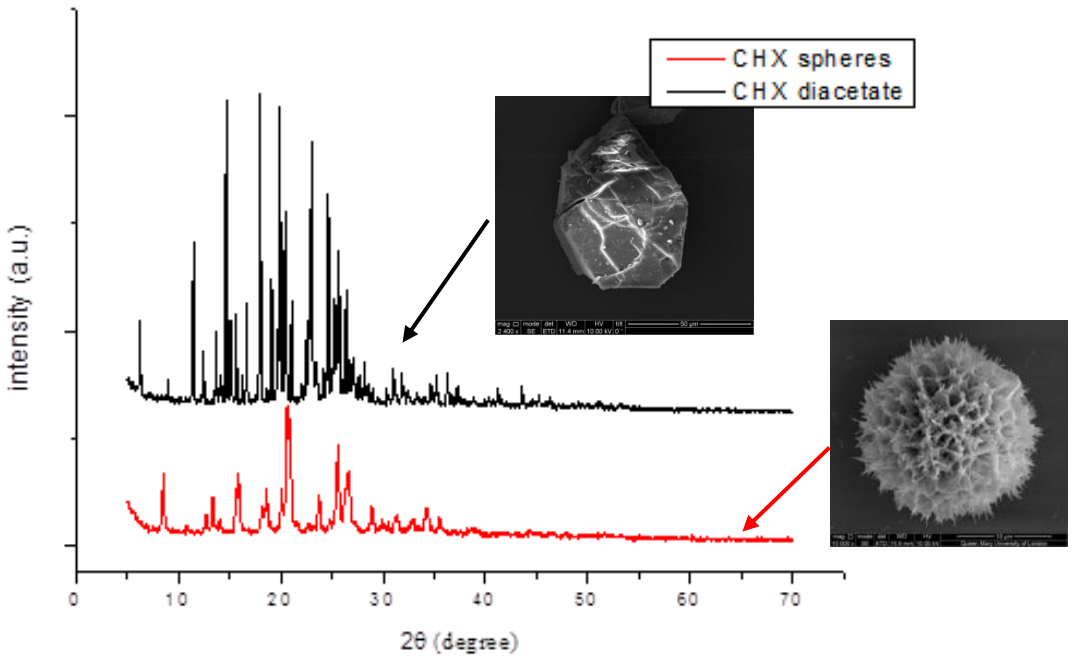

Figure 4.6 XRD of spherical chlorhexidine compounds (lower) and chlorhexidine diacetate (upper). The inset image is a chlorhexidine diacetate crystal.

4.1.1.2 Spherical chlorhexidine particles

Temperature is a key factor which determines the nucleation and crystal growth. In the present study, temperature was explored from 1°C to 25 °C. Figure 4.7 shows the influence of temperature on the morphology and size of the chlorhexidine spheres. As the temperature increased, the mean diameter (SD) of chlorhexidine spheres also increased from 5.6 (1.5) µm (1 °C) to 21 (5.3) µm (25°C). No distinct difference in the particle morphology was observed at this temperature range. There was a correlation ($r^2 = 0.95$) between particle diameter and temperature according to Figure 4.8. It is not surprising that higher temperatures would have encouraged movement of ions and accelerated the heat transfer favoring increased crystal grow rates. The energy required for crystal growth was limited at lower temperatures. The solubility of chlorhexidine at lower temperatures may also effect the process/rate of nucleation and the kinetics of crystal growth. There is also the potential of particle coalescence (Ostwald ripening) in this system, driven by the reduction in interfacial energy when larger particles grow at the expense of smaller ones at increasing temperature.[47]

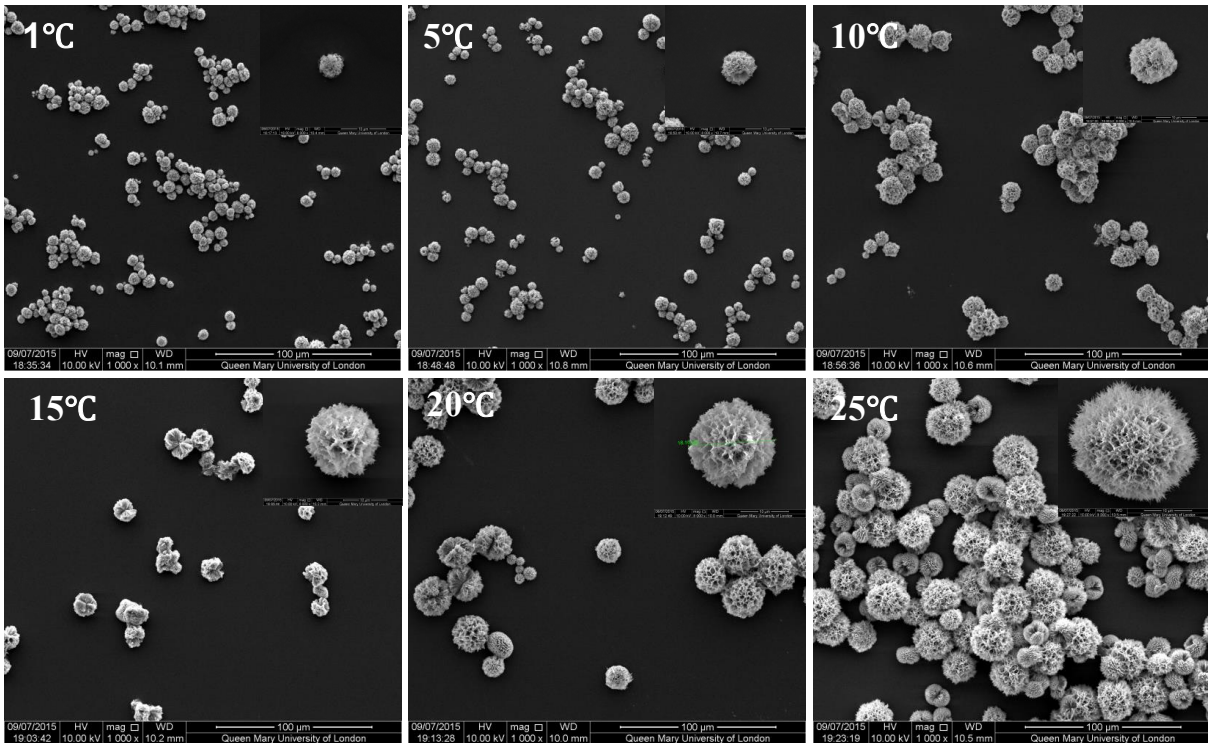

Figure 4.7 SEM images of spherical chlorhexidine particles precipitated with 0.33 M $CaCl_2$ at different temperatures. The inset images are individual particles at high magnification (×8000).

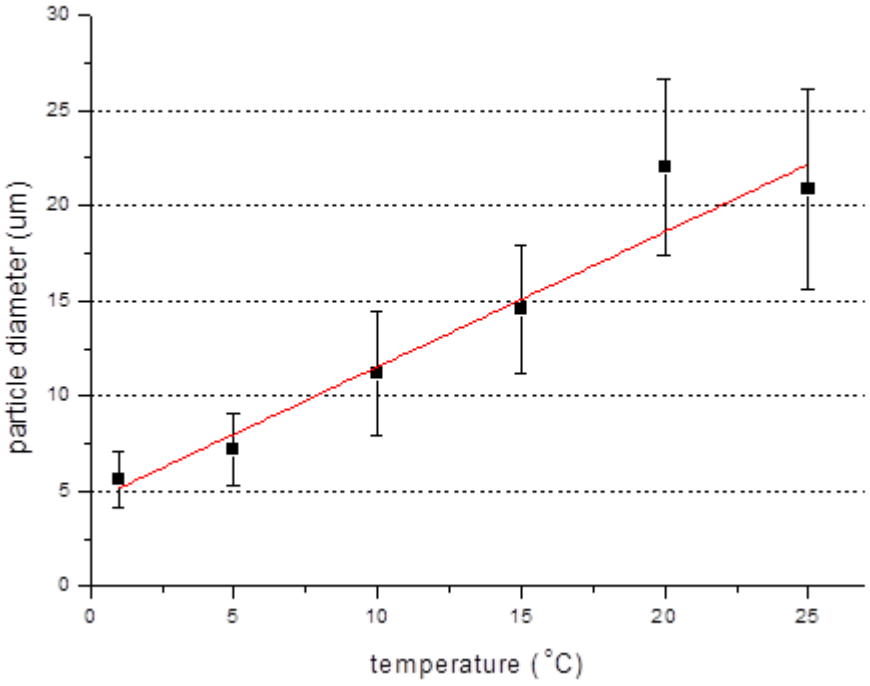

Figure 4.8 Mean diameter (SD) of spherical chlorhexidine particles precipitated with 0.33 M $CaCl_2$ at different temperatures.

4.1.2 Chlorhexidine spheres encapsulation

4.1.2.1 LbL encapsulation of chlorhexidine spheres

The LbL assembly of polyelectrolytes on the surface of crystalline drugs has been extensively studied to stabilize the drug and facilitate sustained release.[195] Many of these drugs (anticancer) are insoluble in H_2O, and coating with polymer shells may improve their solubility.[196] The drugs were either originally charged or tailored with surfactants for polyelectrolyte deposition.[197] Herein, the chlorhexidine spheres were porous with high surface energy which was necessary for sequential assembly of PAH and PSS to yield capsules. Some dissolution of

the drug was always accompanied with the LbL process. To reduce this, 0.33 M $CaCl_2$ was used during the polyelectrolytes deposition, as Cl^- may reduce the solubility of chlorhexidine in H_2O.[30] The SEM images in Figure 4.9, revealed the morphology change after each layer deposition on the particle surface. With the first PAH layer, the dendritic surface structure could still be identified. As the number of polymer layers increased, the shells became thicker until the chlorhexidine spheres were completely covered (Figure 4.9).

LbL assembly on SiO_2 (0.5-5μm) templates provides thin, smooth homogenous layers as compared with the rougher coatings on the chlorhexidine spheres.[96] There are several explanations; firstly, the LbL assembly of PAH and PSS was carried out with 0.33 M $CaCl_2$. The presence of divalent ions in the polyelectrolyte solutions had a fundamental effect on the conformation of polyelectrolyte molecules. The addition of small amounts of ions may help to rearrange the polyelectrolyte chains and form compact layers,[198] while higher ion addition encourages loop formation.[199] The 0.33 M $CaCl_2$ added to PAH and PSS shielded their charge and may further cause shrinkage of the polymers. Thus the LbL assembly of polyelectrolytes in this state did result in thicker layers compared to LbL assembly without adding salts. A similar observation was found for capsule assembly using NaCl solutions.[200] Secondly, complexation of chlorhexidine with PSS did lead to larger wall thickness. Although the LbL assembly process was carried out in $CaCl_2$, the dissolution of chlorhexidine spheres could not be avoided. The dissolved chlorhexidine molecules may have diffused through the polyelectrolyte shells and formed complexes with the PSS layer, as the sulfonic group of PSS could interact with the amine group of chlorhexidine. According to the cross-sectional image of the chlorhexidine capsule, the shell thickness (SD) was 1.02 (0.25) μm (Figure 4.9). The driving force for polymer absorption is mainly electrostatic interactions, and hydrogen bonding and hydrophobic interactions could also be responsible.[197] It was also suggested that polymer chains had a low diffusion rate and less entropy loss, enabling a high affinity to crystalline drug

surfaces.[201] The outermost positively charged layer of the chlorhexidine capsule may help to attract gram negative bacteria and thus enhance the antibacterial properties.

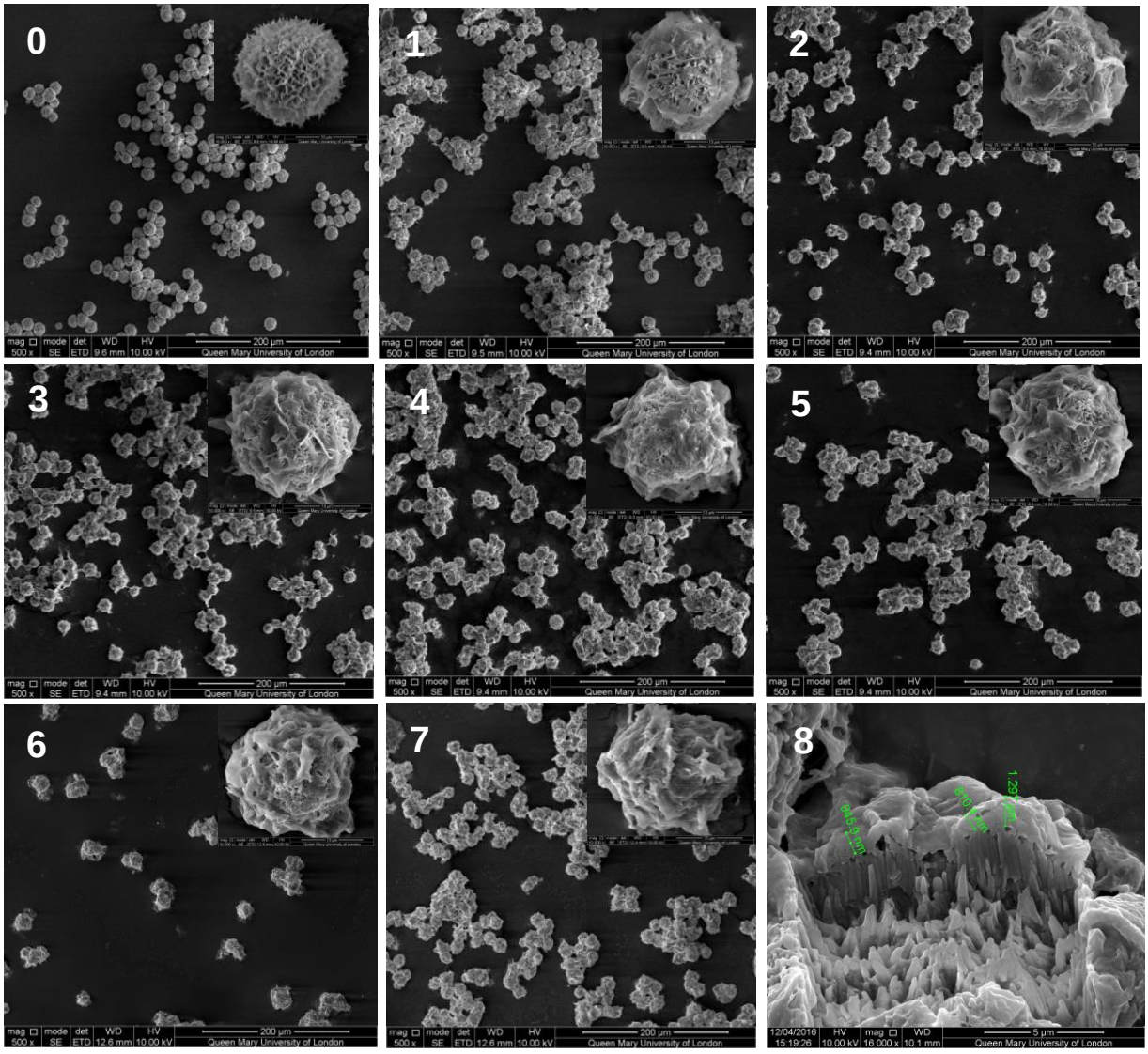

Figure 4.9 SEM images of spherical chlorhexidine particles coated with 0-7 layers of polymers. The inset images are individual particles at high magnification (×8000); Image 8 is the FIB SEM image showing the cross-section of the chlorhexidine capsule.

The chlorhexidine capsules were further characterized with confocal microscopy when the chlorhexidine particle was labelled with RhB and the PAH labelled with FITC. The chlorhexidine particles were still intact after encapsulation (Figure 4.10b) and thick polymer shells were present (green circles, Figure 4.10a). The overlay images (Figure 4.10c) indicated that PAH/PSS had penetrated into the porous chlorhexidine particles, which was in agreement with the FIB /SEM results. According to the inset image of fluorescent intensity, that red fluorescent intensity was strong, whilst the green fluorescent only appeared at the surface (Figure 4.10d). It was a strong evidence of how the PAH and PSS were deposited on the chlorhexidine spheres. Chlorhexidine dissolution during LbL was calculated by measuring the UV-Vis absorption of the supernatant from each layer. Chlorhexidine did dissolve during the LbL assembly process, but only 3wt % was lost after depositing 7 layers. Similarly, confocal microscopy was also used to observe the preservation of fluorescein diacetate crystals from LbL assembly.[202]

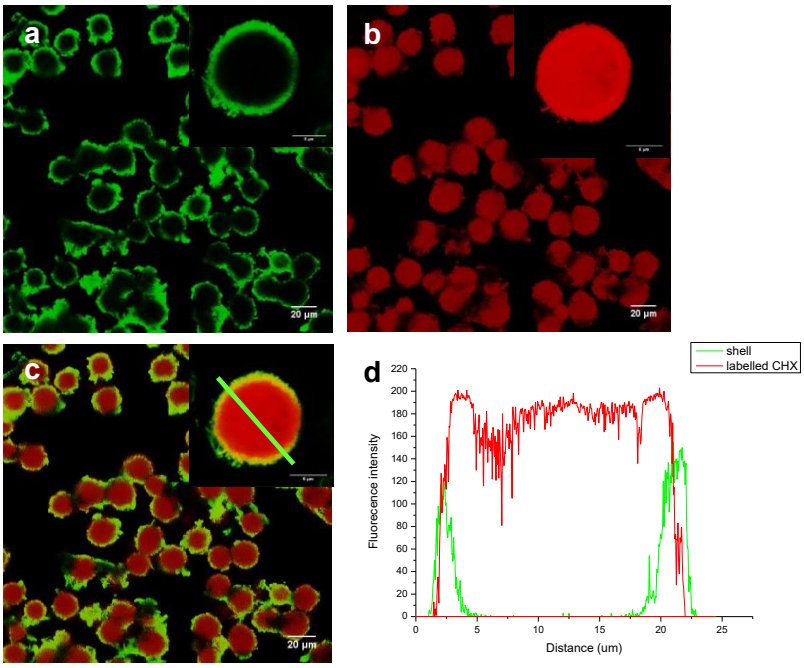

Figure 4.10 Confocal images of chlorhexidine capsules. (a) FITC labelled PAH capsule shells in green channel, (b) RhB labelled chlorhexidine in red channel, (c) overlap image showing the capsule/chlorhexidine relationship, (d) fluorescent intensity across the capsule; the inset images are individual capsules at high magnification.

4.1.2.2 Sustained release of chlorhexidine from LbL capsules

Release kinetics from the capsules was a result of the solubility of the drug, architecture of the polymer multilayers, and the sink condition.[195] In the present work, the release of chlorhexidine from the uncoated spherical particles or capsules was carried out in both H_2O and PBS. The cumulative release curves are presented in Figure 8. Without coating, the chlorhexidine particles were completely dissolved in H_2O within 1 hour, with all the chlorhexidine released. In contrast, the PAH/PSS coated chlorhexidine particles showed a burst release (2 hours) followed by sustained release, and after 7 hours there was still 15 % chlorhexidine within the capsules (Figure 4.11a). The release kinetics for chlorhexidine capsules in PBS was even more sustained, since only 2 % chlorhexidine was released from the capsules after 7 hours. There was a linear relationship between chlorhexidine release and time (r^2=0.99, Figure 4.11b). The sustained release effect was provided by the polymer multilayers, and it was even more obvious for some other insoluble drugs. For Paclitaxel nanocolloids, for instance, release rates after 8 hours could be reduced from 80% (1bilayer of PAH / BSA) to 40%, by the addition of a second bilayer.[107] However, for water soluble drugs, the influence of multilayer coatings was limited; with fluorescein crystal capsules with 18 layers resulting in the dissolution rate starting to level off within 10 mins.[104] Besides the number of layers, the shell architecture also plays a vital role in drug release. The polyelectrolytes the authors used were PAH and PSS and they were assembled in the presence of 0.33 M $CaCl_2$. Therefore, the multilayer shell was thicker than capsules described in the previous literature and less diffusible for small molecules.[200] The mechanism of how the salt within the multilayer films changed the diffusion coefficient was demonstrated by previous study.[203] It is thought that loops formed by polyelectrolytes at high ionic strength and tightly packed polymer layers were less diffusive to small molecules.[203] In terms of the release kinetics in PBS, low release rate and linear release kinetics were mainly

ascribed to low solubility of chlorhexidine, as solubility of chlorhexidine was highly dependent on the salt present in solution.[30] The Cl^- and PO_4^{3-} ions in PBS could greatly reduce solubility of chlorhexidine and it was more likely to saturate during the chlorhexidine release process. The influence of Cl^- and PO_4^{3-} ions on chlorhexidine release kinetics was demonstrated in another experiment by carrying out the release test in a series of descending Cl^- and PO_4^{3-} solutions (Figure 4.12). A remarkable reduction in chlorhexidine release was observed for solutions with Cl^- or PO_4^{3-} concentrations as low as 15.63 mM (Figure 4.12). Compared to the Cl^- solutions, the influence of PO_4^{3-} was even more obvious (at the same ion concentration), as the chlorhexidine release rate in Na_2HPO_4 was lower than that in NaCl. It was feasible that the phosphate ions formed aggregations with the PAH which hindered the diffusion of chlorhexidine. Phosphate ions were reported to bind with polyamine in aqueous solutions, via a defined hydrogen-bonded network, which was stabilized by electrostatic interactions.[146, 204] Therefore, a zero order chlorhexidine release in PBS was observed in our study. Similarly, PAH/PSS coated paclitaxel capsules had more sustained release in PBS and BSA solutions than in H_2O.[105]

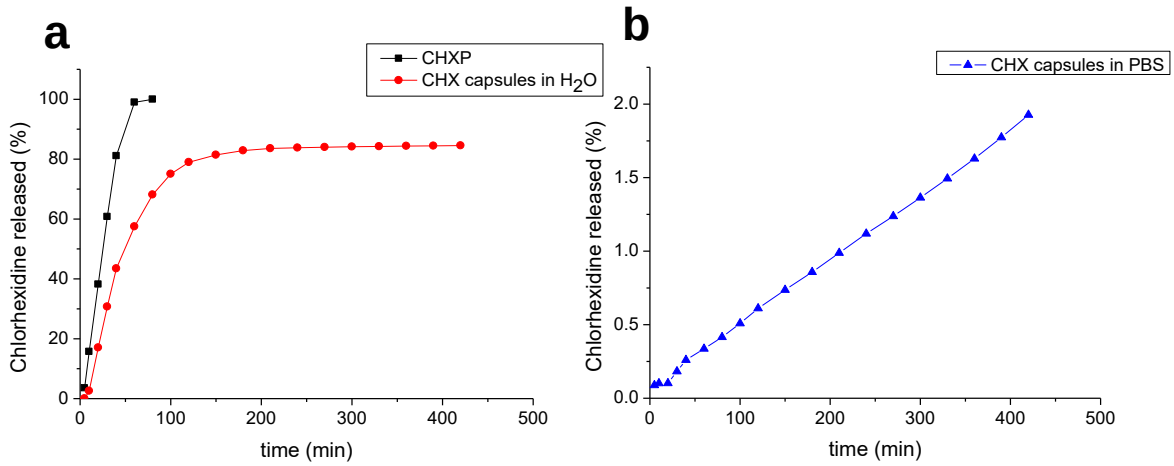

Figure 4.11 Chlorhexidine release kinetics in H_2O and PBS. (a) Release kinetics of uncoated spherical chlorhexidine particles (black line) and chlorhexidine capsules (red line), (b) Release kinetics of chlorhexidine capsule in PBS. Values are the mean of 3 groups and vertical bars represent the SD.

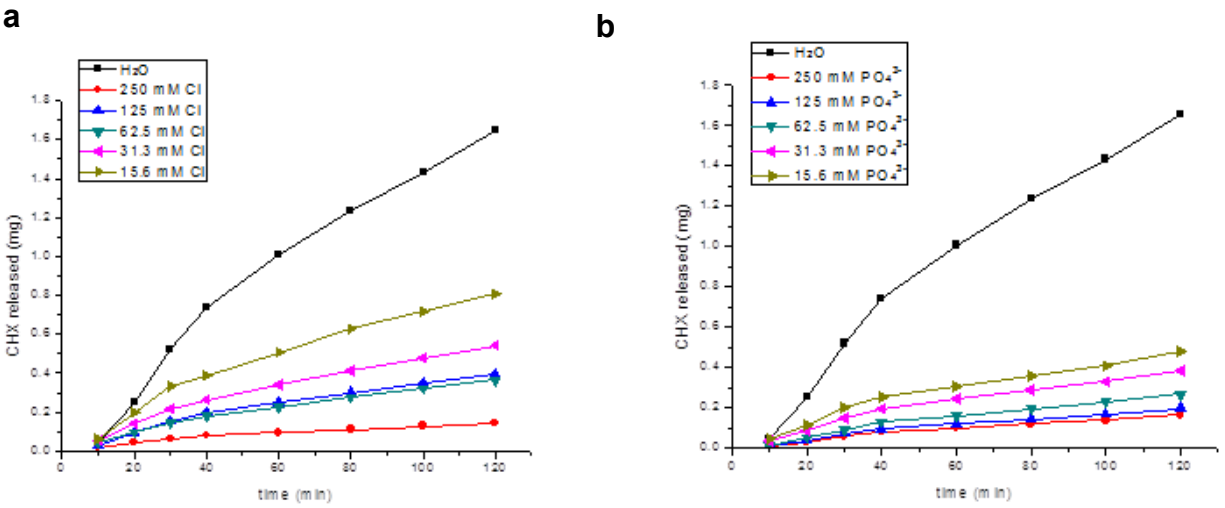

Figure 4.12 Chlorhexidine release kinetics in Cl^- and PO_4^{3-} solutions with different concentration.

Theoretically, the microcapsule assembly from polyelectrolytes were porous and permeable for molecules with molecule weight less than 5 kDa.[96] Chlorhexidine molecules (Mw= 625 Da) may therefore be likely to diffuse out when stored in H_2O, leaving the multilayer shells intact. To illustrate this, the chlorhexidine capsules after the release experiment (H_2O storage, 7 hours) were characterized using SEM (Figure 4.13). The capsules appeared with the center collapsed, indicating that most of the chlorhexidine cores were dissolved and released from the capsules, leaving voids. The collapsed multilayer capsules remained intact and no obvious rupture was observed (Figure 4.13a). Since only 85% of chlorhexidine was released (Figure 4.11a), the remaining drug (15%) inside the capsules suggests that they were not completely hollow, explaining the partially collapsed capsule morphology. PAH/PSS coated ibuprofen and PLL/heparin coated paclitaxel capsules similarly did not show complete drug release in previous studies.[108, 205] The incomplete release of chlorhexidine from the capsules was most likely due to the complexation of chlorhexidine with PSS, as turbidity was observed when mixing chlorhexidine with the PSS solution. By analyzing the PSS and chlorhexidine mixture

with FTIR, the interaction between the sulfonic group of PSS and the amine group of chlorhexidine was confirmed (data not shown). The chlorhexidine and PSS mixture showed peaks at 1621, 3118, 3303 and 3190 cm^{-1} which indicated the chlorhexidine composition. The sulfonic group of PSS had peaks at 1184 and 1042 cm^{-1},[206] which was also identified at the spectrum of PSS-chlorhexidine mixture.

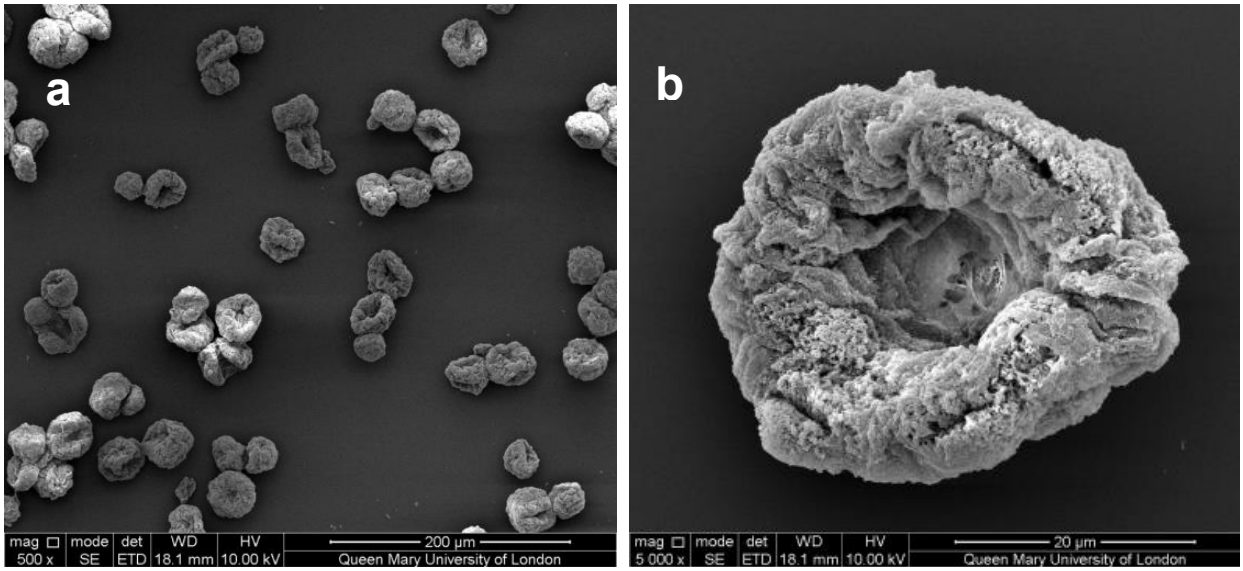

Figure 4.13 SEM images of chlorhexidine capsules after the release test (7 hours in water). (a) chlorhexidine capsules at low magnification, and (b) an individual capsule at high magnification.

Confocal images for the labelled chlorhexidine capsules confirmed the intact polymer shells (Figure 4.14a) and residual chlorhexidine inside the capsules (Figure 4.14b). The overlapping images illustrated that the residual chlorhexidine appeared trapped within the polymer shells (Figures 4.14c, d). This observation was consistent with our hypothesis that residual chlorhexidine formed complexation with PSS in the capsule shells. The highly coordinating ability of guanidinates of the chlorhexidine molecules could form stable complexes with polymers, which was studied in previous research.[31] Chlorhexidine based resins or cements also show reduced release rates, due to chemical bonding of chlorhexidine to polymers.[34, 207]

In terms of capsules size, there was an average 2 μm swelling after 7 hours water storage, which was due to the increased osmotic pressure caused by dissolution of the chlorhexidine core. The chlorhexidine capsules have promising antibacterial applications in dentistry. For instance, they could be injected into periodontal pockets to treat infections,[35] since conventional treatment methods such as chlorhexidine containing mouth rinses may not be able to reach these deep sites. Injection of chlorhexidine capsules into sites of infection could maintain a high local drug concentration and sustained release could also be achieved. Moreover, the LbL architecture could easily be changed to realize a more sustained local release and

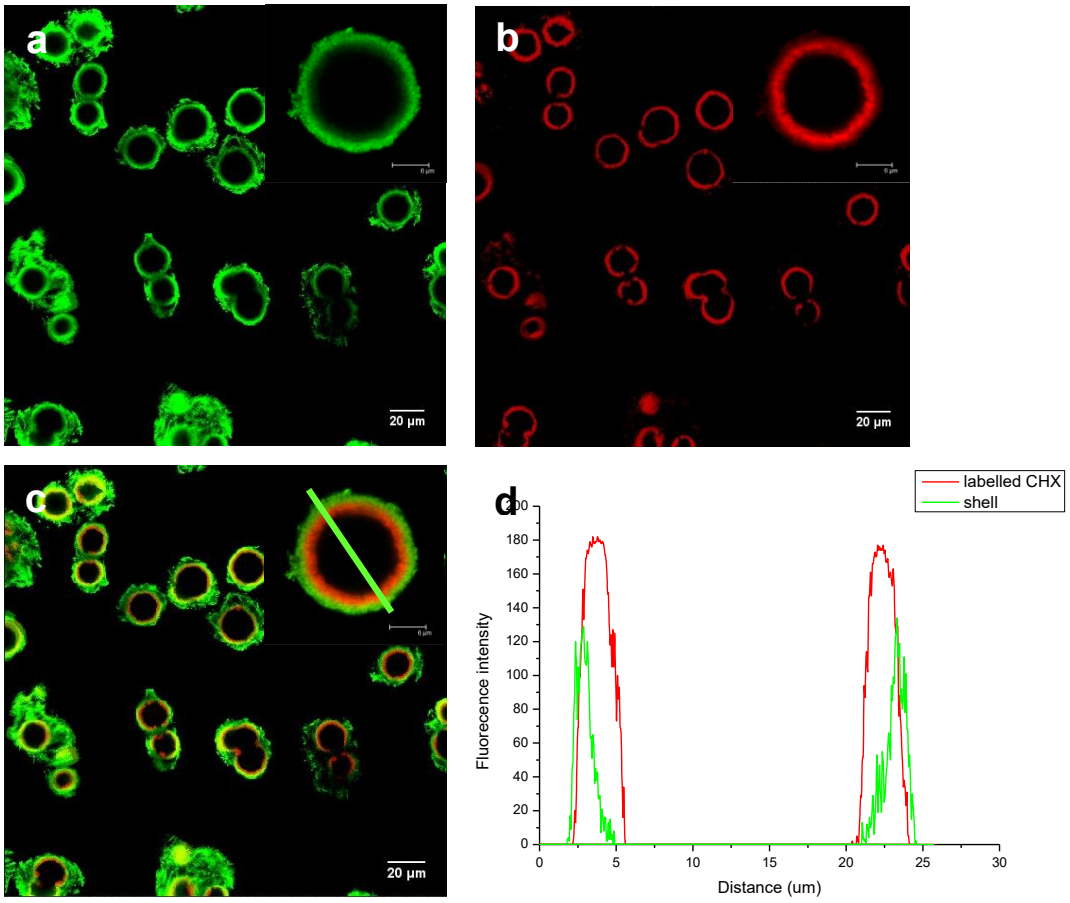

biocompatibility, which will be the focus of our future work.

Figure 4.14 Confocal images of chlorhexidine capsules after the release test. (a) FITC labelled PAH revealing the green capsule shells, (b) RhB labelled chlorhexidine showing residual chlorhexidine, (c) overlap image showing the capsule/chlorhexidine relationship, (d)

fluorescent intensity across the capsule; the inset images are individual capsules at high magnification.

4.1.2.3 PLA encapsulation of chlorhexidine spheres by spray

Since the LbL encapsulation process is quite time consuming and dissolution of chlorhexidine always happens, one step encapsulation by spray-drying would be advantageous. Spray-drying has a higher drug encapsulating rate than any other methods, since all the dissolved substances will precipitate when the solvent evaporates. Therefore, in this part, chlorhexidine particles encapsulation was also carried out using the spray-drying method. Freezing dried chlorhexidine particles are mixed in PLA solutions (Roto Mix) and sprayed immediately to reduce the dissolution of chlorhexidine. The resulted encapsulated particles are presented in Figure 4.15. Without any chlorhexidine particles added, the spray dried PLA particles showed a collapsed morphology and there were pores on the surface of collapsed PLA particles (Figure 4.15a). When chlorhexidine particles were added at a 1:3 ratio to PLA solution, and spray dried, a very thin layer of PLA was revealed on surface of chlorhexidine particles. The typical needle-like surface structure of chlorhexidine particles could still be identified. Similar to the observation of control group, the layer of PLA covered on the surface was also porous (Figure 4.15b). When the ratio of chlorhexidine to PLA was reduced to 1:5, a thicker layer of PLA was deposited on the chlorhexidine particle surface, and the surface was relatively smoother (Figure 4.15c). The chlorhexidine to PLA ratio was tuned because a ratio higher than 1:3 more likely lead to aggregations of particles and a too low ratio would result in large amount of empty particles. From the view of spray-drying, once of the PLA solution was atomized, small droplets were formed in the air and the solvent of the droplet surface was first to evaporate. A fast evaporate of solvent from the surface would lead to solidifying of PLA from the solution and porous surface morphology. By replacing with a lower boiling point solvent (such as dichloromethane),

a more porous surface morphology could be seen (data not shown). With a further evaporation, the solvent in the middle of droplets also got dried, resulting a shrinkage in droplet volume and collapse of produced PLA particles. For the solutions containing chlorhexidine particles, when atomized, solvent evaporation also started from the surface but for the droplets with particles inside, a further collapse was avoided. It explained why much solider particles were observed from the SEM images. But there were still collapsed particles presented which might due to the formation of empty PLA droplets. An increase of PLA concentration did help to enhance the encapsulation of chlorhexidine particles as thicker coating was observed. But it also leaded to an increase of aggregation of particles as the viscosity of solution was increased at the same time.

The encapsulation of chlorhexidine particles was also presented by confocal images when the chlorhexidine particles were labelled with RhB (Figure 4.16). From the overlapped image, all the particles showed red fluorescence. Theoretically, only the PLA particles with chlorhexidine encapsulated would demonstrate fluorescence, but the debris also had a red signal which might be due to dissolution of chlorhexidine particles during the mixing procedure. As the chlorhexidine particles were dispersed in the PLA solution, the dissolved chlorhexidine would homogeneously distribute. Once atomized, there was chlorhexidine remaining in the empty PLA droplets, which leaded to fluorescent for empty PLA particles. However, the fluorescence intensity was not as strong as the chlorhexidine particle encapsulated particles.

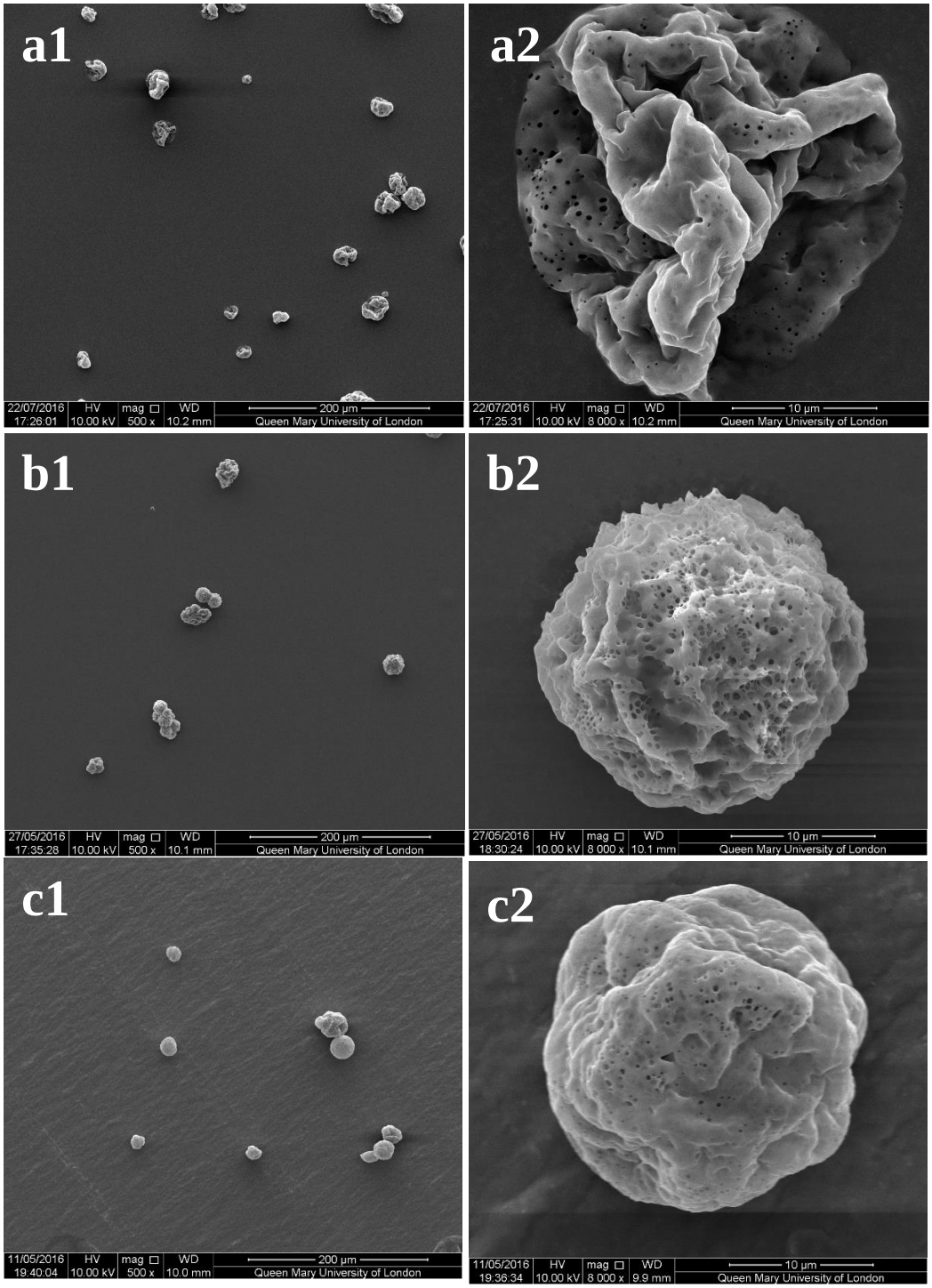

Figure 4.15 SEM images of spray dried PLA particles. (a) control group without chlorhexidine particles added; (b) PLA encapsulated chlorhexidine particles at CHX to PLA ratio of 1:3; (c) PLA encapsulated chlorhexidine particles at CHX to PLA ratio of 1:5.

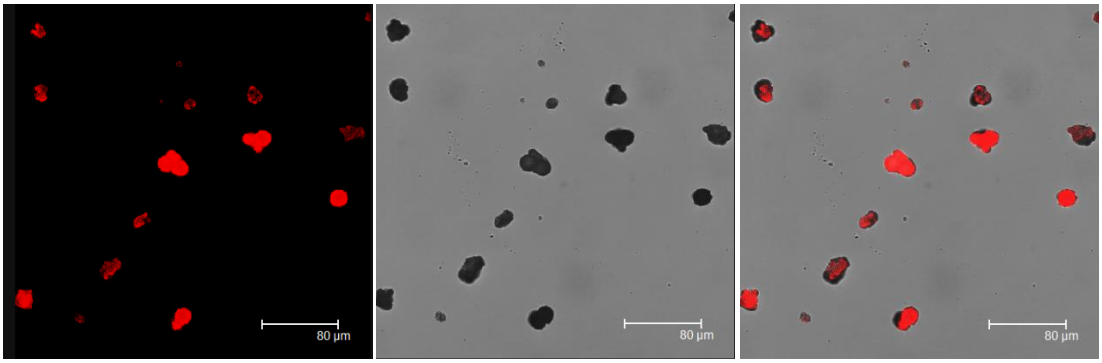

Figure 4.16 Confocal images of PLA encapsulated chlorhexidine particles.

4.1.2.4 Release kinetics of chlorhexidine from PLA capsules

Release kinetics of chlorhexidine from the PLA encapsulated capsules was showed in Figure 4.17. Similar to the release kinetics of LbL encapsulated chlorhexidine particles, the coating of PLA layer can significantly reduce the release rate. Without any coating, the chlorhexidine particles just dissolved within an hour. But with thin PLA coating, the release rate was much slower during the first hour and started to level off then, which after 5 hours there was 58.9% chlorhexidine released. When the thickness of PLA coating was increased, more sustained release was observed and release curve levelled off after 3 hours. It is assumed that with the coating of PLA, chlorhexidine diffusion is hindered and thicker the PLA layer, the harder for chlorhexidine to diffused out. Similar to the release principle demonstrated earlier with the LbL coating. However, since the PLA layer is hydrophobic, the chlorhexidine release rate was lower than that with a LbL coating. Also, the remaining chlorhexidine encapsulated in the particles after a few hours' release test was also higher. It is explainable that since the PLA is hydrophobic while the polyelectrolyte layers are hydrophilic, chlorhexidine trapped in the PLA polymers will not be likely to diffuse out within a few hours. The release of remaining chlorhexidine would be dependent on the degradation of PLA polymers. As demonstrated in most of the cases of drug delivery with polymeric particles.

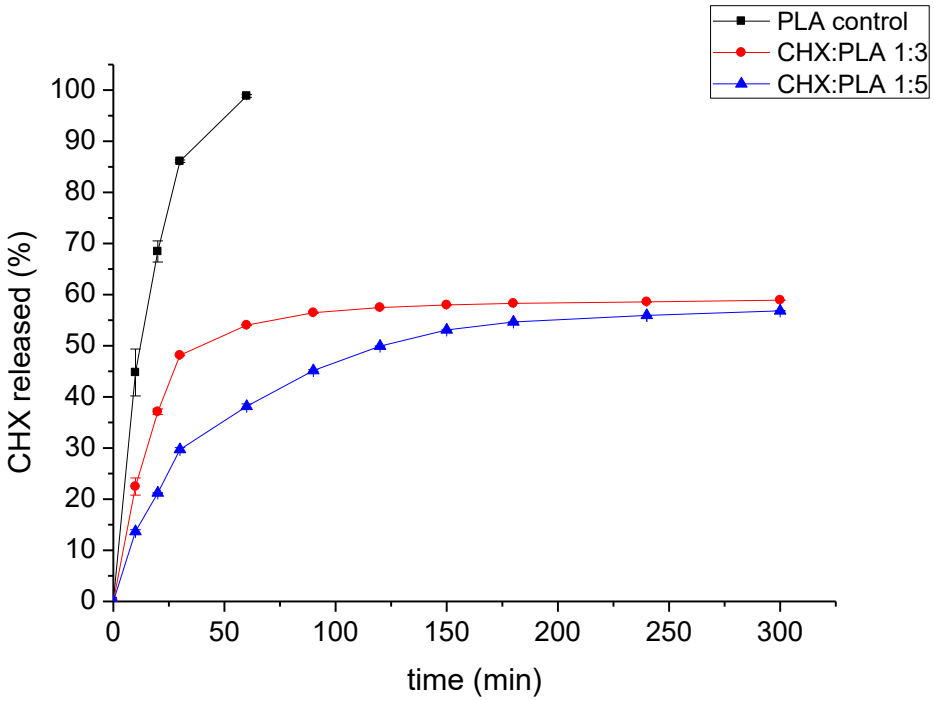

Figure 4.17 Release kinetics of chlorhexidine from encapsulated particles.

The PLA coated chlorhexidine particles after release test were further characterized with SEM. As demonstrated in Figure 4.18, individual solid particles were still identified, however, some of the particles collapsed with only porous PLA shells remained. It was more obvious at a higher magnification, and for the solid particles, some collapse was also observed. It clearly showed that the chlorhexidine particles with a thin PLA coating were more likely released and these with thicker coating, more chlorhexidine was remained in the particles. It was also confirmed by the confocal images (Figure 4.19) that some of red rings were observed after release which indicated released particles and remaining PLA shells, while the other particles were still solid with strong fluorescence. Interestingly, all the debris was still fluorescent which was in agreement with our hypothesis that the release kinetic of this part of chlorhexidine was dependent on PLA degradation.

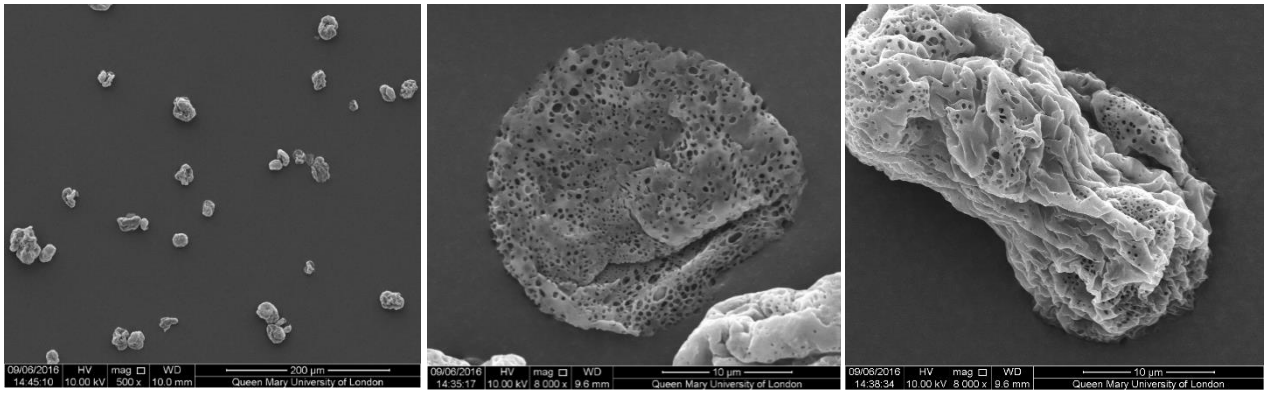

Figure 4.18 SEM images of PLA encapsulated chlorhexidine particles after release.

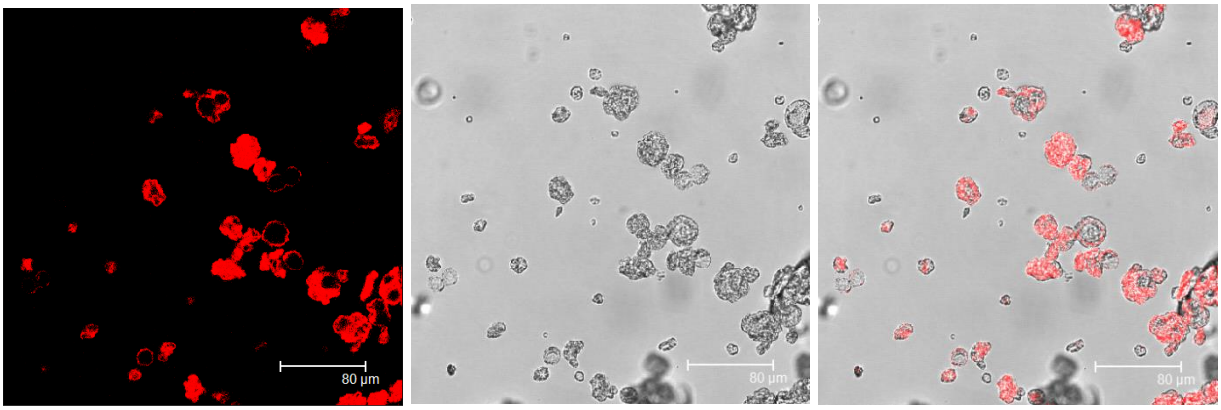

Figure 4.19 Confocal images of PLA encapsulated chlorhexidine particles after release.

4.1.2.5 Chlorhexidine particles imbedding in HEMA-UDMA resin

Once the chlorhexidine spheres were incorporated into resin composites or resin-modified glass-ionomer cements, antimicrobial properties are enabled, and actually this was extensively studied in the last decades by directly incorporating chlorhexidine diacetate crystals [39, 208]. Here, chlorhexidine particles were incorporated into resin and the cross-section images of the filled resin discs are shown in Figure 4.20. As compact and irregular morphology characteristics of chlorhexidine diacetate crystals, the resin could not penetrate the crystals and clear boundary between drug crystals and resin was observed (Figure 4.20a). However, homogeneous

distribution of particles in resin was evidenced and the porous surface morphology of chlorhexidine particles allowed resin to penetrate and there was good coherence at the resin /particle interface for the UDMA-HEMA resin (Figure 4.20b). And no evidence of dissolve or damage of particles was observed, indicating that intact spherical chlorhexidine particles could be preserved during the incorporating process.

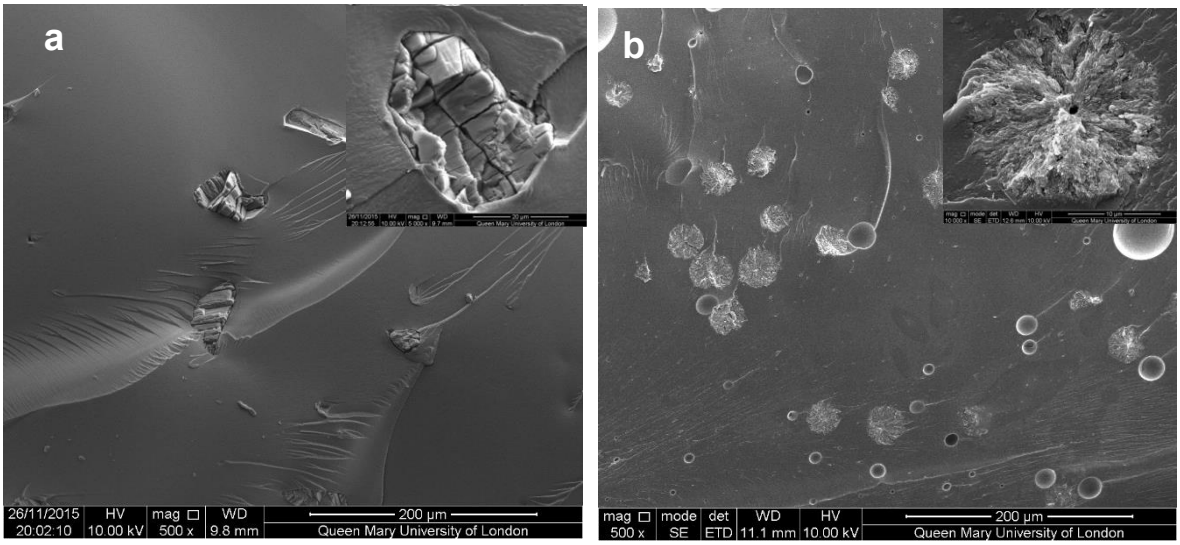

Figure 4.20 Cross-section of resin discs with chlorhexidine diacetate (a) and spherical chlorhexidine particle (b).

4.1.3 Electrospinning PLA fibres with chlorhexidine spheres

4.1.3.1 Fabrication of chlorhexidine fibres

Chlorhexidine was incorporated into the PLA fibers by electrospinning. The SEM images of the fabricated fibers (Figure 4.21) indicate a regular fibrous structure. When the chlorhexidine particles were incorporated a beard-in-string structure was demonstrated, in which the spheres were connected by two ends, with one fiber end much thicker than the other. For the fibers with chlorhexidine particles, a very thin layer of PLA covered the particle surface and the interconnected structure could still be seen (Figure 4.21b). In contrast, when the chlorhexidine particles were encapsulated and electrospun into fibers, a rougher appearance was observed (Figure 4.21c). The mean diameter (SD) of the PLA fibers (control) was 1.35 ± 0.06 μm. When the content of the chlorhexidine was increased (from 0.5% to 25%) the diameter of fibers decreased, as demonstrated in Figure 4.22. There was no significant difference when the chlorhexidine content was below 10%. Further increasing the ratio to 25 % (wt/wt), the chlorhexidine particles significantly ($p<0.01$) reduced the fiber diameter to 0.96 ± 0.06 μm. After incorporating CHX, the mechanical properties of the PLA electrospun fibre mat were also decreased (Table 4.2). While, the contact angle test showed that wettability of fibers was not affected by particle incorporation (123.6±3.7º for control and 121.6±7.2º for 5.0 wt/wt CHX fibers). The uncoated and encapsulated chlorhexidine particles within the fibers could be clearly seen in the confocal images (Figure 4.23). The black shadow around the chlorhexidine particles in the merged images indicates the PLA layer (Figure 4.21 a2). The chlorhexidine particles were still intact after electrospinning and FTIR spectra confirmed the presence of chlorhexidine in the fibers (data not shown).

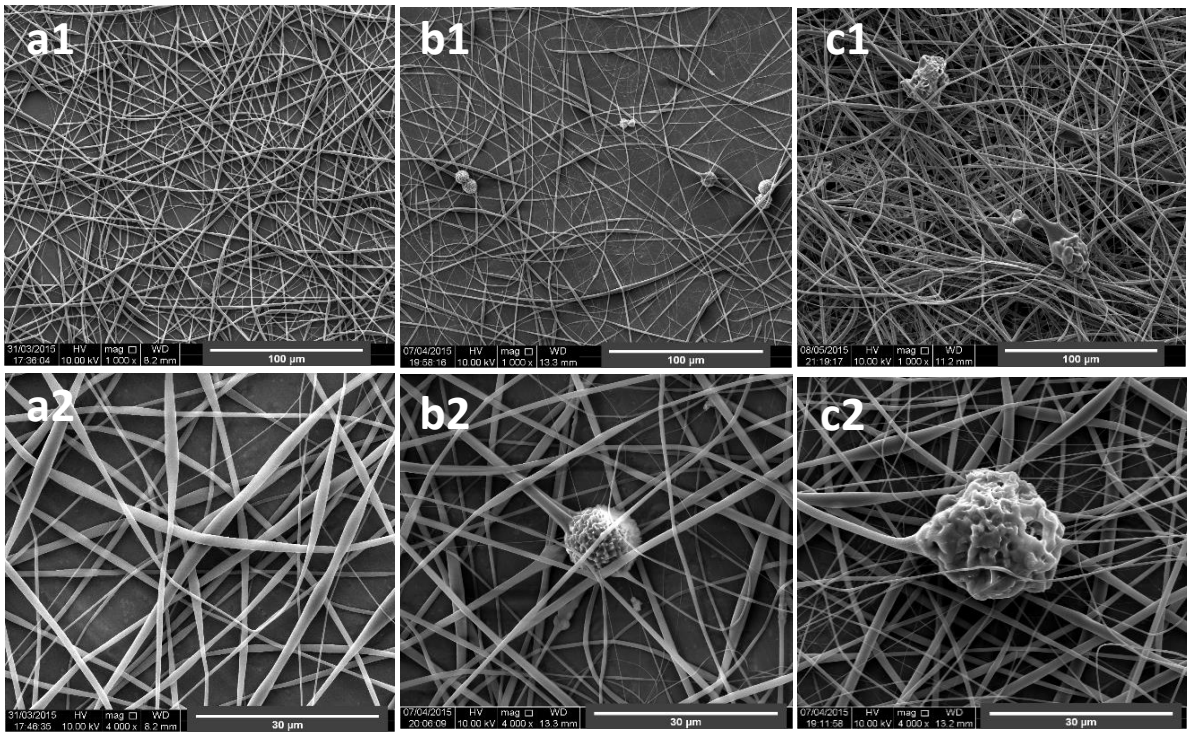

Figure 4.21 SEM images of electrospun fiber. (a) PLA fibers as a control; (b) fibers with chlorhexidine particles; (c) fibers with encapsulated chlorhexidine particles at a magnification of (1) 1000× and (2) 4000×.

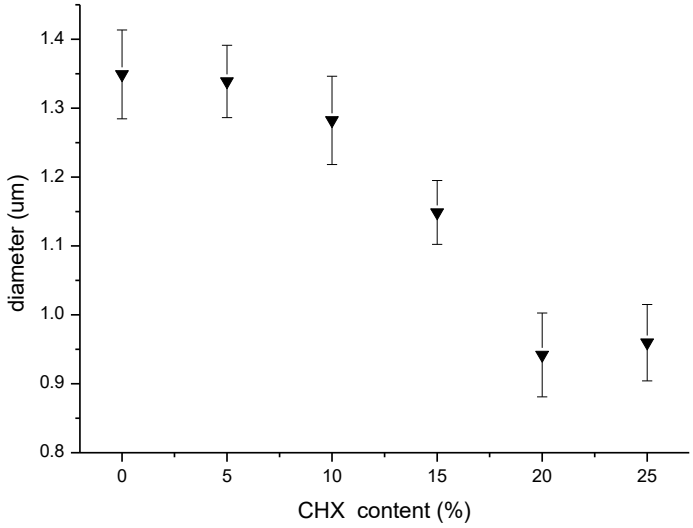

Figure 4.22 Mean (SD) diameter of the PLA fibers as a function of chlorhexidine particle content.

Table 4.2 Tensile properties of PLA fibers containing different amount of chlorhexidine.

Sample name	Young's modulus (MPa)*	Elongation at break (%)	Strength (MPa)
PLA fibre	31.32±5.85	30.43±2.38	1.55±0.14
PLA fibre-0.5% CHX	25.63±3.06	11.89±1.73	0.70±0.05
PLA fibre-1.0% CHX	10.47±1.14	13.84±0.41	0.37±0.02
PLA fibre-5.0% CHX	11.75±1.81	13.40±0.63	0.36±0.02

* Young's modulus was calculated by the slope of the stress-strain curve at 1% strain

According to previous research, the embedding of micro particles resulted in defects and notches in the fibers, but the diameter of the fibers was increased and mechanical properties enhanced [209-210]. The addition of chlorhexidine particles in PLA fibers in the current study did not lead to obvious defects in the fibers, but it did have significant effect (when CHX loading was over 15 % wt/wt) on fiber diameter as a narrowing effect was observed at the distal end, adjacent to the particle. The addition of micro particles (calcium carbonate and HA particles until a 5 % addition) into electrospun polymer solutions previously increased their viscosity, and thus led to an increase of fiber diameters [209-210]. However, the average fiber diameter was dramatically reduced by adding the chlorhexidine particles, which may be associated with the size and volume fraction of the introduced particles, as the diameter of chlorhexidine particles was much larger (17.15 ± 1.99 μm) than the electrospun fibers [91]. Significant amounts of PLA were required to coat and penetrate these larger particles which may have drawn the fibers thinner. The shear force generated during electrospinning may be another explanation, which is strong enough to lead to deformation of spherical particles into ellipsoidal particles [211]. Thus the proximal side of the fiber was always thicker than the distal side. These characteristics of the fibers also led to a mechanical property decrease (Table 4.2). As for the wettability of fibers, it is assumed that all the chlorhexidine particles were covered by a thin layer of PLA, so the hydrophilicity of fiber mesh was not affected. The chlorhexidine was also concentrated in the

particles instead of distributed freely all over the fibers, which may minimize the effect on wettability of fibers.

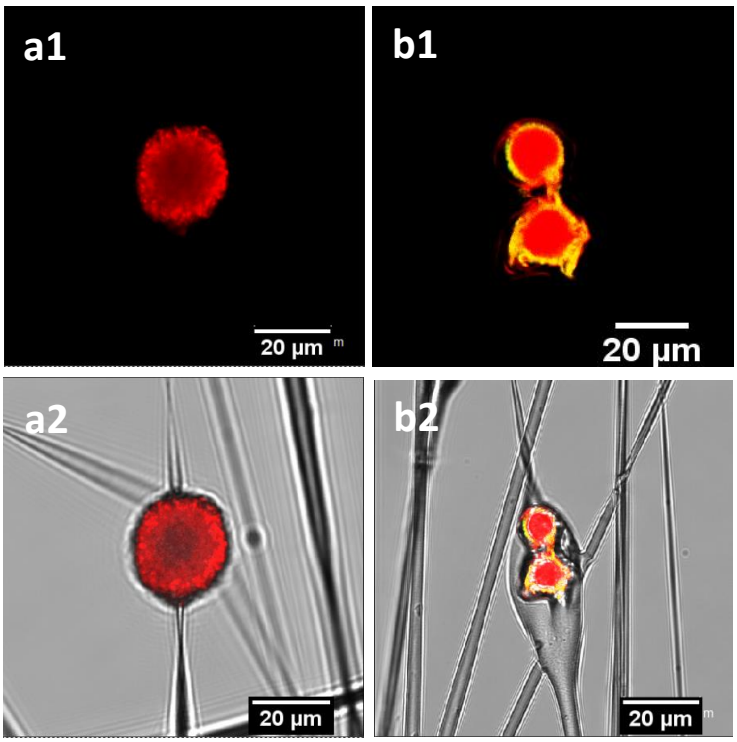

Figure 4.23 Confocal images of: (a) PLA fibers with chlorhexidine particles; (b) fibers with encapsulated chlorhexidine particles (1) in the red channel and (2) merged images with the transmitted channel. Chlorhexidine particles were labelled with RhB and one of PAH layers was labelled with FITC; the yellow colour indicates the overlap of core and shell.

4.1.3.2 Release kinetics of chlorhexidine from fibres

The release profile of chlorhexidine from the PLA fibers containing the chlorhexidine particles was monitored over 650 hours (Figure 4.24). In H_2O the fibers with chlorhexidine particles showed a burst release during the first day, with over 60% of the chlorhexidine released, after which a sustained release was observed. In contrast, the fibers with encapsulated particles displayed a lower (20-25%) sustained release of chlorhexidine. In PBS, both of the fibers had

much lower release rates compared to that in H_2O, and chlorhexidine encapsulation again produced a lower but sustained release rate (Figure 4.24b).

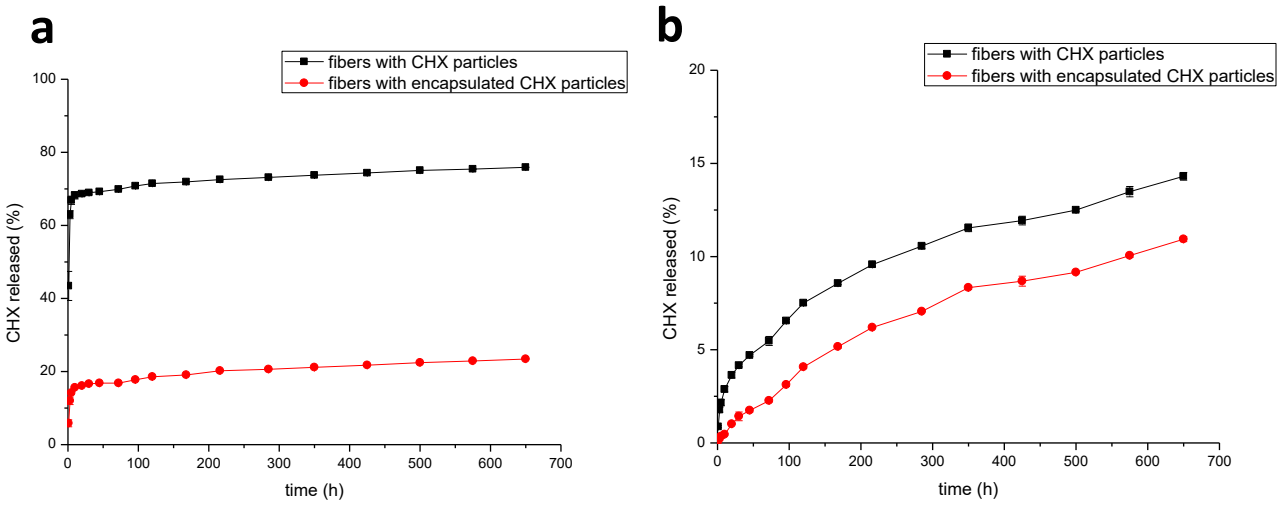

Figure 4.24 Release kinetics of chlorhexidine particle containing fibers in: (a) H_2O and (b) PBS. The PLA fibers with chlorhexidine particles and encapsulated chlorhexidine particles had a chlorhexidine content of 5 % (wt/wt).

The morphology of fibers after the release test in H_2O are shown in Figure 4.25 (a-f). For the fibers containing chlorhexidine particles, most of the chlorhexidine was released and the collapsed spheres were observed (Figure 4.25a). The porous surface of the collapsed sphere revealed the original morphology, indicating that the PLA layer had been penetrated. Fibers containing encapsulated chlorhexidine particles retained more of their surface coating and chlorhexidine content in the collapsed spheres (Figure 4.25d). These observations were confirmed by confocal imaging, as in the fibers with chlorhexidine particles virtually no chlorhexidine was identified (little signal was detected at the red channel), and voids could be seen in the transmitted channel (Figure 4.25 b, c). However, for the fibers with encapsulated particles some chlorhexidine remained inside the fiber, although small voids could be seen

(Figure 4.25 e, f). As for fiber release in PBS, most of the chlorhexidine remained in both of the fibers and corresponding SEM images and confocal images are not showed.

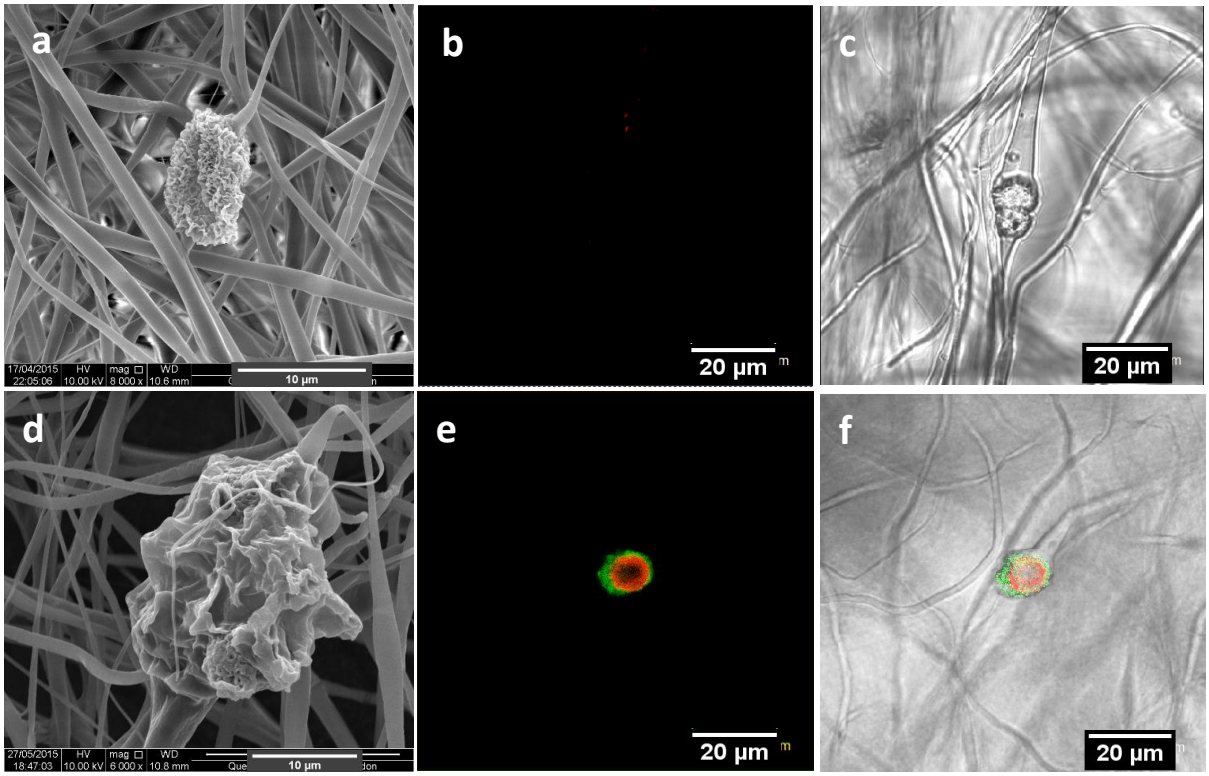

Figure 4.25 SEM and confocal images of electrospun fibers after the 650 h release test. (a, d) SEM images of fibers with chlorhexidine particles and encapsulated chlorhexidine particles; (b, e) confocal images of fibers containing chlorhexidine particles and encapsulated chlorhexidine particles; (c, f) and shown in the merged transmitted channel.

The encapsulation of chlorhexidine spheres by PLA or polyelectrolytes had a fundamental influence on chlorhexidine release kinetics in H_2O, although both kinds of fibers displayed a burst release at the beginning and sustained release afterwards. In order to avoid dissolution of chlorhexidine crystals the electrospun solutions were freshly prepared, and fibers immediately spun. The dissolved chlorhexidine in the fibers may have caused the burst release at the beginning of the release experiment in water. Comparing the difference in the fibers containing

chlorhexidine particles and encapsulated chlorhexidine particles, it is clear that with polyelectrolyte shells it was harder for chlorhexidine to diffuse out. Mixing metronidazole with polymer solutions and electrospinning gave over 90% metroniodazole release from the fibers within the first two days. However, by pre-loading metronidazole in halloysite clay nanotubes a sustained release was achieved [90]. Various carriers such as mesoporous silica or ZnO nanoparticles have been employed to load drugs before electrospinning into fibers to achieve sustained release [87, 212-213]. Electrospinning the LbL encapsulated drug crystals demonstrated another approach, as the LbL shells were already proven to be effective to reduce drug dissolution and diffusion [107-108], and their drug loading rate is much higher than other carriers. Moreover, the release can be further tuned by adjusting the number of deposited polyelectrolyte layers and the type of polyelectrolytes.[32]

4.1.3.3 Cytotoxicity and cell adhesion on chlorhexidine fibres

Cytotoxicity of the fibers (containing particles) to the fibroblasts is shown in Figure 4.26. The fibers containing uncoated and encapsulated chlorhexidine particles with 0.5 % and 1 % (wt/wt) chlorhexidine were not toxic to cells over a period of 5 days, as there was no statistical difference ($p>0.05$) in cell viability between the PLA control and the two test groups. When the chlorhexidine content in the fibers was increased to 5 % (wt/wt), the fibers containing the uncoated chlorhexidine particles reduced the cell viability significantly over 1 day ($p< 0.05$) and more than 2 days ($p< 0.01$). While the fibers with encapsulated particles (5 % chlorhexidine loading ratio) showed better compatibility with cells, with slight cell viability reduction at day 2 and day 5 ($p< 0.05$).

Cell adhesion to the fibers is another indicator of potential cytotoxicity, as demonstrated in Figure 4.27. The number of fluorescent cells on the thin fibers directly reflected the influence

of chlorhexidine content, with fewer cells on the 5 % (wt/wt) chlorhexidine containing fibers than those on the control PLA fibers. The cells appeared less spread out on the fibers and more round shaped cells were observed, which may suggest toxicity at 5 % (wt/wt) chlorhexidine content. Fibers with less chlorhexidine (0.5 and 1 % wt/wt) in the fibers, encouraged cell adherence to the fibers, with typically elongated cell filopodia extensions [90]. A similar observation was made for fibers with encapsulated chlorhexidine particles (data not shown).

The toxicity of chlorhexidine to cells is dose and time dependent, and it was reported that chlorhexidine concentration over 1 µg/ml was toxic to 3T3 cells.[214-215] The chlorhexidine content in the fibers with 5 % (wt/wt) encapsulated particles was 50 µg/ml, which showed no cytotoxicity after 24 hours. Though, cell viability slightly decreased over the 5 days, it still showed much better compatibility over fibers with uncoated particles. We can assume that by chlorhexidine particle encapsulation, the release kinetics is better governed, which ensures a safer performance. Previous work reported that drug crystals encapsulated by LbL shells could reduce toxicity and side effects,[105, 216] and this is in agreement with the current study. Adherence of cells to the fibers was also evidence of good biocompatibility, as cells could adhere, bridge and communicate with the neighbouring cells on the fiber membranes, as revealed with SEM and confocal 3D imaging.[90, 217] Therefore, the PLA fibers produced here are advantageous to ensure a safe performance.

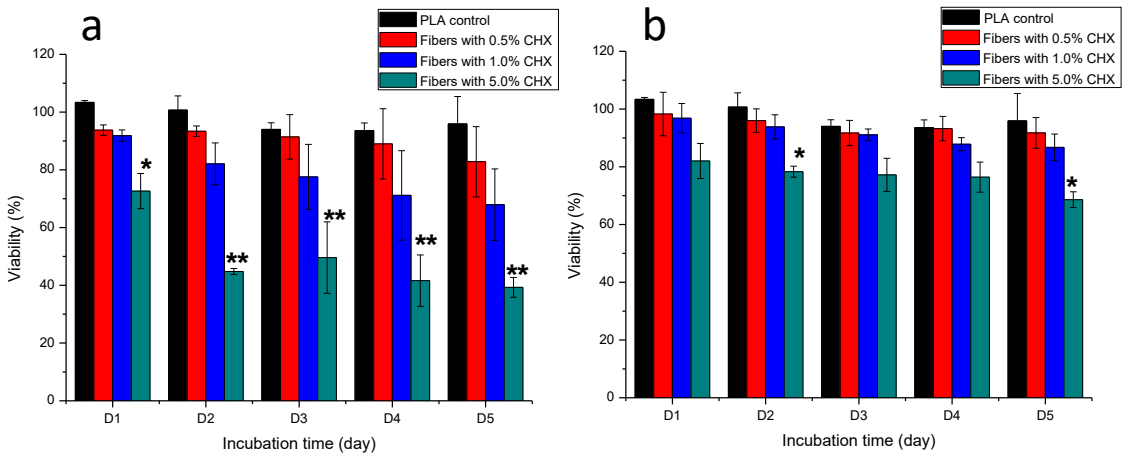

Figure 4.26 Cytotoxicity of chlorhexidine containing fibers with fibroblast cells (3T3). PLA fibers containing chlorhexidine particles (black) and encapsulated chlorhexidine particles (red). Values are the mean of 5 wells and vertical lines are SD, *p< 0.05 and **p< 0.01 indicate statistical differences compared to the control PLA fiber treated cells; ## indicates statistical differences between cells treated by fibers with chlorhexidine particles and encapsulated chlorhexidine particles (p < 0.01).

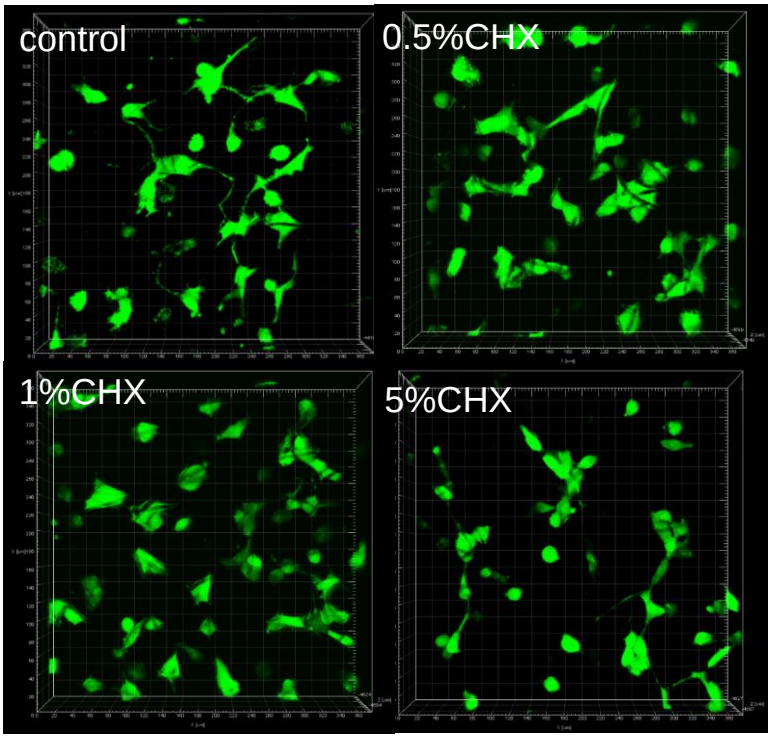

Figure 4.27 3D images of fibroblast adhesion on PLA fibers containing chlorhexidine particles with chlorhexidine loading ratio at 0.5, 1 and 5 % (wt/wt).

4.1.3.4 Antimicrobial activity of chlorhexidine fibres

Antibacterial activity of the fibers against *E. coli* is presented in Figure 4.28. The diameter of clear zone is an indication of the inhibitory effect of the chlorhexidine containing fibers, with higher chlorhexidine ratio in the fibers leading to large inhibition zones. No inhibition against *E. coli* was observed for the control PLA discs. For fibers with chlorhexidine particles, large inhibition zones were observed for all the fiber discs with chlorhexidine ratio at 0.5, 1 and 5 % (wt/wt), and higher chlorhexidine loading rates resulting in larger inhibition zones. In contrast, the inhibitory zones were only observed at 1 and 5 % (wt/wt) for the fibers with encapsulated chlorhexidine particles, which resulted in much smaller inhibitory diameters ($p<0.01$).

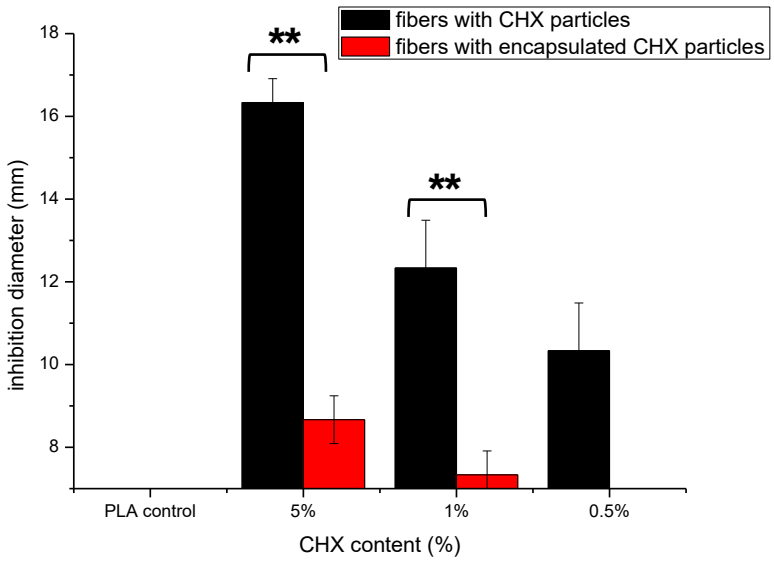

Figure 4.28 *In vitro* inhibition of chlorhexidine containing fibers against *E. coli* using an agar diffusion assay. PLA fibers containing chlorhexidine particles (black) and encapsulated chlorhexidine particles (red), and fibers without chlorhexidine were used as a control, **p< 0.01 indicates statistical differences between the two types of fibers (n=3).

The sustained inhibition effect against *E. coli* was demonstrated by a transfer experiment (Figure 4.29). The chlorhexidine burst release (uncoated particles) within one hour inhibited proliferation of *E. coli* in LB broth suspensions over the next 24 hours. For the control (untreated bacterial suspensions), the bacteria proliferated and a turbidity around 0.8 was found after 24 h (green line). However, 5 % (wt/wt) chlorhexidine in both the fiber containing chlorhexidine particles and encapsulated chlorhexidine particles completely inhibited bacterial growth even after nine transfers (black line, Figure 4.29 a, b). When the chlorhexidine content in the fibers was reduced to 1 % (wt/wt) (red line), no inhibition was observed for the fibers with encapsulated particles and the inhibition effect against *E. coli* depleted quickly after 4 transfers for fibers containing the chlorhexidine particles. Similar observations were displayed for the fibers with 0.5 % (wt/wt) encapsulated chlorhexidine particles (blue line).

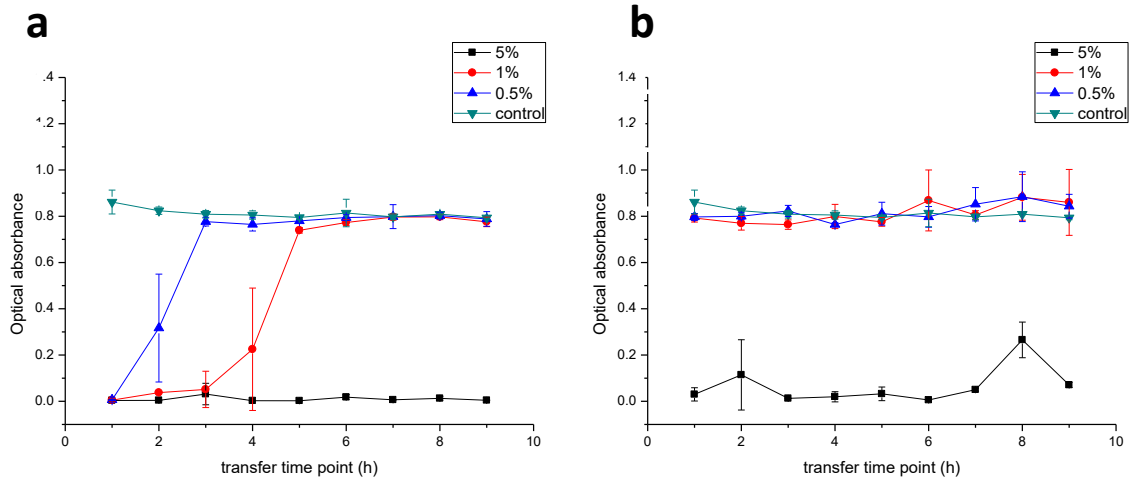

Figure 4.29 *In vitro* inhibition of chlorhexidine containing PLA fibers against *E. coli* using a broth transfer assay. Chlorhexidine loading rate in fibers containing; (a) chlorhexidine particles and (b) encapsulated chlorhexidine particles were 0.5 % (blue), 1 % (red), and 5 % (black) (wt/wt); PLA fibers without chlorhexidine were used as a control (green) (n=3).

Substantial inhibition of the proliferation of bacteria was demonstrated by the agar diffusion inhibition assay. Different bacterial strains have different sensitivities to chlorhexidine concentration, and the minimum inhibitory concentration (MIC) for *E. coli* is 2-8 μg/ml [86]. At lower concentrations, chlorhexidine only interferes with the metabolism of the bacteria [218]. As demonstrated, fibers with 0.5 % (wt/wt) chlorhexidine particles still indicated inhibition against *E. coli*, and the inhibition diameters were substantially affected by the diffusion manner of chlorhexidine in agar. For the fibers containing encapsulated chlorhexidine particles, the dissolution and diffusion of chlorhexidine was effectively hindered, and thus the inhibitory zone of bacterial growth was significantly smaller than the fibers with chlorhexidine particles. Similarly, the sensitivity against *E. coli* was reduced, as proven by comparing chlorhexidine particles and encapsulated chlorhexidine particles at equivalent doses (Figure 4.30). This was consistent with the LB broth transfer results that indicated a sustained inhibitory effect against E. coli for the fibers containing encapsulated chlorhexidine particles at a high chlorhexidine loading ratio (5% wt/wt). However, for 0.5 % or 1 % wt/wt chlorhexidine concentrations, no inhibition against E. coli was observed within one hour transfers (Figure 4.29 b). Bacterial inhibition may be therefore based on contact between chlorhexidine and the bacterial cell membrane, with complete isolation of chlorhexidine particles through encapsulation reducing the chance of direct contact between chlorhexidine particles and *E. coli*, regardless of whether it was dissolved or not. For localized treatment of infections, a sustained release of antibacterial agents is preferred, and thus controlled release by chlorhexidine encapsulation could be beneficial. More interestingly, a combination of uncoated chlorhexidine particles and encapsulated chlorhexidine particles in the same fibers may lead to a burst release at the beginning and more sustained release in the long term, which is attractive for the treatment of bacterial infections [2]. However, to validate the performance of chlorhexidine PLA fibers in our study, further *in vivo* testing is needed.

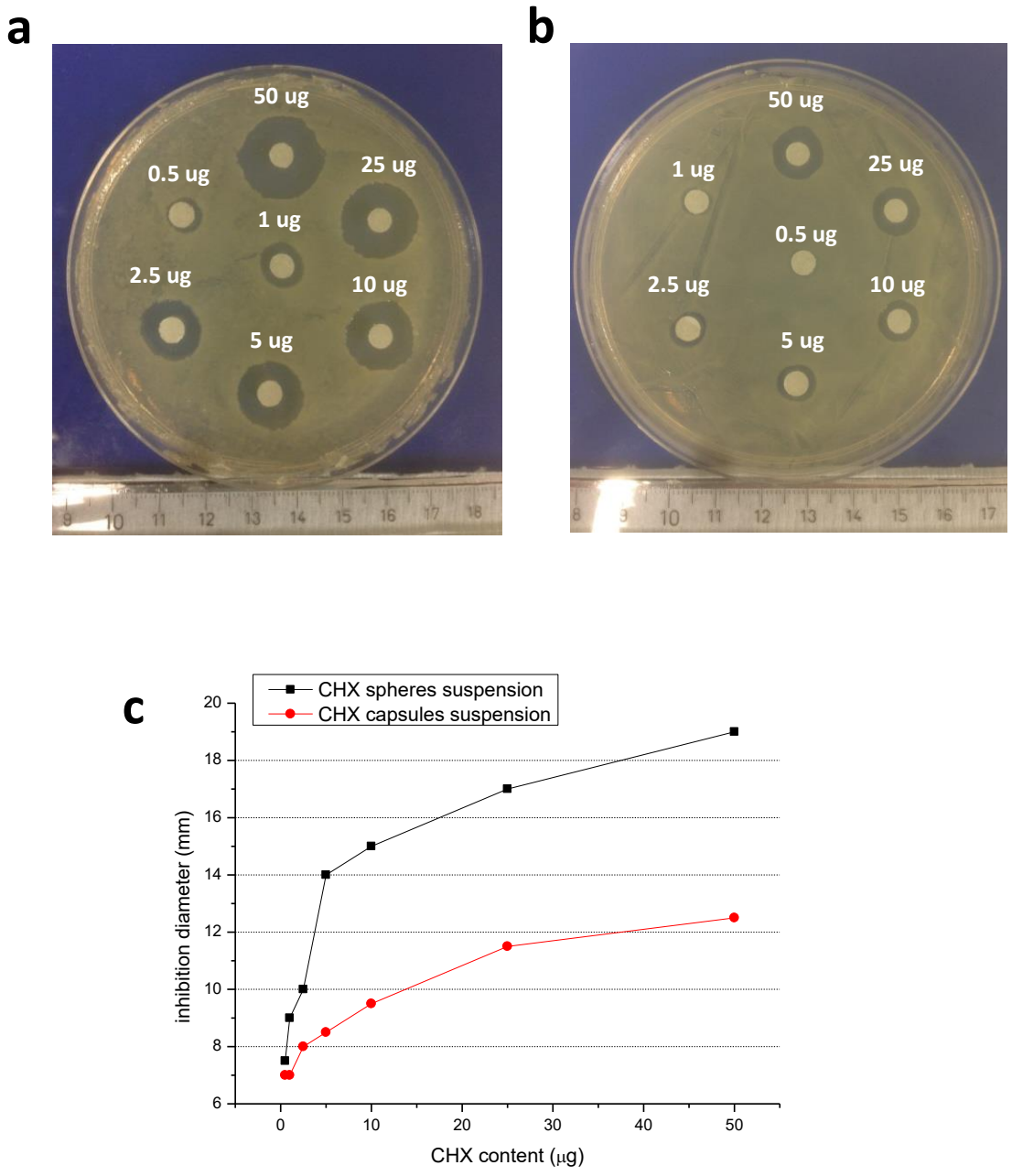

Figure 4.30 Inhibition of (a) chlorhexidine particles and (b) encapsulated particles against E. coli., and (c) comparison of inhibition diameters as a function of chlorhexidine concentration. 10 µl CHX solutions with different amount of CHX content (50, 25, 10, 5, 2.5, 1, 0.5 µg) were added to filters.

4.1.4 Conclusion

In this part, a new structure of the commonly used antimicrobial drug chlorhexidine diacetate was fabricated by co-precipitation with $CaCl_2$. By adjusting the concentration of $CaCl_2$, homogeneous and interconnected spherical chlorhexidine particles were produced, with chlorhexidine content within the particles as high as 90%. Moreover, the size of chlorhexidine spheres could be tailored from 5.6 μm to over 20 μm by controlling the temperature of the original solutions. However, with other salts, no of these perfect structures was observed, which we can conclude that both the Cl^- and Ca^{2+} ions were responsive for the formation of the interconnected structure, as it was confirmed by the FTIR. It is advantageous to have these homogeneous drug crystals, first of all, as secondary fillers in dental materials (resin and resin composites), the size is a very important factor. Also it opens up possibilities for further functionalization of the chlorhexidine particles, which leads to a more controllable and responsive release.

Therefore, the spherical chlorhexidine particles were further encapsulated with different polymers, LbL polyelectrolytes, PLA and the HEMA-UDMA resin, using different techniques. Firstly, the spherical chlorhexidine particles were encapsulated by LbL self-assembly, which oppositely charged PAH and PSS were deposited on their surface, forming multilayer shells. The depositing of polymers on the surface changed the surface morphology as layers of flakes were observed assembly on their surface until the needle-like structure was completely covered. By cutting the encapsulated particles with focus ion beam, the thickness of polyelectrolyte shells was around 1.02±0.25 μm. The coating of polymers did stabilize the chlorhexidine spheres and lead to a sustained release over 7 hours, while the uncoated ones just dissolved within an hour. Though the LbL assembly approach could produce perfect encapsulation, which every chlorhexidine particle was encapsulated, and the coating was even and controllable by just adjusting the number of layers, it was quite time consuming. A one-step

encapsulating approach is desirable, so the spray-drying was carried out. By mixing the chlorhexidine particles with PLA solutions and spraying, a layer of PLA was successfully coated on the surface, and generally, the thickness of PLA layer could be tuned by tuning the chlorhexidine to PLA ratio. With higher chlorhexidine to PLA ratio (1:3), the PLA layer was quite thin and increasing the reducing the ratio to 1:5, thicker PLA layer was deposited. As a result, chlorhexidine particles with a thick PLA coating demonstrated a more sustained release than the thin coated ones, than the uncoated ones. This method was fast and productive, but compared to the LbL encapsulated, the resulted particles were not so perfect. Though the chlorhexidine to PLA ratio was tuned, the thickness of PLA coating was not even and aggregations could not be avoided. Also, due to the fast evaporation of organic solvent, there were always pored formed on the PLA layer which leaded to the burst release at the beginning. Another shortage was the occupancy of the sprayed particles, that empty PLA clusters were always appeared regardless of the chlorhexidine to PLA ratio.

On the other hand, both the uncoated and LbL encapsulated chlorhexidine particles could be electrospun in PLA fibers to enable the fibers with sustained antibacterial properties. The incorporation of chlorhexidine particles into fibers greatly improved the drug loading ratio, and more sustained release was achieved by pre-encapsulating chlorhexidine particles with polyelectrolyte multilayers. Both fibers showed no cytotoxicity to fibroblasts at low chlorhexidine loading rate (from 0.5 % to 1 % wt/wt), and by encapsulating the particles, biocompatibility was significantly improved at 5 % (wt/wt). Similar results were illustrated by 3D imaging of cell adhesion on the fibers. Both fibers showed good inhibition against *E. coli* growth in the agar diffusion assay, and sustained antibacterial effect via broth transfer experiments (5 % wt/wt). Therefore, the developed PLA fibers containing chlorhexidine particles may have promising applications for the localized treatment of infections. By incorporating the chlorhexidine particles into fibers, it is easier to hand and place them to

specific site which is a big advantage to treat infections. The encapsulated particles in the fibers should also allow a tailored drug release, that might be matched to the disease stages, to allow a more effective and responsive treatment.

As a most commonly used antibacterial drug in dentistry, the chlorhexidine particles were incorporated into HEMA-UDAM resin discs, which had the potential to be used as restorations. The release of chlorhexidine and more detail are demonstrated in section 4.2.

Overall, the spherical chlorhexidine particles can be encapsulated or embedded into many polymer matrixes to achieve a sustained release and antibacterial activity. The process of chlorhexidine particles fabrication is simple, and it is also possible to make further functionalization to the interconnected structures and achieve stimuli responsive release, which is advantageous in a variety of applications required in medicine and dentistry.

4.2 External stimuli responsive chlorhexidine formulation

4.2.1 NIR light stimulus responsive chlorhexidine release

4.2.1.1 Gold nanorods synthesise

Based on the seed mediated growth method, the homogeneous gold nanorods used are shown in Figure 4.31a. According to the TEM image, the gold nanorods have an average length of 85 nm and width of 20 nm. UV-vis NIR spectroscopy of the gold nanorods (Figure 4.31b) displayed their absorbance peak at 840 nm. The surface plasmon resonance band was largely dependent on the shape and ratio of length to width of the gold nanorods, their surface properties, as well as the mediums surrounding the particles.[126-127] The plasmonic properties of gold nanorods make them promising candidates in light responsive drug delivery, since they have great photothermal conversion ability and their absorption band in the near infrared range is especially preferred for *in vivo* applications.[219]

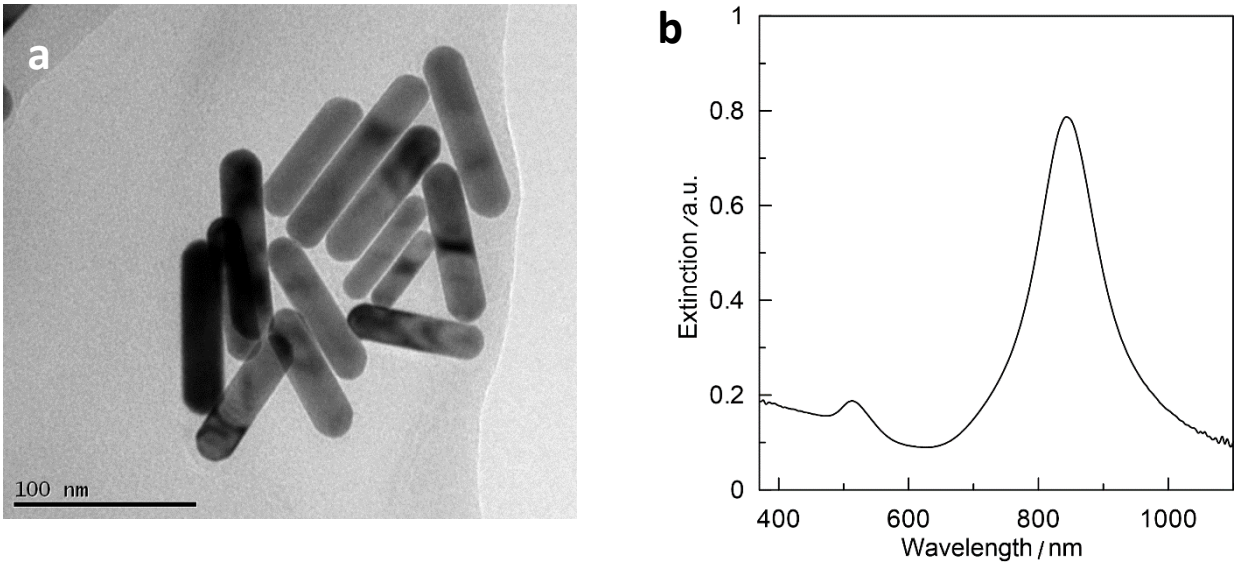

Figure 4.31 TEM images of gold nanorods (a) and UV-vis spectrum of gold nanorods (b).

4.2.1.2 Effect of Gold nanorods on chlorhexidine crystal growth

In a previous study, it is reported that chlorhexidine spheres, with homogeneous size and morphology, were produced, and proved that the crystal growth of the drug spheres could be tuned by temperature and ion concentration. In Medicine and Dentistry[24] a more sustained and stimuli responsive chlorhexidine delivery system against bacteria is also desirable. This could be achieved by combining the chlorhexidine spheres with the gold nanorods. As demonstrated in Figure 4.32, gold nanorod functionalized chlorhexidine spheres were synthesized by introducing the gold nanorods into the $CaCl_2$ solution. Without gold nanorods, the chlorhexidine spheres had a porous interconnected surface morphology, which were comprised of small dendrites (Figure 4.32b). In contrast, for the gold nanorods functionalized spheres (with 400 µl Nanorods), gold was clearly observed in the backscattered images (Figure 4.32c), and at high magnification small gold nanorod clusters were present on the chlorhexidine dendrites (Figure 4.32d). The incorporation of gold particles into drug delivery carriers has been extensively studied. For instance, hollow gold nanospheres were loaded into PLGA microspheres together with paclitaxel, via a double-emulsion solvent evaporation method, and the paclitaxel release was modulated by using a NIR light.[220] Gold nanorods and doxorubicin were incorporated into crosslinked poly(β-amino ester) particles, with the glass transition temperature (Tg) close to body temperature. Therefore, transformation of the polymer from a glassy to a rubbery state induced by an NIR light produced an instant burst release of doxorubicin.[221] For both examples drug release benefited from enhanced diffusion through the polymer networks. The choice of polymers with either a lower Tg or high thermal sensitivity, such as poly(N-isopropylacrylamide) (PNIPAm),[166] is essential for the design of NIR responsive drug carriers. The incorporated gold nanorods in the chlorhexidine drug crystals

have the potential to generate heat upon NIR light irradiation, and thus deconstruct the interconnected drug crystals and induce chlorhexidine release.

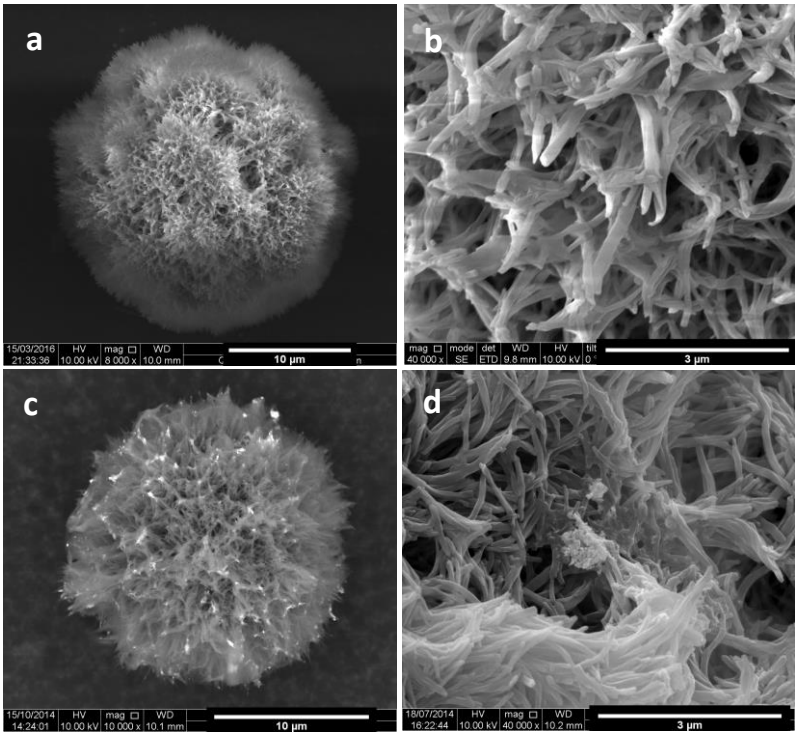

Figure 4.32 SEM and BSEM images of gold functionalized chlorhexidine particles. (a) BSEM image of chlorhexidine sphere at ×10,000; (b) SEM image shows the surface morphology of chlorhexidine sphere at ×40,000; (c) BSEM image of gold-chlorhexidine composites at ×10,000; (d) SEM image shows the surface morphology of gold-chlorhexidine composites at ×40,000.

To further understand the role of gold nanorods in chlorhexidine crystal growth, different amounts of gold nanorods was dispersed into $CaCl_2$ solutions. Figure 4.33 illustrates the influence of gold nanorods on the size of chlorhexidine spheres. Without the addition of gold nanorods the chlorhexidine spheres had a mean (SD) diameter of 24.0 (5.0) µm. Adding 5 µl

of gold nanorods produced a slight size reduction of 22.9 (4.6) μm. The average chlorhexidine sphere diameters gradually decreased on increasing addition of gold nanorods, with a 400 μl gold nanorod addition giving a mean (SD) diameter of 14.5 (1.6) μm. There was a correlation between the amount of gold nanorods added and the mean chlorhexidine particle diameter (r^2=0.98, Figure 4.34a). SEM images indicated there was no distinct difference in the morphology of chlorhexidine spheres at different gold nanorods addition. The chlorhexidine precipitation efficiency (>98%) was also similar for all the samples (data not shown). In terms of the particles size distribution, with less gold nanorods added, the size distribution was broader (data not shown). When increasing the amount gold nanorods however, the chlorhexidine spheres were more homogeneous. The crystallisation of the chlorhexidine spheres involves a rapid nucleation and crystal growth process, so it is likely that the gold nanorods in the solution may act as sites for crystallization. This is supported by the data in Figure 4.34b where chlorhexidine particle number and size was correlated with the amount of gold nanorods added to solution (r^2=0.98, Figure 4.34a, r^2=0.98, x from 0 to 200, Figure 4.34b). The remaining weight of functionalized chlorhexidine spheres also increased as a function of increased amount of gold nanorods as indicated by the TGA result (data not shown). Gold nanoparticles were previously used as seeds to produce hybrid silica particles,[147] and CdSe/ZnS quantum dots were also used to grow mesoporous silica shells on their surface.[222] Therefore, we assume that the amount of gold nanorods in the solution was a key factor to determine the chlorhexidine sphere size and number. It was however noted that any excess gold nanorods could cluster and be trapped in the crystals, as showed in Figure 4.35. It is a common approach to control crystals size by adjusting the seed amount in nanoparticle synthesis. Similarly for gold nanoparticle synthesis, the mean particle size can also be tuned, with the mean particle size decreased with increased seed concentration, and at low seed and gold precursor ratio, large particles and secondary nucleation were observed.[123] Interestingly, gold nanorods can

also be replaced by other nanoparticles (e.g. Fe_3O_4 nanoparticles), and the same effect on chlorhexidine crystallization has been demonstrated by the authors. The current functionalization of chlorhexidine crystals with Gold or Fe_3O_4 nanoparticles also opens up a door for its stimuli responsive release.

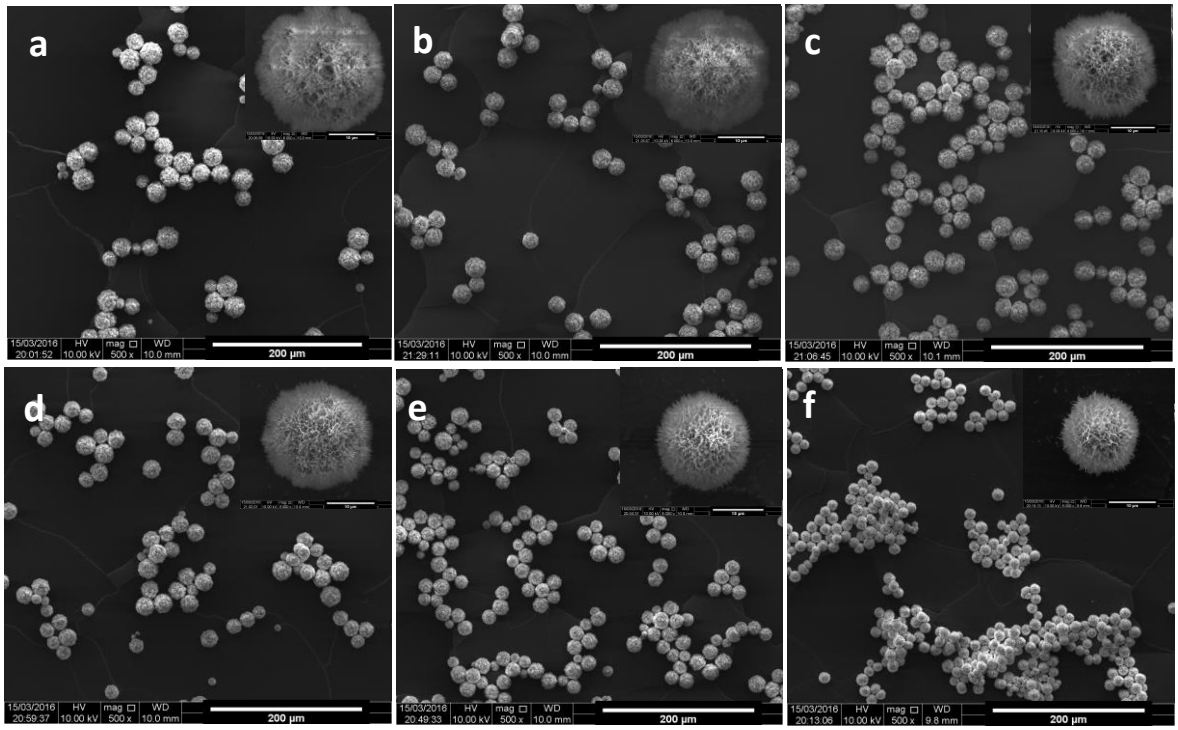

Figure 4.33 SEM images of gold-chlorhexidine composites with different amount of gold nanorods. (a) no gold nanorods; (b) 5 µl; (c) 50 µl; (d) 100 µl; (e) 200 µl; (f) 400 µl gold nanorods (0.45 mg/mL). Inset images are individual particles at high magnification (×8000).

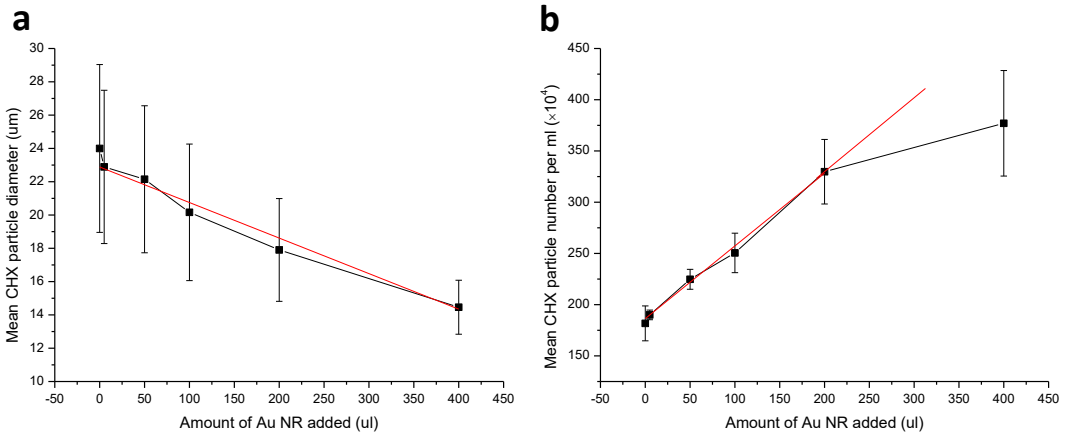

Figure 4.34 Effect of gold nanorod addition on the size and number of chlorhexidine particles. (a) Mean chlorhexidine particle diameter as a function of gold nanorod amount; and (b) Mean chlorhexidine particle numbers as a function of gold nanorod amount.

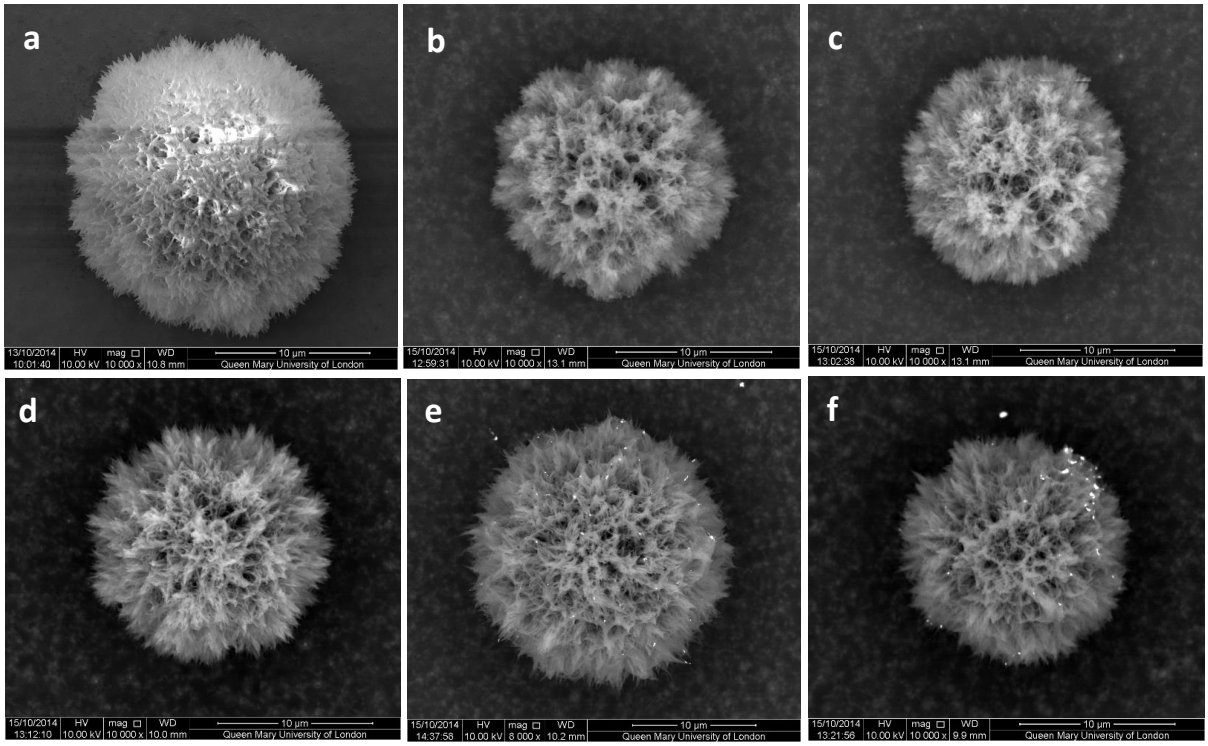

Figure 4.35 BSEM images of gold-chlorhexidine composites with different amount of Au nanorods loaded. (a) no Au nanorods; (b) 5 µl; (c) 50 µl; (d) 100 µl; (e) 200 µl; (f) 400 µl Au nanorods.

In a parallel experiment, small chlorhexidine spheres were used as primary particles instead of gold nanorods to further reveal chlorhexidine crystallization. This was achieved by keeping the original chlorhexidine diacetate and $CaCl_2$ solutions in an ice bath and carrying out the synthesis to produce primary chlorhexidine particles with a mean (SD) diameter of 5.2 (1.7) μm (Figure 4.36a), while chlorhexidine spheres synthesized at room temperature had a mean (SD) diameter of 17.2 (1.9) μm (Figure 4.36b). By introducing the chlorhexidine primary particles into the $CaCl_2$ solution, growth of a second shell of chlorhexidine crystals were successfully achieved. FITC labelled chlorhexidine primary particles were presented as the core (green label, Figure 4.36a, c) and the new shells grown from the interface around the primary particles were visible when labelled with RhB (red label, Figure 4.36 d, e). At the transmitted channel, a clear boundary between the chlorhexidine primary particles and outside shell was identified (Figure 4.36f). These observations suggest a seed mediated crystallisation of chlorhexidine crystals, which supports the previous hypothesis. Similarly, the mean particle diameter of the chlorhexidine spheres decreased as the amount of primary chlorhexidine particles increased (date not shown). The chlorhexidine particle size distribution also narrowed at increasing primary particle concentration (Figures 4.37). An epitaxial growth on the surface of the primary seed crystal may also be likely and is present in other systems where the chemistry and crystal lattice constants are favourable.[223]

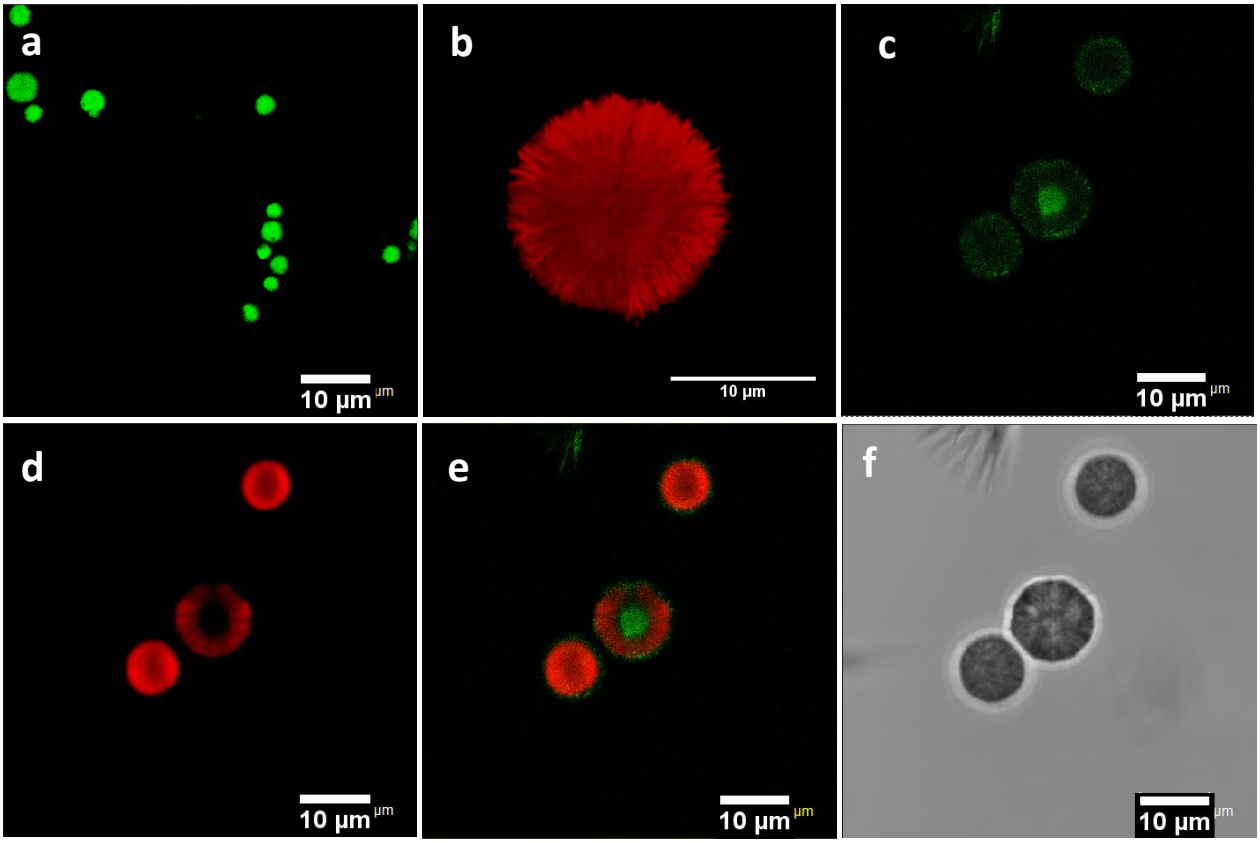

Figure 4.36 Confocal images of core-shell chlorhexidine spheres. (a) chlorhexidine primary particles produced in an ice bath (labelled with FITC); (b) large chlorhexidine spheres produced at room temperature (labelled with RhB); core-shell chlorhexidine particles produced based on the small chlorhexidine primary particles at (c) green channel, (d) red channel and (e) merged image; (f) at transmission channel.

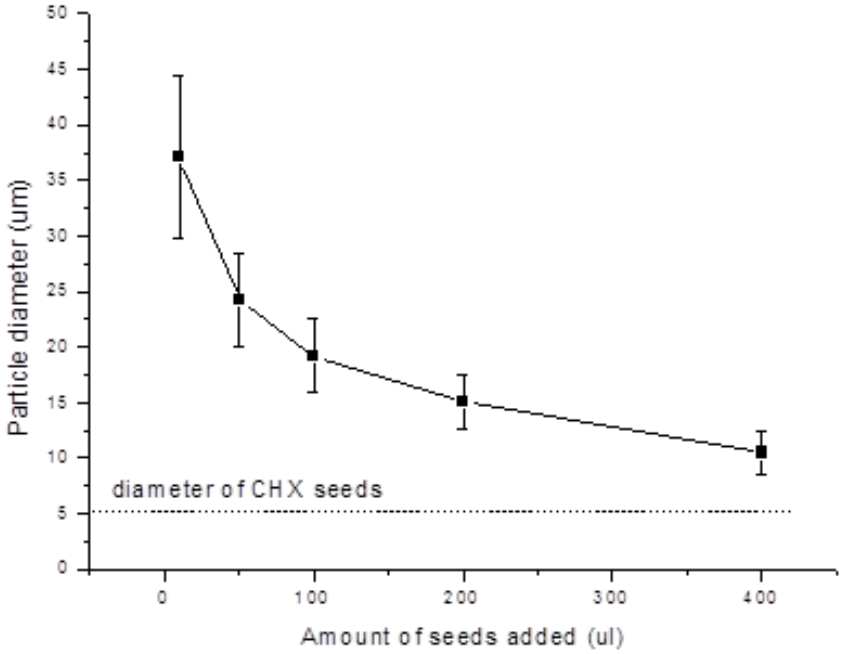

Figure 4.37 Effect chlorhexidine seeds amount on the size of chlorhexidine spheres (dash line indicates the size of the chlorhexidine seeds).

4.2.1.3 Mechanism of chlorhexidine growth

Theoretically, the growth of nano/micro particles involved two main stages: rapid nucleation to form primary seeds and sustained growth of precursors on the primary seeds.[224] The formation of homogenous interconnected chlorhexidine spheres was a very rapid process, which was dependent on the type and concentration of ions and temperature of the bulk solutions, as proposed in our previous study.[225] Herein, with gold nanorods or chlorhexidine primary particles, the chlorhexidine particle forming process is presented schematically in Figure 4.38. At the first stage of synthesis, when chlorhexidine diacetate was mixed with $CaCl_2$, monomers were formed immediately following basic coordination chemistry of guanidines.[31] The biguanidines of chlorhexidine have strong coordination capability with ions, such as Cu^{2+}, Zn^{2+} or Ag^{+}.[28-29] According to the inset FTIR spectrum (Figure 4.38), the typical chlorhexidine

band of C=N was shifted from 1610 cm^{-1} to 1621cm^{-1} and N-H stretching vibration of the Alkyl-NH-Aryl, $(Alkyl)_2NH$ and =NH at 3118, 3303 and 3190 cm^{-1} was distinctly increased.[28] This is evidence that Ca^{2+} had coordinated with chlorhexidine. The presence of Cl^- may also help to accelerate the precipitation of these complexes since the Cl^- ion is thought to reduce chlorhexidine solubility.[30] Interestingly there was a homogenous and copious distribution of Ca^{2+} and Cl^- in the chlorhexidine spheres via EDX mapping (Figure 4.39). Therefore, the addition of $CaCl_2$ to the chlorhexidine diacetate solution facilitated the formation of chlorhexidine nucleation and monomers for crystal growth. The addition of gold nanorods or chlorhexidine primary particles in the solution, appears to have encouraged surface crystallization to produce more primary crystallites. Research on the growth of mesoporous silica shells on gold nanoparticles, indicates the ratio of gold nanoparticles to silica precursors was a key factor to determine the gold occupancy and cluster sizes for the synthesized composites.[148] This could explain why gold was only detected in the backscattered SEM images for samples with excess addition of gold nanorods. At more reduced additions of gold particles crystallization sites were favoured, while excess gold particles could lead to flocculation and clusters observed on the chlorhexidine sphere surfaces. In addition, the negatively charged gold nanorods may have a high affinity to positively charged chlorhexidine molecules, which encouraged crystallization of chlorhexidine on their surfaces. This is advantageous as coating of gold colloids with silica requires a surface modification using a silane coupling agent to make them vitreophilic.[145, 147] For the second stage, growth of chlorhexidine spheres proceeded via continuous deposition of monomers on the primary particles. This process was monitored by labelling the chlorhexidine primary particles and chlorhexidine monomers with different dyes and a core-shell structure was displayed (Figure 4.36). At low temperature, chlorhexidine crystal growth rate was limited, so small (5.2 ± 1.7μm) crystals were produced. Once the primary particles were transferred into solutions with

monomers, crystal growth continued until the chlorhexidine monomers were depleted. There was also evidence of Ostwald Ripening, as the sacrifice of small particles and bridging between particles was observed in the SEM images of the chlorhexidine precipitates at different time intervals (10, 20, 30, 40, 50 and 60s) (Figure 4.40).

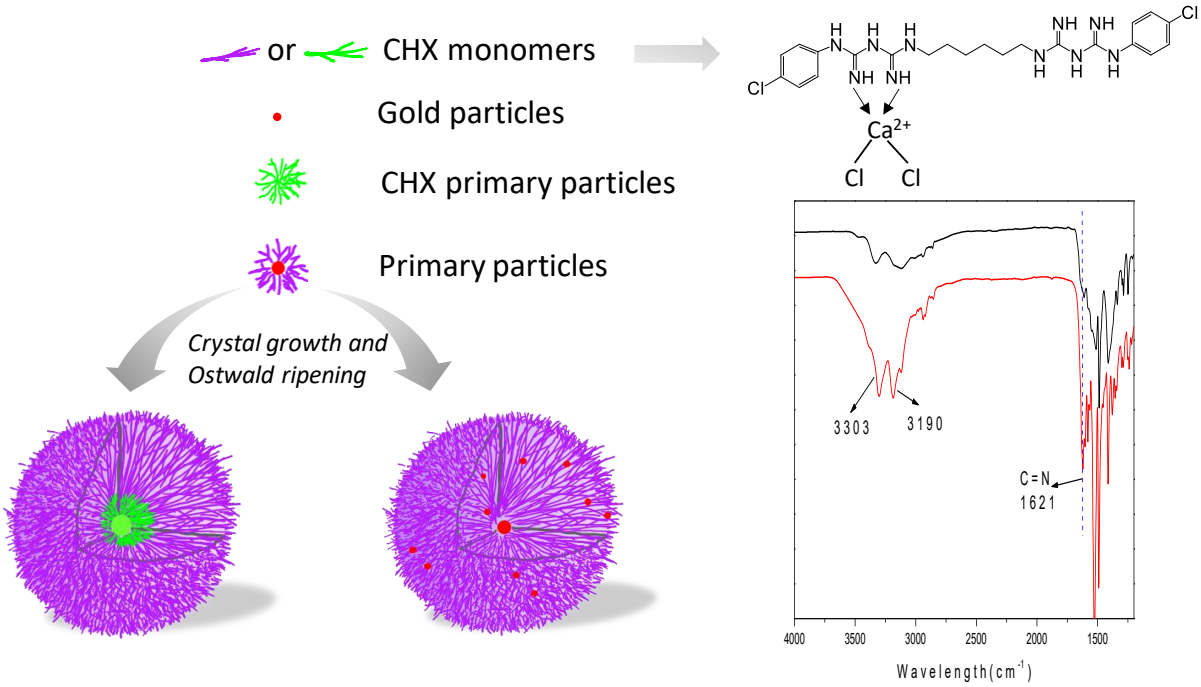

Figure 4.38 Schematic illustration of chlorhexidine crystallization. Gold particles (red) and small chlorhexidine spheres (green) were used as seeds for chlorhexidine crystals growth; inset is the FTIR spectrum of the chlorhexidine spheres (red) and chlorhexidine diacetate (black).

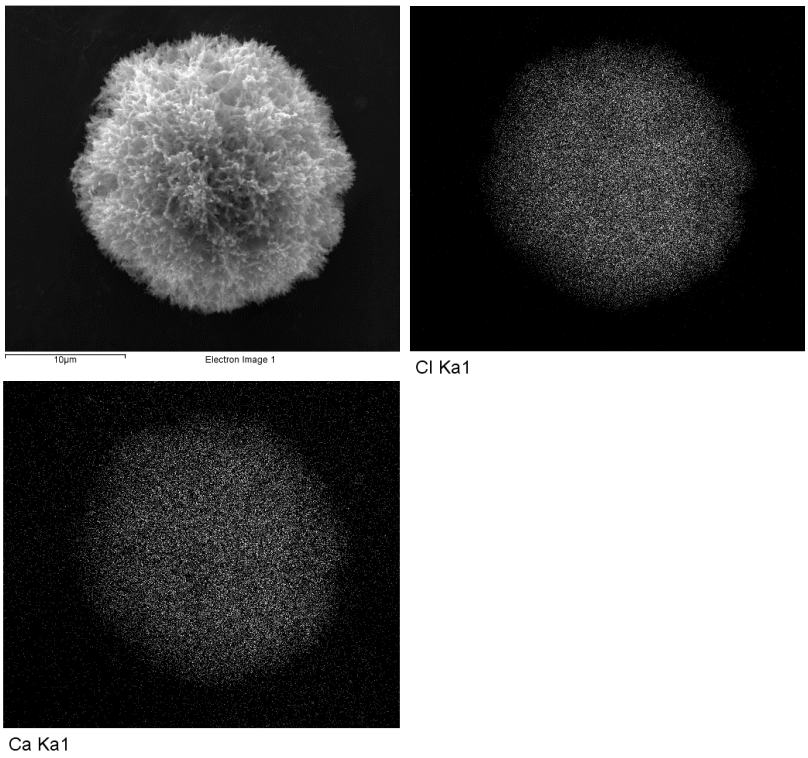

Figure 4.39 EDX mapping of elements distribution on the chlorhexidine sphere.

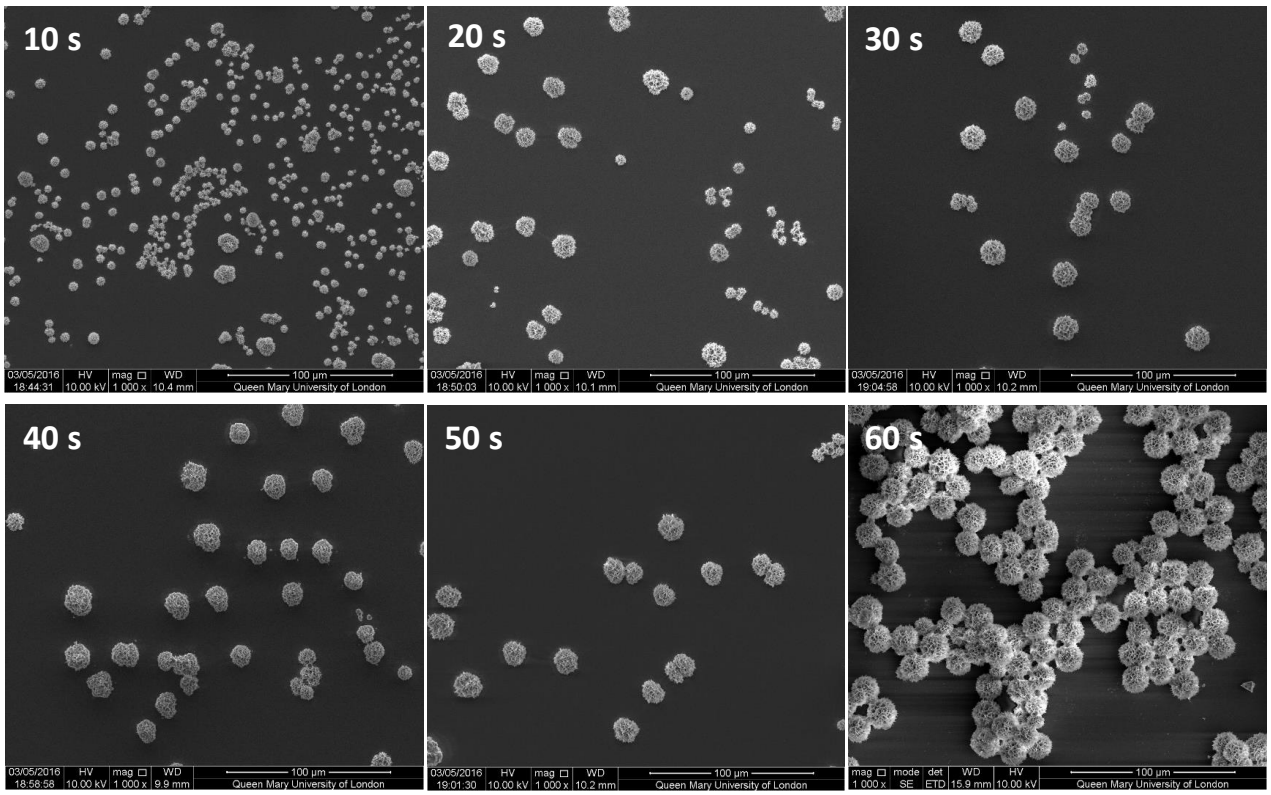

Figure 4.40 SEM images of chlorhexidine crystal growth as a function of time.

4.2.1.4 Infrared laser induced release of chlorhexidine

LbL encapsulation of drug crystals is an efficient approach to achieve sustained drug release and improve the solubility for some anticancer drugs.[108, 196] The advantage of drug colloid encapsulation over other delivery methods is the high drug loading rate since the cores consist of the drug, and their toxicity can be reduced at the same time compared to the equivalent free dose.[216] LbL encapsulation of the chlorhexidine composites was necessary to stabilize the interconnected structure as the spheres were sensitive and could be dissolved in H_2O within a few minutes. Successful encapsulation of the chlorhexidine spheres was achieved by carrying out the assembly at moderate conditions and in high salt polyelectrolyte solutions. As presented in Figure 4.40a, the chlorhexidine sphere cores still remained intact after encapsulating 6 layers of polyelectrolytes (shells appear in green). The overlapped images indicated that the polyelectrolytes had penetrated into the porous chlorhexidine sphere surface (Figure 4.41a). Compared to the conventional LbL capsules, the polymer shells here were much thicker, which was due to the deposition of polyelectrolytes at high salt concentration, and also chlorhexidine dissolution during the LbL process.[200] The shell thickness of the chlorhexidine capsules was 1.02 μm according to a cross-sectional measurement in our previous study.[225] SEM images showed that the chlorhexidine capsules had completely coated the chlorhexidine structure and no dendritic structure could be identified.

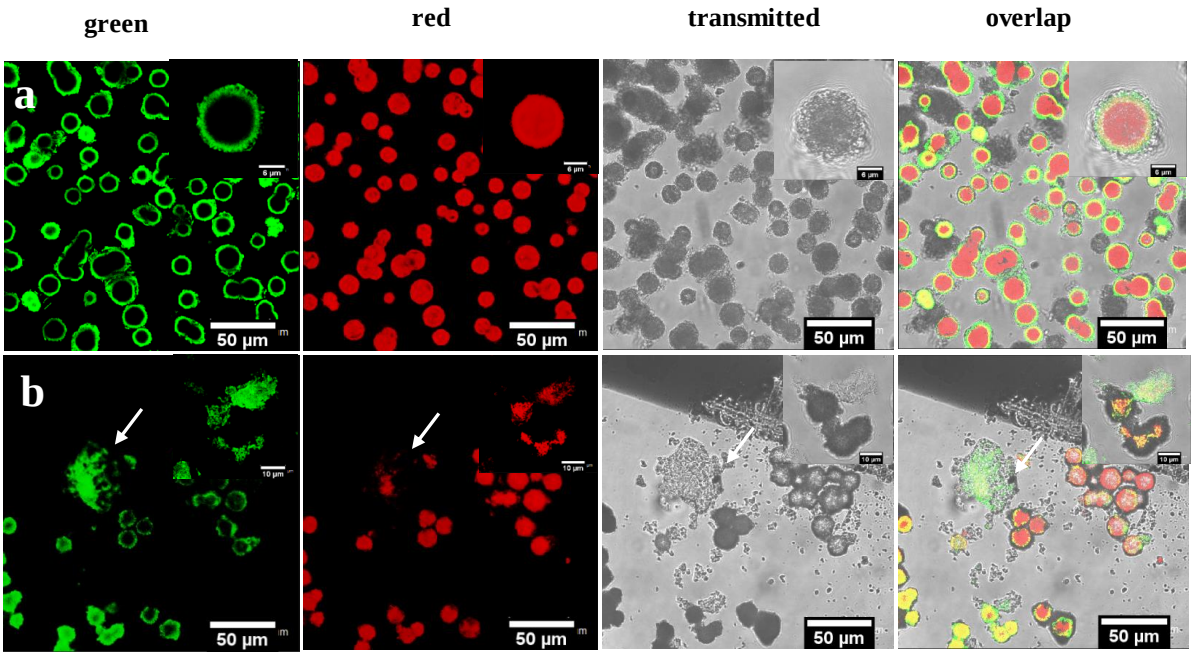

Figure 4.41 Confocal images of gold functionalized chlorhexidine capsules before (a) and after laser irradiation (b). One of the PAH layers is labelled with FITC (green) and the chlorhexidine particles were labelled with RhB (red). Arrows indicated the remaining polyelectrolyte shells and inset images are taken at high magnification.

Gold nanorods have a strong photothermal conversion ability,[135] so it was assumed it would be possible to trigger the release of functionalized chlorhexidine capsules with NIR light irradiation. Using an 840 nm NIR light (up to 100 mW) with our laser setup, the chlorhexidine capsules could be ruptured while the others stayed intact (Figure 4.41b). Once targeted by the laser beam, the capsule erupted and the exposed chlorhexidine spheres dissolved, as a result only polyelectrolyte shells remained as indicated by the arrows in Figure 4.41b. There was however still some weak red signal detected within the residual shells, indicating residual chlorhexidine. This was due to complexation between the chlorhexidine molecules and the PSS layer via an interaction of its amine group and sulfonic group of PSS.

According to the transmitted channel images, debris around the broken polyelectrolyte shells was also observed and confirmed by the SEM images (Figure 4.42a, b). It was not surprising that the gold nanorod functionalized chlorhexidine capsules were responsive to NIR light since the chlorhexidine crystals were directly grown on top of the nanorods. The energy generated by NIR light irradiation was able to disrupt the chlorhexidine crystal structures. In a previous study of silica coated gold nanoparticles, the surface temperature of gold particles was suggested to be more than 100 ºC upon laser irradiation.[226-227] The local heating by using NIR light irradiation was therefore a more efficient trigger for drug release than simply heating the solution to an equivalent temperature.[141] Gold nanoparticles deposited into polyelectrolyte capsules previously revealed rupture of the capsules upon laser irradiation,[228] even with a SiO_2 layer deposited on the surface of capsules, which allowed snap intracellular cargo release.[139] Since the chlorhexidine crystal growth is based on the coordination of Ca^{2+} and biguanidines, heat generated by gold nanorods could interrupt the binding and even cause a conformational change of chlorhexidine molecules, thus leading to destruction of the crystals.

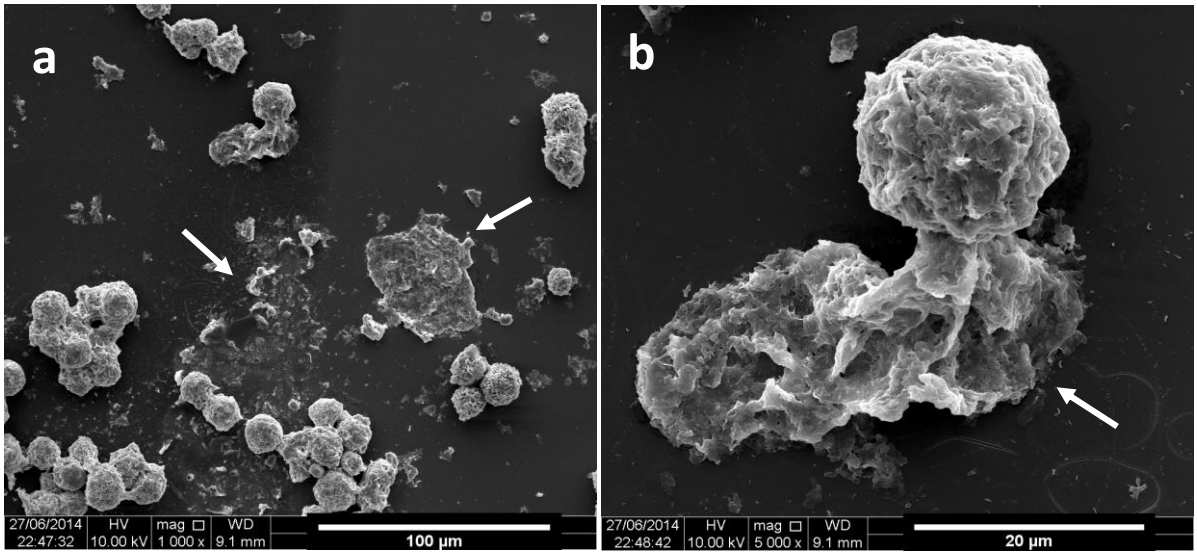

Figure 4.42 SEM images of gold functionalized chlorhexidine capsules after laser irradiation. Untreated capsules were still intact but laser triggered ones were broken with polymer shells remaining as indicated by white arrows.

Local heating of gold nanorods may also accelerate dissolution and diffusion of chlorhexidine molecules. According to the *in vitro* release kinetics (Figure 4.43), chlorhexidine release occurred in a stepwise fashion after each cycle of laser treatment. A burst release was observed during each laser irradiation cycle. In contrast, the released chlorhexidine content during each cycle for the control was lower, although both groups exhibited a sustained release.

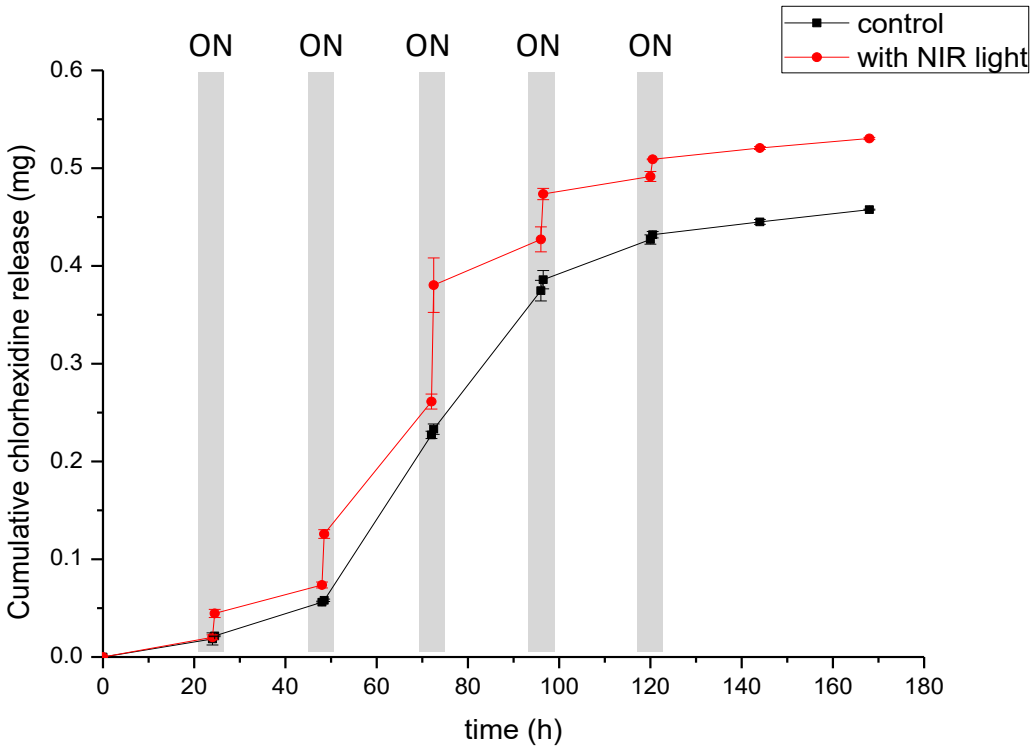

Figure 4.43 Cumulative release of chlorhexidine from capsules with (red) and without (black) NIR light irradiation. Five cycles of NIR light on (30 min, 100 mW) were indicated by grey shades; values are the mean of three groups and vertical bars represent the SD.

The proposed chlorhexidine capsules with high drug loading rate and NIR light responsive properties have advantages and promising applications in medicine and dentistry. Many current products used in dentistry have a limitations due to lack of controlled drug release and duration.[35] The gold nanorod functionalized chlorhexidine capsules are useful as they may be injected into sites such as periodontal pockets. As the periodontitis disease is caused by biofilms which are highly resistant to antimicrobial agents, a burst release triggered by NIR light is essential to eliminate the pathogens, which cannot be achieved otherwise as the minimum bactericidal concentration (MBC) is hardly be reached without any triggers. Any bacteria remained may cause a secondary infection, and the non-invasive approach of NIR light induced release can open up ways to solve this problem. Photodynamic therapy using a diode laser is used in conjunction with a photosensitizer to decrease or eliminate bacteria[229] and it may be possible to combine these therapies to increase its efficacy. The *in vitro* NIR light induced chlorhexidine release and their antibacterial activities will be evaluated in our future work.

4.2.2 Magnetic field responsive chlorhexidine release

4.2.2.1 Fe_3O_4 nanoparticles synthesis

TEM image of synthesized Fe_3O_4 nanoparticles was showed in Figure 4.44. It can be seen that diameter of the nanoparticles was around 20 nm and they were not monodispersed as appeared in clusters. These nanoparticles were stored under argon protection to prevent oxidation and used to functionalize the chlorhexidine spheres.

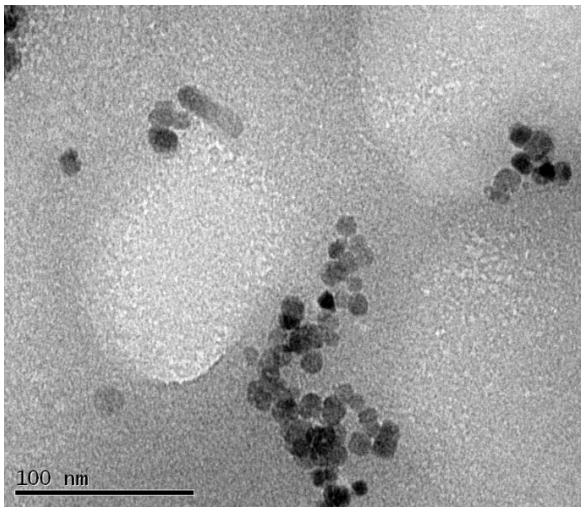

Figure 4.44 TEM image of Fe_3O_4 nanoparticles.

4.2.2.2 Fe_3O_4 nanoparticles functionalization of chlorhexidine spheres

When the Fe_3O_4 nanoparticles were added, similar results were produced. Without Fe_3O_4 nanoparticles added, the mean diameter (SD) for particles was 17.15 (1.99) um, while the Fe_3O_4 nanoparticles functionalized chlorhexidine spheres had a mean diameter (SD) of 10.39 (2.61) um. According to the images at high magnification (×40000), clusters Fe_3O_4 nanoparticles could be observed (Figure 4.45a). The presence of Fe in the chlorhexidine spheres was further confirmed by XRD analysis as shown in Figure 4.44b, c. The peaks of Fe were strong and clearly identified.

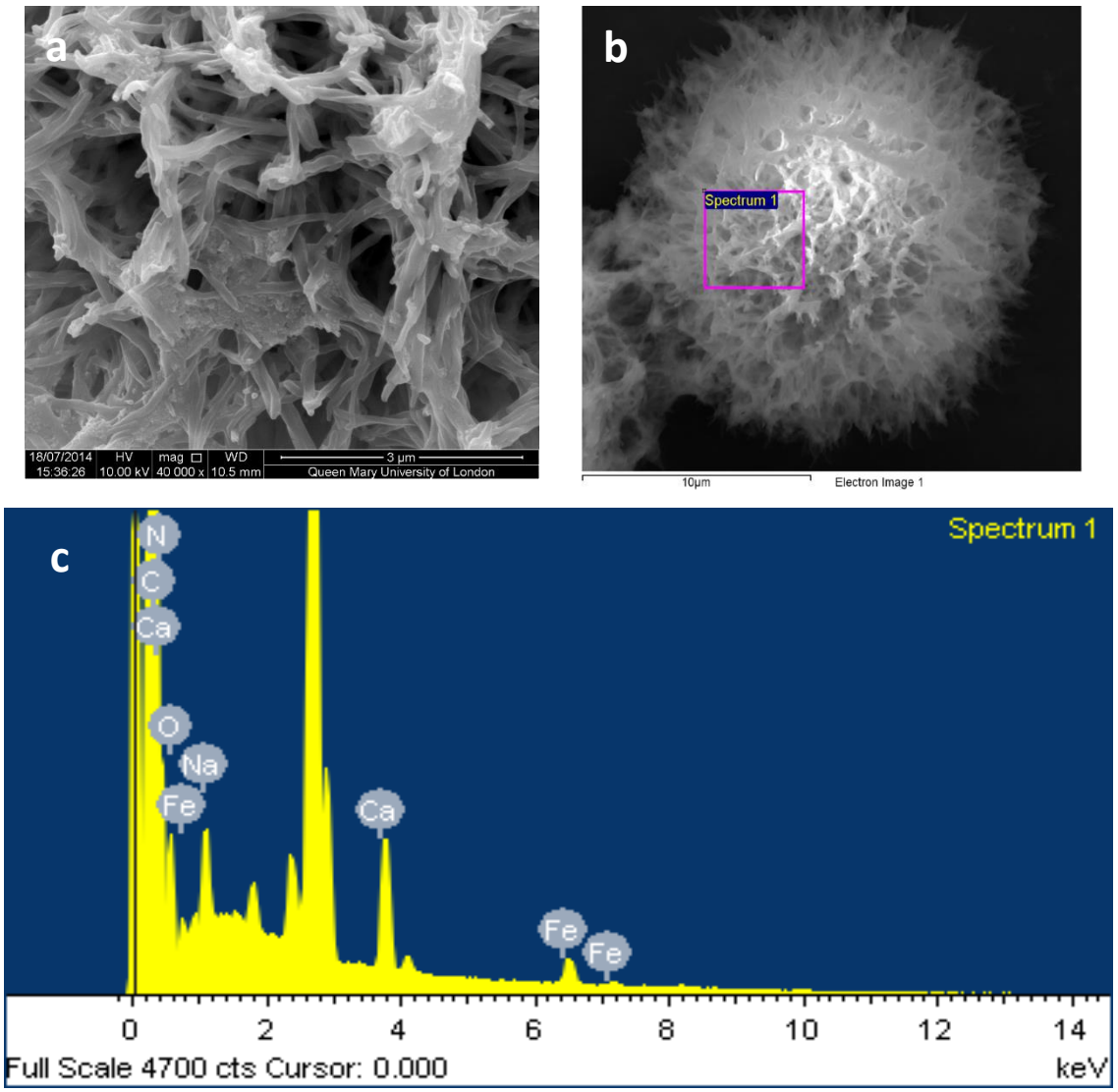

Figure 4.45 SEM image (a) and EDX (b, c) of Fe_3O_4 nanoparticles functionalized chlorhexidine spheres.

4.2.2.3 Magnetic controlled chlorhexidine release from HEMA-UDAM resin

The Fe_3O_4 nanoparticles functionalized chlorhexidine spheres were freeze dried and the powder was incorporated into HEMA-UDMA resin composites. The continuous cross-section images of resin discs were joint together to make panoramic images and were presented in Figure 4.46. The chlorhexidine spheres were clearly identified as white dots in the resin, which

were intact with resin penetrated into the porous surface of chlorhexidine spheres. No dissolution of chlorhexidine spheres was observed as clear boundary of chlorhexidine and resin was presented. For the control group resin disc (Figure 4.46a), the chlorhexidine spheres were homogeneously distributed inside the resin discs. Whilst, when treated in magnetic field for 5 min, the magnetic chlorhexidine spheres moved to the end of magnet, which resulted more chlorhexidine spheres at the magnet end (Figure 4.46b). The closest two frames in the panoramic had significantly more chlorhexidine spheres than the most far away two frames which no chlorhexidine spheres were identified. It was even more dramatic when extending the magnetic field treatment time to 10 min that most of the magnetic chlorhexidine spheres were distributed in the four frames close to the magnet (Figure 4.46c).

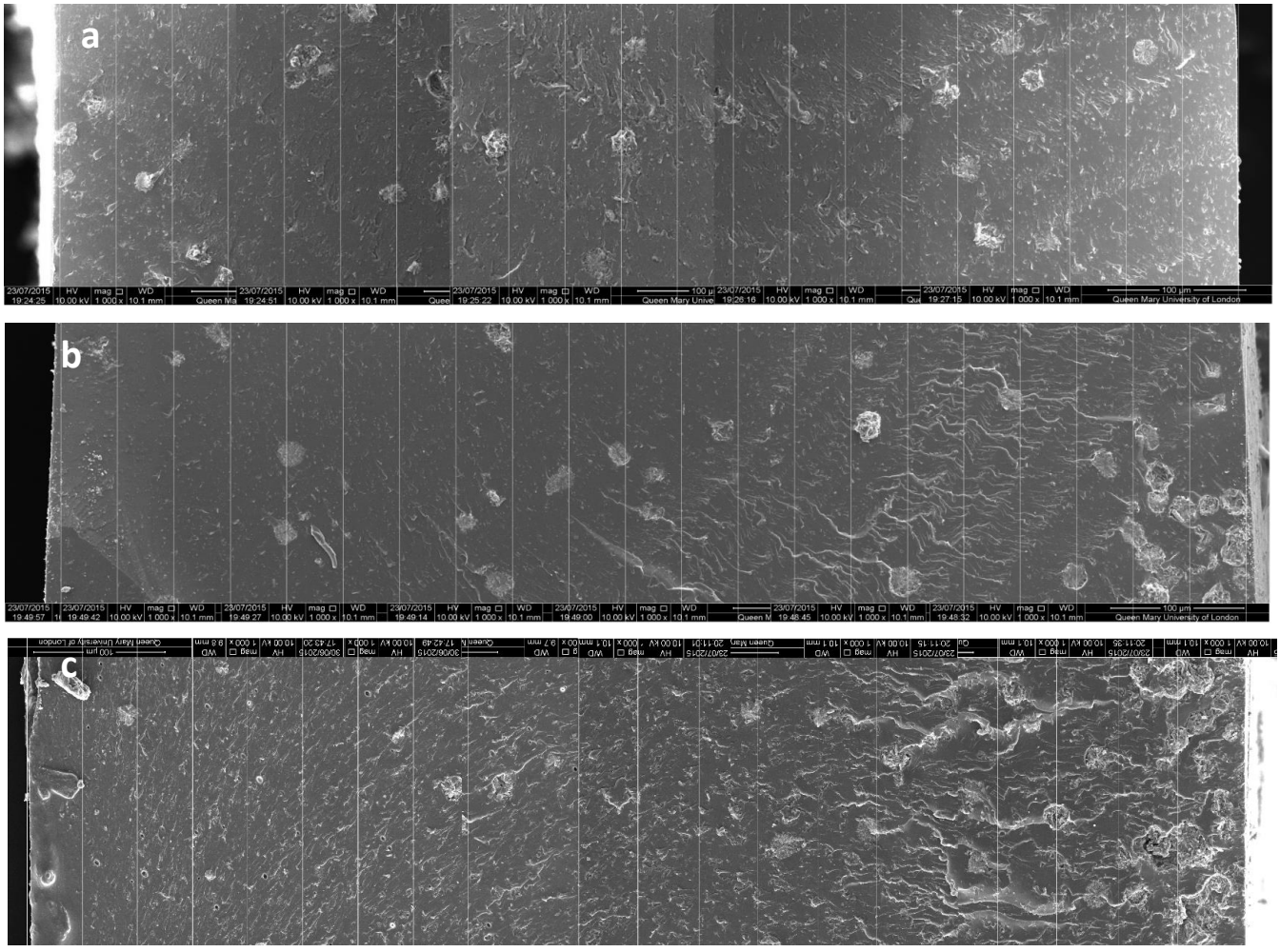

Figure 4.46 Cross-section SEM images of HEMA-UDMA resin with Fe_3O_4-CHX spheres. (a) control without magnetic field treatment; (b) with magnetic field treatment for 5 min; (c) with magnetic treatment for 10 min.

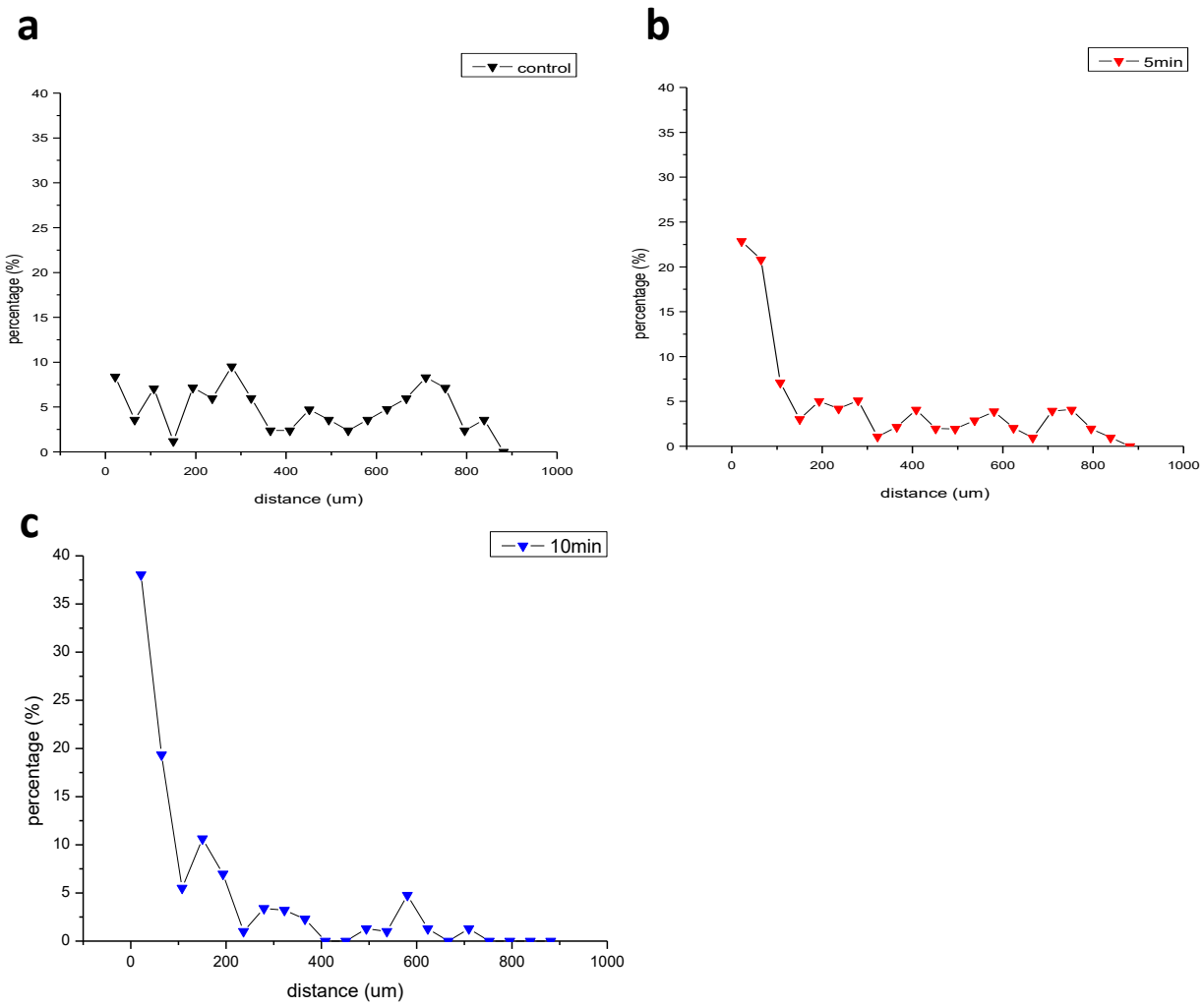

Figure 4.47 Distribution of Fe_3O_4-CHX spheres in HEMA-UDMA resin as a function of magnetic field treatment. (a) control without magnetic field treatment; (b) with magnetic field treatment for 5 min; (c) with magnetic treatment for 10 min.

According to the numbers of magnetic chlorhexidine spheres counted in each of the frames, their distribution was plotted as a function of distance to magnet (Figure 4.47). As for the control resin disc, the chlorhexidine spheres were homogeneously distributed so that numbers of spheres in each frame were quite even with average of 5 % particles in each frame. Though the first frame at the bottom was slightly higher with 8.4 % particles (Figure 4.47a). For the resin disc with 5 min magnetic field treatment, half of the magnetic chlorhexidine spheres distributed in the first three frames near the magnet with 22.9%, 20.8% and 7.1% for the first, second and third frames respectively. The rest of frames had an 2.5% average chlorhexidine spheres distribution (Figure 4.47b). The magnetic effect was most dramatic for the 10 min treatment group that 38% and 19.3% of magnetic chlorhexidine spheres was located in the first and second frames near the magnet, and the half of the resin disc at the other end of magnetic field had almost no chlorhexidine spheres distributed, though one or two particles were rarely seen (Figure 4.47c).

Release kinetics of chlorhexidine from HEMA-UDMA resin discs was showed in Figure 4.48. Generally, the release of chlorhexidine had two stages, with a fast release at the beginning 125 hours and a more sustained release afterwards. For the control group, the release is the most sustained, with 4.4 % of chlorhexidine released at the end of 650 hours. With 5 min magnetic field treatment, the release was accelerated, and there was 5.9% chlorhexidine release at 650 hours. The release kinetics for the 10 min treatment group was the most dramatic, that there was 7.4% release at the end.

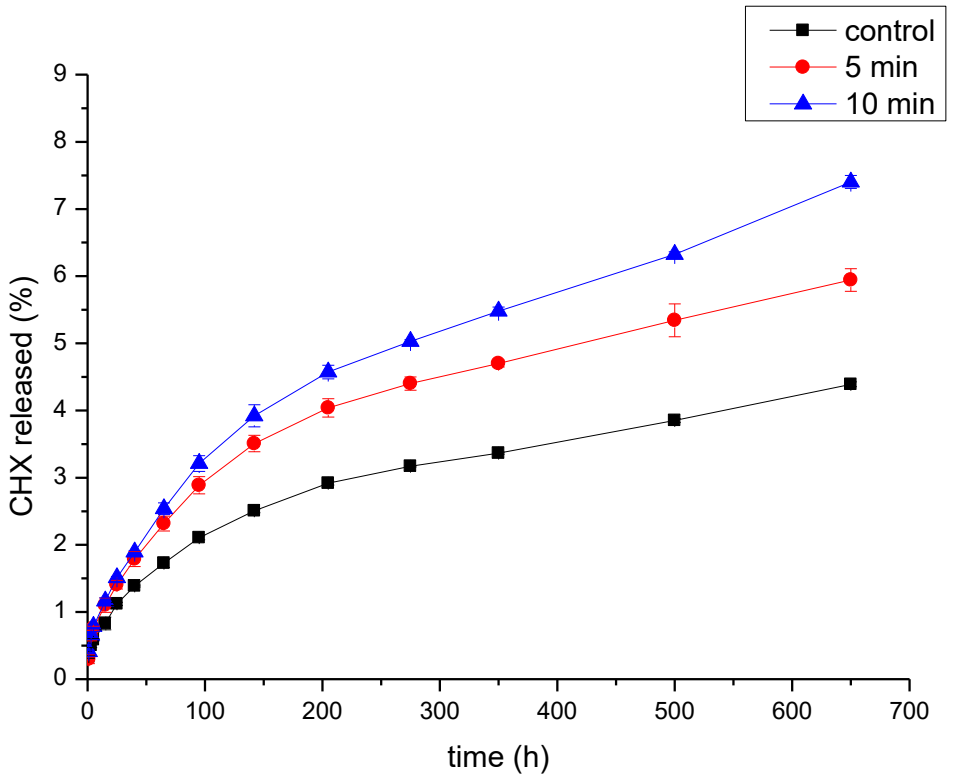

Figure 4.48 Release kinetics of chlorhexidine from HEMA-UDMA resin as a function of magnetic field treatment. (black line) control without magnetic field treatment; (red line) with magnetic field treatment for 5 min; (blue line) with magnetic treatment for 10 min.

4.2.3 Ultrasound triggered chlorhexidine release from HEMA-UDAM resin

The release process of the chlorhexidine from spherical particles filled UDMA-HEMA resin was much slower than that from chlorhexidine diacetate filled resin (Figure 4.49). Without any triggers, chlorhexidine diacetate filled resin discs released 16.2% chlorhexidine (Figure 4.49a, black line), in contrast, the chlorhexidine spheres filled resin discs had only 7.7% chlorhexidine released (Figure 4.49b, black line)

The effect of ultrasound on chlorhexidine release kinetics was significant, which the longer sonication duration, the higher release rate was observed. By 650 hours, chlorhexidine release rate for chlorhexidine diacetate incorporated resin discs were 23.5% (10s), 42.6% (20s), and 51.2% (30s), while 9.8% (10s), 12.3% (20s), and 14.0% (30s) for chlorhexidine spheres resin discs. And chlorhexidine diacetate crystals were more sensitive to ultrasound, which once the ultrasound treatment was stopped (at 205h, as indicated by red arrow), the release curve levelled off, whilst the spherical chlorhexidine compounds did not show so obvious trend.

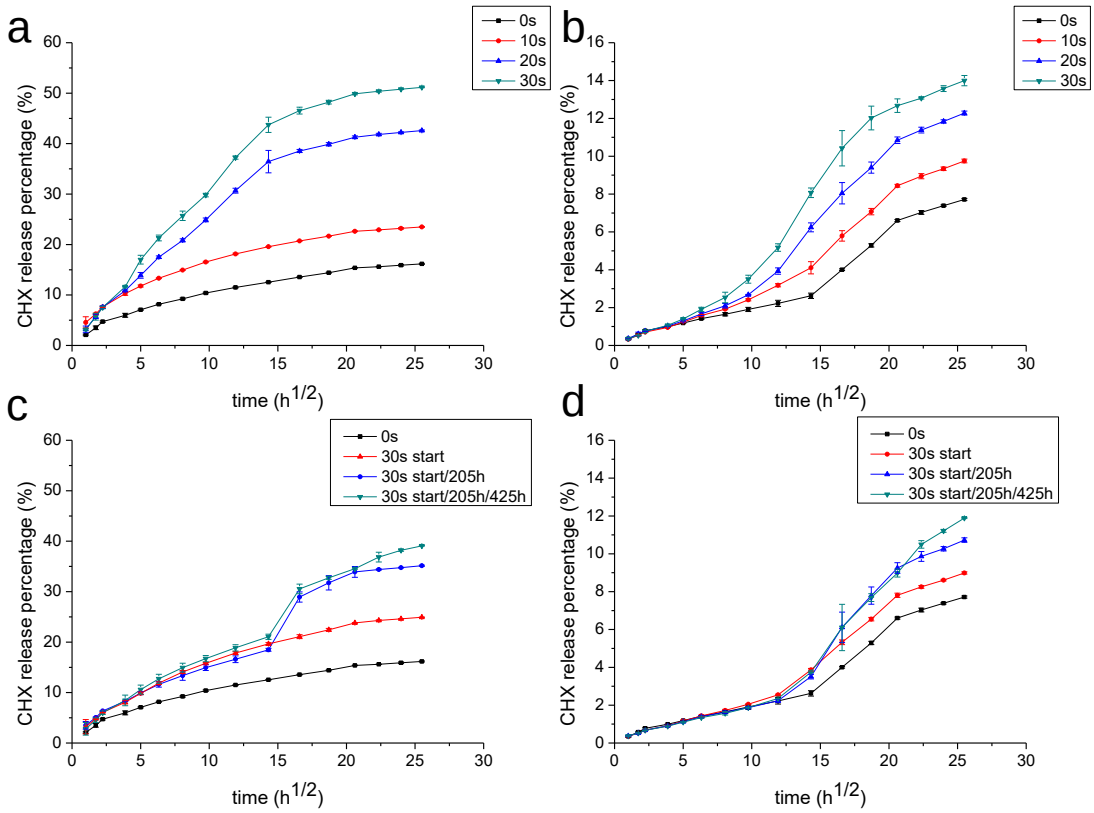

Figure 4.49 Release kinetics of chlorhexidine diacetate (a, c) and chlorhexidine spheres (b, d) contained UDMA-HEMA resin discs. Repetitive ultrasound treatment of 0 s (black), 10 s (red), 20 s (blue) and 30 s (green) and terminated at the 205h (a, b); And without ultrasound treatment (black), sonication for 30 s only at the beginning (red), sonication for 30 s twice at the 0h and 205h (blue), and sonication for 30 s three times at the 0h, 205h and 425h (green) (c, d). Red arrows indicated the point of termination of sonication (a, b) and each ultrasound treatment (c, d).

To further demonstrate the sensitivity to ultrasound and to control the release kinetics of chlorhexidine from UDMA-HEMA resin discs, ultrasound was only carried out at some specific time intervals (0h, 205h and 425h). The release kinetic of resin discs for each ultrasound treatment was illustrated in Figure 3c and d. For the chlorhexidine diacetate resin discs (Figure 4.49c), influence of sonication was dramatic that once treated for 30 s at the beginning, burst release was observed (indicated by first arrow), and when second treatment was applied (at 205h for 30s), more dramatic burst release was showed (indicated by second arrow), and the same jump of the release curve at 425 h could be seen when third sonication was applied. In comparison, chlorhexidine spheres contained resin discs were less sensitive to the sonication (Figure 4.49d), that no significant increase in release was observed for the first sonication, though obvious release curve jumps at 205 h and 425 h were also illustrated. These results demonstrated the ability to produce a burst or slow controlled/graduated release with the chlorhexidine compound within a resin.

The release profile of chlorhexidine from resin composite was a complicated process, which dissolution of drug may be ascribed for burst release only at the beginning, while the sustained release profile is dependent on Fickian diffusion [34]. This result was consistent with the previous studies that chlorhexidine and other antimicrobial agents had relatively higher release rate from methacrylate polymers [41, 230], which more than 50% of chlorhexidine could be released, while less than 5% was released from glass ionomer cements over 30 days [207, 231]. Similarly, increased chlorhexidine release rate was observed when hydrophilic components were increased and drug release had a correlation with the H_2O sorption [41].

Chlorhexidine release was also enhanced by ultrasound treatment for both the chlorhexidine diacetate and chlorhexidine spheres incorporated resin composites. With longer sonication (from 10s to 30s for each intervals), more chlorhexidine was released. And it was more obvious for the chlorhexidine diacetate crystals incorporated resin discs. It is feasible that micro

streaming induced by ultrasound was the main reason, which cavitation effect of ultrasound will be beneficial for fluid exchange which promotes the chance for chlorhexidine to diffuse out [232]. As aqueous channel/pathway is needed for chlorhexidine to leak out from resin composites, the influence of sonication on this process may be dramatic. In addition, thermal effect generated by sonication should also be taken into consideration. As indicated that influence of ultrasound on gentamicin release was equal to that caused by increasing 3℃ [115]. We could assume that heat generated during sonication helped dissolution of chlorhexidine compounds in the resin composites. Besides, the size of incorporated chlorhexidine compounds also had influence on release kinetics as bigger chlorhexidine crystals were more sensitive to ultrasound triggers than the homogeneous spheres, more dramatic jumps on release curve were observed corresponding to each of the ultrasound treatment.

Cross-section of chlorhexidine diacetate and spherical chlorhexidine compounds doped resin discs after 650 hours release were observed by SEM. As chlorhexidine was dissolved and released from the resin, voids could be observed. For the chlorhexidine diacetate incorporated resin, the dissolution of chlorhexidine started from crystal boundaries. The remaining chlorhexidine crystals were isolated in the cavity and small debris appeared (Figure 4.50a, no ultrasonication). In contrast, for the chlorhexidine spheres, the dissolution of chlorhexidine was started from the middle of particles, which voids were observed only at the central of particles and the particle/resin interface remained as intact as before. This was more obvious when comparing the discs with different ultrasound treatment duration. Longer ultrasound treatment lead to more chlorhexidine release and larger voids left in the middle of original particles (Figure 4.50b, no ultrasonication).

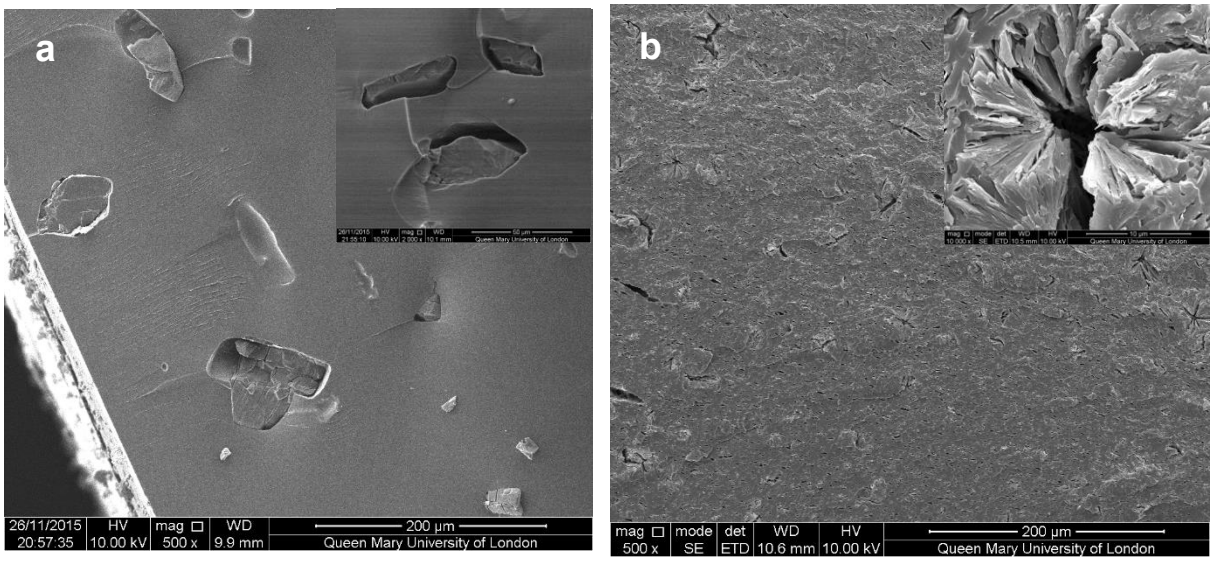

Figure 4.50 Cross-section of resin discs with chlorhexidine diacetate (a) and spherical chlorhexidine particle (b) after release test.

Confocal images of labelled chlorhexidine particles inside UDMA-HEMA film also revealed the similar chlorhexidine dissolve process (Figure 4.51). When the spherical particles were labelled with RhB, their distribution in the resin film could be observed, which at the red channel typical radiate needle structure was clearly seen. And before release, they were intact and had distinct edges. However, dissolution and release of chlorhexidine resulted in dark center in original particles, indicating that there was no chlorhexidine was there, though the interfaces of particles/resin remained distinct. The results further confirmed that dissolve of chlorhexidine was started at original particles center, and there was still large amount of chlorhexidine remained in the resin composite.

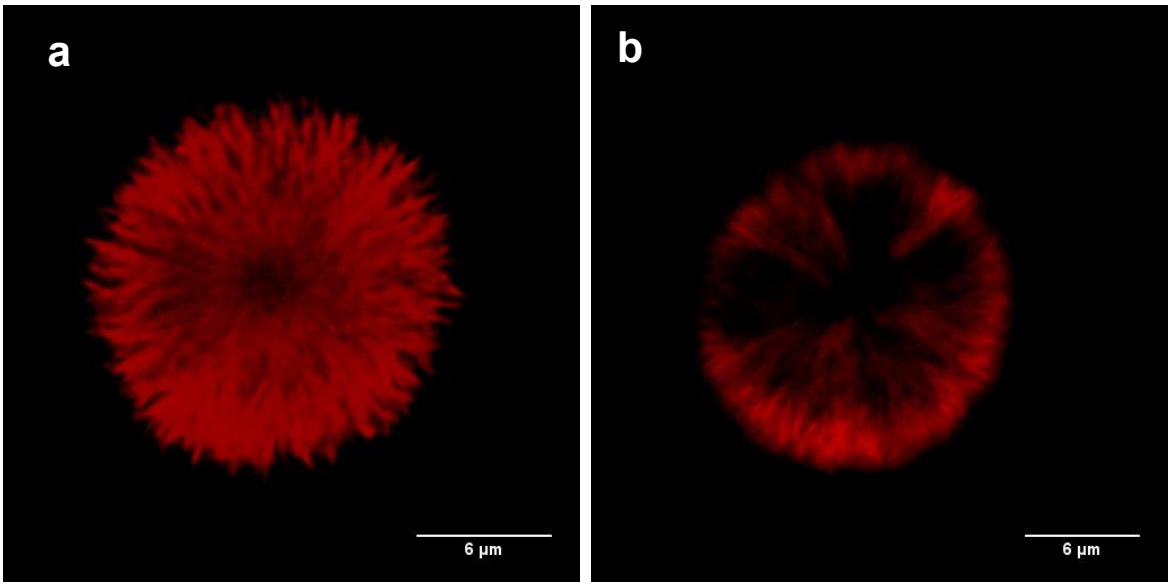

Figure 4.51 Confocal images of UDMA- HEMA resin film containing spherical chlorhexidine particles before (a) and after release (b).

4.2.4 Conclusion

In this section, chlorhexidine particles with multiple responsiveness were produced. When the chlorhexidine particles were functionalized with gold nanorods, a NIR light responsive property was achieved. By introducing gold nanorods into chlorhexidine solutions it was possible to control the amount and size of chlorhexidine spheres. Formation of gold functionalized chlorhexidine crystals was demonstrated in a gold nanorod assisted crystallisation and Ostwald Ripening mechanism. This process was also demonstrated by using chlorhexidine primary particles control chlorhexidine crystallisation, which a core-shell structure was demonstrated. Encapsulation of the gold nanorod functionalized chlorhexidine crystals using LbL polyelectrolyte multilayers allowed a sustained release and stimuli responsive release when NIR light irradiation was used.

When replacing the gold nanorods with Fe_3O_4 nanoparticles, similar size reducing effect was observed. The advantage to have Fe_3O_4 nanoparticle incorporated into the chlorhexidine spheres was that the drug particles could be attracted with an external magnetic field, and moved to the site of interest. So the magnetic chlorhexidine particles were imbedded into HEMA-UDMA resin and attracted by magnetic field for different durations before light curing. The distribution of magnetic chlorhexidine particles was successfully manipulated with magnetic field that with longer treatment more chlorhexidine particles were distributed at the surface of resin discs, and thus leaded to a higher release rate.

In addition, the chlorhexidine particles incorporated in the resin could be triggered with ultrasound. Compared to resin discs with chlorhexidine diacetate crystals imbedded directly, the resin with chlorhexidine particles showed a lower release rate, and upon ultrasound treatment, a more controllable burst release was demonstrated, which was beneficial for a safer performance in dentistry.

Overall, it is promising to have a chlorhexidine release on demand, either with ultrasound, NIR light or magnetic field, because bacterial infection treatment is always a tough and complicated process. Generally, a burst release is always needed at the beginning to kill most of the bacteria at infection site and then a sustained activity to inhibit any potential growth. So if any secondary infection occurs, it is likely to achieve another burst release with external triggers to get rid of the bacteria. Combined with magnetic responsive properties, it is even more attractive as we can easily increase the local drug concentration by targeting delivery with magnetic field. For the biofilm treatment, a very high local drug concentration is needed, chlorhexidine particles have the potential to be navigated to biofilms and transport through their barriers and triggered locally. It is an ideal concept for antibacterial agent delivery in the future medicine and dentistry.

5. Doxycycline delivery

5.1 Local and sustained delivery of doxycycline

5.1.1 Doxycycline encapsulation

Small molecule drugs can be incorporated into microcapsules through electrostatic interactions following a post loading approach.[99, 233] Doxycycline as a small molecular drug (structure showed in Figure 5.1a), in our study, was encapsulated by precipitating with DS (Figure 5.2). Typically, two types of capsule were assembled, synthetic capsules consisting of PAH/PSS layers and biodegradable ones composed of Parg/DS, both of which had DS in the interior for doxycycline loading (Figure 5.3a and d). Upon incubation, doxycycline penetrated the microcapsule layers forming a less soluble complex with DS in the core, as well as being trapped within the layers. The synthetic capsules became smaller in size and had a more protuberant structure after doxycycline loading (Figure 5.3 b), indicating that doxycycline-DS complex was formed in the core. Whilst, the biodegradable capsules did not undergo such notable morphological change, but according to the increased capsule shell thickness (Figure 5.3 e), we could assume that more doxycycline was absorbed in the microcapsule walls. The principle of the complex forming was based on the ion paring ability of dextran sulphate, as indicated by the FTIR spectrum (Figure 5.1b), which was also used to promote minocycline loading efficiency in PLGA nanoparticles.[4] Similar phenomenon was observed when ciprofloxacin was deposited into capsules, with a black shadow seen in the capsule interior under TEM and an increase in average capsule height by 500 nm.[234] According to measurement of supernatants from encapsulation, doxycycline loaded in synthetic and biodegradable capsules was determined to be 5.4 pg and 4.8 pg per capsule, respectively. Doxycycline amount per gram of capsules was determined to be around 9.74 wt.% according to the net weight increase compared to the empty microcapsules. The results were confirmed by fluorescence

imaging, synthetic capsules with doxycycline had more blue fluorescence in the core, while blue fluorescence in biodegradable capsules was within the rings of microcapsule shells (Figure 5.4) in both instances doxycycline is complexed with DS.

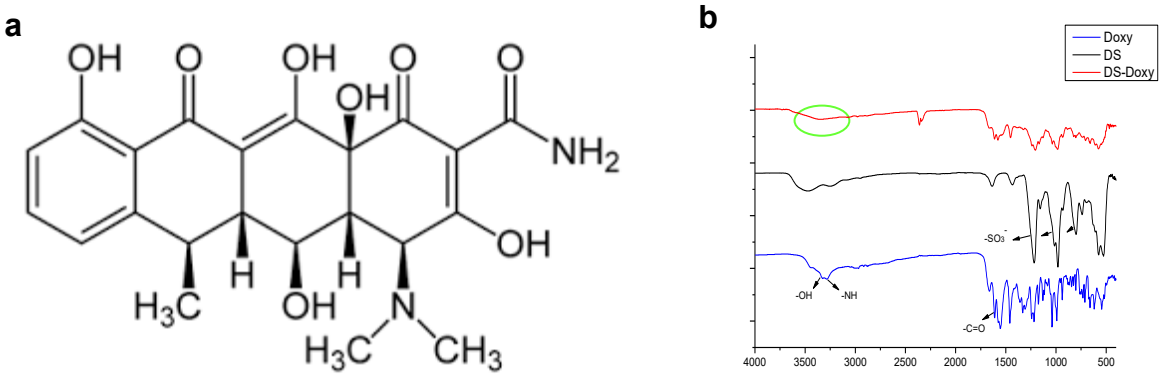

Figure 5.1 Doxycycline and FTIR spectrum. Molecule structure of doxycycline (a), FTIR spectrum of doxycycline (blue), dextran sulfate sodium salt (black) and doxycycline-DS complex (red) (b).

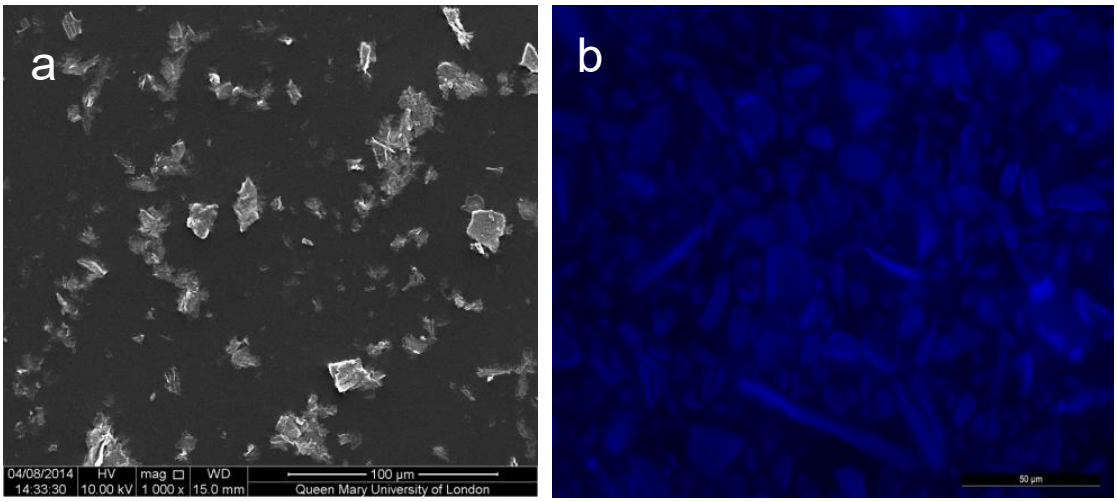

Figure 5.2 SEM and fluorescence image of doxycycline-DS complex (a, b).

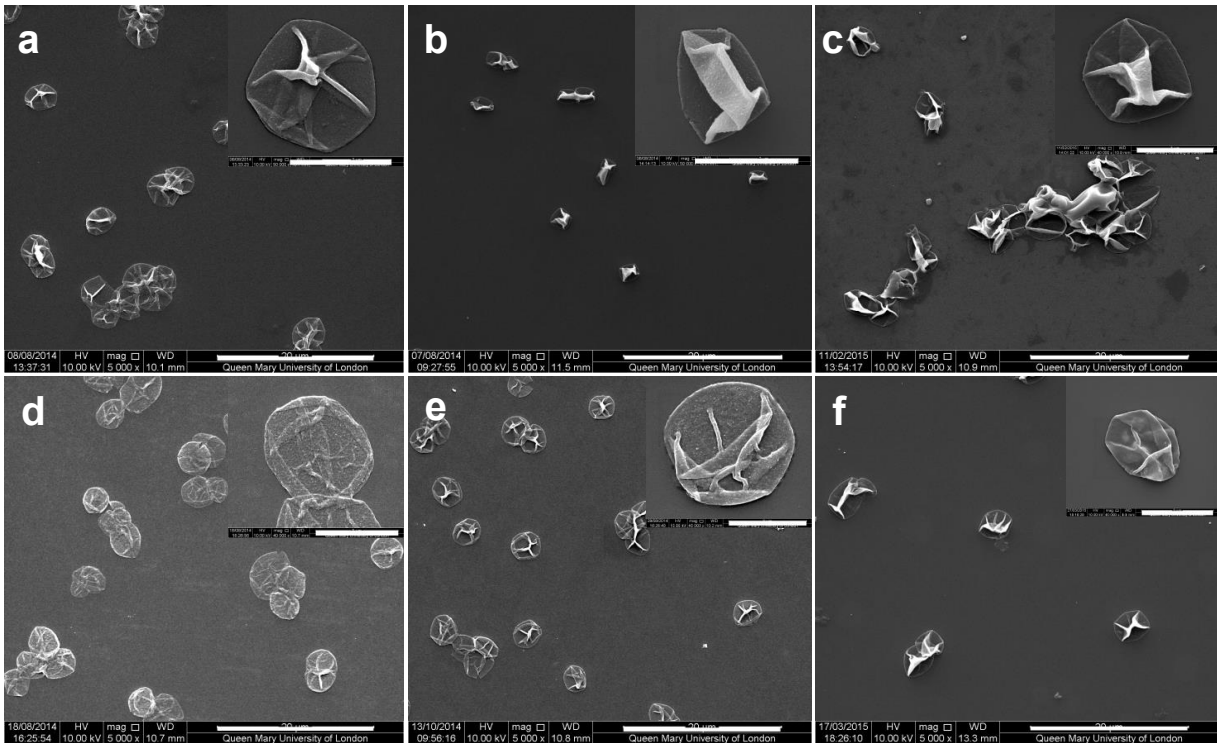

Figure 5.3 SEM images of synthetic capsules (a-c) and biodegradable capsules (d-f), before being loaded with doxycycline (a, d), after loading with doxycycline (b, e), and coated with a lipid layer on the surface (c, f) (scale bar of 20 μm). The inset images are individual capsules at high magnification (×40000) (scale bar of 3 μm).

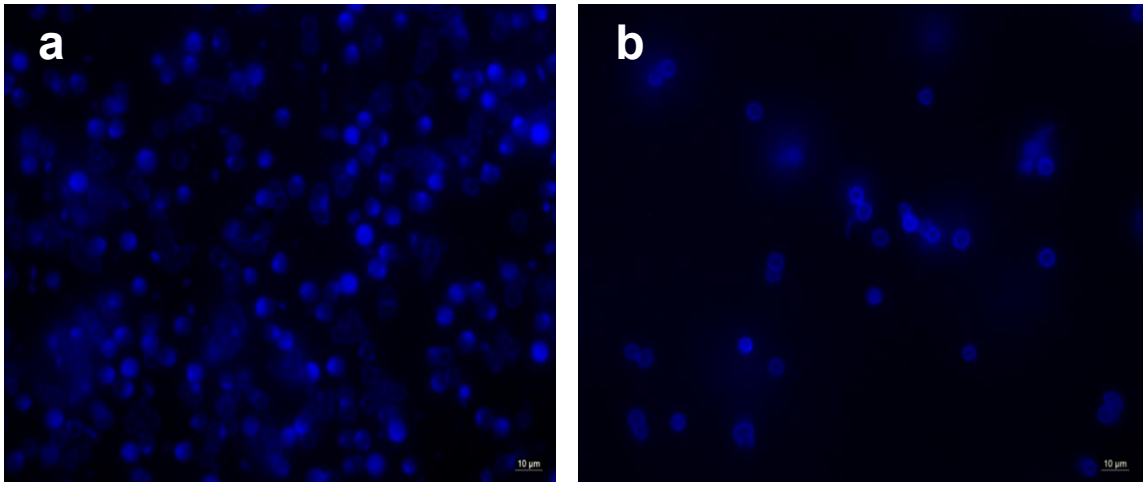

Figure 5.4 Fluorescence images of doxycycline-loaded synthetic capsules (a) and biodegradable capsules (b).

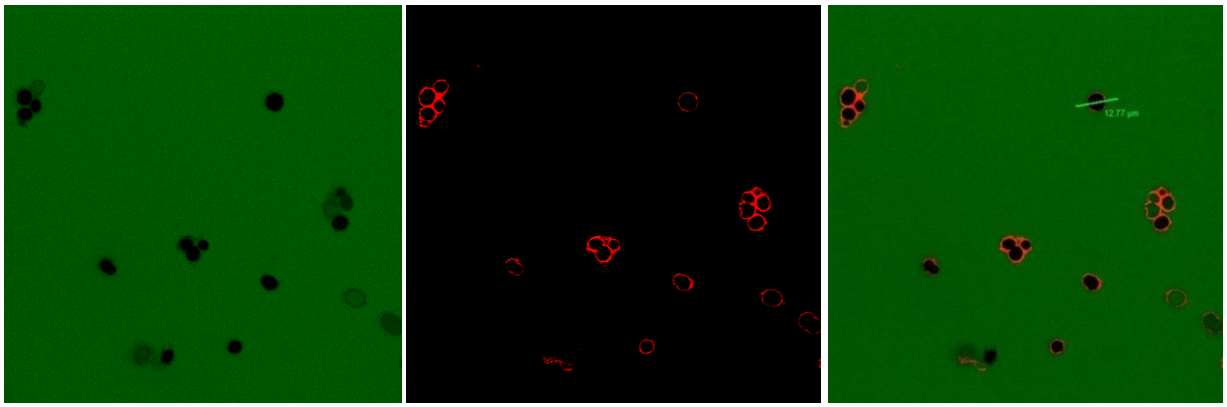

Figure 5.5 Permeability of DPPC coated synthetic capsules to FITC (outmost lipid layer was labelled with Rhodamine B).

Since the microcapsule shells are permeable, extra layers are often assembled to enable longer drug retention. Such layers are either more hydrophobic or have a denser meshwork. The phospholipids DPPC and lecithin were used as an outer layer for synthetic and biodegradable capsules respectively. As could be seen by changes in zeta potential (data not shown), the outmost DPPC coating altered the negative charge of PSS to slightly positive, which confirmed addition of the lipid layer on the surface. In addition, confocal images of capsules show red circles when the lipid was labelled with Rhodamine B. In the permeability test, the outer lipid layer also effectively hindered penetration of FITC through capsules. Whilst an incomplete lipid layer on the microcapsule surface only rendered them partially permeable to FITC (Figure 5.5). These results provide evidence that microcapsule permeability was reduced by the lipid coating. SEM images of lipid coated capsules (Figure 2c and f) shows that DPPC, or lecithin coating smoothed the capsule surface (inset image), which was evidenced as a more compact outer shell was formed. Similar morphological changes were previously observed when biotinylated lipid was assembled on the surface of PAH/PSS capsules resulting in an uncollapsed structure.[235] According to measurement of supernatants, doxycycline loaded in

DPPC-coated synthetic and lecithin-coated biodegradable capsules was 5.3 pg and 5.4 pg per capsule, respectively.

5.1.2 Release kinetics of doxycycline

Release kinetics of a drug from LbL assembled microcapsules is primarily dependent on physio-chemical properties of the polymeric shells[200] and the binding characteristics between the drug molecules and capsules.[233, 236] In our study, doxycycline was trapped by forming a complex with DS, and the release of payload was affected by both factors. Due to the porous structure of polymeric shells, doxycycline was able to diffuse through, but the capsules shell thickness, polyelectrolyte molecular weight and ionic strength of the medium all affect the diffusion rate.[200] Changes in the ionic strength of solution alter the strength of electrostatic interactions within the microcapsule shell structure and in the binding between doxycycline and DS. By shaking in water, 0.15M NaCl or PBS, doxycycline release from all microcapsules was monitored, and the rate of doxycycline release from all microcapsules was PBS>0.15M NaCl>water (Figure 5.6). In low ionic strength solution, a tightly packed microcapsule structure is observed, but when the polymeric structure is transferred to high ionic strength solution, the charge of polymers is shielded and the rearranged microcapsule structure is more permeable to small molecules.[203] With regards to doxycycline and DS binding, in water, there would be a stronger binding between the two molecules, due to charge interaction of negatively charged DS and amino groups of doxycycline, but PBS and NaCl might accelerate the dissociation of the DS-doxycycline complex via charge decoupling in salt solution. What facilitates release of free doxycycline from the capsule interior. And in general, the release of doxycycline from microcapsules was bi-phasic; a primary burst release within the first 40 minutes and a slower secondary release after 40 minutes (Table 5.1). The first phase is relevant to detaching of more loosely bound doxycycline and second phase is salt induced dissolution

of complex between DS and doxycycline. In case of pure water the effect of different stage is less notable. By mixing the microcapsules with 2 M NaOH, all microcapsules disassembled[186] and all the encapsulated doxycycline was released immediately. After being centrifuged, doxycycline capsules without NaOH had yellow pellet at the bottom of tube (means doxycycline was still encapsulated in capsules). However, with 2 M NaOH added, there was no pellet but the dissolution was yellow. By measure the solution, 100% release rate was identified.

The release kinetics were however slower when microcapsules were coated with a lipid layer as shown in Figure 3c and 3d. The retention of doxycycline with the lipid coated capsules can be attributed to lipophilic nature of doxycycline[237] and to the hydrophobic barrier formed at the outmost capsule surface by phospholipids which would be less permeable aqueous solutions. A phospholipid outer layer seal was previously employed in the encapsulation of the small molecule drug doxorubicin.[185] The difference in the release kinetics for lipid coated synthetic and biodegradable capsules may be due to the fact that lecithin, a natural phospholipid, is a heterogeneous molecule with a range of molecular weights which may prohibit the formation of a more compact coating layer observed with synthetic DPPC.

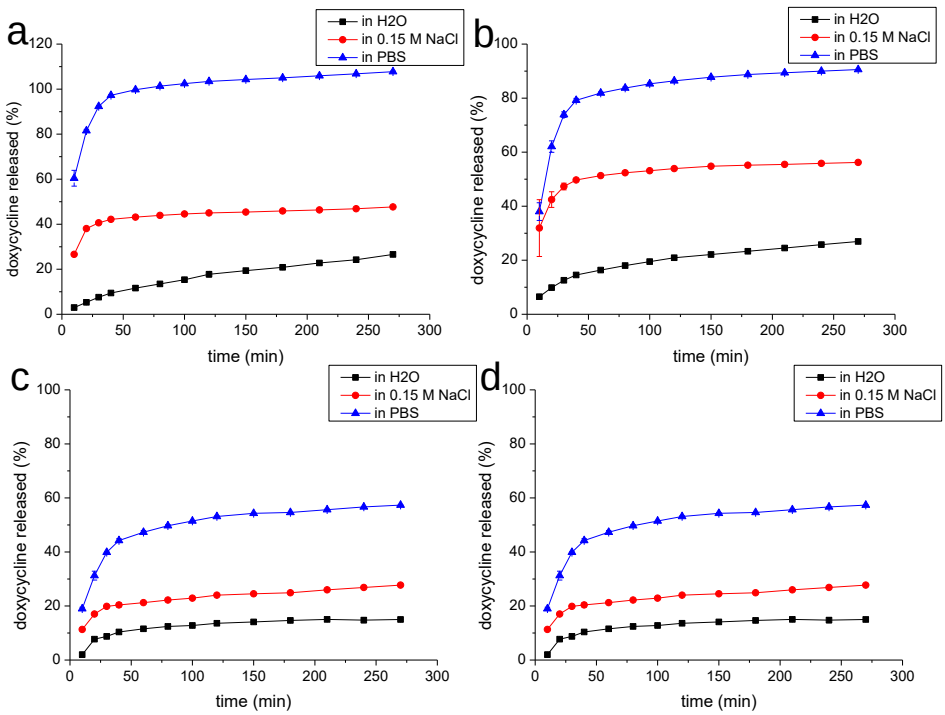

Figure 5.6 Kinetics of doxycycline release from microcapsules. Release profile of doxycycline from synthetic capsules (a), biodegradable capsules (b), synthetic capsules with DPPC coating (c) and biodegradable capsules with lecithin coating (d) in water, 0.15 M NaCl, and PBS. Values are the mean of 3 groups and vertical bars represent the SD.

Table 5.3 Rate of doxycycline release rates from microcapsules in different solutions. Phase 1 release is the kinetic in the first 40 minutes whilst phase 2 release relates to the kinetic during the subsequent 235 minutes.

Doxycycline release rate	In H_2O		In NaCl		In PBS	
(ug/min)	Phase1	Phase2	Phase1	Phase2	Phase1	Phase2
Syn capsules	0.229	0.067	0.700	0.019	1.595	0.032
DPPC coated syn capsules	0.263	0.016	0.428	0.029	1.045	0.043
Bio capsules	0.305	0.043	0.769	0.021	1.794	0.039
Lecithin coated bio capsules	0.313	0.019	0.599	0.029	1.476	0.059

5.1.3 Local and sustained activity of doxycycline in Engineered C2C12 cells

Viability of cells treated with doxycycline solution, synthetic and biodegradable capsules (w/o doxycycline encapsulated) is shown in Figure 5.7. Compared to the control group, cells treated with doxycycline solution (2.5 µg/ml) had a viability of 89% after 48 hours incubation. With both synthetic and biodegradable capsules, over 80% cell viability was observed at the same time point. In addition, no significant difference was observed between empty and doxycycline loaded capsules which was consistent with previous studies of capsule cytotoxicity *in vitro* and *in vivo*.[20, 238-239]

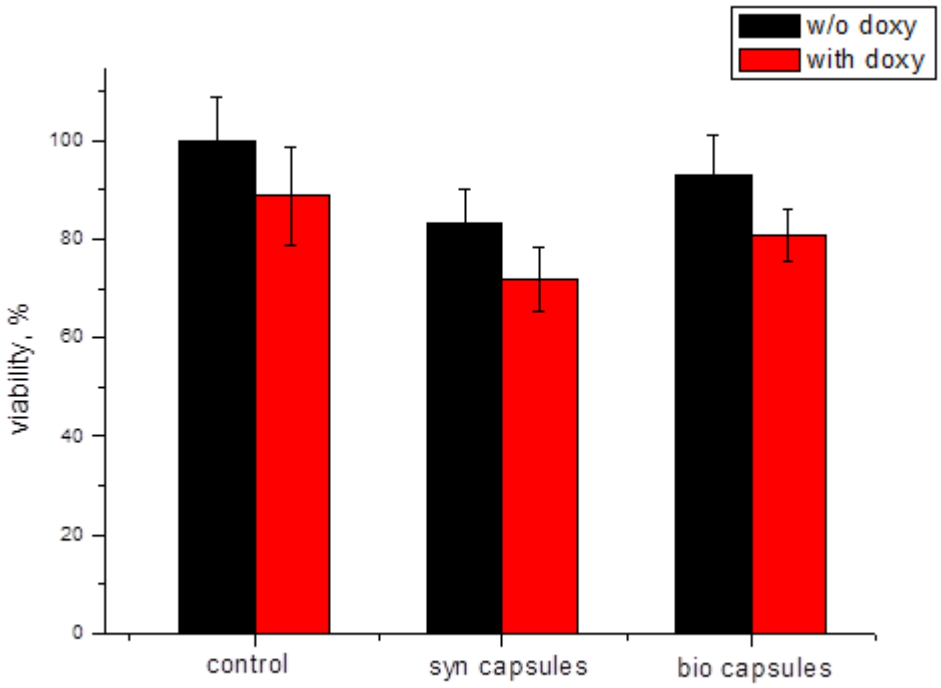

Figure 5.7 Cell viability of engineered C2C12 cells incubated with doxycycline solution, synthetic and biodegradable capsules with and without (w/o) doxycycline. Values are the mean of six values and vertical bars represent the SD.

When reporter cells were treated with doxycycline solution or encapsulated doxycycline the different cell delivery routes impacts on the kinetics of EGFP expression from the tetracycline responsive promoter (P*tet*). The promoter is activated by rtTA-2SM2 in the presence of doxycycline and is actively switched off upon removal of doxycycline through binding of the repressor *tet*RKRAB. This *tet-on* system has shown high gene regulation efficiency in our previous study,[50] and this was confirmed here. Confocal images were taken to assess whether doxycycline loaded capsules were internalized by myoblast cells and subsequently induce EGFP expression in C2C12 cells via the *tet-on* system. Synthetic capsules were incubated with cells for 2 days at a ratio of 10 capsules per cell, and the same amount of free doxycycline was used as control. As illustrated in Figure 5.8, EGFP expression was successfully switched on by doxycycline solution with homogenous fluorescence in every cell (Figure 5.8A). However, when delivered as cargo by microcapsules, doxycycline was released after cell uptake of capsules, so cells without internalized capsules had no fluorescence as indicated by red circles in Figure 5.8B. The results highlighted that doxycycline delivery from microcapsules can be targeted to specific cells via capsule internalization which then function *in situ*.

To evaluate the efficiency of doxycycline delivered by capsules, cells were classified into four categories (Green/red, green, red and none – see methods for details) and the number of cells in each category was counted within the panoramic confocal image, and was presented as a percentage in Figure 5.9. The capsule uptake ratio by cells was about 70%, and doxycycline capsules induced EGFP expression was as high as 61.8% (shown as green and red in the histogram), but there were a small proportion of these cells with red microcapsules that were devoid of EGFP expression (8.9%). When no capsules were engulfed 18% of cells were not green as expected, but 11% were fluorescent. There are potential explanations for this observation, firstly, capsules were not visible in these cells (hidden under the nucleus); secondly, after cell division a daughter cell could contain EGFP but not a microcapsule from

the parent cell; alternatively, doxycycline could leak from extracellular microcapsules located nearby or in other cells. A similar phenomenon was observed when EGFP was delivered as cargo in capsules to A549 cells, when cells with no engulfed capsules had EGFP in the cytosol.[144] As for the non-fluorescent cells that had internalized microcapsules, the absence of fluorescence may be due to capsules being devoid of doxycycline or containing an amount of doxycycline below the threshold to induce EGFP expression, though the baseline for doxycycline to switch on gene expression is known to be very low (1 pg/ml).[50] Previous studies have tried to chemically modify doxycycline to achieve spatial and temporal gene expression regulation,[54, 240] in which doxycycline was inactivated in a 'cage' so that transcription was only promoted after photo-activation. But, delivery by versatile microcapsule carriers is a preferable approach as minimum modification to molecular structure is introduced and side products of chemical reactions are not generated.

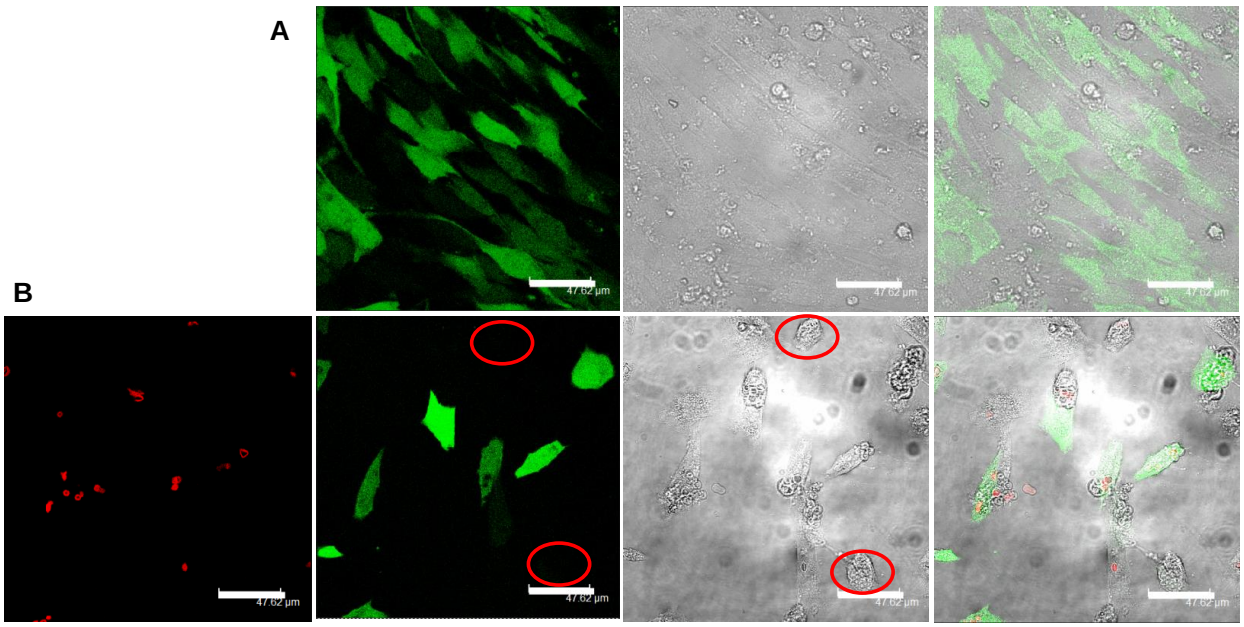

Figure 5.8 Images of doxycycline induced EGFP expression. Cells treated with a solution of doxycycline (A) and doxycycline-loaded synthetic capsules (B) (capsules to cells ratio 10:1, incubate time 48 hours, red circles indicate cells that have no internalized capsules or EGFP expression) (scale bar of 50 μm).

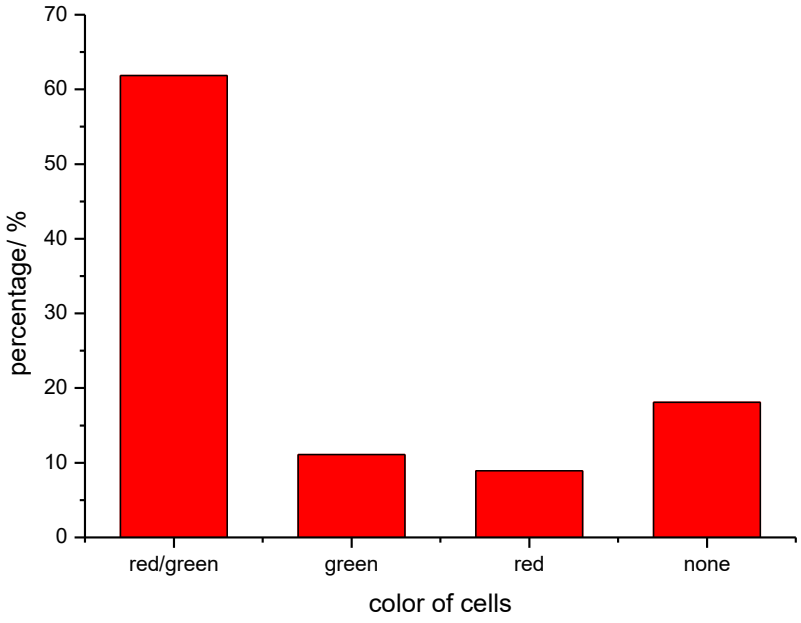

Figure 5.9 Correlation of microcapsule delivery and EGFP expression in C2C12 cells. After incubation with doxycycline-loaded synthetic microcapsules that were labelled red due to use of TRITC labelled PAH cells exposed to doxycycline express EGFP. The distribution of cells in the four categories (Red/green: cells with microcapsules and expressing EGFP; Green: cells expressing EGFP but have no capsules; Red: cells with microcapsules have no EGFP expression; None: neither red or green) was determined by microscopic examination with results expressed as a percentage of all cells (total number 459).

To demonstrate the sustained effect of doxycycline delivered by microcapsules, the kinetics of EGFP expression was monitored by fluorescence intensity change in long-term experiments. Four types of capsules, synthetic (PAH/PSS) and biodegradable (DS/Parg) were compared with their lipid coated counterparts. EGFP fluorescence intensity at specific time intervals was measured for each type of capsule. Cells treated with free doxycycline had the maximum fluorescence intensity at day 2 and declined to baseline values after 10 days (Figure 5.10a). For

all the capsule-treated cells, the fluorescence intensity increased and peaked on the fourth day, then fluorescence decreased gradually, and there were significant differences compared with the free doxycycline treated cells after the sixth day ($p < 0.05$). Doxycycline molecules are lipophilic enabling them to rapidly enter cells and induce gene expression, while microcapsules enter cells following membrane adherence, phagocytosis and macropinocytosis mechanisms, and are finally targeted to phagolysosomes[95, 238] doxycycline released from microcapsules in these compartments can still penetrate lipid membranes but clearly the kinetics of nuclear delivery are slower than the free doxycycline. For the synthetic capsules, DPPC coating resulted in elevated and prolonged EGFP expression compared with the uncoated microcapsules ($p<0.01$) (Figure 5.10b). Whilst for the biodegradable capsules, the lecithin coating only improved expression from day 4 to day 8 ($p < 0.01$) (Figure 5.10c).

The fluorescence intensity kinetics indicated that all doxycycline loaded capsules had a sustained effect *in vitro,* which was optimal with DPPC coated synthetic capsules. The EGFP fluorescence peak intensity was higher for lipid coated capsules than the uncoated ones. It is feasible that the DPPC lipid not only promoted microcapsule retention of lipophilic doxycycline but may also promote cell uptake of capsules.[185, 241] If this is the case then higher levels of EGFP expression observed with DPPC coated capsules could, in part be attributed to a higher total doxycycline dose delivered to cells. For the lecithin coated biodegradable capsules, though, the *in vitro* release kinetics of coated microcapsules is more sustained than the uncoated ones, the EGFP kinetics are similar. It is feasible that digestion of outmost lecithin layer could limit lipid retention and result in a similar intracellular doxycycline release rate as uncoated microcapsules.

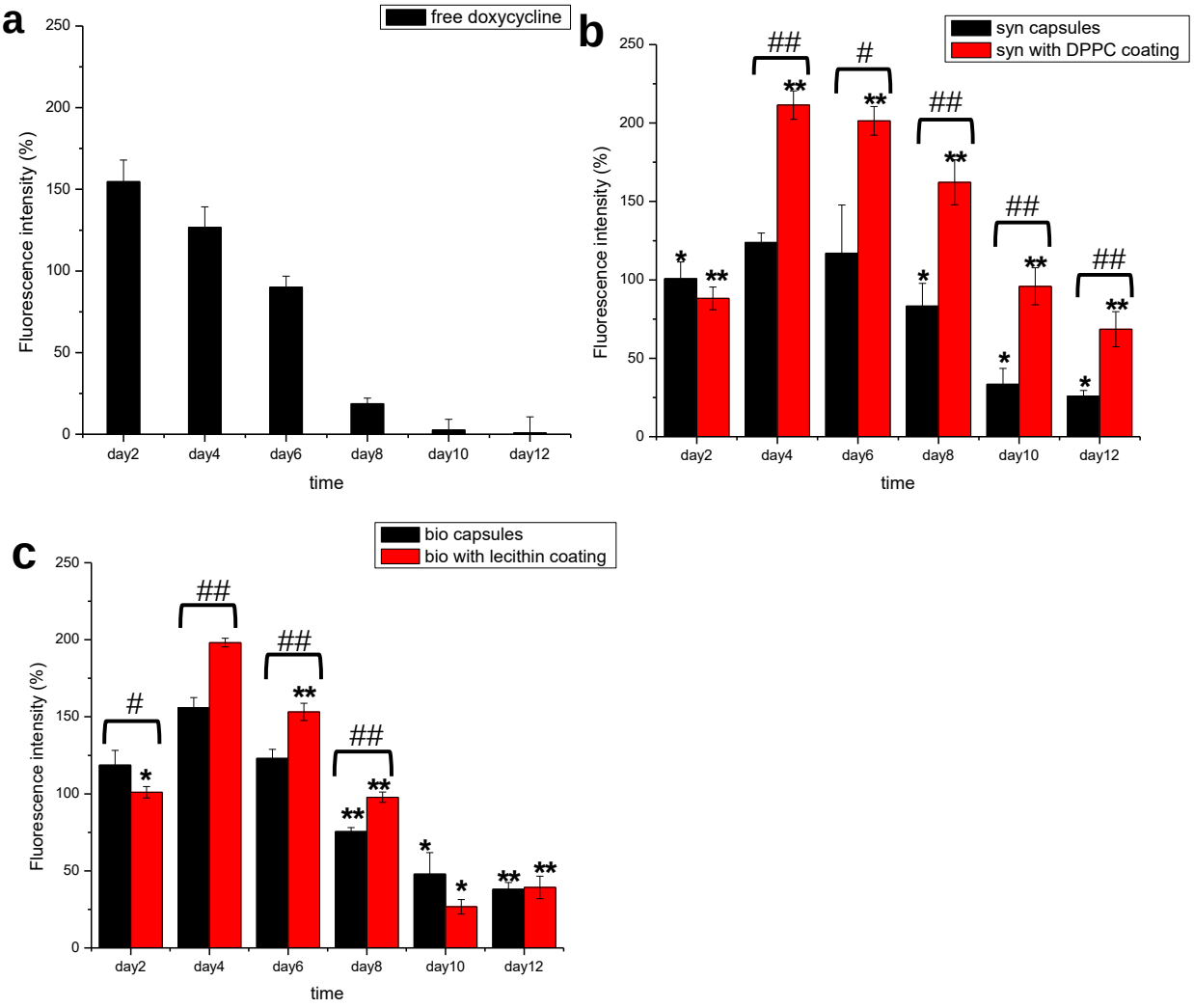

Figure 5.10 Kinetics of EGFP expression following delivery of free or encapsulated doxycycline. Cells were cultured in 96-well plates with 1×10^4 cells in each well and the following day were incubated with free doxycycline (a), doxycycline-loaded synthetic and DPPC coated synthetic capsules (b), and doxycycline-loaded biodegradable and Lecithin coated biodegradable capsules (c) at a ratio of 10 microcapsules per cell (n=7), medium was changed every two days, and after 2, 4, 6, 8, 10 and 12days cells were lysed and fluorescence intensity was measured with excitation at 488nm, emission at 520nm. Values are the mean of 5 wells and vertical lines are SD, $^{*}p< 0.05$, $^{**}p< 0.01$, compared with free doxycycline treated cells; $^{\#}p< 0.05$, $^{\#\#}p < 0.01$, compared between lipid coated and uncoated capsule treated cells.

The observations were further explored in a parallel experiment that monitored EGFP expression by confocal microscopy. As shown in Figure 5.11, the same amount of doxycycline, delivered by capsules could extend the duration of EGFP expression. For cells treated with free doxycycline, EGFP fluorescence began to decline after six days, and by the eighth day, dark nuclei appeared and only the cytoplasm was fluorescent. The decline of EGFP continued until to the twelfth day when no fluorescence was observed. For uncoated synthetic and biodegradable capsules, EGFP expression was maintained for twelve days, after which dark nuclei also appeared, and the decline in EGFP expression continued to day 34. EGFP expression was prolonged to eighteen days for the DPPC coated synthetic capsules, indicating that sustained release from engulfed capsules at levels sufficient to induce EGFP expression. As for the lecithin coated biodegradable capsules, the lipid layer did not dramatically enhance the duration of EGFP expression, which was similar to the duration of uncoated biodegradable microcapsules. Although a biodegradable or synthetic microcapsule structure can have a big influence on release of contents this is of less importance for the release of low molecular weight drugs which can pass through the microcapsule structure even in the intact state. However, release of low molecular weight doxycycline will be sensitive to permeability changes in microcapsules associated with degradation and digestion of the lipid layer. In our studies with myoblast cells, though some 'intact' biodegradable capsules were observed inside cells after 34 days, the degradation of the lecithin layer might have occurred much earlier. As shown in previous research, 6-carboxyfluorescein could penetrate DPPC/DMPA lipid capsules immediately after partial hydrolysis by the enzyme phospholipase A2, while untreated capsules were impermeable. High-resolution surface force microscopy further revealed the increased capsule surface roughness after enzyme treatment.[242] The combination of the versatility of LbL microcapsules and the sensitivity of the Tet-on system have enabled us to accurately monitor the delivery of doxycycline in a cellular system. From our previous investigations it should be

possible to include doxycycline into capsules engineered with nanoparticles or enzymes within the shells, so that release of doxycycline could be regulated in response to lasers, magnetism or in an endogenously responsive manner.[19, 243] Magnetism could also be used to target microcapsule delivery to specific cells or tissues.

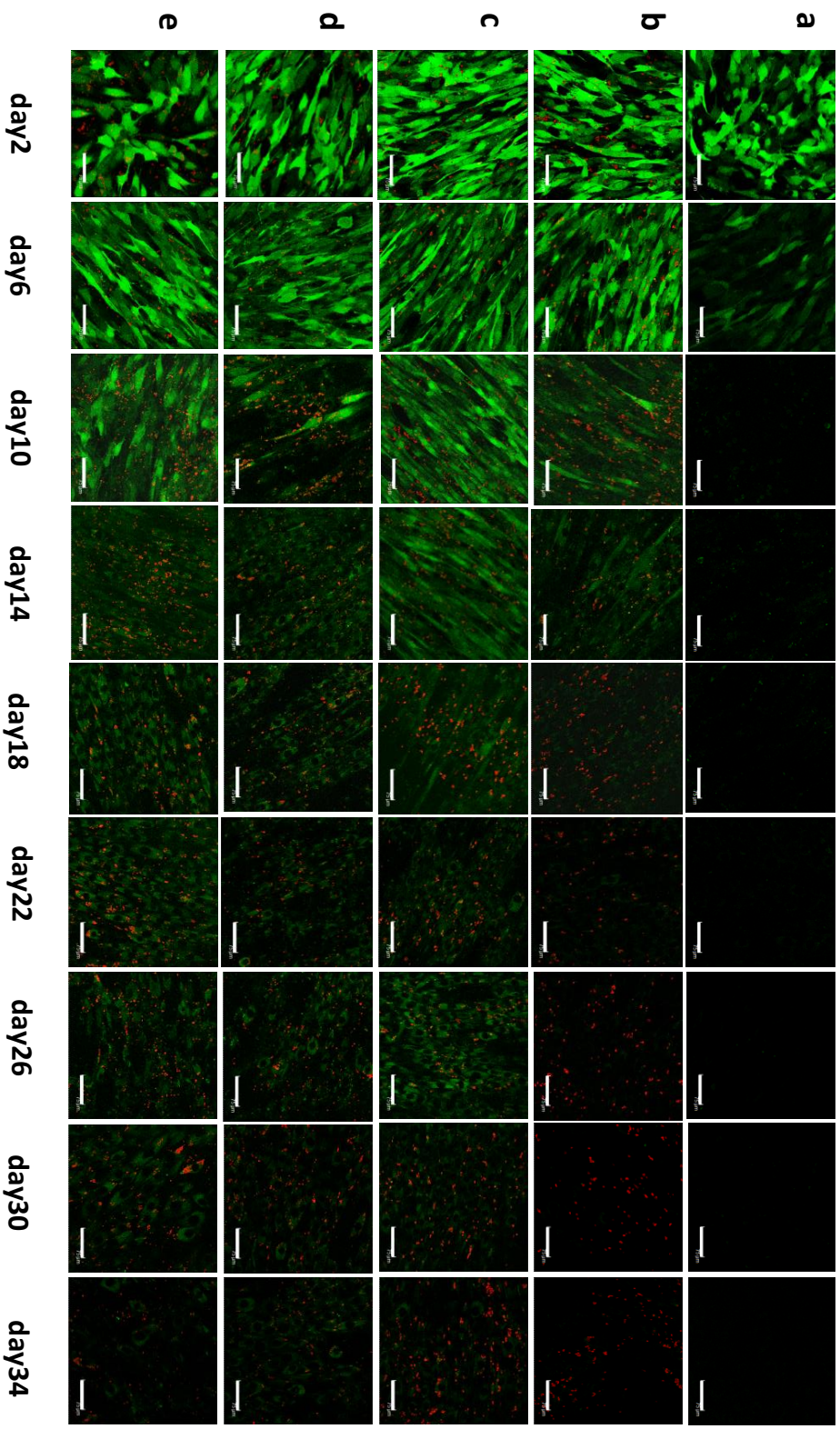

Figure 5.11 Comparison of EGFP expression kinetics following delivery of free and encapsulated doxycycline to engineered C2C12 cells. Cells were incubated with free doxycycline (a), doxycycline-loaded (b) and DPPC coated (c) synthetic capsules, and doxycycline loaded (d) and lecithin coated (e) biodegradable capsules at a ratio of 10:1 as indicated. The free doxycycline concentration in culture medium was 2 μg/ml, and medium was changed every two days. Images were captured using Leica confocal microscope with 40× oil emersion objective. Microcapsules are labelled with TRITC and are red in images of microcapsule treated cells (scale bar of 75 μm).

5.1.4 Antimicrobial activity of doxycycline capsules

The activity of doxycycline in the C2C12 cell assay opened the possibility for delivering antimicrobial effects with LbL microcapsules. Since persistent infections are challenging to treat that overuse of antibiotics will lead to resistant bacteria,[2] a deposit of sustained antibiotic release may be an attractive treatment approach for local infections. The sensitivity of *E. coli* growth to inhibition with doxycycline was initially demonstrated in a dose response experiment in which the relationship between diameter of clear zone and doxycycline concentration was pictured (Figure 5.12a) and plotted (Figure 5.12b). Clear zones in this assay show that higher doxycycline concentrations have greater inhibitory effect and the assay is sensitive to doxycycline concentrations as low as 40 μg/ml. The inhibitory zone against *E. coli* was dependent on the concentration of doxycycline, with more doxycycline diffused into the agar larger clear zones were formed. In the transfer experiment, free doxycycline (1 mg/ml) was devoid of any antimicrobial activity after 6 hours, whilst inhibitory activity for the 0.1 mg/ml solution was lost after 3 hours (Figure 5.12c). In contrast, doxycycline loaded microcapsules had more sustained antimicrobial effect, clear zones were still visible for all the microcapsules

after 7.5 hours and for synthetic microcapsules with a DPPC outer layer activity persisted beyond 10.5 hours (Figure 5.12c). The kinetics of inhibition are plotted in Figure 5.12d, and clearly illustrate the sustained antimicrobial effect of doxycycline loaded microcapsules with a gradual decline in activity compared to the more rapid decline seen with doxycycline solutions. It is likely that diffusion of encapsulated doxycycline was more sustained because more liquid exchange was needed to detach doxycycline from microcapsule shells and the DS-doxycycline complex. Microcapsules may be particularly suited to topical application here their size permits them to reside around root hair cells[244] and also in situations where prolonged local delivery of antibiotic is beneficial such as post-operative and dental applications.

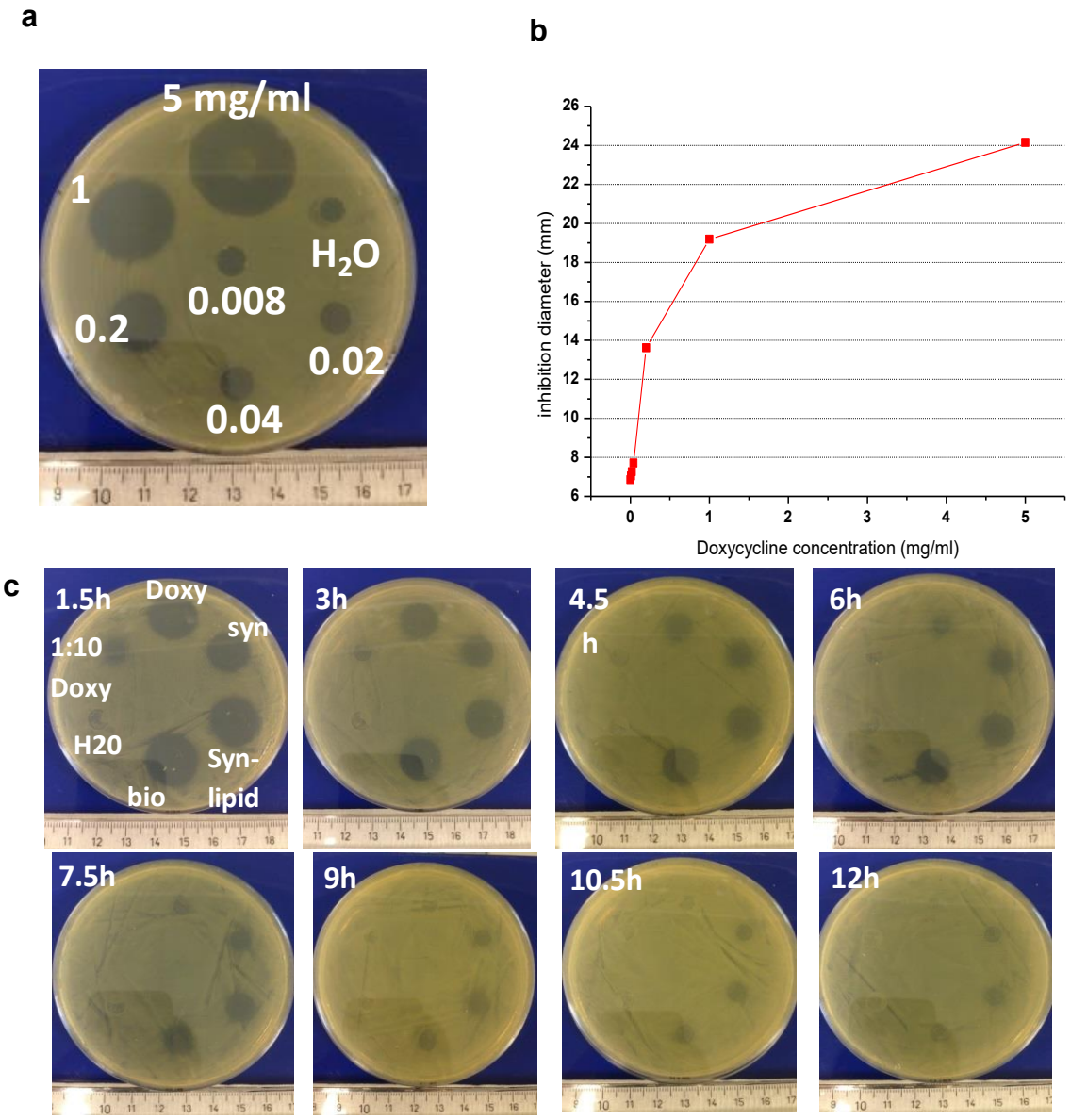

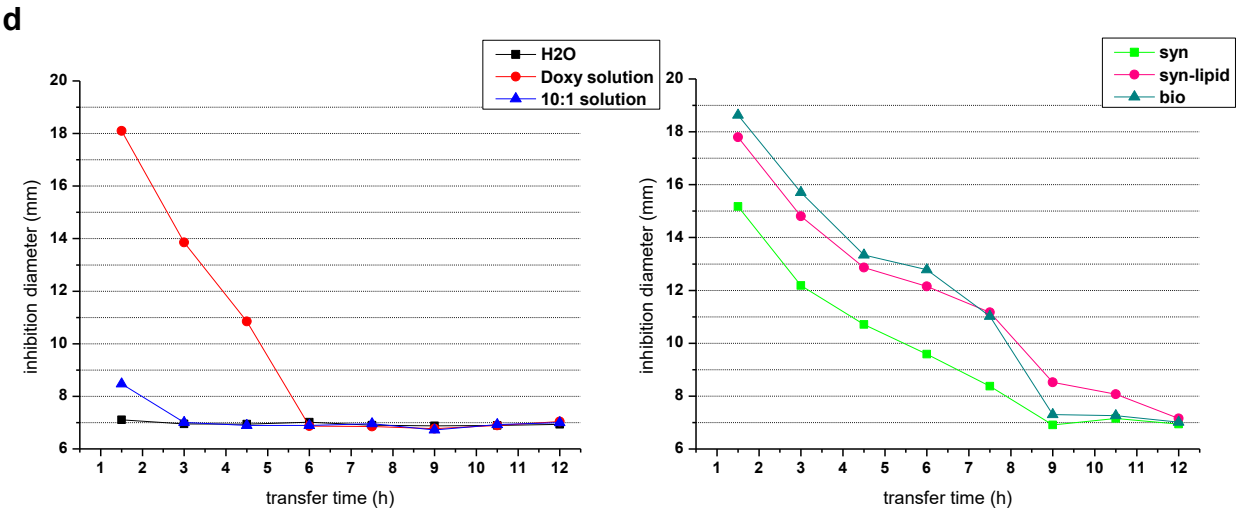

Figure 5.12 Antimicrobial activity of doxycycline with an agar diffusion assay against *E. coli*. The sensitivity of *E. coli* growth to inhibition by doxycycline is shown by a dose response experiment pictured in (a) and the diameter of the growth inhibition zones for this experiment is plotted in (b). Pictures of plates following the sustained activity of doxycycline solutions (1 and 0.1 mg/ml) and microcapsules in the transfer assay are shown in (c) and the change in diameter of the growth inhibition zones are plotted against time in (d) with water (black), doxycycline solutions of 0.1 mg/ml (blue) and 1 mg/ml (red), along with microcapsules - biodegradable (dark green), synthetic (light green) and synthetic with a lipid layer (pink) shown.

5.1.5 Conclusion

The results of this section illustrate that low-molecular-weight doxycycline could be encapsulated in LbL microcapsules via attraction to DS in the microcapsule core, and specific and sustained activity of doxycycline is observed in a gene expression system via the *Ptet* promoter and in an anti-bacterial diffusion assay. Slower release and sustained activity is enhanced by coating capsules with a lipid layer, which retards the leakage of doxycycline and may promote cell uptake as well. However, a lecithin coating was less effective for sustained release *in vitro* perhaps due to degradation by intracellular lipases. Sustained delivery of doxycycline with engineered microcapsules could provide an improved formulation for pharmaceutical application especially in situations where long-term local effects would be beneficial.

5.2 Alternating magnetic field (AMF) triggered release of doxycycline

5.2.1 Magnetic capsules with doxycycline

Negative charged iron oxide nanoparticles with average size of 13.0 nm were deposited as one layer of multilayered microcapsules, which resulted in a rough appearance according to the SEM images (Figure 5.13a). The electronic interaction was commonly used for functionalization of microcapsules with nanoparticles, though a directly growth and deposition of Fe_3O_4 nanoparticles on LbL multilayered shells was also reported.[245-246] The inclusion of magnetic nanoparticles into microcapsules is beneficial for either targeted delivery of cargos of interest or a further external responsive release. Herein, the doxycycline molecules were loaded into the magnetic capsules via a post interaction with DS in the core.[4] Compared to the empty capsules which displayed a flat morphology, the doxycycline loaded ones had a more protuberant appearance, indicating that doxycycline-DS complex was formed (Figure 5.13b). In addition, physically trapped doxycycline molecules between the shells may be another reason which changed the rigidity of capsules as shell thickness was increased. According to measurement, doxycycline encapsulated per capsules was 4.6 pg.

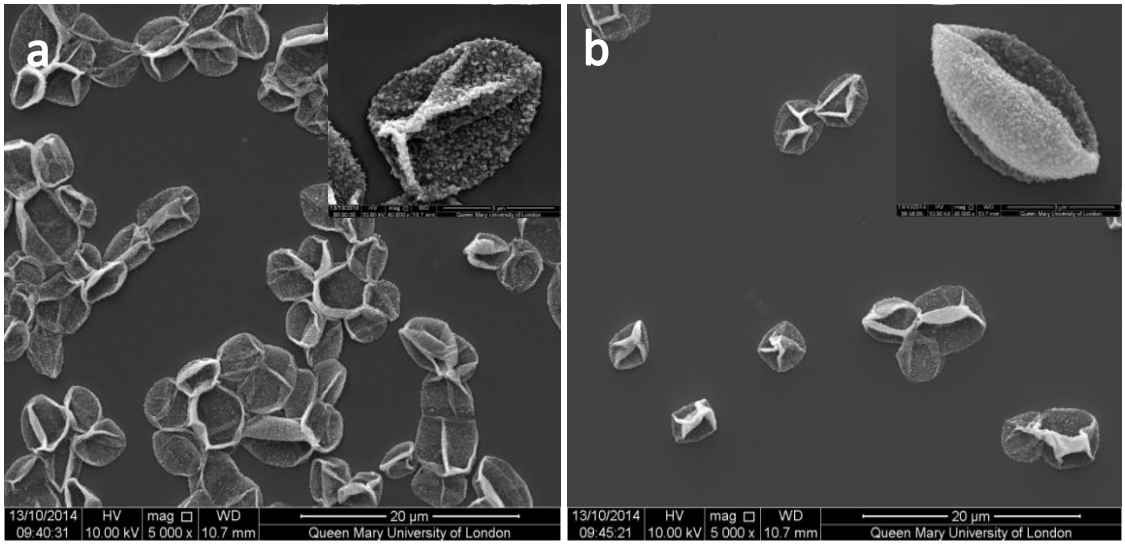

Figure 5.13 SEM images of magnetic microcapsule (a) before and (b) after loading with doxycycline. Inset images are individual capsules at high magnification.

5.2.2 Capsules permeability change by AMF

It is known that microcapsules are not permeable to molecules with molecule weight larger than 5 kDa,[247] so here we used FITC labelled dextran (70 kDa) as model dye to monitor the permeability changes induced by AMF, and the microcapsules were labelled with TRITC. When microcapsules were mixed with FITC-dextran, theoretically, the dyes would be isolated by the capsules walls, resulting dark in the capsule cavity. According to the confocal images, the control capsules without AMF treatment has complete isolation for FITC-dextran (Figure 5.14a), and with longer incubation (until 60 min), only one or two capsules were filled with green fluorescence. When the microcapsules were exposed to the AMF for 20 min, the number of dye penetrated capsules increased to 13.5%, and with longer AMF exposure, more capsules were permeable to FITC-dextran, from 18.1% at 30 min to 52.8% at 360 min (Figure 5.14b, c). However, most of the microcapsules were still intact after 60 min's AMF treatment. The morphology of microcapsules was further examined by SEM imaging. The as-synthesized

microcapsules showed no visible cracks or pores as shown in Figure 1a. After AMF stimulus, the microcapsules were still intact overall, but some cracks and holes on the capsules walls could be observed, which may be corresponding to the percentage of capsules which were permeable to FITC-dextran (Figure 5.14d). Besides, microcapsules also underwent slight shrinkage during AMF stimulus, as some free-standing capsules were displayed.

The increased permeability induced by AMF was ascribed to the agitation of Fe_3O_4 nanoparticles within the polymer shells. The nanoparticles twisted and vibrated in the corresponding frequency as the AMF, leading to the distortion of the polyelectrolyte multilayers and promoting the diffusion of FITC-dextran molecules into capsules. Different from the AMF used in the other studies, the frequency of which was as high as 300 kHz,[23] the AMF used in our study was only 50Hz, so it was more likely to disturb the polymer shell mechanically and the energy generated was also limited. It has been reported that AMF with frequency higher than 300 Hz did lead to negligible permeability increase regardless the exposure time.[178] The high frequency AMF is more likely to destroy the microcapsules thermally since the local heat generated by it was incredibly high. According to Hu et. al, a 10 min exposure of magnetic capsules to 50-100 kHz AMF did result in numerous nanocavities up to 100 nm on surface of microcapsules, and 15 min stimulus directly ruptured the capsules.[174] Some of the pores and small cracks were also observed in our study (Figure 5.14d, indicated by arrows). It was feasible that big aggregation of Fe_3O_4 nanoparticles in capsule shells would tried to align in the magnetic field, which caused large stresses to the capsule shells and thus resulted pores and cracks. Therefore, using of low frequency AMF may be a gentle way to trigger the release of encapsulated cargos.

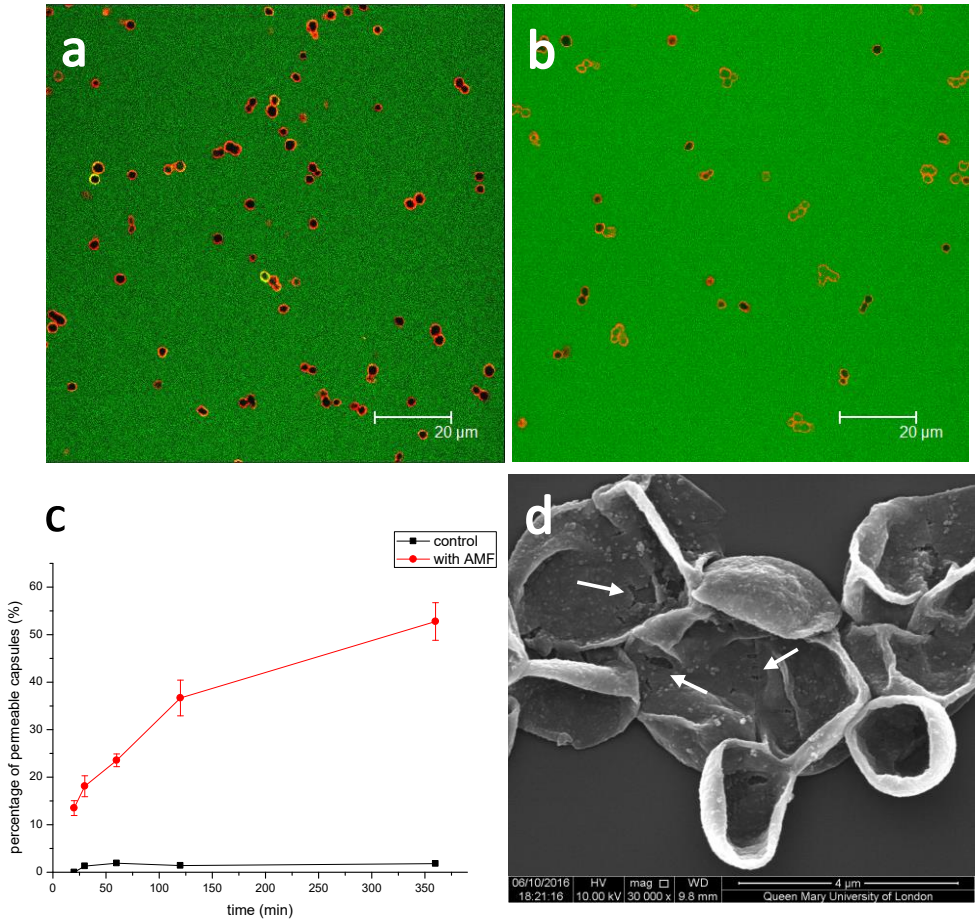

Figure 5.14 Permeability of microcapsule to dextran-FITC (70 kDa). (a) without and (b) with AMF treatment for 360 min, and (c) the percentage of microcapsules which were permeable to FITC-Dextran (70 kDa) as a function of AMF exposure time; (d) SEM image of microcapsules after AMF treatment for 360 min. Arrows indicate the defect of microcapsules caused by AMF.

5.2.3 AMF triggered release of doxycycline

As a small molecular weight drug, doxycycline is easy to diffuse from the microcapsules, and in our previous study, it has been proved that doxycycline release could be divided into two stages, dissociation of doxycycline-DS complex and doxycycline diffusion from the capsule walls.[248] Therefore, factors such as ionic strength and polyelectrolyte shell composition would influence the release profile. In the case here, the AMF had a dominating effect on capsule wall permeability, and thus promoted the doxycycline diffusion. According to the release kinetics,

AMF did obviously accelerate doxycycline release from microcapsules, which 3% more payload doxycycline was release over 4.5 hours compared to the control group (Figure 5.15). To further evaluate the effect of AMF, another group of doxycycline loaded microcapsules were exposed at the 120 h, and an immediate increase in doxycycline release was displayed. As demonstrated earlier in with the FITC-dextran, AMF could facilitate the diffusion of big molecules into microcapsules. Since the molecule weight of doxycycline was much smaller, it was easy to diffusion even without any external triggers, so no dramatic burst release was observed. The result was in agreement with a similar AMF assistant doxorubicin release. According to their study, the doxorubicin release profile was divided into two stages, a slow and steady release stage was maintained when microcapsule structure was still integrity, while a burst release was occurred until the microcapsules were ruptured by the AMF.[174]

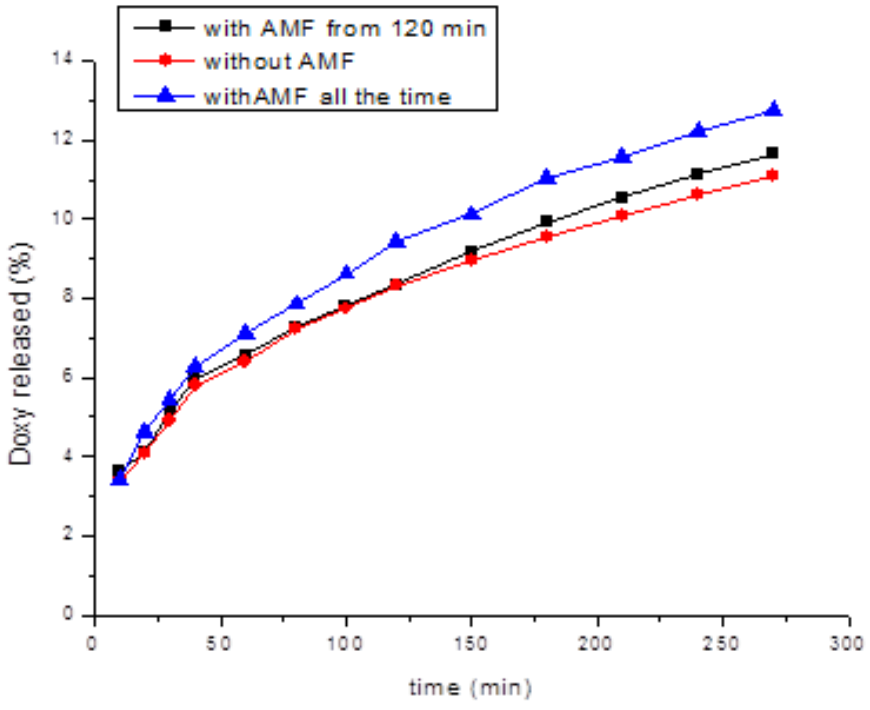

Figure 5.15 Release kinetics of doxycycline from magnetic capsules with (blue line and black line) and without (red line) being exposed to AMF.

5.2.4 Local delivery of doxycycline by magnet

Cell viability after incubated with free doxycycline, normal and magnetic microcapsules was presented in Figure 5.16. With 4 μg/ml free doxycycline, it showed slight toxicity, while microcapsules loaded with equivalent amount of doxycycline showed excellent biocompatibility. Either the normal or magnetic microcapsules were already proved to be biocompatible *in vitro* until the capsule to cell ratio was as high as 100 to 1.[249] Compared to free doxycycline, the encapsulated drug would enter the cells via a routine which started with phagocytosis and micropinocytosis and finally reached the lysosomes.[238] The carriers would protect the drug during the whole process and thus reduced its toxicity. However, the free doxycycline could diffuse quickly into cells and nucleus, and lead to cytotoxicity. It was evidenced by cells incubated with doxorubicin which the free drug molecules displayed significant red fluorescence in the nucleus within 30 min, whilst micelles with doxorubicin were only found in the cytoplasm up to 4 hours.[18] When the cells with magnetic microcapsules internalized were exposed to AMF, no evidence of toxicity was displayed for cells treated for 10 min and 30 min. However, when extending the AMF exposure time to 60 min, slight decrease in cell viability was displayed (87.3%, $p<0.05$), and further elongating it to 90 min and 120 min, cell viability was significantly reduced to 81.2% and 75.0% respectively ($p<0.01$). It is strongly evidenced that the low frequency AMF used in our study was friendly to cells, even after exposing for 60 min. Interestingly, as demonstrated in previous studies that a high frequency AMF (300 kHz) was used, the temperature of microcapsule bulk solution could reach 90 °C within 10 min exposure, which may be dangerous for intracellular drug delivery.[23] That is why the thermal effect was utilized for tuber ablation in which tumor cells were killed by the heat generated by external magnetic field. The local hyperthermia induced by high frequency AMF was able to significantly enhance the performance of doxorubicin to kill 4T1 cells when it was delivered by magnetic PLGA microspheres.[164] However, for drug delivery to

healthy cells and tissue, the local hyperthermia will be toxic, therefore, the low frequency AMF demonstrated in our study will be beneficial.

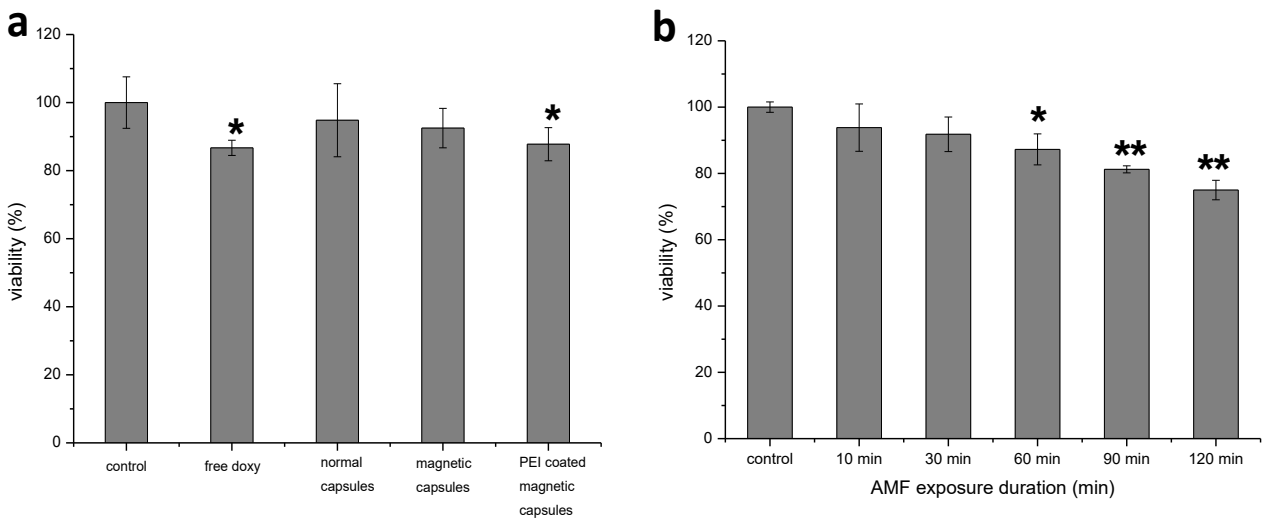

Figure 5.16 Cytotoxicity of C2C12 cells (a) after treated with free doxycycline, doxycycline loaded normal and magnetic capsules, and PEI coated magnetic capsules; (b) with AMF exposure for different duration. Doxycycline concentration in each well was 4 ug/ml. *$p<0.05$, **$p<0.01$ compared to control group cells, n=5.

Magnetically targeted drug delivery and gene transfection were of great interest to design high efficient carriers,[250] and in fact, there are already magnetically *in vivo* targeted dene transfection demonstrated using liposomes.[251] To further demonstrate to potential of microcapsules for targeted doxycycline delivery, the *tet-on* system was utilized to engineer the myoblast cells which acted as reporters of intracellular doxycycline activity. Basically, as showed in Figure 5.17a, this *tet-on* system was based on the tetracycline responsive promoter (Ptet), which can be activated by rtTA-2SM2 and repressed by *tet*RKRAB. The magnetic microcapsules were added to cells chambers with a magnet placed at the bottom, so the doxycycline loaded capsules

were engulfed and released their cargos locally, and further intracellular activated the EGFP expression. The results were demonstrated by monitoring the microcapsules distribution and EGFP expression in the whole chamber. As illustrated in Figure 5.17b, the control group with no static magnet placed at the bottom of chamber had a random and homogeneous distribution of microcapsules and thus cells with green fluorescence. Since the *tet-on* system had shown excellent EGFP regulation capability in our previous study,[248] it was certain here that the green cells located in the whole chamber were activated by microcapsules internalization. So if the magnetic microcapsules were attracted to the specific site, the EGFP expression could be activated locally. As displayed in Figure 5.17c, red microcapsules were only appeared at the site of magnet, and accordingly, only the cells at where there were microcapsules located had green fluorescence while cells at the rest of chamber were completely dark. We can conclude that local delivery and EGFP expression activation was achieved by exert of magnetic field, and no free doxycycline was located elsewhere away from the magnet, as the threshold for doxycycline to switch on EGFP expression is very low (1 pg/ml).[50] It is an important observation that the magnetic microcapsule could be navigated with magnetic field and release their cargo locally while avoiding the unnecessary exposure of doxycycline to the other cells. It will be advantages for antibiotics delivery as the local drug concentration could be effectively increased without improving a systematic administration. In addition, the selectively switch on of EGFP expression also showed a potential for gene therapies as the expression of the gene of interest can be modulated in a spatial and temporal manner via the *tet-on* system.[55, 240, 252]

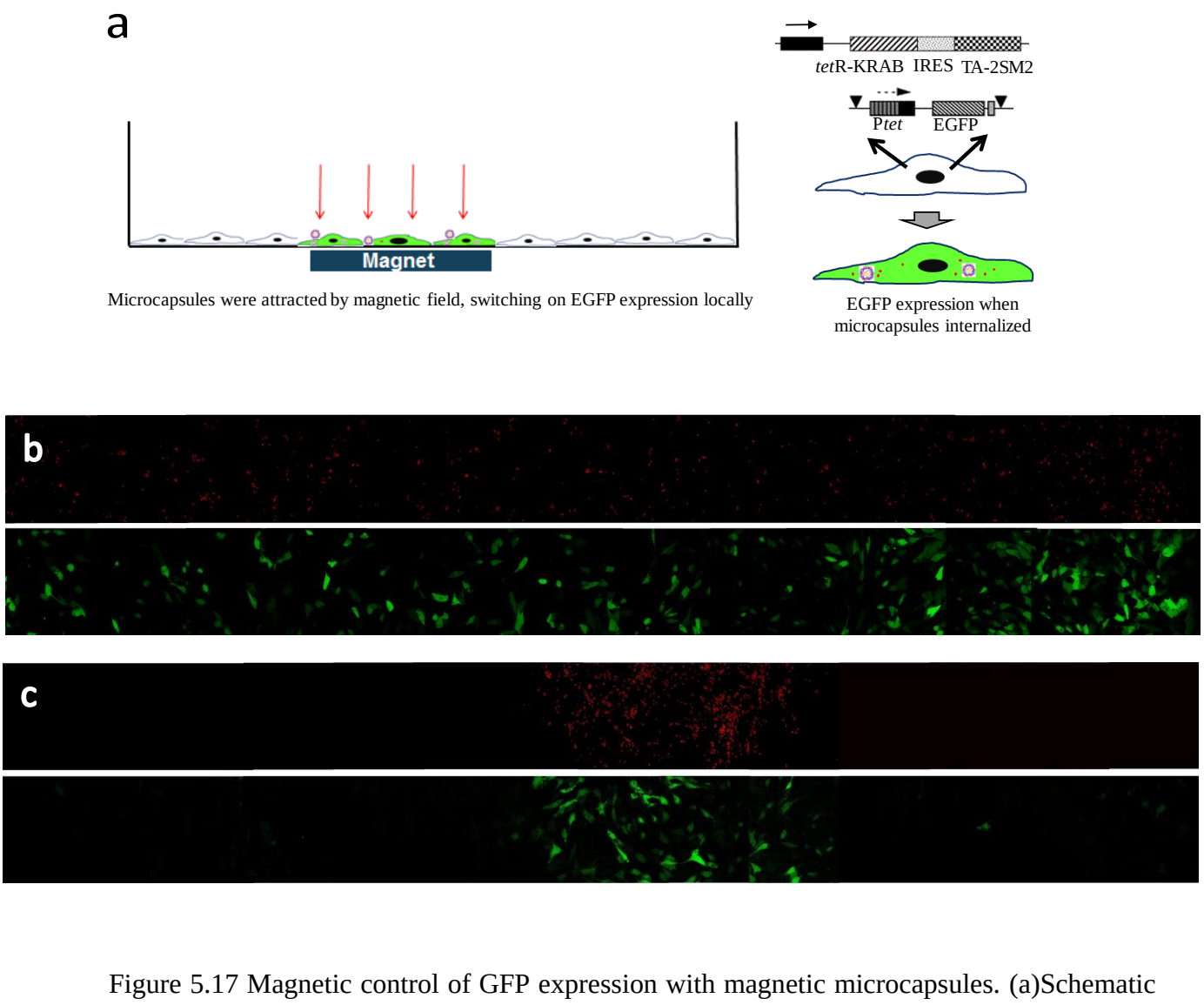

Figure 5.17 Magnetic control of GFP expression with magnetic microcapsules. (a)Schematic illustration of magnetic targeted delivery and vector used for C2C12 engineering; (b) control group without magnet targeting; (c) cells with magnet placed under the chamber. Microcapsules in red channel were labelled with TRITC and cells with doxycycline delivered had EGFP expression.

5.2.5 Intracellular AMF-induced doxycycline release and EGFP expression

To further demonstrate the possibility of intracellularly promoting the EGFP expression via an external AMF, the engineered myoblast cells with microcapsule internalized were exposed to AMF and lysed to examine the EGFP fluorescence intensity. Both the normal and magnetic microcapsules with different capsule to cell ratio were tested, and the PEI coating was to promote the cell internalization. According to Figure 5.18, cells with free doxycycline had significantly higher EGFP expression compared to equivalent doxycycline delivered by normal microcapsules at all ratios ($p<0.05$). This was due to the fast diffusion of free doxycycline into cells, while once encapsulated by microcapsules it was engulfed via an endocytosis pathway. However, the internalization of magnetic capsules was enhanced and the EGFP expression was significantly promoted at both 10:1 and 5:1 capsule to cell ratio ($p<0.01$). According to a similar observation in our previous study that magnetic capsules could promote luciferase delivery and increase cell transfection efficiency, it was because magnetic microcapsules had a higher sedimentation rate than the normal capsules, which was beneficial for the interaction of cells and microcapsules.[249] At capsule to cell ratio of 1:1, there was no difference between these two types of capsules. In comparison, with PEI coated as the outmost layer, the doxycycline induced EGFP expression was further enhanced at all ratios ($p<0.01$). It was explainable that the strong positive charge of PEI enabled a rapid interaction between capsules and cells. Besides, the proton sponge effect of PEI could also promote the transition of doxycycline molecules from endosome to cytosol, which was also proved to be effective for plasmid DNA and siRNA delivery with microcapsules.[13, 253]

Under the AMF, the intracellular doxycycline delivery was further enhanced, as an increase of EGFP expression was demonstrated (Figure 5.18, red and blue column). With an extension of AMF exposure from 10 min to 20 min, the EGFP fluorescence intensity also displayed an increasing tendency at all ratios. For magnetic microcapsules group, there was significant

difference between cells with and without AMF treatment at both 10:1 and 5:1 capsule to cell ratio ($p<0.01$), and for the PEI coated magnetic capsules, the promoted EGFP expression by AMF was also remarkable at the ratio of 5:1 ($p<0.05$). These results were consistent with the *in vitro* doxycycline release profile, indicating that the release of cargo intracellularly was also achievable via an external AMF. Increasing the AMF treatment time to 30 min did lead to higher EGFP expression intensity, however, it decreased when further extending the exposure time to 60 min and 90 min (Figure 5.18d). We can hypothesize that the applying of AMF did facilitate a fast diffusion of doxycycline from microcapsules and liberation from endosomes, but too longer AMF exposure man not be beneficial as it will damage the cells and reduce cell viability. It was clearly evidenced by confocal images that fluorescent doxorubicin was sequestered inside intracellular endosomes and no cancer cell death was induced, but until when AMF was exerted, the cell viability was dramatically reduced.[254] However, different from the use of high frequent AMF, the hyperthermia effect of which could directly lead to *in vitro* cytotoxicity and *in vivo* tumor growth inhibition,[164] the low frequent AMF used here had a much gentler effect and a safe performance for drug delivery could be ensured.

The demonstration of navigated delivery of doxycycline with magnetic microcapsules, and subsequent AMF intracellular triggered release highlighted a perspective in *in vivo* drug delivery. Though, some studies have showed the possibility for targeted drug delivery and remote AMF triggered release *in vivo* using other carriers,[164, 255-256] the microcapsules still show great advantages due to their versatility, and the intravascular delivery of microcapsules is also possible.[257] Further studies will be carried out to seal the microcapsules to ensure a precise on-off control of drug release with the AMF, and the frequency of AMF will also be optimized.

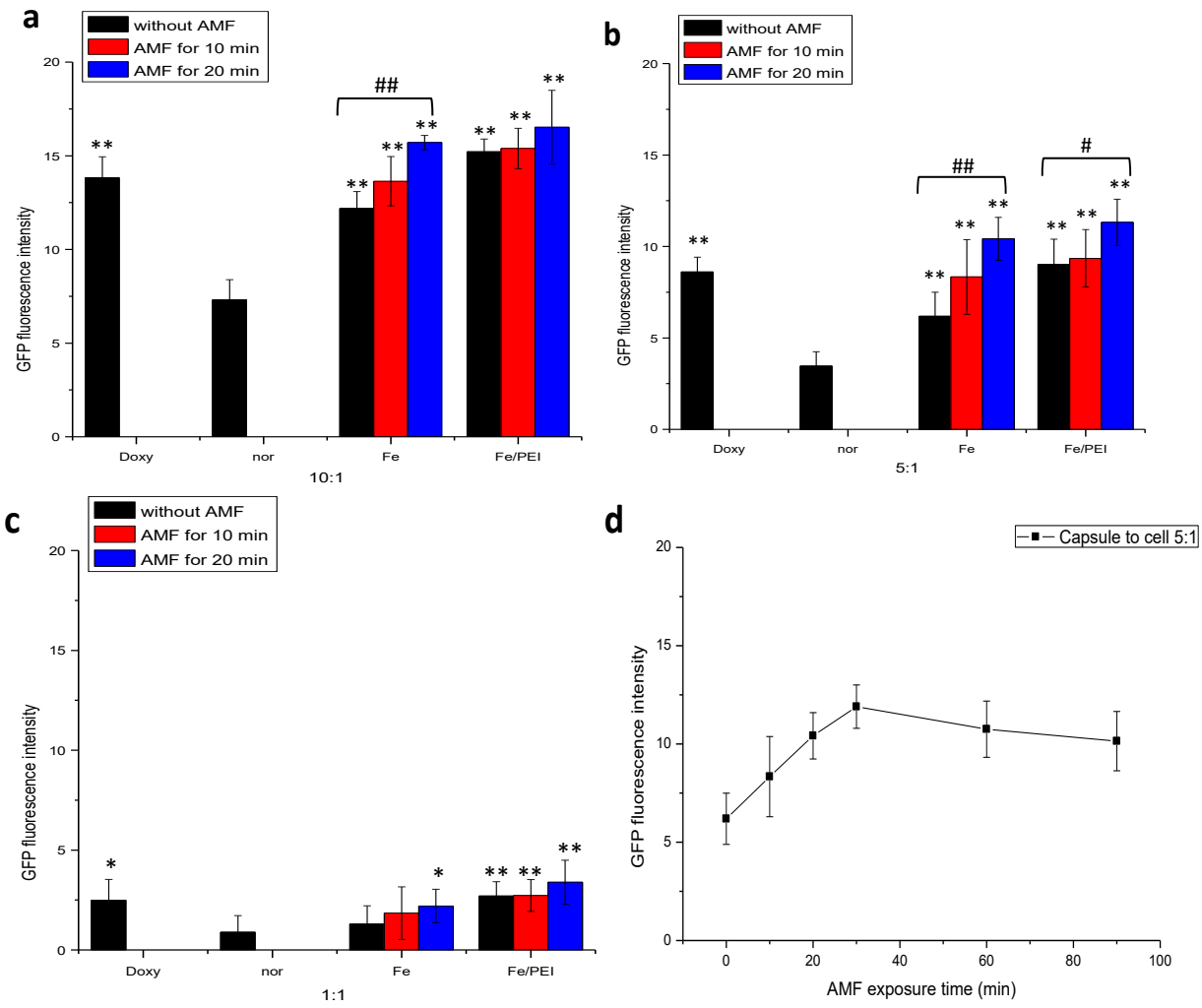

Figure 5.18 EGFP fluorescence intensity of cells treated with free doxycycline, doxycycline loaded normal and magnetic synthetic capsules. Doxycycline concentration in each well was 4 ug/ml (a), 2 ug/ml (b) and 0.4 ug/ml (c). Cells were exposed to AMF for 10 min and 20 min each well (a-c), and 30 min, 60 min and 90 min for (d). After which, cells were lysed and tested. * $p<0.05$, ** $p<0.01$, compared to normal capsules, # $p<0.05$, ## $p<0.001$, compared between no AMF treated and AMF treated cells, n=5.

5.2.6 Conclusion

A low frequent AMF in this section was proved to be effective to trigger doxycycline release from microcapsules without destroying their architecture or damaging the cells with 30 min exposure, and further up-regulate the EGFP expression via the *tet-on* system. The low frequent AMF enhanced the permeability of microcapsules as a function of exposure duration and induced more doxycycline release. Doxycycline delivered by magnetic microcapsules enable a specific site delivery and local function with static magnetic, while non-targeted sites remained unaffected. In addition, the local function was further promoted by the AMF. The targeted delivery of doxycycline and remote AMF enhanced activity open up exciting perspective for its *in vivo* applications.

6. Conclusions and future work

6.1 General conclusions

Delivery of antibacterial agents with carriers is not a new concept that many systems were utilized ranging from micro/nano-particles (polymeric particles, nanogels, micelles, liposomes), electrospinning fibers to polymer films. These kinds of carriers did greatly improve the delivery efficiency and prolong the activity of antibacterial agents, and enhance their performance against bacteria. This work was intended to make a step further to enable a sustained and external responsive antibacterial agent delivery. Two different type of antibacterial drug, chlorhexidine and doxycycline, were delivered with layer-by-layer assembly microcapsules, spray PLA particles, HEMA-UDMA polymer matrix and electrospinning fibers to achieve a sustained effect. On the other hand, to facilitate an external trigger (NIR light and alternating magnetic field) responsive release, either the drug formulation or the carrier were functionalized with components, such as gold nanorods or magnetite nanoparticles.

In the chlorhexidine chapter, a new formulation of chlorhexidine was produced taking advantage of the coordinating ability of chlorhexidine molecules. It was easy to precipitate chlorhexidine by mixing with a range of salts, however, the formation of homogeneous particles was dependent on the type and concentration of ions in the solutions. Combining 15 mg/ml chlorhexidine diacetate solution with 0.33 M $CaCl_2$ solution, spherical drug crystals with an interconnected structure were produced. The forming of this structure was due to the interaction of Ca^{2+} and Cl^- with guanidine groups. Moreover, the size of chlorhexidine particles could be tuned from a few micrometers to over 20 micrometers by temperature. The advantage of this chlorhexidine formulation is the possibility of further modification. Used as templates, polyelectrolyte multilayers were deposited on the surface, which stabilized the drug crystals and prolonged the release kinetics. The solid chlorhexidine capsules with an average shell

thickness of 1.02 μm showed a high drug retention since chlorhexidine could interact with PSS layers. On the other hand, the encapsulation of chlorhexidine drug crystals was simplified with the spray-drying technique, which by mixing the chlorhexidine particles with PLA solutions and spraying, layer of PLA was deposited on the particle surface. The thickness of PLA shell depended on the concentration of PLA solution, and thus affected chlorhexidine release kinetics. The chlorhexidine spheres were also advantageous over the commercially used chlorhexidine diacetate, since a more sustained and controllable chlorhexidine release was demonstrated when both of them were incorporated into the HEMA-UDMA resin.

More importantly, the formulation of chlorhexidine was possible to be directly functionalized with metal nanoparticles. With gold nanorods pre-added into the $CaCl_2$ solution, the nanorods were incorporated into the interconnected structure. The presence of gold nanorods did affect the crystalline of chlorhexidine that with more nanorods in the system, chlorhexidine particles with a smaller size would be produced but the number of chlorhexidine particles were increased. The nanorods were likely to act as crystallization sites for chlorhexidine which was illustrated by using chlorhexidine seeds (5.2 μm) as primary particles for chlorhexidine growth and a core-shell structure was observed. Similarly, when gold nanorods were replaced with Fe_3O_4 nanoparticles, size of resulted chlorhexidine particles was also reduced. It can be concluded that introducing of nanoparticles into the chlorhexidine system led to a surface crystallization and thus achieved a multi-functionalization, which opened possibilities for an external manipulated release. When the gold functionalized chlorhexidine particles were focused by NIR light, local heating of drug crystals led to rupture of solid chlorhexidine capsules and chlorhexidine release, and step-wise chlorhexidine release was demonstrated with NIR light illumination. This strategy offered a novel way to control the release of chlorhexidine upon demand. Also, the magnetite nanoparticles functionalized chlorhexidine particles could be

attracted by magnetic field, and distribution of drug crystals in resin was manipulated, leading to different release kinetics.

The chlorhexidine particles were further incorporated into the electrospun PLA fibers, producing antibacterial fiber meshes. With chlorhexidine particles incorporated, the size of PLA fibers reduced, as well as the mechanical properties. Due to the high surface area, fibers with uncoated chlorhexidine particles showed a burst release in H_2O, but when the particles were LbL encapsulated, the burst release could be reduced, improving the biocompatibility at the same time. It was beneficial to have a moderate chlorhexidine release to ensure safe performance. Both PLA fibers with uncoated and encapsulated chlorhexidine particles demonstrated good antibacterial activity sustained effect against *E. coli*.

For doxycycline delivery, the low molecular weight drug was encapsulated into LbL microcapsules by interaction with the DS in the capsule cavity. Since the microcapsules were porous and diffusible for small molecule drugs, the doxycycline encapsulated capsules were sealed with a lipid layer, facilitating a more sustained release kinetics than the non-lipid coated capsules. Doxycycline delivered by microcapsules has the potential to enhance the treatment for intracellular infections. So myoblast cells engineered with tetracycline regulated gene expression system were used to demonstrate the intracellular doxycycline release. By encapsulation, doxycycline was delivered to cells via capsule internalization, which only the cells with capsules engulfed expressed EGFP while gene expression in the other cells was silenced. The sustained doxycycline release in cells was monitored via EGFP fluorescence. Cells with doxycycline loaded synthetic capsules and biodegradable capsules showed longer EGFP expression than the free doxycycline, and it was further extended by coating with a DPPC on the synthetic capsules. However, lecithin coated biodegradable capsules did not prolong the EGFP expression since the intracellular degradation. Doxycycline delivered by microcapsules also showed a more sustained antibacterial activity against *E. coli*.

The release of doxycycline from microcapsules was further tuned by an external alternating magnetic field when magnetite nanoparticles were assembled in the capsule shells. Upon AMF exposure, the magnetic nanoparticle rotated within the shells, leading to permeability improvement. As demonstrated with FITC labelled dextran (70 kDa), more capsules were permeable with an increase of AMF exposure duration. Doxycycline release was also enhanced by AMF *in vitro*. When the doxycycline loaded magnetic capsules were internalized by cells, the intracellular release was also possible to enhanced, up-regulating the EGFP expression. Moreover, with magnetic capsules, the doxycycline could be delivered to specific site and switched on the EGFP expression locally with a static magnet. It was an exciting observation since targeted delivery of antibiotics could greatly improve the efficiency and reduce side effect to normally cells or tissues. And a local triggered release by AMF may further enhance its activity, which is attractive for infections treatment.

6.2 Future work

This thesis has initiated new formulation of antibacterial agents and demonstrated possibilities to burst the release with various triggers such as NIR light, magnetic field, and ultrasound. The results are promising for treat of infections in reality, but more experiments are needed to be carried out to evaluate their safety and activity against bacteria *in vitro* and *in vivo*. Also some improvement for the formulations demonstrated in the thesis needed to be achieved.

1) Crystal structure of chlorhexidine spheres and the formation mechanism. Though the crystallization of chlorhexidine particles were controlled by ions, temperature and nanoparticles existing in the system, and primarily the chemical interactions between chlorhexidine molecules and ions was revealed by FTIR, the mechanism of how this interconnected structure formed was not fully understood. With the help of further XRD

analysis, simulation, or other techniques, this spherical crystal structure might be better understood.

2) Chlorhexidine particles encapsulation. The spherical chlorhexidine particles were encapsulated with both LbL polyelectrolyte multilayers and PLA shell. However, either of these two methods solved the problem of chlorhexidine burst release at the beginning. For LbL encapsulation, multilayer architecture could be optimized and biodegradable polymers need be used for encapsulation to meet the potential applications *in vivo*. For the spray-dried chlorhexidine particles, same exploring of the usage of polymers for encapsulation is also needed to solve the problem of porous morphology of coating, as well as temperature, solvents, concentrations. If possible, the spray-drying equipment might be updated that the parameters such as temperature, flow of gas would be better controlled to produce higher quality particles.

3) Safety evaluation and antibacterial assay for chlorhexidine product. The chlorhexidine particles were successfully encapsulated with different polymers or embedded into polymer matrixes, and when the particles were functionalized, an external responsive release was demonstrated. However, no experiments were carried out to assess their biocompatibility or their antibacterial activity. As there are already some commercial chlorhexidine products available, it is important to address the safety and antibacterial activity, and advantage of products we fabricated. For example, there is no studies that even reported magnetic control the distribute of drug crystals. This strategy is so attractive to treat the infection and biofilm in periodontal pockets. So it is beneficial to evaluate their biocompatibility, optimize the drug loading amount, explore the possibility to attract the chlorhexidine particle *in vivo*, and to see their antibacterial activity.

4) *In vivo* antibacterial activity for chlorhexidine fibers. The uncoated and encapsulated chlorhexidine particles containing PLA fibers showed good biocompatibility and *in vitro* antibacterial activity. Further *in vivo* experiments could be carried out.

5) More controllable doxycycline release from microcapsules. In chapter 5, doxycycline was successfully encapsulated by forming complex with DS, and release was reduced by lipid coating, and a AMF triggered release was demonstrated when the microcapsules were magnetic. But, as the doxycycline molecules are so small that they are diffusing from the microcapsules all the time even without any triggers. It will be beneficial to have the microcapsule completely sealed to trap them inside, so that an on-demand release could be achieved. Strategies such as depositing a layer of silica on capsule surface are likely to achieve this goal.

6) Intracellularly antibacterial of doxycycline loaded microcapsules. When the doxycycline encapsulated microcapsules were internalized by cells, a sustained intracellular release was demonstrated via monitoring the EGFP expression and AMF also could increase the release in cells. It was exciting observations that the sustained doxycycline activity might also be promising to treat intracellular infections. So in the future, some intracellular infection models could be established and the doxycycline loaded microcapsule might be used to kill the bacteria inside cells.

7) Generally, any other drugs or antibacterial agent formulations could be fabricated with the same methods, and functionalized with metal nanoparticles to achieve a responsive release.

7. References

1. Xiong, M. H.; Bao, Y.; Yang, X. Z.; Zhu, Y. H.; Wang, J., Delivery of antibiotics with polymeric particles. *Advanced drug delivery reviews* **2014,** *78* (30), 63-76.
2. Duncan, B.; Li, X.; Landis, R. F.; Kim, S. T.; Gupta, A.; Wang, L. S.; Ramanathan, R.; Tang, R.; Boerth, J. A.; Rotello, V. M., Nanoparticle-Stabilized Capsules for the Treatment of Bacterial Biofilms. *ACS Nano* **2015,** *9* (8), 7775-82.
3. Hajipour, M. J.; Fromm, K. M.; Ashkarran, A. A.; Jimenez de Aberasturi, D.; de Larramendi, I. R.; Rojo, T.; Serpooshan, V.; Parak, W. J.; Mahmoudi, M., Antibacterial properties of nanoparticles. *Trends Biotechnol* **2012,** *30* (10), 499-511.
4. Kashi, T. S.; Eskandarion, S.; Esfandyari-Manesh, M.; Marashi, S. M.; Samadi, N.; Fatemi, S. M.; Atyabi, F.; Eshraghi, S.; Dinarvand, R., Improved drug loading and antibacterial activity of minocycline-loaded PLGA nanoparticles prepared by solid/oil/water ion pairing method. *International journal of nanomedicine* **2012,** *7*, 221-34.
5. Xue, J.; He, M.; Liu, H.; Niu, Y.; Crawford, A.; Coates, P. D.; Chen, D.; Shi, R.; Zhang, L., Drug loaded homogeneous electrospun PCL/gelatin hybrid nanofiber structures for anti-infective tissue regeneration membranes. *Biomaterials* **2014,** *35* (34), 9395-405.
6. Zeng, P.; Zhang, G.; Rao, A.; Bowles, W.; Wiedmann, T. S., Concentration dependent aggregation properties of chlorhexidine salts. *International journal of pharmaceutics* **2009,** *367* (1-2), 73-8.
7. Yue, I. C.; Poff, J.; Cortes, M. E.; Sinisterra, R. D.; Faris, C. B.; Hildgen, P.; Langer, R.; Shastri, V. P., A novel polymeric chlorhexidine delivery device for the treatment of periodontal disease. *Biomaterials* **2004,** *25* (17), 3743-50.
8. Maya, S.; Indulekha, S.; Sukhithasri, V.; Smitha, K. T.; Nair, S. V.; Jayakumar, R.; Biswas, R., Efficacy of tetracycline encapsulated O-carboxymethyl chitosan nanoparticles against intracellular infections of Staphylococcus aureus. *International journal of biological macromolecules* **2012,** *51* (4), 392-9.
9. Phaechamud, T.; Charoenteeraboon, J., Antibacterial activity and drug release of chitosan sponge containing doxycycline hyclate. *AAPS PharmSciTech* **2008,** *9* (3), 829-35.
10. Monteiro, N.; Martins, M.; Martins, A.; Fonseca, N. A.; Moreira, J. N.; Reis, R. L.; Neves, N. M., Antibacterial activity of chitosan nanofiber meshes with liposomes immobilized releasing gentamicin. *Acta biomaterialia* **2015,** *18*, 196-205.
11. Sukhorukov, G. B.; Donath, E.; Davis, S.; Lichtenfeld, H.; Caruso, F.; Popov, V. I.; MoÈhwald, H., Step-Wise Polyelectrolyte Assembly on Particle Surfaces – A Novel Approach to Colloid Design. *Polym. Adv. Technol.* **1998,** *9*, 759-767.
12. Pavlov, A. M.; Sukhorukov, G. B.; Gould, D. J., Lessons in Microcapsule Assembly from Imaging Delivery of a Bioluminescent Enzyme. *Biomacromolecules* **2013,** *14* (3), 608-612.

13. Pavlov, A. M.; Sukhorukov, G. B.; Gould, D. J., Location of molecules in layer-by-layer assembled microcapsules influences activity, cell delivery and susceptibility to enzyme degradation. *J. Controlled Release* **2013,** *172* (1), 22-29.
14. Sridhar, R.; Lakshminarayanan, R.; Madhaiyan, K.; Barathi, V. A.; Lim, K.; Ramakrishna, S., Electrosprayed nanoparticles and electrospun nanofibers based on natural materials: applications in tissue regeneration, drug delivery and pharmaceuticals. *Chem. Soc. Rev.* **2015,** *44*, 790--814.
15. Hu, X.; Liu, S.; Zhou, G.; Huang, Y.; Xie, Z.; Jing, X., Electrospinning of polymeric nanofibers for drug delivery applications. *Journal of controlled release : official journal of the Controlled Release Society* **2014,** *185*, 12-21.
16. Okuda, T.; Tominaga, K.; Kidoaki, S., Time-programmed dual release formulation by multilayered drug-loaded nanofiber meshes. *Journal of controlled release : official journal of the Controlled Release Society* **2010,** *143* (2), 258-64.
17. Yu, J.; Ju, Y.; Zhao, L.; Chu, X.; Yang, W.; Tian, Y.; Sheng, F.; Lin, J.; Liu, F.; Dong, Y.; Hou, Y., Multistimuli-Regulated Photochemothermal Cancer Therapy Remotely Controlled via Fe5C2 Nanoparticles. *ACS Nano* **2016,** *10* (1), 159-69.
18. Panja, S.; Maji, S.; Maiti, T. K.; Chattopadhyay, S., A Smart Magnetically Active Nanovehicle for on-Demand Targeted Drug Delivery: Where van der Waals Force Balances the Magnetic Interaction. *ACS applied materials & interfaces* **2015,** *7* (43), 24229-41.
19. Deshmukh, P. K.; Ramani, K. P.; Singh, S. S.; Tekade, A. R.; Chatap, V. K.; Patil, G. B.; Bari, S. B., Stimuli-sensitive layer-by-layer (LbL) self-assembly systems: targeting and biosensory applications. *Journal of controlled release : official journal of the Controlled Release Society* **2013,** *166* (3), 294-306.
20. Pavlov, A. M.; Gabriel, S. A.; Sukhorukov, G. B.; Gould, D. J., Improved and targeted delivery of bioactive molecules to cells with magnetic layer-by-layer assembled microcapsules. *Nanoscale* **2015,** *7* (21), 9686-93.
21. Lu, Z.; Prouty, M. D.; Guo, Z.; Golub, V. O.; Kumar, C. S. S. R.; Lvov, Y. M., Magnetic Switch of Permeability for Polyelectrolyte Microcapsules Embedded with Co@Au Nanoparticles. *Langmuir* **2005,** *21* (5), 2042-2050.
22. Katagiri, K.; Imai, Y.; Koumoto, K., Variable on-demand release function of magnetoresponsive hybrid capsules. *Journal of Colloid and Interface Science* **2011,** *361* (1), 109-114.
23. Carregal-Romero, S.; Guardia, P.; Yu, X.; Hartmann, R.; Pellegrino, T.; Parak, W. J., Magnetically triggered release of molecular cargo from iron oxide nanoparticle loaded microcapsules. *Nanoscale* **2015,** *7* (2), 570-6.
24. Beyth, N.; Farah, S.; Domb, A. J.; Weiss, E. I., Antibacterial dental resin composites. *Reactive and Functional Polymers* **2014,** *75*, 81-88.
25. Rai, M.; Yadav, A.; Gade, A., Silver nanoparticles as a new generation of antimicrobials. *Biotechnology advances* **2009,** *27* (1), 76-83.
26. Rabea, E. I.; Badawy, M. E.; Stevens, C. V.; Smagghe, G.; Steurbaut, W., Chitosan as Antimicrobial Agent: Applications and Mode of Action. *Biomacromolecules* **2003,** *4* (6), 1457-1465.
27. Barbour, M. E.; Maddocks, S. E.; Grady, H. J.; Roper, J. A.; Bass, M. D.; Collins, A. M.; Dommett, R. M.; Saunders, M., Chlorhexidine hexametaphosphate as a wound care

material coating: antimicrobial efficacy, toxicity and effect on healing. *Nanomedicine* **2016,** *11* (16), 2049-2057.
28. Badea, M.; Olar, R.; Iliş, M.; Georgescu, R.; Călinescu, M., Synthesis, characterization, and thermal decomposition of new copper (II) complex compounds with chlorhexidine. *Journal of Thermal Analysis and Calorimetry* **2012,** *111* (3), 1763-1770.
29. Călinescu, M.; Negreanu-Pîrjol, T.; Georgescu, R.; Călinescu, O., Synthesis and characterization of new copper(II) complex compounds with chlorhexidine. Part I. *Central European Journal of Chemistry* **2010,** *8* (3), 543-549.
30. Zeng, P.; Rao, A.; Wiedmann, T. S.; Bowles, W., Solubility properties of chlorhexidine salts. *Drug development and industrial pharmacy* **2009,** *35* (2), 172-6.
31. Bailey, P. J.; Pace, S., The coordination chemistry of guanidines and guanidinates. *Coordination Chemistry Reviews* **2001,** *214*, 91–141.
32. Barbour, M. E.; Maddocks, S. E.; Wood, N. J.; Collins, A. M., Synthesis, characterization, and efficacy of antimicrobial chlorhexidine hexametaphosphate nanoparticles for applications in biomedical materials and consumer products. *International journal of nanomedicine* **2013,** *8*, 3507-19.
33. Farrugia, C.; Camilleri, J., Antimicrobial properties of conventional restorative filling materials and advances in antimicrobial properties of composite resins and glass ionomer cements-A literature review. *Dental materials : official publication of the Academy of Dental Materials* **2015,** *31* (4), e89-99.
34. Anusavice, K. J.; Zhang, N. Z.; Shen, C., Controlled Release of Chlorhexidine from UDMA-TEGDMA Resin. *Journal of dental research* **2006,** *85* (10), 950-954.
35. Tabary, N.; Chai, F.; Blanchemain, N.; Neut, C.; Pauchet, L.; Bertini, S.; Delcourt-Debruyne, E.; Hildebrand, H. F.; Martel, B., A chlorhexidine-loaded biodegradable cellulosic device for periodontal pockets treatment. *Acta biomaterialia* **2014,** *10* (1), 318-29.
36. Lboutounne, H.; Chaulet, J.; Ploton, C.; Falson, F.; Pirot, F., Sustained ex vivo skin antiseptic activity of chlorhexidine in poly(e-caprolactone) nanocapsule encapsulated form and as a digluconate. *Journal of Controlled Release* **2002,** *82*, 319–334.
37. Giunchedi, P.; Juliano, C.; Gavini, E.; Cossu, M.; Sorrenti, M., Formulation and in vivo evaluation of chlorhexidine buccal tablets prepared using drug-loaded chitosan microspheres. *European Journal of Pharmaceutics and Biopharmaceutics* **2002,** *53*, 233–239.
38. Tallury, P.; Alimohammadi, N.; Kalachandra, S., Poly(ethylene-co-vinyl acetate) copolymer matrix for delivery of chlorhexidine and acyclovir drugs for use in the oral environment: effect of drug combination, copolymer composition and coating on the drug release rate. *Dental materials : official publication of the Academy of Dental Materials* **2007,** *23* (4), 404-9.
39. Stanislawczuk, R.; Reis, A.; Malaquias, P.; Pereira, F.; Farago, P. V.; Meier, M. M.; Loguercio, A. D., Mechanical properties and modeling of drug release from chlorhexidine-containing etch-and-rinse adhesives. *Dental materials : official publication of the Academy of Dental Materials* **2014,** *30* (4), 392-9.
40. Stanislawczuk, R.; Pereira, F.; Munoz, M. A.; Luque, I.; Farago, P. V.; Reis, A.; Loguercio, A. D., Effects of chlorhexidine-containing adhesives on the durability of resin-dentine interfaces. *Journal of dentistry* **2014,** *42* (1), 39-47.

41. Hiraishi, N.; Yiu, C. K.; King, N. M.; Tay, F. R.; Pashley, D. H., Chlorhexidine release and water sorption characteristics of chlorhexidine-incorporated hydrophobic/hydrophilic resins. *Dental materials : official publication of the Academy of Dental Materials* **2008,** *24* (10), 1391-9.
42. Zhang, J. F.; Wu, R.; Fan, Y.; Liao, S.; Wang, Y.; Wen, Z. T.; Xu, X., Antibacterial dental composites with chlorhexidine and mesoporous silica. *Journal of dental research* **2014,** *93* (12), 1283-9.
43. Xie, S.; Tao, Y.; Pan, Y.; Qu, W.; Cheng, G.; Huang, L.; Chen, D.; Wang, X.; Liu, Z.; Yuan, Z., Biodegradable nanoparticles for intracellular delivery of antimicrobial agents. *Journal of controlled release : official journal of the Controlled Release Society* **2014,** *187C*, 101-117.
44. Golub, L. M.; Ramamurthy, N. S.; McNamara, T. F.; Greenwald, R. A.; Rifkin, B. R., Tetracyclines Inhibit Connective Tissue Breakdown: New Therapeutic Implications for an Old Family of Drugs. *Critical Reviews in Oral Biology & Medicine* **1991,** *2* (3), 297-321.
45. Greenwald, R. A., The road forward: The scientific basis for tetracycline treatment of arthritic disorders. *Pharmacological Research* **2011,** *64* (6), 610-613.
46. Wei, G. X.; Campagna, A. N.; Bobek, L. A., Effect of MUC7 peptides on the growth of bacteria and on Streptococcus mutans biofilm. *The Journal of antimicrobial chemotherapy* **2006,** *57* (6), 1100-9.
47. Ostwald, W., Studien über die Bildung und Umwandlung fester Körper. 1. Abhandlung: Übersättigung und Überkaltung. *Z Phys Chem* **1897,** *22*, 289–330.
48. Das, B.; Brown, D. D., Controlling transgene expression to study Xenopus laevis metamorphosis. *Proceedings of the National Academy of Sciences of the United States of America* **2004,** *101* (14), 4839-42.
49. X Zhou, M. V., B Klaver, B Berkhout and AT Das, Optimization of the Tet-On system for regulated gene expression through viral evolution. *gene therapy* **2006,** *13*, 1382–1390.
50. Gould, D.; Yousaf, N.; Fatah, R.; Subang, M. C.; Chernajovsky, Y., Gene therapy with an improved doxycycline-regulated plasmid encoding a tumour necrosis factor-alpha inhibitor in experimental arthritis. *Arthritis research & therapy* **2007,** *9* (1), R7.
51. Centlivre, M.; Zhou, X.; Pouw, S. M.; Weijer, K.; Kleibeuker, W.; Das, A. T.; Blom, B.; Seppen, J.; Berkhout, B.; Legrand, N., Autoregulatory lentiviral vectors allow multiple cycles of doxycycline-inducible gene expression in human hematopoietic cells in vivo. *Gene Ther* **2010,** *17* (1), 14-25.
52. P. Orth, D. S., W. Hillen, W. Saenger, W. Hinrichs, Structural basis of gene regulation by the tetracycline inducible Tet repressor–operator system. *Nat. Struct. Biol.* **2000,** *7*, 215–219.
53. Sidney B Cambridge, D. G., Federico Calegari, Konstantinos Anastassiadis, Mazahir T Hasan,; A Francis Stewart, W. B. H., Volker Hagen & Tobias Bonhoeffer, Doxycycline-dependent photoactivated gene expression in eukaryotic systems. *Nature methods* **2009,** *6* (7), 527-531.
54. Sauers, D. J.; Temburni, M. K.; Biggins, J. B.; Ceo, L. M.; Galileo, D. S.; Koh, J. T., Light-Activated Gene Expression Directs Segregation of Co-cultured Cells in Vitro. *ACS Chem Biol.* **2010,** *5* (3), 313-320.

55. Gajbhiye, V.; Escalante, L.; Chen, G.; Laperle, A.; Zheng, Q.; Steyer, B.; Gong, S.; Saha, K., Drug-loaded nanoparticles induce gene expression in human pluripotent stem cell derivatives. *Nanoscale* **2014,** *6* (1), 521-31.
56. Moszner, N.; Salz, U., New developments of polymeric dental composites. *Progress in Polymer Science* **2001,** *26* (4), 535-576.
57. Ferracane, J. L., Resin composite--state of the art. *Dental materials : official publication of the Academy of Dental Materials* **2011,** *27* (1), 29-38.
58. Peutzfeldt, A., Resin composites in dentistry: the monomer systems. *Ear J Oral Sci* **1997,** *105*, 97-116.
59. Ferracane, J. L., Current Trends in Dental Composites. *Critical Reviews in Oral Biology & Medicine* **1995,** *6* (4), 302-318.
60. Kleverlaan, C. J.; Feilzer, A. J., Polymerization shrinkage and contraction stress of dental resin composites. *Dental materials : official publication of the Academy of Dental Materials* **2005,** *21* (12), 1150-7.
61. Ensaff, H.; O'Doherty, D. M.; Jacobsen, P. H., Polymerization shrinkage of dental composite resins. *Journal of Engineering in Medicine* **2001,** *215* (4), 367-375.
62. Brunthaler, A.; Konig, F.; Lucas, T.; Sperr, W.; Schedle, A., Longevity of direct resin composite restorations in posterior teeth. *Clinical oral investigations* **2003,** *7* (2), 63-70.
63. Bertolini, M. M.; Portela, M. B.; Curvelo, J. A.; Soares, R. M.; Lourenco, E. J.; Telles, D. M., Resins-based denture soft lining materials modified by chlorhexidine salt incorporation: an in vitro analysis of antifungal activity, drug release and hardness. *Dental materials : official publication of the Academy of Dental Materials* **2014,** *30* (8), 793-8.
64. Lim, B. S.; Cheng, Y.; Lee, S. P.; Ahn, S. J., Chlorhexidine release from orthodontic adhesives after topical chlorhexidine treatment. *European journal of oral sciences* **2013,** *121* (3 Pt 1), 211-7.
65. Carrilho, M. R. O.; Carvalho, R. M.; de Goes, M. F.; di Hipólito, V.; Geraldeli, S.; Tay, F. R.; Pashley, D. H.; Tjäderhane, L., Chlorhexidine Preserves Dentin Bond in vitro. *Journal of dental research* **2007,** *86* (1), 90-94.
66. Shen, C.; Zhang, N. Z.; Anusavice, K. J., Fluoride and chlorhexidine release from filled resins. *Journal of dental research* **2010,** *89* (9), 1002-6.
67. Yan, S.; Cai, X.; Yan, W.; Dai, X.; Wu, H., Continuous Wave Ultrasound Enhances Vancomycin Release and Antimicrobial Efficacy of Antibiotic-Loaded Acrylic Bone Cement In Vitro and In Vivo. *Journal of Biomedical Materials Research Part B: Applied Biomaterials* **2007,** *82B* (1), 57-64.
68. Huynh, T. T.; Padois, K.; Sonvico, F.; Rossi, A.; Zani, F.; Pirot, F.; Doury, J.; Falson, F., Characterization of a polyurethane-based controlled release system for local delivery of chlorhexidine diacetate. *European journal of pharmaceutics and biopharmaceutics : official journal of Arbeitsgemeinschaft fur Pharmazeutische Verfahrenstechnik e.V* **2010,** *74* (2), 255-64.
69. Hook, E. R.; Owen, O. J.; Bellis, C. A.; Holder, J. A.; O'Sullivan, D. J.; Barbour, M. E., Development of a novel antimicrobial-releasing glass ionomer cement functionalized with chlorhexidine hexametaphosphate nanoparticles. *Journal of Nanobiotechnology* **2014,** *12* (1), 3.

70. Cheng, L.; Weir, M. D.; Xu, H. H.; Kraigsley, A. M.; Lin, N. J.; Lin-Gibson, S.; Zhou, X., Antibacterial and physical properties of calcium-phosphate and calcium-fluoride nanocomposites with chlorhexidine. *Dental materials : official publication of the Academy of Dental Materials* **2012,** *28* (5), 573-83.
71. Kim, H.-J.; Kwon, T.-Y.; Kim, K.-H.; Kwon, S.-T.; Cho, D.-H.; Son, J. S., Long-term release of chlorhexidine from dental adhesive resin system using human serum albumin nanoparticles. *Polymer Bulletin* **2014,** *71* (4), 875-886.
72. Sosnik, A.; Seremeta, K. P., Advantages and challenges of the spray-drying technology for the production of pure drug particles and drug-loaded polymeric carriers. *Adv Colloid Interface Sci* **2015,** *223*, 40-54.
73. Liu, W.; Chen, X. D.; Selomulya, C., On the spray drying of uniform functional microparticles. *Particuology* **2015,** *22*, 1-12.
74. Wan, F.; Wu, J. X.; Bohr, A.; Baldursdottir, S. G.; Maltesen, M. J.; Bjerregaard, S.; Foged, C.; Rantanen, J.; Yang, M., Impact of PLGA molecular behavior in the feed solution on the drug release kinetics of spray dried microparticles. *Polymer* **2013,** *54* (21), 5920-5927.
75. Dierendonck, M.; De Koker, S.; De Rycke, R.; De Geest, B. G., Just spray it--LbL assembly enters a new age. *Soft Matter* **2014,** *10* (6), 804-7.
76. Johnson, P. E.; Muttil, P.; MacKenzie, D.; Carnes, E. C.; Pelowitz, J.; Mara, N. A.; Mook, W. M.; Jett, S. D.; Dunphy, D. R.; Timmins, G. S.; Brinker, C. J., Spray-Dried Multiscale Nano-biocomposites Containing Living Cells. *ACS Nano* **2015,** *9* (7), 6961-6977.
77. Jensen, D. M.; Cun, D.; Maltesen, M. J.; Frokjaer, S.; Nielsen, H. M.; Foged, C., Spray drying of siRNA-containing PLGA nanoparticles intended for inhalation. *Journal of controlled release : official journal of the Controlled Release Society* **2010,** *142* (1), 138-45.
78. O'Toole, M. G.; Henderson, R. M.; Soucy, P. A.; Fasciotto, B. H.; Hoblitzell, P. J.; Keynton, R. S.; Ehringer, W. D.; Gobin, A. S., Curcumin encapsulation in submicrometer spray-dried chitosan/Tween 20 particles. *Biomacromolecules* **2012,** *13* (8), 2309-14.
79. De Koker, S.; Fierens, K.; Dierendonck, M.; De Rycke, R.; Lambrecht, B. N.; Grooten, J.; Remon, J. P.; De Geest, B. G., Nanoporous polyelectrolyte vaccine microcarriers. A formulation platform for enhancing humoral and cellular immune responses. *Journal of controlled release : official journal of the Controlled Release Society* **2014,** *195*, 99-109.
80. Llorens, E.; Calderon, S.; del Valle, L. J.; Puiggali, J., Polybiguanide (PHMB) loaded in PLA scaffolds displaying high hydrophobic, biocompatibility and antibacterial properties. *Materials science & engineering. C, Materials for biological applications* **2015,** *50*, 74-84.
81. Wu, J.; Wang, N.; Zhao, Y.; Jiang, L., Electrospinning of multilevel structured functional micro-/nanofibers and their applications. *Journal of Materials Chemistry A* **2013,** *1* (25), 7290.
82. Goh, Y.-F.; Shakir, I.; Hussain, R., Electrospun fibers for tissue engineering, drug delivery, and wound dressing. *Journal of Materials Science* **2013,** *48* (8), 3027-3054.
83. Xie, Z.; Paras, C. B.; Weng, H.; Punnakitikashem, P.; Su, L. C.; Vu, K.; Tang, L.; Yang, J.; Nguyen, K. T., Dual growth factor releasing multi-functional nanofibers for wound healing. *Acta biomaterialia* **2013,** *9* (12), 9351-9.
84. Agarwal, A.; Nelson, T. B.; Kierski, P. R.; Schurr, M. J.; Murphy, C. J.; Czuprynski, C. J.; McAnulty, J. F.; Abbott, N. L., Polymeric multilayers that localize the release of chlorhexidine from biologic wound dressings. *Biomaterials* **2012,** *33* (28), 6783-92.

85. Kenawy, E. R.; Bowlin, G. L.; Mansfield, K.; Layman, J.; Simpson, D. G.; Sanders, E. H.; Wnek, G. E., Release of tetracycline hydrochloride from electrospun poly(ethylene-co-vinylacetate), poly(lactic acid), and a blend. *Journal of Controlled Release* **2002,** *81* 57–64.
86. Chen, L.; Bromberg, L.; Hatton, T. A.; Rutledge, G. C., Electrospun cellulose acetate fibers containing chlorhexidine as a bactericide. *Polymer* **2008,** *49* (5), 1266-1275.
87. Song, B.; Wu, C.; Chang, J., Dual drug release from electrospun poly(lactic-co-glycolic acid)/mesoporous silica nanoparticles composite mats with distinct release profiles. *Acta biomaterialia* **2012,** *8* (5), 1901-7.
88. Hongxu Qi; Ping Hu ; Jun Xu; Wang, A., Encapsulation of drug reservoirs in fibers by emulsion electrospinning: morphology characterization and preliminary release assessment. *Biomacromolecules* **2006,** *7,* 2327-2330.
89. Wang, Y.; Wang, B.; Qiao, W.; Yin, T., A novel controlled release drug delivery system for multiple drugs based on electrospun nanofibers containing nanoparticles. *J Pharm Sci* **2010,** *99* (12), 4805-11.
90. Jiajia Xue; Yuzhao Niu; Min Gong; Rui Shi; Dafu Chen; Liqun Zhang; Lvov, Y., ElectrospunMicrofiber Membranes Embedded with Drug-Loaded Clay Nanotubes for Sustained Antimicrobial Protection. *ACS Nano* **2015,** *9* (2), 1600–1612.
91. Zhang, C. L.; Yu, S. H., Nanoparticles meet electrospinning: recent advances and future prospects. *Chemical Society reviews* **2014,** *43* (13), 4423-48.
92. Han, D.; Steckl, A. J., Triaxial electrospun nanofiber membranes for controlled dual release of functional molecules. *ACS applied materials & interfaces* **2013,** *5* (16), 8241-5.
93. Shi, X.; Shen, M.; Mohwald, H., Polyelectrolyte multilayer nanoreactors toward the synthesis of diverse nanostructured materials. *Progress in Polymer Science* **2004,** *29* (10), 987-1019.
94. Pilar Rivera Gil, L. L. d. M., Pablo del_Pino, Almudena Muñoz_Javier, and Wolfgang J. Parak, Nanoparticle-modified polyelectrolyte capsules. *nanotoday* **2008**.
95. Rivera-Gil, p.; De Koker, S.; De Geest, B. G.; Parak, W. J., Intracellular Processing of Proteins Mediated by Biodegradable Polyelectrolyte Capsules. *Nano letters* **2009,** *9* (12), 4398-4402.
96. De Cock, L. J.; De Koker, S.; De Geest, B. G.; Grooten, J.; Vervaet, C.; Remon, J. P.; Sukhorukov, G. B.; Antipina, M. N., Polymeric multilayer capsules in drug delivery. *Angewandte Chemie* **2010,** *49* (39), 6954-73.
97. Anton M. Pavlov, G. B. S., and David J. Gould, Lessons in Microcapsule Assembly from Imaging Delivery of a Bioluminescent Enzyme. *Biomacromolecules* **2013,** *14*, 608-612.
98. Shen, H.; Shi, H.; Xie, M.; Ma, K.; Li, B.; Shen, S.; Wang, X.; Jin, Y., Biodegradable chitosan/alginate BSA-gel-capsules for pH-controlled loading and release of doxorubicin and treatment of pulmonary melanoma. *Journal of Materials Chemistry B* **2013,** *1* (32), 3906.
99. Shen, H. J.; Shi, H.; Ma, K.; Xie, M.; Tang, L. L.; Shen, S.; Li, B.; Wang, X. S.; Jin, Y., Polyelectrolyte capsules packaging BSA gels for pH-controlled drug loading and release and their antitumor activity. *Acta biomaterialia* **2013,** *9* (4), 6123-33.
100. Köhler, K.; Shchukin, D. G.; Möhwald, H.; Sukhorukov, G. B., Thermal behavior of polyelectrolyte multilayer microcapsules. 1. The effect of odd and even layer number. *The Journal of Physical Chemistry B* **2005,** *109* (39), 18250-18259.

101. Leporatti, S.; Gao, C.; Voigt, A.; Donath, E.; Möhwald, H., Shrinking of ultrathin polyelectrolyte multilayer capsules upon annealing: a confocal laser scanning microscopy and scanning force microscopy study. *The European Physical Journal E* **2001,** *5* (1), 13-20.
102. Andreeva, D. V.; Gorin, D. A.; Shchukin, D. G.; Sukhorukov, G. B., Magnetic Microcapsules with Low Permeable Polypyrrole Skin Layer. *Macromolecular rapid communications* **2006,** *27* (12), 931-936.
103. Yi, Q.; Sukhorukov, G. B., Photolysis triggered sealing of multilayer capsules to entrap small molecules. *ACS applied materials & interfaces* **2013,** *5* (14), 6723-31.
104. Antipov, A. A.; Sukhorukov, G. B.; Donath, E., Sustained Release Properties of Polyelectrolyte Multilayer Capsules. *J. Phys. Chem. B* **2001,** *105*, 2281-2284.
105. Agarwal, A.; Lvov, Y.; Sawant, R.; Torchilin, V., Stable nanocolloids of poorly soluble drugs with high drug content prepared using the combination of sonication and layer-by-layer technology. *Journal of controlled release : official journal of the Controlled Release Society* **2008,** *128* (3), 255-60.
106. Lvov, Y. M.; Pattekari, P.; Zhang, X.; Torchilin, V., Converting poorly soluble materials into stable aqueous nanocolloids. *Langmuir* **2011,** *27* (3), 1212-7.
107. Pattekari, P.; Zheng, Z.; Zhang, X.; Levchenko, T.; Torchilin, V.; Lvov, Y., Top-down and bottom-up approaches in production of aqueous nanocolloids of low solubility drug paclitaxel. *Physical chemistry chemical physics : PCCP* **2011,** *13* (19), 9014-9.
108. Santos, A. C.; Pattekari, P.; Jesus, S.; Veiga, F.; Lvov, Y.; Ribeiro, A. J., Sonication-Assisted Layer-by-Layer Assembly for Low Solubility Drug Nanoformulation. *ACS applied materials & interfaces* **2015,** *7* (22), 11972-83.
109. Matthieu F. Bédard, B. G. D. G., Andre G. Skirtach, Helmuth Möhwald, Gleb B. Sukhorukov, Polymeric microcapsules with light responsive properties for encapsulation and release. *Advances in Colloid and Interface Science* **2010**.
110. Martien A. Cohen Stuart, W. T. S. H., Jan Genzer, Marcus Müller, Christopher Ober, Manfred Stamm, Gleb B. Sukhorukov, Igal Szleifer, Vladimir V. Tsukruk, Marek Urban, Françoise Winnik, Stefan Zauscher, Igor Luzinov and Sergiy Minko*, Emerging applications of stimuli-responsive polymer materials. *nature materials*

2010.
111. Husseini, G. A.; Pitt, W. G., Micelles and nanoparticles for ultrasonic drug and gene delivery. *Advanced drug delivery reviews* **2008,** *60* (10), 1137-52.
112. Yu, T., A review of research into the uses of low level ultrasound in cancer therapy. *Ultrasonics Sonochemistry* **2004,** *11* (2), 95-103.
113. Kishen, A.; Khoo, B. C.; Shrestha, A.; Ohl, S. W., Characterizing bubble dynamics created by high-intensity focused ultrasound for the delivery of antibacterial nanoparticles into a dental hard tissue. *Proceedings of the Institution of Mechanical Engineers, Part H: Journal of Engineering in Medicine* **2010,** *224* (11), 1285-1296.
114. Pavlov, A. M.; Saez, V.; Cobley, A.; Graves, J.; Sukhorukov, G. B.; Mason, T. J., Controlled protein release from microcapsules with composite shells using high frequency ultrasound—potential for in vivo medical use. *Soft Matter* **2011,** *7* (9), 4341–4347.

115. Hendriks, J. G. E.; Ensing, G. T.; van Horn, J. R.; Lubbers, J.; van der Mei, H. C.; Busscher, H. J., Increased release of gentamicin from acrylic bone cements under influence of low-frequency ultrasound. *Journal of Controlled Release* **2003,** *92* (3), 369-374.
116. Shrestha, A.; Fong, S. W.; Khoo, B. C.; Kishen, A., Delivery of antibacterial nanoparticles into dentinal tubules using high-intensity focused ultrasound. *Journal of endodontics* **2009,** *35* (7), 1028-33.
117. Needham, D.; Anyarambhatla, G.; Kong, G.; Dewhirst, M. W., A New Temperature-sensitive Liposome for Use with Mild Hyperthermia: Characterization and Testing in a Human Tumor Xenograft Model. *Cancer Research* **2000,** *60* (5), 1197-1201.
118. Schroeder, A.; Kost, J.; Barenholz, Y., Ultrasound, liposomes, and drug delivery: principles for using ultrasound to control the release of drugs from liposomes. *Chemistry and physics of lipids* **2009,** *162* (1-2), 1-16.
119. Ibsen, S.; Benchimol, M.; Simberg, D.; Schutt, C.; Steiner, J.; Esener, S., A novel nested liposome drug delivery vehicle capable of ultrasound triggered release of its payload. *Journal of controlled release : official journal of the Controlled Release Society* **2011,** *155* (3), 358-66.
120. Gao, H.; Wen, D. S.; Sukhorukov, G. B., Composite silica nanoparticle/polyelectrolyte microcapsules with reduced permeability and enhanced ultrasound sensitivity. *J. Mater. Chem. B* **2015,** *3*, 1888-1897.
121. Wang, S.; Huang, P.; Chen, X., Stimuli-Responsive Programmed Specific Targeting in Nanomedicine. *ACS Nano* **2016,** *10* (3), 2991-4.
122. Wang, H.; Han, R. L.; Yang, L. M.; Shi, J. H.; Liu, Z. J.; Hu, Y.; Wang, Y.; Liu, S. J.; Gan, Y., Design and Synthesis of Core-Shell-Shell Upconversion Nanoparticles for NIR-Induced Drug Release, Photodynamic Therapy, and Cell Imaging. *ACS applied materials & interfaces* **2016,** *8* (7), 4416-23.
123. Bastus, N. G.; Comenge, J.; Puntes, V., Kinetically controlled seeded growth synthesis of citrate-stabilized gold nanoparticles of up to 200 nm: size focusing versus Ostwald ripening. *Langmuir* **2011,** *27* (17), 11098-105.
124. Khanadeev, V. A.; Khlebtsov, N. G.; Burov, A. M.; Khlebtsov, B. N., Tuning of plasmon resonance of gold nanorods by controlled etching. *Colloid Journal* **2015,** *77* (5), 652-660.
125. Khlebtsov, B.; Khanadeev, V.; Pylaev, T.; Khlebtsov, N., A New T-Matrix Solvable Model for Nanorods: TEM-Based Ensemble Simulations Supported by Experiments. *The Journal of Physical Chemistry C* **2011,** *115* (14), 6317-6323.
126. Zhang, Q.; Han, L.; Jing, H.; Blom, D. A.; Lin, Y.; Xin, H. L.; Wang, H., Facet Control of Gold Nanorods. *ACS Nano* **2016,** *10* (2), 2960-74.
127. Zhang, Q.; Jing, H.; Li, G. G.; Lin, Y.; Blom, D. A.; Wang, H., Intertwining Roles of Silver Ions, Surfactants, and Reducing Agents in Gold Nanorod Overgrowth: Pathway Switch between Silver Underpotential Deposition and Gold–Silver Codeposition. *Chemistry of Materials* **2016**.
128. Govorov, A. O.; Zhang, W.; Skeini, T.; Richardson, H.; Lee, J.; Kotov, N. A., Gold nanoparticle ensembles as heaters and actuators: melting and collective plasmon resonances. *Nanoscale Research Letters* **2006,** *1* (1), 84-90.

129. Fedoruk, M.; Meixner, M.; Carretero-Palacios, S.; Lohmüller, T.; Feldmann, J., Nanolithography by Plasmonic Heating and Optical Manipulation of Gold Nanoparticles. *ACS Nano* **2013,** *7* (9), 7648-7653.
130. Bédard, M. F.; Braun, D.; Sukhorukov, G. B.; Skirtach, A. G., Toward Self-Assembly of Nanoparticles on Polymeric Microshells: Near-IR Release and Permeability. *ACS Nano* **2008,** *2* (9), 1807-1816.
131. Lee , J.; Govorov, A. O.; Dulka, J.; Kotov, N. A., Bioconjugates of CdTe Nanowires and Au Nanoparticles-Plasmon Exciton Interactions, Luminescence Enhancement, and Collective Effects. *Nano letters* **2004,** *4* (12), 2323-2330.
132. Liu, J.; Detrembleur, C.; De Pauw-Gillet, M. C.; Mornet, S.; Jerome, C.; Duguet, E., Gold nanorods coated with mesoporous silica shell as drug delivery system for remote near infrared light-activated release and potential phototherapy. *Small* **2015,** *11* (19), 2323-32.
133. Liu, Y.; Yang, M.; Zhang, J.; Zhi, X.; Li, C.; Zhang, C.; Pan, F.; Wang, K.; Yang, Y.; Martinez de la Fuentea, J.; Cui, D., Human Induced Pluripotent Stem Cells for Tumor Targeted Delivery of Gold Nanorods and Enhanced Photothermal Therapy. *ACS Nano* **2016,** *10* (2), 2375-85.
134. Yahia-Ammar, A.; Sierra, D.; Merola, F.; Hildebrandt, N.; Le Guevel, X., Self-Assembled Gold Nanoclusters for Bright Fluorescence Imaging and Enhanced Drug Delivery. *ACS Nano* **2016,** *10* (2), 2591-9.
135. Alkilany, A. M.; Thompson, L. B.; Boulos, S. P.; Sisco, P. N.; Murphy, C. J., Gold nanorods: their potential for photothermal therapeutics and drug delivery, tempered by the complexity of their biological interactions. *Advanced drug delivery reviews* **2012,** *64* (2), 190-9.
136. Zhang, P.; Wang, C.; Zhao, J.; Xiao, A.; Shen, Q.; Li, L.; Li, J.; Zhang, J.; Min, Q.; Chen, J.; Chen, H. Y.; Zhu, J. J., Near Infrared-Guided Smart Nanocarriers for MicroRNA-Controlled Release of Doxorubicin/siRNA with Intracellular ATP as Fuel. *ACS Nano* **2016,** *10* (3), 3637-47.
137. You, J.; Wang, Z.; Du, Y.; Yuan, H.; Zhang, P.; Zhou, J.; Liu, F.; Li, C.; Hu, F., Specific tumor delivery of paclitaxel using glycolipid-like polymer micelles containing gold nanospheres. *Biomaterials* **2013,** *34* (18), 4510-9.
138. Lajunen, T.; Viitala, L.; Kontturi, L. S.; Laaksonen, T.; Liang, H.; Vuorimaa-Laukkanen, E.; Viitala, T.; Le Guevel, X.; Yliperttula, M.; Murtomaki, L.; Urtti, A., Light induced cytosolic drug delivery from liposomes with gold nanoparticles. *Journal of controlled release : official journal of the Controlled Release Society* **2015,** *203*, 85-98.
139. Ott, A.; Yu, X.; Hartmann, R.; Rejman, J.; Schütz, A.; Ochs, M.; Parak, W. J.; Carregal-Romero, S., Light-Addressable and Degradable Silica Capsules for Delivery of Molecular Cargo to the Cytosol of Cells. *Chemistry of Materials* **2015,** *27* (6), 1929-1942.
140. Wang, H.; Yi, J.; Mukherjee, S.; Banerjee, P.; Zhou, S., Magnetic/NIR-thermally responsive hybrid nanogels for optical temperature sensing, tumor cell imaging and triggered drug release. *Nanoscale* **2014,** *6* (21), 13001-11.
141. Niikura, K.; Iyo, N.; Matsuo, Y.; Mitomo, H.; Ijiro, K., Sub-100 nm gold nanoparticle vesicles as a drug delivery carrier enabling rapid drug release upon light irradiation. *ACS applied materials & interfaces* **2013,** *5* (9), 3900-7.

142. Shi, P.; Ju, E.; Ren, J.; Qu, X., Near-Infrared Light-Encoded Orthogonally Triggered and Logical Intracellular Release Using Gold Nanocage@Smart Polymer Shell. *Advanced Functional Materials* **2014,** *24* (6), 826-834.
143. Li, N.; Yu, Z.; Pan, W.; Han, Y.; Zhang, T.; Tang, B., A Near-Infrared Light-Triggered Nanocarrier with Reversible DNA Valves for Intracellular Controlled Release. *Advanced Functional Materials* **2013,** *23* (18), 2255-2262.
144. Carregal-Romero, S.; Ochs, M.; Rivera-Gil, P.; Ganas, C.; Pavlov, A. M.; Sukhorukov, G. B.; Parak, W. J., NIR-light triggered delivery of macromolecules into the cytosol. *Journal of controlled release : official journal of the Controlled Release Society* **2012,** *159* (1), 120-7.
145. Nooney, R. I.; Dhanasekaran, T.; Chen, Y.; Josephs, R.; Ostafin, A. E., Self-Assembled Highly Ordered Spherical Mesoporous Silica/Gold Nanocomposites. *Advanced materials* **2002,** *14* (7), 529-532.
146. Yang, X.; Liu, X.; Liu, Z.; Pu, F.; Ren, J.; Qu, X., Near-infrared light-triggered, targeted drug delivery to cancer cells by aptamer gated nanovehicles. *Advanced materials* **2012,** *24* (21), 2890-5.
147. Liz-Marzan, L. M.; Giersig, M.; Mulvaney, P., Synthesis of Nanosized Gold-Silica Core-Shell Particles. *Langmuir* **1996,** *12* (18), 4329-4335.
148. Nooney, R. I.; Thirunavukkarasu, D.; Chen, Y.; R., J.; Ostafin, A. E., Self-Assembly of Mesoporous Nanoscale Silica/Gold Composites. *Langmuir* **2003,** *19*, 7628-7637.
149. Lee, J.; Jeong, C.; Kim, W. J., Facile fabrication and application of near-IR light-responsive drug release system based on gold nanorods and phase change material. *J. Mater. Chem. B* **2014,** *2*, 8338–8345.
150. Chen, F.; Hong, H.; Zhang, Y.; Valdovinos, H. F.; Shi, S.; Kwon, G. S.; Theuer, C. P.; Barnhart, T. E.; Cai, W., In Vivo Tumor Targeting and Image-Guided Drug Delivery with Antibody-Conjugated, Radiolabeled Mesoporous Silica Nanoparticles. *ACS Nano* **2013,** *7* (10), 9027-9039.
151. Kilinc, D.; Dennis, C. L.; Lee, G. U., Bio-Nano-Magnetic Materials for Localized Mechanochemical Stimulation of Cell Growth and Death. *Advanced materials* **2016,** *28* (27), 5672-80.
152. Arias, J. L.; Reddy, L. H.; Couvreur, P., Fe3O4/chitosan nanocomposite for magnetic drug targeting to cancer. *Journal of Materials Chemistry* **2012,** *22* (15), 7622.
153. Zheng, Y. Y.; Wang, X. B.; Shang, L.; Li, C. R.; Cui, C.; Dong, W. J.; Tang, W. H.; Chen, B. Y., Fabrication of shape controlled Fe3O4 nanostructure. *Materials Characterization* **2010,** *61* (4), 489-492.
154. Yan, A.; Liu, X.; Qiu, G.; Wu, H.; Yi, R.; Zhang, N.; Xu, J., Solvothermal synthesis and characterization of size-controlled Fe3O4 nanoparticles. *Journal of Alloys and Compounds* **2008,** *458* (1-2), 487-491.
155. Wu, J.-H.; Ko, S. P.; Liu, H.-L.; Kim, S.; Ju, J.-S.; Kim, Y. K., Sub 5 nm magnetite nanoparticles: Synthesis, microstructure, and magnetic properties. *Materials Letters* **2007,** *61* (14-15), 3124-3129.
156. Sheparovych, R.; Sahoo, Y.; Motornov, M.; Wang, S.; Luo, H.; Prasad, P. N.; Sokolov, I.; Minko, S., Polyelectrolyte Stabilized Nanowires from Fe3O4Nanoparticles via Magnetic Field Induced Self-Assembly. *Chemistry of Materials* **2006,** *18* (3), 591-593.

157. Liu, Y.; Gao, Z.-F.; Sun, Q.; Zeng, Y.-P., The structure-tunable synthesis and magnetic properties of Fe3O4 nanocrystals. *Hyperfine Interactions* **2013,** *219* (1-3), 107-112.
158. Guardia, P.; Riedinger, A.; Nitti, S.; Pugliese, G.; Marras, S.; Genovese, A.; Materia, M. E.; Lefevre, C.; Manna, L.; Pellegrino, T., One pot synthesis of monodisperse water soluble iron oxide nanocrystals with high values of the specific absorption rate. *Journal of Materials Chemistry B* **2014,** *2* (28), 4426.
159. Zhang, W.; Jia, S.; Wu, Q.; Ran, J.; Wu, S.; Liu, Y., Convenient synthesis of anisotropic Fe3O4 nanorods by reverse co-precipitation method with magnetic field-assisted. *Materials Letters* **2011,** *65* (12), 1973-1975.
160. Wang, F.; Liu, J.; Kong, J.; Zhang, Z.; Wang, X.; Itoh, M.; Machida, K.-i., Template free synthesis and electromagnetic wave absorption properties of monodispersed hollow magnetite nano-spheres. *Journal of Materials Chemistry* **2011,** *21* (12), 4314.
161. Lin, X.; Ji, G.; Liu, Y.; Huang, Q.; Yang, Z.; Du, Y., Formation mechanism and magnetic properties of hollow Fe3O4 nanospheres synthesized without any surfactant. *CrystEngComm* **2012,** *14* (24), 8658.
162. Kuo, C. Y.; Liu, T. Y.; Chan, T. Y.; Tsai, S. C.; Hardiansyah, A.; Huang, L. Y.; Yang, M. C.; Lu, R. H.; Jiang, J. K.; Yang, C. Y.; Lin, C. H.; Chiu, W. Y., Magnetically triggered nanovehicles for controlled drug release as a colorectal cancer therapy. *Colloids and surfaces. B, Biointerfaces* **2016,** *140*, 567-73.
163. Kakwere, H.; Leal, M. P.; Materia, M. E.; Curcio, A.; Guardia, P.; Niculaes, D.; Marotta, R.; Falqui, A.; Pellegrino, T., Functionalization of strongly interacting magnetic nanocubes with (thermo)responsive coating and their application in hyperthermia and heat-triggered drug delivery. *ACS applied materials & interfaces* **2015,** *7* (19), 10132-45.
164. Fang, K.; Song, L.; Gu, Z.; Yang, F.; Zhang, Y.; Gu, N., Magnetic field activated drug release system based on magnetic PLGA microspheres for chemo-thermal therapy. *Colloids and surfaces. B, Biointerfaces* **2015,** *136*, 712-20.
165. Todd Hoare, J. S., Gerardo F. Goya, Silvia Irusta, Debora Lin, Samantha Lau, Robert Padera, Robert Langer, and Daniel S. Kohane, A Magnetically Triggered Composite Membrane for On-Demand Drug Delivery. *Nano letters* **2009**.
166. Hoare, T.; Timko, B. P.; Santamaria, J.; Goya, G. F.; Irusta, S.; Lau, S.; Stefanescu, C. F.; Lin, D.; Langer, R.; Kohane, D. S., Magnetically triggered nanocomposite membranes: a versatile platform for triggered drug release. *Nano Lett* **2011,** *11* (3), 1395-400.
167. Peça, I. N.; Bicho, A.; Gardner, R.; Cardoso, M. M., Control of doxorubicin release from magnetic Poly(dl-lactide-co-glycolide) nanoparticles by application of a non-permanent magnetic field. *Journal of Nanoparticle Research* **2015,** *17* (11).
168. Baeza, A.; Guisasola, E.; Ruiz-Hernández, E.; Vallet-Regí, M., Magnetically Triggered Multidrug Release by Hybrid Mesoporous Silica Nanoparticles. *Chemistry of Materials* **2012,** *24* (3), 517-524.
169. Kong, S. D.; Zhang, W.; Lee, J. H.; Brammer, K.; Lal, R.; Karin, M.; Jin, S., Magnetically vectored nanocapsules for tumor penetration and remotely switchable on-demand drug release. *Nano Lett* **2010,** *10* (12), 5088-92.
170. Dan, N., Compound release from core–shell carriers triggered by oscillating fields: Monte Carlo simulations. *Colloids and Surfaces A: Physicochemical and Engineering Aspects* **2015,** *481*, 80-86.

171. Hardiansyah, A.; Huang, L.; Yang, M.; Liu, T.; Tsai, S.; Yang, C.; Kuo, C.; Chan, T.; Zou, H.; Lian, W.; Lin, C., Magnetic liposomes for colorectal cancer cells therapy by high-frequency magnetic field treatment. *Nanoscale Research Letters* **2014,** *9* (497).
172. Zou, H.; Yuan, W., Temperature- and redox-responsive magnetic complex micelles for controlled drug release. *J. Mater. Chem. B* **2015,** *3*, 260-269.
173. Liu, J.; Detrembleur, C.; Debuigne, A.; De Pauw-Gillet, M. C.; Mornet, S.; Vander Elst, L.; Laurent, S.; Labrugere, C.; Duguet, E.; Jerome, C., Poly(acrylic acid)-block-poly(vinyl alcohol) anchored maghemite nanoparticles designed for multi-stimuli triggered drug release. *Nanoscale* **2013,** *5* (23), 11464-77.
174. Shang-Hsiu Hu, C.-H. T., Chen-Fu Liao, Dean-Mo Liu,* and San-Yuan Chen*, Controlled Rupture of Magnetic Polyelectrolyte Microcapsules for Drug Delivery. *Langmuir* **2008**.
175. Riedinger, A.; Guardia, P.; Curcio, A.; Garcia, M. A.; Cingolani, R.; Manna, L.; Pellegrino, T., Subnanometer local temperature probing and remotely controlled drug release based on azo-functionalized iron oxide nanoparticles. *Nano Lett* **2013,** *13* (6), 2399-406.
176. Nappini, S.; Bonini, M.; Bombelli, F. B.; Pineider, F.; Sangregorio, C.; Baglioni, P.; Nordèn, B., Controlled drug release under a low frequency magnetic field: effect of the citrate coating on magnetoliposomes stability. *Soft Matter* **2011,** *7* (3), 1025-1037.
177. Klyachko, N. L.; Sokolsky-Papkov, M.; Pothayee, N.; Efremova, M. V.; Gulin, D. A.; Pothayee, N.; Kuznetsov, A. A.; Majouga, A. G.; Riffle, J. S.; Golovin, Y. I.; Kabanov, A. V., Changing the enzyme reaction rate in magnetic nanosuspensions by a non-heating magnetic field. *Angewandte Chemie* **2012,** *51* (48), 12016-9.
178. Lu, Z. H.; Prouty, M. D.; Guo, Z. H.; Golub, V. O.; Kumar, C. S. S. R.; Lvov, Y. M., Magnetic Switch of Permeability for Polyelectrolyte Microcapsules Embedded with Co@Au Nanoparticles. *Langmuir* **2005**.
179. Griffiths, G.; Nystrom, B.; Sable, S. B.; Khuller, G. K., Nanobead-based interventions for the treatment and prevention of tuberculosis. *Nature reviews. Microbiology* **2010,** *8* (11), 827-34.
180. Pieters, J., Evasion of host cell defense mechanisms by pathogenic bacteria. *Current Opinion in Immunology* **2001,** *13* (1), 37-44.
181. Das, D.; Saha, S. S.; Bishayi, B., Intracellular survival of Staphylococcus aureus: correlating production of catalase and superoxide dismutase with levels of inflammatory cytokines. *Inflammation research : official journal of the European Histamine Research Society ... [et al.]* **2008,** *57* (7), 340-9.
182. Costerton, J. W.; Stewart, P. S.; Greenberg, E. P., Bacterial Biofilms: A Common Cause of Persistent Infections. *Science* **1999,** *284*, 1318-1322.
183. Briones, E.; Colino, C. I.; Lanao, J. M., Delivery systems to increase the selectivity of antibiotics in phagocytic cells. *Journal of controlled release : official journal of the Controlled Release Society* **2008,** *125* (3), 210-27.
184. Köhler, K.; Sukhorukov, G. B., Heat Treatment of Polyelectrolyte Multilayer Capsules: A Versatile Method for Encapsulation. *Advanced Functional Materials* **2007,** *17* (13), 2053-2061.

185. Qi, W.; Wang, A.; Yang, Y.; Du, M.; Bouchu, M. N.; Boullanger, P.; Li, J., The lectin binding and targetable cellular uptake of lipid-coated polysaccharide microcapsules. *Journal of Materials Chemistry* **2010,** *20* (11), 2121-2127.
186. Pavlov, A. M.; De Geest, B. G.; Louage, B.; Lybaert, L.; De Koker, S.; Koudelka, Z.; Sapelkin, A.; Sukhorukov, G. B., Magnetically engineered microcapsules as intracellular anchors for remote control over cellular mobility. *Advanced materials* **2013,** *25* (48), 6945-50.
187. Urlinger, S.; Baron, U.; Thellmann, M.; Hasan, M. T.; Bujard, H.; Hillen, W., Exploring the sequence space for tetracycline-dependent transcriptional activators: novel mutations yield expanded range and sensitivity. *Proc Natl Acad Sci U S A* **2000,** *97* (14), 7963-8.
188. Forster, K.; Helbl, V.; Lederer, T.; Urlinger, S.; Wittenburg, N.; Hillen, W., Tetracycline-inducible expression systems with reduced basal activity in mammalian cells. *Nucleic Acids Res* **1999,** *27* (2), 708-10.
189. Yousaf, N.; Gould, D. J.; Aganna, E.; Hammond, L.; Mirakian, R. M.; Turner, M. D.; Hitman, G. A.; McDermott, M. F.; Chernajovsky, Y., Tumor necrosis factor receptor I from patients with tumor necrosis factor receptor-associated periodic syndrome interacts with wild-type tumor necrosis factor receptor I and induces ligand-independent NF-kappaB activation. *Arthritis Rheum* **2005,** *52* (9), 2906-2916.
190. Wissel, K.; Stover, T.; Hofmann, N. S.; Chernajovsky, Y.; Daly, G.; Sasse, S.; Warnecke, A.; Lenarz, T.; Gross, G.; Hoffmann, A., Fibroblast-mediated delivery of GDNF induces neuronal-like outgrowth in PC12 cells. *Otology & neurotology : official publication of the American Otological Society, American Neurotology Society [and] European Academy of Otology and Neurotology* **2008,** *29* (4), 475-81.
191. Kulbe, H.; Thompson, R.; Wilson, J. L.; Robinson, S.; Hagemann, T.; Fatah, R.; Gould, D.; Ayhan, A.; Balkwill, F., The inflammatory cytokine tumor necrosis factor-alpha generates an autocrine tumor-promoting network in epithelial ovarian cancer cells. *Cancer Res* **2007,** *67* (2), 585-92.
192. Skirtach, A. G.; Antipov, A. A.; Shchukin, D. G.; Sukhorukov, G. B., Remote Activation of Capsules Containing Ag Nanoparticles and IR Dye by Laser Light. *Langmuir* **2004,** *20* (17), 6988-6992.
193. Dupont, N.; Lazar, A. N.; Perret, F.; Danylyuk, O.; Suwinska, K.; Navaza, A.; Coleman, A. W., Solid state structures of the complexes between the antiseptic chlorhexidine and three anionic derivatives of calix[4]arene. *CrystEngComm* **2008,** *10* (8), 975.
194. Bharatam, P. V.; Patel, D. S.; Iqbal, P., Pharmacophoric Features of Biguanide Derivatives: An Electronic and Structural Analysis. *J. Med. Chem.* **2005,** *48*, 7615-7622.
195. Shutava, T. G.; Fakhrullin, R. F.; Lvov, Y. M., Spherical and tubule nanocarriers for sustained drug release. *Current opinion in pharmacology* **2014,** *18*, 141-8.
196. Fuhrmann, K.; Schulz, J. D.; Gauthier, M. A.; Leroux, J., PEG Nanocages as Non-sheddable Stabilizers for Drug Nanocrystals. *ACS Nano* **2012,** *6* (2), 1667–1676.
197. Sun, W.; Tian, W.; Zhang, Y.; He, J.; Mao, S.; Fang, L., Effect of novel stabilizers--cationic polymers on the particle size and physical stability of poorly soluble drug nanocrystals. *Nanomedicine* **2012,** *8* (4), 460-7.
198. Schwiertz, J.; Meyer-Zaika, W.; Ruiz-Gonzalez, L.; González-Calbet, J. M.; Vallet-Regí, M.; Epple, M., Calcium phosphate nanoparticles as templates for nanocapsules prepared by the layer-by-layer technique. *Journal of Materials Chemistry* **2008,** *18* (32), 3831-3834.

199. Antipov, A. A.; Sukhorukov, G. B., Polyelectrolyte multilayer capsules as vehicles with tunable permeability. *Adv Colloid Interface Sci* **2004,** *111* (1-2), 49-61.
200. Ai, H.; Jones, S. A.; de Villiers, M. M.; Lvov, Y. M., N ano-encapsulation of furosemide microcrystals for controlled drug release. *Journal of Controlled Release* **2003,** *86*, 59–68.
201. Choi, J. Y.; Park, C. H.; Lee, J., Effect of Polymer Molecular Weight on Nanocomminution of Poorly Soluble Drug. *Drug delivery* **2008,** *15* (5), 347-353.
202. Caruso, F.; Yang, W.; Trau, D.; Renneberg, R., Microencapsulation of Uncharged Low Molecular Weight Organic Materials by Polyelectrolyte Multilayer Self-Assembly. *Langmuir* **2000,** *16*, 8932-8936.
203. Klitzing, R. V.; Möhwald, H., A Realistic Diffusion Model for Ultrathin Polyelectrolyte Films. *macromolecules* **1996,** *29* (21), 6901–6906.
204. Jang, J.; Ha, J.; Cho, J., Fabrication of Water-Dispersible Polyaniline-Poly(4-styrenesulfonate) Nanoparticles For Inkjet-Printed Chemical-Sensor Applications. *Advanced materials* **2007,** *19* (13), 1772-1775.
205. Shutava, T. G.; Pattekari, P. P.; Arapov, K. A.; Torchilin, V. P.; Lvov, Y. M., Architectural layer-by-layer assembly of drug nanocapsules with PEGylated polyelectrolytes. *Soft Matter* **2012,** *8* (36), 9418-9427.
206. Yang, X.; Liu, X.; Liu, Z.; Pu, F.; Ren, J.; Qu, X., Near-infrared light-triggered, targeted drug delivery to cancer cells by aptamer gated nanovehicles. *Advanced materials* **2012**.
207. Palmer, G.; Jones, F. H.; Billington, R. W.; Pearson, G. J., Chlorhexidine release from an experimental glass ionomer cement. *Biomaterials* **2004,** *25* (23), 5423-31.
208. Hiraishi, N.; Yiu, C. K.; King, N. M.; Tay, F. R., Chlorhexidine release and antibacterial properties of chlorhexidine-incorporated polymethyl methacrylate-based resin cement. *Journal of biomedical materials research. Part B, Applied biomaterials* **2010,** *94* (1), 134-40.
209. Metwally, H. A.; Ardazishvili, R. V.; Severyukhina, A. N.; Zaharevich, A. M.; Skaptsov, A. A.; Venig, S. B.; Sukhorukov, G. B.; Gorin, D. A., The Influence of Hydroxyapatite and Calcium Carbonate Microparticles on the Mechanical Properties of Nonwoven Composite Materials Based on Polycaprolactone. *BioNanoScience* **2014,** *5* (1), 22-30.
210. Sy, J. C.; Klemm, A. S.; Shastri, V. P., Emulsion as a Means of Controlling Electrospinning of Polymers. *Advanced materials* **2009,** *21* (18), 1814-1819.
211. Herrmann, C.; Turshatov, A.; Crespy, D., Fabrication of Polymer Ellipsoids by the Electrospinning of Swollen Nanoparticles. *ACS Macro Letters* **2012,** *1* (7), 907-909.
212. Qiu, K.; He, C.; Feng, W.; Wang, W.; Zhou, X.; Yin, Z.; Chen, L.; Wang, H.; Mo, X., Doxorubicin-loaded electrospun poly(l-lactic acid)/mesoporous silica nanoparticles composite nanofibers for potential postsurgical cancer treatment. *Journal of Materials Chemistry B* **2013,** *1* (36), 4601-4611.
213. Wei, J.; Hu, J.; Li, M.; Chen, Y.; Chen, Y., Multiple drug-loaded electrospun PLGA/gelatin composite nanofibers encapsulated with mesoporous ZnO nanospheres for potential postsurgical cancer treatment. *RSC Advances* **2014,** *4* (53), 28011-28019.
214. del Valle, L. J.; Roa, M.; Díaz, A.; Casas, M. T.; Puiggalí, J.; Rodríguez-Galán, A., Electrospun nanofibers of a degradable poly(ester amide). Scaffolds loaded with antimicrobial agents. *Journal of Polymer Research* **2012,** *19* (2), 1-13.

215. Naghavi, N.; Ghoddusi, J.; Sadeghnia, H. R.; Asadpour, E.; Asgary, S., Genotoxicity and cytotoxicity of mineral trioxide aggregate and calcium enriched mixture cements on L929 mouse fibroblast cells. *Dental Materials Journal* **2014,** *33* (1), 64-69.
216. Zhao, J.; Cui, Y.; Wang, A.; Fei, J.; Yang, Y.; Li, J., Side effect reduction of encapsulated hydrocortisone crystals by insulin/alginate shells. *Langmuir* **2011,** *27* (4), 1499-504.
217. Stachewicz, U.; Qiao, T.; Rawlinson, S. C.; Almeida, F. V.; Li, W. Q.; Cattell, M.; Barber, A. H., 3D imaging of cell interactions with electrospun PLGA nanofiber membranes for bone regeneration. *Acta biomaterialia* **2015,** *27*, 88-100.
218. Chen, Y.-T.; Hung, S.-L.; Lin, L.-W.; Chi, L.-Y.; Ling, L.-J., Attachment of Periodontal Ligament Cells to Chlorhexidine-Loaded Guided Tissue Regeneration Membranes. *J Periodontol* **2003,** *74* (11), 1652-1659.
219. Timko, B. P.; Dvir, T.; Kohane, D. S., Remotely triggerable drug delivery systems. *Advanced materials* **2010,** *22* (44), 4925-43.
220. You, J.; Shao, R.; Wei, X.; Gupta, S.; Li, C., Near-infrared light triggers release of Paclitaxel from biodegradable microspheres: photothermal effect and enhanced antitumor activity. *Small* **2010,** *6* (9), 1022-31.
221. Hribar, K. C.; Lee, M. H.; Lee, D.; Burdick, J. A., Enhanced release of small molecules from near-infrared light responsive polymer-nanorod composites. *ACS Nano* **2011,** *5* (4), 2948–2956.
222. Gorelikov, I.; Matsuura, N., Single-Step Coating of Mesoporous Silica on Cetyltrimethyl Ammonium Bromide-Capped Nanoparticles. *Nano letters* **2008,** *8* (1), 369-373.
223. Koutsoukos, P. G.; Nancollas, G. H., Crystal growth of calcium phosphates - epitaxial considerations. *Journal of Crystal Growth* **1981,** *53* (1), 10-19.
224. LaMer, V. K.; Dinegar, R. H., Theory, Production and Mechanism of Formation of Monodispersed Hydrosols. *J. Am. Chem. Soc.* **1950,** *72* (11), 4847-4854.
225. Luo, D.; Shahid, S.; Wilson, R. M.; Cattell, M. J.; Sukhorukov, G. B., Novel Formulation of Chlorhexidine Spheres and Sustained Release with Multilayered Encapsulation. *ACS applied materials & interfaces* **2016,** *8* (20), 12652-60.
226. Croissant, J.; Zink, J. I., Nanovalve-controlled cargo release activated by plasmonic heating. *Journal of the American Chemical Society* **2012,** *134* (18), 7628-31.
227. Kyrsting, A.; Bendix, P. M.; Stamou, D. G.; Oddershede, L. B., Heat profiling of three-dimensionally optically trapped gold nanoparticles using vesicle cargo release. *Nano Lett* **2011,** *11* (2), 888-92.
228. Yi, Q.; Sukhorukov, G. B., Single-Component Diazo-resin Microcapsules for Encapsulation and Triggered Release of Small Molecules. *Particle & Particle Systems Characterization* **2013,** *30* (11), 989-995.
229. Haag, P. A.; Steiger-Ronay, V.; Schmidlin, P. R., The in Vitro Antimicrobial Efficacy of PDT against Periodontopathogenic Bacteria. *International journal of molecular sciences* **2015,** *16* (11), 27327-38.
230. Leung, D.; Spratt, D. A.; Pratten, J.; Gulabivala, K.; Mordan, N. J.; Young, A. M., Chlorhexidine-releasing methacrylate dental composite materials. *Biomaterials* **2005,** *26* (34), 7145-53.

231. Sanders, B. J.; Gregory, R. L.; Moore, K.; Avery, D. R., Antibacterial and physical properties of resin modified glass-ionomers combined with chlorhexidine. *Journal of Oral Rehabilitation* **2002,** *29* (6), 553-558.
232. Joshi, A.; Raje, J., Sonicated transdermal drug transport. *Journal of controlled release : official journal of the Controlled Release Society* **2002,** *83* (1), 13–22.
233. Jing, J.; Szarpak-Jankowska, A.; Guillot, R.; Pignot-Paintrand, I.; Picart, C.; Auzély-Velty, R., Cyclodextrin/Paclitaxel Complex in Biodegradable Capsules for Breast Cancer Treatment. *Chem. Mater.* **2013,** *25* (19), 3867-3873.
234. Mao, Z.; Ma, L.; Gao, C.; Shen, J., Preformed microcapsules for loading and sustained release of ciprofloxacin hydrochloride. *Journal of controlled release : official journal of the Controlled Release Society* **2005,** *104* (1), 193-202.
235. Battle, A. R.; Valenzuela, S. M.; Mechler, A.; Nichols, R. J.; Praporski, S.; di Maio, I. L.; Islam, H.; Girard-Egrot, A. P.; Cornell, B. A.; Prashar, J.; Caruso, F.; Martin, L. L.; Martin, D. K., Novel Engineered Ion Channel Provides Controllable Ion Permeability for Polyelectrolyte Microcapsules Coated with a Lipid Membrane. *Advanced Functional Materials* **2009,** *19* (2), 201-208.
236. Cui, J.; Yan, Y.; Such, G. K.; Liang, K.; Ochs, C. J.; Postma, A.; Caruso, F., Immobilization and intracellular delivery of an anticancer drug using mussel-inspired polydopamine capsules. *Biomacromolecules* **2012,** *13* (8), 2225-8.
237. Barza, M.; Brown, R. B.; Shanks, C.; Gamble, C.; Weinstein, L., Relation between lipophilicity and pharmacological behavior of minocycline, doxycycline, tetracycline, and oxytetracycline in dogs. *Antimicrob Agents Chemother* **1975,** *8* (6), 713-20.
238. Javier, A. M.; Kreft, O.; Semmling, M.; Kempter, S.; Skirtach, A. G.; Bruns, O. T.; del Pino, P.; Bedard, M. F.; Rädler, J.; Käs, J.; Plank, C.; Sukhorukov, G. B.; Parak, W. J., Uptake of Colloidal Polyelectrolyte-Coated Particles and Polyelectrolyte Multilayer Capsules by Living Cells. *Adv. Mater.* **2008,** *20* (22), 4281–4287.
239. De Koker, S.; De Geest, B. G.; Cuvelier, C.; Ferdinande, L.; Deckers, W.; Hennink, W. E.; De Smedt, S. C.; Mertens, N., In vivo Cellular Uptake, Degradation, and Biocompatibility of Polyelectrolyte Microcapsules. *Advanced Functional Materials* **2007,** *17* (18), 3754-3763.
240. Cambridge, S. B.; Geissler, D.; Calegari, F.; Anastassiadis, K.; Hasan, M. T.; Stewart, A. F.; Huttner, W. B.; Hagen, V.; Bonhoeffer, T., Doxycycline-dependent photoactivated gene expression in eukaryotic systems. *Nature methods* **2009,** *6* (7), 527-531.
241. Yang, Y. S.; Carney, R. P.; Stellacci, F.; Irvine, D. J., Enhancing Radiotherapy by Lipid Nanocapsule-Mediated Delivery of Amphiphilic Gold Nanoparticles to Intracellular Membranes. *ACS Nano* **2014,** *8* (9), 8992–9002.
242. Ge, L.; Mohwald, H.; Li, J., Phospholipase A2 hydrolysis of mixed phospholipid vesicles formed on polyelectrolyte hollow capsules. *Chem. Eur. J.* **2003,** *9* (11), 2589-94.
243. Delcea, M.; Möhwald, H.; Skirtach, A. G., Stimuli-responsive LbL capsules and nanoshells for drug delivery. *Adv Drug Deliv Rev.* **2011,** *63*, 730-741.
244. J., L.; C., R.; H., B.; H., S.; G., M.; W., S., Penetration of Titanium Dioxide Microparticles in a Sunscreen Formulation into the Horny Layer and the Follicular Orifice. *Skin Pharmacol Appl Skin Physiol* **1999,** *12*, 247–256

245. Yan, S.; Zhang, X.; Sun, Y.; Wang, T.; Chen, X.; Yin, J., In situ preparation of magnetic Fe3O4 nanoparticles inside nanoporous poly(L-glutamic acid)/chitosan microcapsules for drug delivery. *Colloids and surfaces. B, Biointerfaces* **2014,** *113*, 302-11.
246. Bukreeva, T. V.; Orlova, O. A.; Sulyanov, S. N.; Grigoriev, Y. V.; Dorovatovskiy, P. V., A new approach to modification of polyelectrolyte capsule shells by magnetite nanoparticles. *Crystallography Reports* **2011,** *56* (5), 880-883.
247. Liesbeth J. De Cock, S. D. K., BrunoG. De Geest, Johan Grooten, Chris Vervaet, Jean Paul Remon, Gleb B. Sukhorukov, and Maria N. Antipina, Polymeric Multilayer Capsules in Drug Delivery. *Angew. Chem. Int. Ed.* **2010**.
248. Luo, D.; Gould, D. J.; Sukhorukov, G. B., Local and Sustained Activity of Doxycycline Delivered with Layer-by-Layer Microcapsules. *Biomacromolecules* **2016,** *17* (4), 1466-76.
249. Pavlov, A. M.; Gabriel, S. A.; Sukhorukov, G. B.; Gould, D. J., Improved and targeted delivery of bioactive molecules to cells with magnetic layer-by-layer assembled microcapsules. *Nanoscale* **2015,** *7* (21), 9686-9693.
250. Sukhorukov, G. B.; Rogach, A. L.; Zebli, B.; Liedl, T.; Skirtach, A. G.; Kohler, K.; Antipov, A. A.; Gaponik, N.; Susha, A. S.; Winterhalter, M.; Parak, W. J., Nanoengineered polymer capsules: tools for detection, controlled delivery, and site-specific manipulation. *Small* **2005,** *1* (2), 194-200.
251. Hu, S. H.; Hsieh, T. Y.; Chiang, C. S.; Chen, P. J.; Chen, Y. Y.; Chiu, T. L.; Chen, S. Y., Surfactant-Free, Lipo-Polymersomes Stabilized by Iron Oxide Nanoparticles/Polymer Interlayer for Synergistically Targeted and Magnetically Guided Gene Delivery. *Adv. Healthcare Mater.* **2014,** *3* (2), 273-282.
252. Aytar, B. S.; Muller, J. P.; Kondo, Y.; Abbott, N. L.; Lynn, D. M., Spatial control of cell transfection using soluble or solid-phase redox agents and a redox-active ferrocenyl lipid. *ACS applied materials & interfaces* **2013,** *5* (17), 8283-8.
253. Ganas, C.; Weiss, A.; Nazarenus, M.; Rosler, S.; Kissel, T.; Rivera Gil, P.; Parak, W. J., Biodegradable capsules as non-viral vectors for in vitro delivery of PEI/siRNA polyplexes for efficient gene silencing. *Journal of controlled release : official journal of the Controlled Release Society* **2014,** *196*, 132-8.
254. Griffete, N.; Fresnais, J.; Espinosa, A.; Wilhelm, C.; Bée, A.; Ménager, C., Design of magnetic molecularly imprinted polymer nanoparticles for controlled release of doxorubicin under an alternative magnetic field in athermal conditions. *Nanoscale* **2015,** *7* (45), 18891-18896.
255. Lee, G. Y.; Qian, W. P.; Wang, L.; Wang, Y. A.; Staley, C. A.; Satpathy, M.; Nie, S.; Mao, H.; Yang, L., Theranostic Nanoparticles with Controlled Release of Gemcitabine for Targeted Therapy and MRI of Pancreatic Cancer. *ACS Nano* **2013,** *7* (3), 2078-2089.
256. Ding, X.; Liu, Y.; Li, J.; Luo, Z.; Hu, Y.; Zhang, B.; Liu, J.; Zhou, J.; Cai, K., Hydrazone-bearing PMMA-functionalized magnetic nanocubes as pH-responsive drug carriers for remotely targeted cancer therapy in vitro and in vivo. *ACS applied materials & interfaces* **2014,** *6* (10), 7395-407.
257. Yi, Q.; Li, D.; Lin, B.; Pavlov, A. M.; Luo, D.; Gong, Q.; Song, B.; Ai, H.; Sukhorukov, G. B., Magnetic Resonance Imaging for Monitoring of Magnetic Polyelectrolyte Capsule In Vivo Delivery. *BioNanoScience* **2013,** *4* (1), 59-70.

8. Publications

Patent

1. D. Luo, S. Shahid, M. J. Cattell, G. B. Sukhorukov: Chlorhexidine crystal forms and uses thereof in medicine, UK Patent, Application No. 1604639.3. filed at 18.3.2016.

Papers

1. Q. Yi, D. Li, B. Lin, A. M. Pavlov, D. Luo, Q. Gong, B. Song, H. Ai, G. B. Sukhorukov: Magnetic Resonance Imaging for Monitoring of Magnetic Polyelectrolyte Capsule In Vivo Delivery. *BioNanoScience* 2013**,** *4* (1), 59-70.
2. D. Luo, D. J. Gould, G. B. Sukhorukov: Local and Sustained Activity of Doxycycline Delivered with Layer-by-Layer Microcapsules. *Biomacromolecules* 2016, 17(4), 1466-1476.
3. D. Luo, S. Shahid, R. M. Wilson, M. J. Cattell, G. B. Sukhorukov: Novel Formulation of Chlorhexidine Spheres and Sustained Release with Multilayered Encapsulation. *ACS Appl. Mater. Interfaces* 2016, 8, 12652-12660.
4. D. Luo, X. Zhang, S. Shahid, M. J. Cattell, D. J. Gould, G. B. Sukhorukov: Electrospun Poly(lactic acid) Fibers Containing Novel Chlorhexidine Particles with Sustained Antibacterial Activity. *Biomater Sci*. 2017, 5, 111-119.
5. D. Luo, S. Shahid, G. B. Sukhorukov, M. J. Cattell: Synthesis of novel Chlorhexidine Spheres with Controlled Release from UDMA-HEMA Resin using Ultrasound. Submitted to *Dental Materials*.
6. D. Luo, S. Shahid, B. N. Khlebtsov, M. J. Cattell, G. B. Sukhorukov: Gold Nanorod Mediated Chlorhexidine Crystallization and Near-infrared Light Stimuli Responsive Release. Submitted to *Nanomedicine: NBM*.
7. D. Luo, R. N. Poston, D. J. Gould, G. B. Sukhorukov: Targeted Delivery of Doxycycline with Magnetic Capsules and Alternating Magnetic Field Induced Intracellular Release. In preparation.
8. D. Luo, S. Shahid, M. J. Cattell, D. J. Gould, G. B. Sukhorukov: One-step Encapsulation of Chlorhexidine Particles with PLA and its Sustained Antibacterial Activity. In preparation.